Role of cryptochromes from the marine worm in the circadian/circalunar clock

Dissertation

to obtain the degree

Doctor of Science

At the Department of Biology

The Johannes Gutenberg University Mainz

by

Shruthi Krishnan

Contents

Abbreviations

AEBSF	4-(2-aminoethyl)benzenesulfonyl fluoride hydrochloride
APS	Ammonium per sulfate
At	*Arabidopsis thaliana*
bHLH	Basic helix-loop-helix
Bis-Tris	Bis(2-hydroxythyl)amino-tris(hydroxymethyl)methane
BMAL1	Brain and muscle ARNT-like 1
bZIP	Basic leucine zipper
cAMP	Cyclic adenosine monophosphate
CCGs	Clock-controlled genes
CD	Circular dichroism
CK1	Casein kinase 1
CLOCK	Circadian locomotor output cycles kaput
CLK	CLOCK
CPD	Cyclobutane pyrimidine dimer
CPF	Cryptochrome/Photolyase family
CRE	cAMP response element
CREB	cAMP response element binding protein
CRY	CRYPTOCHROME
CRY-DASH	Cryptochrome-*Drosophila, Arabidopsis, Synechocystis, Human*
CRYO EM	Cryogenic electron microscopy
CV	Column volume
CYC	CYCLE
Da	Daltons
DBT	DOUBLETIME
DMSO	Dimethyl sulfoxide
DNA	Deoxyribonucleic acid
dNTP	Deoxyribonucleotide triphosphate
DTT	1,4-dithiothreitol
E.coli	*Escherichia coli*
EDTA	Ethylenediaminetetraacetic acid
EPR	Electron paramagnetic resonance
FAD	Flavin adenine dinucleotide
FBXL3	F-box and leucine-rich repeat protein 3
FF	Fast flow
FL	Full length
FMN	Flavin mononucleotide
FP	Forward primer
GSK3	Glycogen synthase kinase 3

GST	Glutathione S transferase
G3BP	Ras GTPase-activating protein-binding protein 1/2
HEPES	4-(2-Hydroxyethyl)piperazine-1-ethanesulfonic acid
IBS	Illustrator of biological sequences
IMAC	Immobilized metal ion chromatography
IPTG	Isopropyl β-D-1-thiogalactopyranoside
ipRGCs	Intrinsically photoreceptive retinal ganglion cells
kDa	Kilodaltons
LB	Luria Bertani
MALS	Multi-angle light scattering
mAU	Milli-absorbance units
Mettl3	Methyltransferase-like 3
$MgCl_2$	Magnesium chloride
MTHF	Methylenetetrahydrofolate
MOPS	3-(N-morpholino)propanesulfonic acid
NaCl	Sodium chloride
NEMO	NF-kappa-B essential modulator
NMDA	N-methyl-D-aspartate receptor
NTF2	Nuclear transport factor 2 domain
PAS	PER-ARNT-SIM
PCR	Polymerase chain reaction
PDP1	PAR DOMAIN PROTEIN1
PEG	Polyethylene glycol
PER	PERIOD
PFD	Photon flux density
PHR	Photolyase homology region
PITH	Proteasome-interacting thioredoxin domain
PITHD1	PITH domain-containing protein 1-like
PMSF	Phenylmethylsulfonyl fluoride
PPαRα	Peroxisome proliferator-activator α
PPFD	Photosynthetic photon flux density
PSIPRED	PSI-blast based secondary structure prediction
REV-ERB	Reverse strand of ERB
RGG box	Arginine-glycine rich box
RHT	Retinohypothalamic tract
RNA	Ribonucleic acid
ROR	Retinoic-acid related orphan receptor
ROREs	Retinoic acid-related orphan receptor response elements
RP	Reverse primer
RPM	Revolutions per minute
RRM	RNA recognition motif

SART3	Squamous cell carcinoma antigen recognized by T cells 3
SAXS	Small angle X-ray scattering
SCN	Suprachiasmatic nucleus
SDS-PAGE	Sodium dodecyl sulfate-polyacrylamide gel electrophoresis
SEC	Size-exclusion chromatography
Sf	*Spodoptera frugiperda*
SGG	segment polarity gene SHAGGY
SH3	SRC Homology 3 Domain
SLIC	Sequence and ligation independent cloning
SMAD	Mothers Against Decapentaplegic Homolog 1 (Drosophila)
SOC	Super optimal broth with added glucose
Src/FAK	Steroid receptor coactivator/Focal adhesion kinase
ss	Single stranded
TAD	Transactivation domain
TAE	Tris-acetate-EDTA
TB	Terrific broth
TCEP	Tris(2-carboxyethyl)phosphin
TEMED	N,N,N,N'-Tetramethylethylenediamine
TIM	TIMELESS
Tris	2-Amino-2-(hydroxymethyl)-1,3-propanediol
VRI	VRILLE
X-Gal	5-Bromo-4-chloro-3-indolyl-β-D-galactopyranoside
YFP	Yellow Fluorescent Protein
YTHDF	YTH domain-containing family protein 2-like isoform X2

Zusammenfassung

In den meisten Organismen, einschließlich des Menschen, werden physiologische Prozesse und Verhalten durch eine molekulare innere Uhr koordiniert. Diese Rhythmen sind mit dem 24-Stunden-Tag synchronisiert und werden als zirkadiane Rhythmen bezeichnet. Die Uhren-Proteine sind teilweise zwischen Insekten- und Säugetiersystemen konserviert. Viele Organismen richten ihr Verhalten nicht nur auf den Stand der Sonne aus, sondern auch auf die Zyklen des Mondes (monatliches Timing). Borstenwürmer wie z.B. *Platynereis dumerilli* waren unter den ersten Organismen, bei denen gezeigt wurde, dass das Erkennen eines Mondzyklus nur von nächtlichen Lichtreizen abhängt. Daher verfügt *Platynereis dumerilli* zusätzlich zur zirkadianen (täglichen) Uhr über eine zirkalunare (monatliche) Uhr.

Cryptochrome sind gut untersuchte Bestandteile der zirkadianen Uhr, die bei einigen Organismen als Lichtrezeptoren fungieren. Die vorliegende Dissertationsarbeit konzentriert sich auf die biochemische und strukturelle Charakterisierung der Cryptochrome aus *Platynereis dumerilli*, um Einblicke in deren Rolle in zirkadianen und/oder zirkalunaren Uhren zu erhalten. *Platynereis dumerilli* besitzt drei verschiedene Cryptochrome, von denen je eines Sequenzähnlichkeit zu dem Cryptochrom aus *Drosophila* (L-CRY), den Säugetieren (TR-CRY) oder dem Pflanzen-Cryptochrom (P-CRY) aufweist. Studien mit S2-Zellen ergaben, dass TR-CRY wie bei den Säugetieren als Transkriptionsrepressor-Cryptochrom fungiert. Die Rolle von L-CRY und P-CRY muss jedoch noch geklärt werden.

In dieser Arbeit wurden die *Platynereis* L-CRY und P-CRY Proteine aufgereinigt und mit Hilfe von UV / VIS- und Fluoreszenzspektroskopie, Hochleistungsflüssigchromatographie (HPLC) und statischer Lichtstreuung (MALS / SLS) analysiert, um den oligomeren Zustand und die gebundenen Cofaktoren der Cryptochrome zu bestimmen, sowie ein Modell für ihre Photoreaktionsmechanismen vorzuschlagen. Unsere Analysen legen mögliche Rollen von *Platynereis* L-CRY und P-CRY als Flavin-abhängige Photorezeptoren nahe. L-CRY reagiert auf Mondlicht, was zur teilweisen Photoreduktion zum anionischen FAD ° -Radikal führt.

Zudem lieferten Kleinwinkel-Röntgenstreuung (SAXS) Experimente und Cryo-Elektronenmikroskopie strukturelle Informationen zu L-CRY. Um weitere Einblicke in die funktionelle Rolle dieser Cryptochrome zu erhalten, half ein massenspektrometrischer Ansatz, um potenzielle Interaktionspartner zu bestimmen. Die nächste Ebene des

Verständnisses wird darin bestehen, zu erkennen, wie die Cryptochrome und ihre Interaktoren molekular verbunden sind und inwieweit diese Interaktionen bei zirkalunaren Uhren eine Rolle spielen.

Abstract

In most organisms including humans, physiology and behavior are coordinated by an internal molecular clock. These rhythms are synchronized with the 24h solar day and termed as circadian rhythms. At a molecular level, the circadian clock is governed by the interplay between several proteins such as CLOCK, CYCLE, PERIOD and CRY and is regulated by transcription-translation feedback loop. These regulatory proteins are partially conserved between several insect and mammalian systems indicating a possible evolutionary function. Many organisms align their behavior not only to the changes of the sun but also to the cycles of the moon (monthly timing). The bristle worm *Platynereis* was among the first organisms for which the entrainment to a lunar cycle was shown to only depend on nocturnal light stimuli. Thus, *Platynereis dumerilli* has a circalunar (monthly) clock in addition to the circadian (daily) clock. The locomotor activity of the worm is under the control of the circadian clock. The circalunar clock regulates the maturation of *Platynereis* adjusting its reproduction to the lunar phase. *Platynereis* is a suitable model to study the interplay between circadian and circalunar clock components and the influence of this on the behavior of the organism. It has been established that the circalunar clock of the worm affects the circadian clock at several levels and the circalunar clock persists even when the circadian clock is disrupted.

Cryptochromes are well studied components of the circadian clock which have the potential to function as light receptors in some species. This study focuses on the characterization of the cryptochromes from *Platynereis dumerilli* to provide insights to their role in circadian and/or circalunar clocks. *Platynereis dumerilli* possess 3 different kinds of cryptochromes, one each similar to the drosophila (L-CRY), mammalian repressor (TR-CRY) and plant (P-CRY) cryptochromes. Studies with S2 cells also established that TR-CRY functions as a transcriptional repressor cryptochrome as in mammals. However, the role of L-CRY and P-CRY remain to be elucidated.

In this thesis, characterization of L-CRY and P-CRY has been carried out with purified proteins. Here, we have purified the *Platynereis* L-CRY and P-CRY proteins and analyzed them by UV/VIS- and fluorescence spectroscopy, high performance liquid chromatography (HPLC) and static light scattering (MALS/SLS) to determine the oligomeric state, their cofactors bound and to propose their photoreaction mechanisms. Our analyses suggest possible roles of *Platynereis* L-CRY and P-CRY as flavin-dependent photoreceptors. SAXS and electron

microscopy analysis provided structural information regarding L-CRY with the detection of a novel dimer interface. To gain further insights into the functional role of these cryptochromes, a mass spectrometry-based approach helped to determine potential interacting partners. The next level of understanding will be to discern how these different cryptochromes and their interactors are molecularly connected and to what extent underlying molecular clocks share same components.

1 Introduction

1.1 Rhythms governing life

The periodic phenomena in living organisms to adapt their behavior to environmental solar and lunar cues is studied in the field of chronobiology (Jay C Dunlap et al., 2004). The daily biological activity and behavior of unicellular and multicellular organisms such as cyanobacteria, fungi, plants, insects and mammals is coordinated by internal molecular clocks (Dibner, Schibler, and Albrecht 2009; Bell-Pedersen et al. 2005; Reppert and Weaver 2002) . These daily rhythms are synchronized with the 24h solar day and hence termed as circadian rhythms. In humans, physiological processes such as sleep, secretion of hormones, neurotransmitters, metabolism, and regulation of body temperature are linked to circadian rhythms. Any disruption of the circadian rhythm or chronodisruption severely impacts health, for example, leading to fatigue due to jet-lag in travelers, sleep disorders and increased cancer risk in shift workers (Julius, Yin, and Wen 2019; Tagaya, Murayama, and Fukase 2015; Bonmati-Carrion et al. 2014; Rea et al. 2008). The significance of the field was recognized by the 2017 Nobel Prize in Physiology/Medicine being awarded for the discovery of the molecular mechanisms controlling circadian rhythms. In addition to the circadian rhythms, there exist several other important cycles such as the circannual cycles (in many plants and animals), circalunar, circasemilunar rhythms (seen in marine organisms) governing the migration and reproduction success and circatidal rhythms controlling the locomotion of intertidal crustaceans (De La Iglesia & Hsu, 2010; de la Iglesia & Johnson, 2013; Raible et al., 2017). Avoiding predation, to align with favorable environmental conditions for sexual maturation and successful mating, several organisms from algae, corals, worms to vertebrates use the lunar phase (H.-D. Franke, 1985; Zantke et al., 2013). The impact of the circalunar rhythm on mammalian reproduction extends to humans. It has also be suggested that sleep and mental health is affected by the lunar cycle (Chaput et al. 2016; Turányi et al. 2014; Cajochen et al. 2013). Molecular and cellular mechanisms governing these different rhythms as well as the interdependence among them has long held the interest of chronobiologists.

1.2 Connecting rhythms to clocks

Naturally occurring time cues termed as Zeitgeber are signals with 24h or 12-month periodicity (Ehlers et al., 1988; Grandin et al., 2006). Observations in nature triggered the

curiosity if rhythmic behavior in plants and animals was governed by internal endogenous clocks or a response to external environmental cues such as light signal or tidal waves (Palmer, 2000; Reppert & Weaver, 2002). Jean Jacques de Mairan observed that the leaves of the mimosa plant maintained their rhythmic opening and closing at the appropriate time of the day even in absence of light cues. This was the first indication towards the existence of endogenous circadian clocks. Later, German plant physiologist recorded leaf movements using a kymograph and observed that leaf movements were persistent even under constant light conditions. Jürgen Aschoff discovered that endogenous biological clocks exist and also certain external zeitgebers influence the timing of internal clock (Aschoff & Pohl, 1978; Lewis et al., 2018). This is also true in the case of circalunar/circasemilunar clocks where endogenous oscillators persist and changes in nocturnal light also have an impact (Raible et al., 2017).

Light as a primary zeitgeber regulating circadian rhythms is well studied (Moore MD, 1997). Simple organisms such as medusae possess specialized photoreceptors, ocelli (eye spots), to respond to light changes and coordinate phototaxis (Martin, 2002). In mammals, the photopigment melanopsin in the retina of the eye perceives light signal through the intrinsically photoreceptive retinal ganglion cells (ipRGCs) (Berson, 2003; Mohawk et al., 2012). There is a direct connection between the melanopsin-containing ganglion cells in the retina to the ventrolateral suprachiasmatic nucleus (SCN) in the hypothalamus of the brain. The SCN hosts the master circadian oscillator synchronizing the circadian rhythm to the 24h day based on the light cue. Destruction of the SCN leads to loss of circadian rhythmicity (Bernard et al., 2007; Hatori et al., 2014; Michel & Meijer, 2020; Ralph et al., 1990; Stephan & Zucker, 1972). In addition to the SCN (the central pacemarker), there are numerous peripheral clocks located in various tissues and organs which exhibit their own 24h rhythms under the control of the SCN (Fig. 1) . These peripheral clocks have diverse physiological outputs but interact with each other and the master clock, SCN to maintain healthy functioning of the body (Dibner et al., 2009). Unlike the SCN, these subsidiary clocks are not entrained by light, rather neuronal and hormonal output signals from the SCN or stimuli like feeding control their rhythmicity. Glucocorticoids released in rhythmic patterns also impact the functioning of peripheral clocks (Reddy et al., 2007; So et al., 2009). It was shown that endogenous and environmental temperature cues help synchronize peripheral clocks in

mammals and these temperature changes do not impact the phase of the central circadian pacemaker in the SCN (Brown et al., 2002).Despite differences, the molecular basis of both the central and peripheral clocks are quite similar (Kwon et al., 2011).

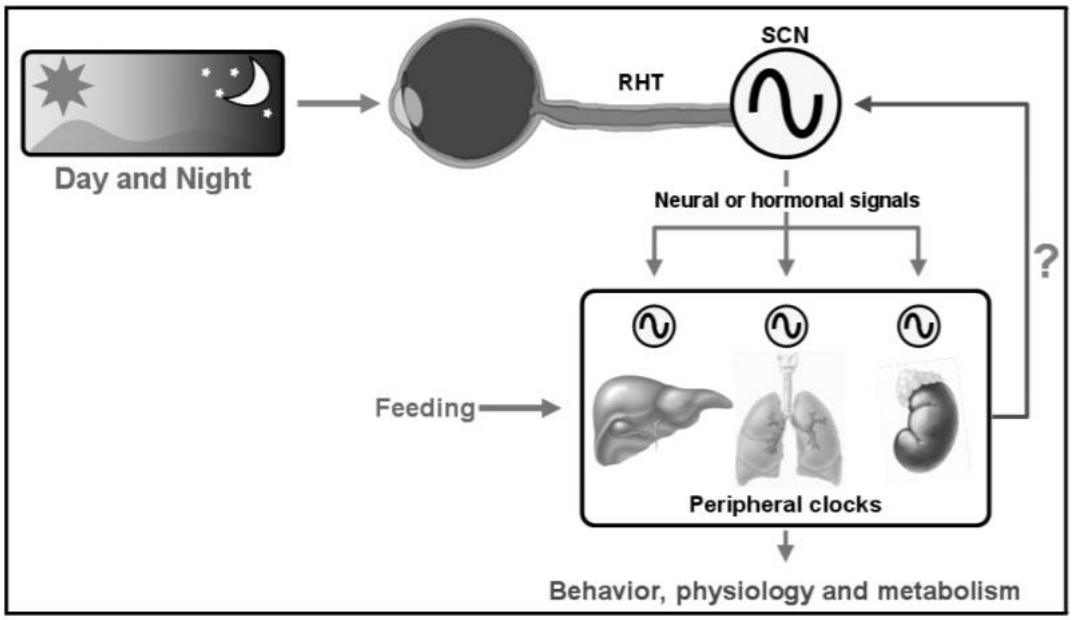

Fig 1: Master and peripheral circadian clock system in mammals. Light is perceived by the retina and this information transferred to the master clock in the suprachiasmatic nucleus (SCN) by the Retinohypothalamic tract (RHT). The SCN generated circadian rhythmicity acts as the input signal for various peripheral clocks residing in organs and tissues. (Kwon et al., 2011)

1.3 Molecular clock in mammals

At the molecular level, the mammalian circadian clock comprises of interlinked transcription-translation feedback loops (Fig. 2). The core transcription factors are the Circadian Locomotor Output Cycles Kaput (CLOCK) and Brain and Muscle ARNT-Like 1 (BMAL1) (Crane & Young, 2014). They belong to the family of basic helix-loop-helix (bHLH)-PAS (Period-Arnt-Single-minded) transcription factors. CLOCK and BMAL1 form a heterodimer which bind to E-box elements in the promoters of several clock-controlled genes (CCGs) such as *Cry1*, *Cry2,* three *Period* genes and *Rev-erbα* among others (Gekakis et al., 1998; Ko & Takahashi, 2006; Kume et al., 1999; Preitner et al., 2002). The transcription of *per* and *cry* genes results in the accumulation of circadian repressors PERIOD (PER) and CRYPTOCHROME (CRY) during the day. The PER and CRY heterodimer translocates back into the nucleus during night repressing its own transcription. Degradation of PER:CRY complex allows the transcription by

CLOCK:BMAL1 to continue and the feedback loop is closed regulating circadian gene expression. The repressor activity of CRYs is dependent on their interaction with PER proteins and E3 ubiquitin ligase F-box and leucine-rich repeat protein 3 (FBXL3) (Gatfield & Schibler, 2007; Lamia et al., 2009). In addition, post translational modifications such as ubiquitylation, acetylation/deacetylation, phosphorylation and sumoylation influence the stability and subcellular localization of clock proteins (N. Liu & Zhang, 2016; Mehra et al., 2009; Vanselow & Kramer, 2007).

The CLOCK protein is continuously produced, however, the expression of BMAL1 is rhythmically controlled by a second transcription-translation feedback loop which is governed by the orphan nuclear receptors reverse strand of ERB (REV-ERB) and the retinoic-acid related orphan receptor (ROR). CLOCK:BMAL1 activate *Rev-erbα* and *Rorα.* ROR and REV-ERB regulate Bmal1 through retinoic acid-related orphan receptor response elements (ROREs). RORs and REV-ERBs act as transcription activator and repressors of Bmal1 respectively thus regulating circadian oscillations (Akashi & Takumi, 2005; Guillaumond et al., 2005; Preitner et al., 2002; Ueda et al., 2002)

Studies suggest that the main photic signal for the SCN is glutamate. Glutamate induces NMDA-induced calcium influx into SCN leading to signal transduction cascades such as calmodulin kinase II (CaMKII), mitogen-activated protein kinase (MAPK), and neuronal nitric oxide synthase (nNOS). These diverse cascades lead to the phosphorylation of cAMP response element binding protein (CREB), binding to the cAMP response element (CRE) in the promoter region of *per* genes activating transcription.

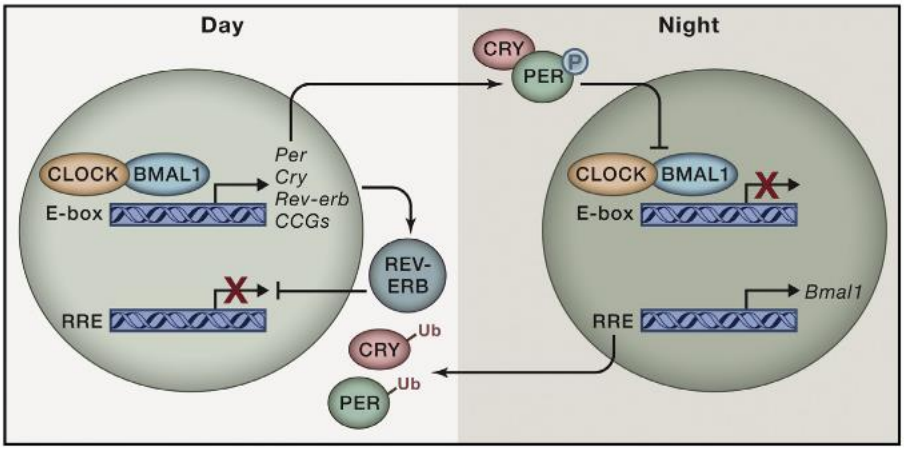

Fig 2: Mammalian circadian clock at the molecular level. CLOCK:BMAL1 complex activates the transcription of PER, CRY, and several CCGs. PER:CRY complex translocates back into nucleus to repress CLOCK:BMAL1 controlled transcription. Ubiquitination of PER and CRY leads to their degradation by the proteasome, allowing the feedback loop to be completed by the reactivation of transcription by CLOCK:BMAL1 (Asher & Sassone-Corsi, 2015)

1.4 Molecular clock in Drosophila

Similar to the mammalian circadian clock, the Drosophila clock is also driven by transcription-translation feedback loops. The transcription is activated by CLOCK (CLK) and CYCLE (CYC) which bind to the CACGTG E-box element in the promoter of *Cry*, *Period* and *Timeless* genes (Fig. 3). The initial levels of PER and TIM proteins are low and accumulate in cytoplasm during the day upto sunset (Darlington et al., 1998; Maurer et al., 2009; Rutila et al., 1998). Casein kinase 1 (CK1) homolog, DOUBLETIME (DBT) phosphorylates PER leading to its degradation through the E3 ubiquitin ligase SLIMB (Chiu et al., 2008; Kloss et al., 1998, 2001; Nawathean & Rosbash, 2004). The kinase NEMO controls the phosphorylation of DBT(Chiu et al., 2011). PER is stabilized by the binding of TIM to PER:DBT complex. A homolog of glycogen synthase kinase 3 (GSK3), segment polarity gene SHAGGY (SGG) phosphorylates TIM, promoting the entry of the PER:TIM:DBT complex into the nucleus. The heterodimer complex of PER:TIM repress CLOCK:CYC mediated transcription and thus regulating their own expression. Thereby, TIM replaces the function of mammalian CRYs as a transcription repressor and binding partner of PER. The degradation of TIM is regulated by the light driven interaction between CRY and TIM. Light induced conformational change of CRY enable binding to TIM, which facilitates the proteasomal degradation of TIM through the E3 ubiquitin ligase JETLAG (JET) (J C Dunlap, 1999; Koh et al., 2006; Peschel et al., 2009). Unlike the mammalian CRYs,

the Drosophila CRY is involved in photoreception in addition to the maintenance of circadian rhythmicity (Baik et al. 2019; Allada and Chung 2010; Yu and Hardin 2006; Hardin 2005; Krishnan et al. 2001).

A secondary interconnected feedback loop exists wherein the basic leucine zipper (bZIP) family of transcription factors VRILLE (VRI) and PAR DOMAIN PROTEIN1 (PDP1) act as transcription activator and repressor of CYCLE respectively thus regulating circadian oscillations (Hardin, 2005; Merbitz-Zahradnik & Wolf, 2015).

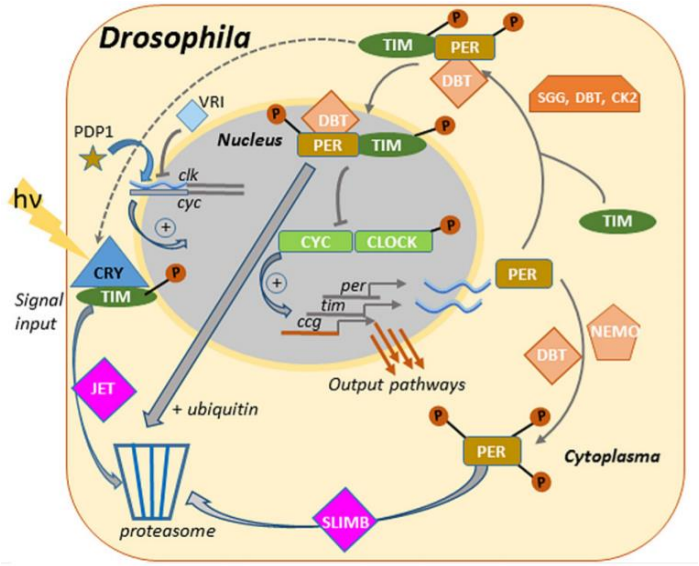

Fig 3: Drosophila circadian clock at the molecular level. CLOCK:CYC complex activates the transcription of PER, CRY, and several CCGs. PER:TIM:DBT complex translocates back into nucleus to repress CLOCK:CYC controlled transcription. Phosphorylation of PER and TIM is carried out SGG, NEMO, CK2 and DBT. E3 ligase SLIMB mediates proteasomal degradation of PER and TIM, allowing the feedback loop to be completed by the reactivation of transcription by CLOCK:CYC. CYC levels are regulated by the secondary feedback loop via VRI and PDP1. Light dependent conformational change of CRY, facilitates its binding to TIM leading to its degradation (Merbitz-Zahradnik & Wolf, 2015)

1.5 Role of chromophores

The DNA repair enzymes (photolyases) and the closely related cryptochromes are described in 1.6. One of their common features is the binding of chromophores. The chromophores and their role is described briefly here and further highlighted for members of the CPF family in the respective sections. Photolyases usually consist of non-covalently bound flavin adenine dinucleotide (FAD) as the catalytic chromophore (Fig 4B). This is located in the C-terminal part of the protein within a structural cavity. FAD in photolyases in its various redox states are

involved in the mechanism of photoreactivation. Five different redox states of FAD exist which can be detected by differences in their absorption spectrum. FAD_{ox} absorbs UV-A and blue-light with characteristic absorption peaks at 368 nm, 425 nm, 450 nm, and 475 nm. Semiquinone anion radical (FAD^{o-}) absorbs blue-light and has two absorption peaks at 370 nm and 405 nm while neutral semiquinone $FADH^{o}$ absorbs blue, green, and red light with peaks at 495 nm, 580 nm, and 620 nm. FAD bound to photolyases in the dark state is usually in the full oxidized state (FAD_{ox}) for e.g. *X. laevis* (6-4) photolyase or semi-reduced state ($FADH^{o}$) for e.g. *E.coli* CPD photolyase. FAD_{ox} / $FADH^{o}$ are converted to the fully reduced $FADH^{-}$ by the process of photoactivation. The fully reduced ($FADH^{-}$) absorbs light of wavelength between 350-500 nm in order to repair UV lesions. By tracking the transition between flavin intermediate redox states in photolyases and cryptochromes, it is possible examine their mechanism of action (Byrdin et al., 2004; Chaves, Pokorny, et al., 2011; Kao, Saxena, et al., 2008; J. Wang et al., 2015).

A second chromophore also known as the antenna chromophore is usually a pterin or a flavin derivative. This is located at the N-terminal region of the protein near the surface. The antenna chromophore is the primary light-harvesting molecule, which transfers the excitation energy to the fully reduced flavin via resonance transfer. Some of the known antenna chromophores are flavin mononucleotide (FMN), flavin adenine dinucleotide (FAD), 8-Hydroxy-7,8-didemethyl-5-deazariboflavin (8-HDF) or methylenetetrahydrofolate (MTHF) (Fig. 4A). The excitation energy from the absorption of light by the primary chromophore is transferred to FAD via resonance transfer.

Both cryptochromes and photolyases undergo photoactivation which leads to flavin reduction by electron transfer. Photolyases accumulate fully reduced flavin while cryptochromes (plant and insect CRYs) accumulate radical flavin which undergoes reoxidation in the dark (Fig. 5). The downstream signaling in the case of cryptochromes is proposed to be mediated either via conformational change or interaction with signaling partner. In addition to light dependent redox changes in flavin states, studies also indicate the possible role of FAD in a light-independent manner. It has been reported from studies in mice that CRY expression and stability is dependent on the cycling of cellular FAD and in turn regulates cellular metabolism (Hirano et al., 2017).

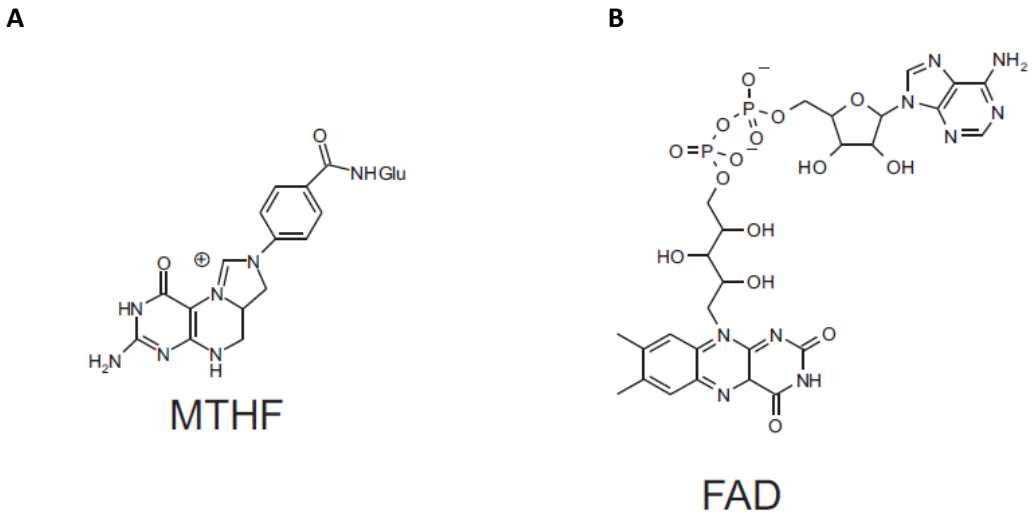

Fig 4 : Chemical structure of chromophores A) Methylenetetrahydrofolate (MTHF) and B) Flavin adenine dinucleotide (FAD).

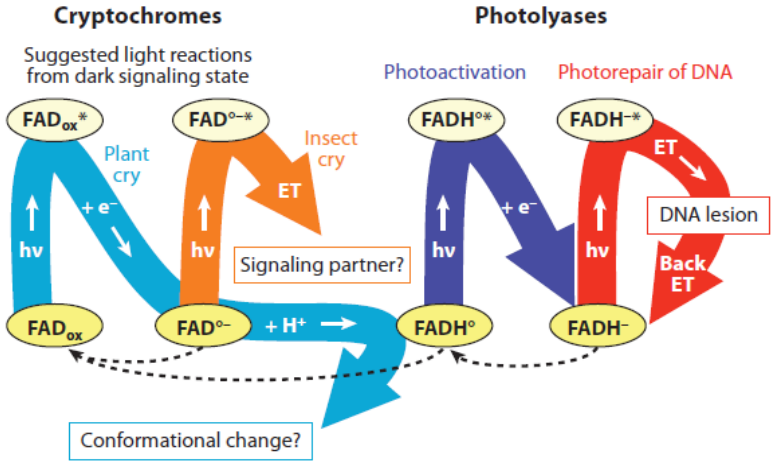

Fig 5 : General scheme of flavin photoreduction in cryptochromes and photolyases. Plant CRYs in vivo consist of oxidized flavin which on photoreduction are converted to the neutral radical $FADH^{o}$. Reoxidation back to the FAD_{ox} state occurs in darkness. Similar to plant CRYs, the insect CRYs show oxidized flavin as the resting state which is transformed to the radical form. Cryptochromes may facilitate signaling either by undergoing conformational changes or direct electron transfer to signaling partners. In vitro purified photolyases contain partially oxidized flavin as $FADH^{o}$ which on photoactivation is converted to the fully reduced state. DNA photolyases utilize fully reduced flavin $FADH^{-}$ to repair DNA lesions. (Chaves, Pokorny, et al., 2011)

1.6 Cryptochrome/Photolyase family (CPF)

In 1949, Kelner and Dulbecco discovered that UV irradiation could inactivate bacteria. It was later possible to reactivate these bacteria on exposure to suitable light (Dulbecco, 1949; Kelner, 1949). The enzyme responsible for this phenomenon was demonstrated by Rupert and named as DNA photolyase (Rupert, 1960). Photolyases are enzymes that catalyze the process of photoreactivation which is the repair of UV-C/UV-B damaged DNA with the help of light with wavelength between 300 to 500 nm (Brettel & Byrdin, 2010). Cryptochromes on the other hand, have lost this DNA repair activity and gained novel signaling functions such as in the entrainment of circadian rhythms. Photolyases and cryptochromes belong to the same family of photoactive proteins present in several organisms. Photolyases are widespread, found in all species of prokaryotes and eukaryotes except mammals, whereas cryptochromes are found only in higher plants, most insect and animal species (Cashmore et al., 1999; Y. F. Li et al., 1993; Mei & Dvornyk, 2015). Phylogenetic analysis of the CPF has led to several classes and subclasses of the superfamily being assigned which however do not converge in all aspects (Fig. 6). For example, the distant relation among the three classes of the CPD photolyases is not supported by the fact that they perform similar functions (Ozturk, 2017). The family is broadly classified into a) (6-4) pyrimidine-pyrimidine adduct photolyases b) cyclobutane pyrimidine dimer (CPD) photolyases and c) cryptochromes (CRY). Photolyases are water-soluble, globular, monomeric protein of 55 to 70 kDa which bind two chromophores with high affinity in the dark. At a sequence level, photolyases and cryptochromes are quite similar sharing a photoactive domain called the photolyase homology region (PHR) (Sancar, 2003). However, cryptochromes have no demonstrable DNA repair activity. Cryptochromes on the other hand possess additional C-terminal tail extending beyond the PHR region responsible for signal transduction and protein-protein interaction. Domain architecture of proteins from the CPF indicates that they usually harbor homologous N-terminal domains comprising the chromophore binding regions and possess variable C-terminal domains (Fig. 7).

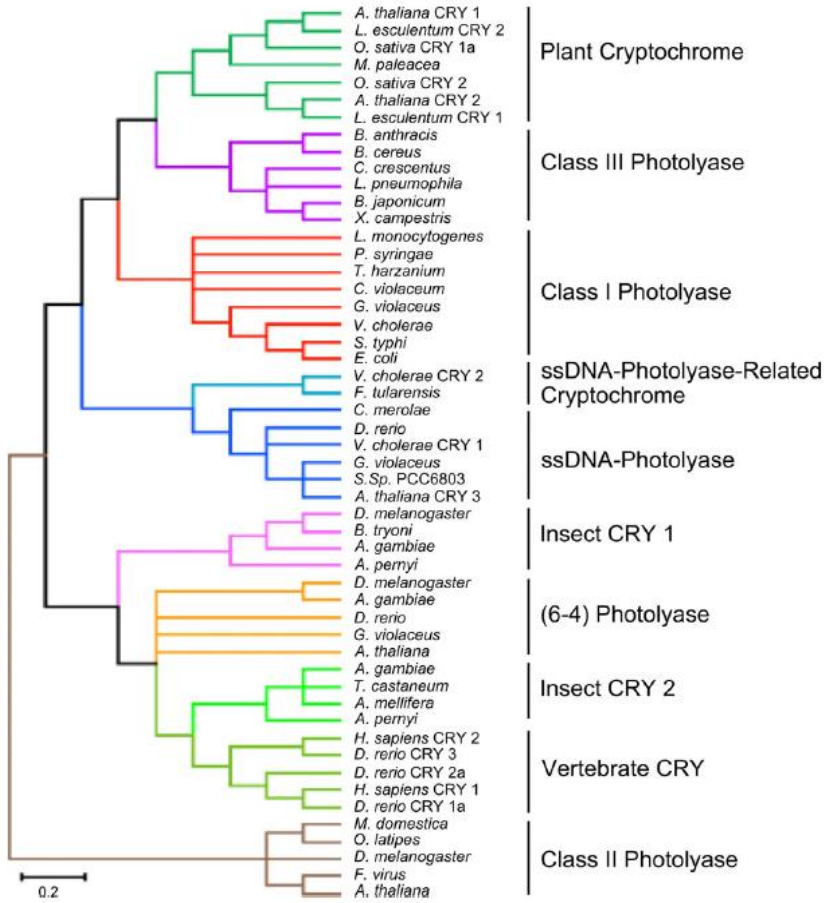

Fig 6: Phylogenetic analysis of the cryptochrome/photolyase family (CPF). Photolyases are classified as (6-4) photolyases and CPD photolyases, which are further subdivided into 3 distinct classes I,II and III based on sequence similarity. The ssDNA-Photolyase also known as CRY-DASH have higher similarity to Insect and Vertebrate CRYs than to bacterial photolyases. Plant CRYs are phylogenetic closer to CPD photolyases and Vertebrate CRYs to the (6-4) photolyases (Kavakli et al., 2017; Öztürk et al., 2008).

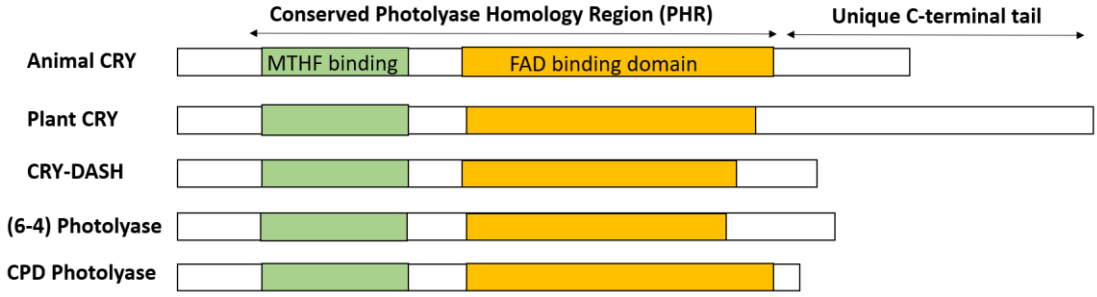

Fig 7: Schematic representation of photolyase/cryptochrome family domain architecture. All members of the superfamily contain N-terminal photolyase homology region comprising the binding sites for chromophores, MTHF (depicted in green) and FAD (depicted in yellow). The C-terminal extensions are of variable length ranging from 40 to

250 amino acids. (Adapted from Chaves, Nijman, et al., 2011; Kavakli et al., 2017; Mei & Dvornyk, 2015)

1.6.1 (6-4) pyrimidine-pyrimidine adduct photolyases

Photons of high energy in the UV-C range (~265 nm) extending beyond 290 nm into the UV-B region cause modifications of the DNA which can inhibit replication and transcription leading to loss of genetic information, mutagenesis, carcinogenesis or cell death (Cadet et al., 2005). (6-4) photolyases were first discovered in 1993 in *Drosophila melanogaster*. Since then they have been studied in several species such as *Arabidopsis thaliana, Xenopus Laevis* and other higher organisms (Jiang et al., 1997; Kim et al., 1996; Y. Kobayashi et al., 2000; T Todo et al., 1993; Uchida et al., 1997).

20-30% of the DNA lesions are (6-4) photoproducts which are formed via an oxetane or azetidine intermediate which are thermodynamically unstable (Marguet & Markovitsi, 2005; Varghese & Wang, 1968; Yamamoto et al., 2017). The most common (6-4) photoproducts induced are T(6-4)C, T(6-4)T (Fig. 8), C(6-4)T and C(6-4)C (T Douki et al., 2000; Thierry Douki & Cadet, 2001). (6-4) photolyases carry FAD as the primary chromophore and photoinduced electron transfer from the flavin leads to the cleavage of the C6-C4’ bond between the 5’ and 3’ yielding two damaged nucleotides. The transfer of the functional group O4’ (or N4’H) from the 5’ to the 3’ base has to be carried out as part of the repair. The excess electron is returned back to the flavin molecule (Kenichi Hitomi et al., 2001; Kim et al., 1994; Yamada et al., 2015).

Crystal structure of *Drosophila melanogaster* (6-4) photolyase bound to 15-mer dsDNA with a T(6-4)T lesion was resolved, depicting the His365, His369 and Y423 as the key residues involved in a hydrogen bond network during the photorepair. Light illumination of the crystal, revealed photoreactivation and repair of the lesion without displacement of vicinity amino acids refuting the thermal oxetane formation mechanism (Maul et al., 2008). Several other repair mechanisms have been proposed over the years (Domratcheva & Schlichting, 2009; Faraji et al., 2016; Faraji & Dreuw, 2012; Harbach et al., 2010; Sadeghian et al., 2010).

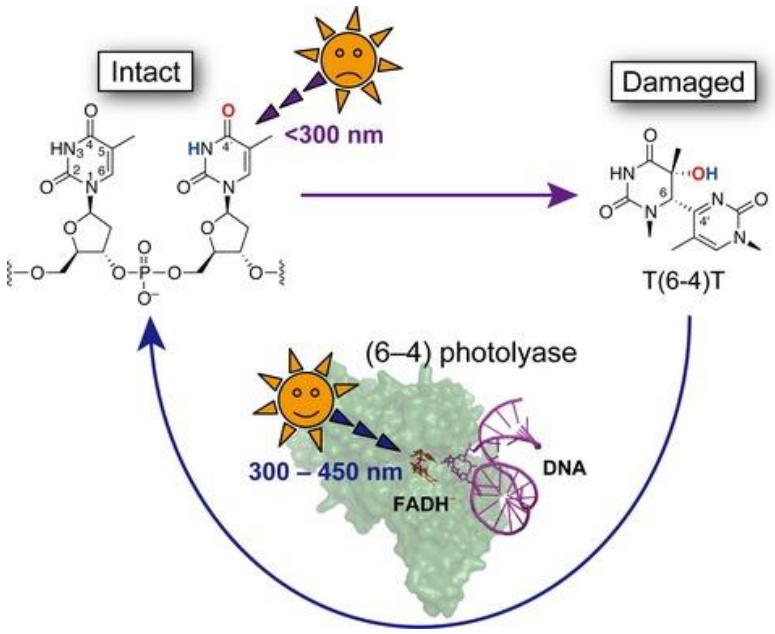

Fig 8: Formation of T(6-4)T photoproduct induced by UV. UV-C damages intact DNA at the TT site leading to a T(6-4)T lesion through a T(ox)T oxetane intermediate. The lesion is rectified by the action of (6-4) DNA photolyases using the FAD in the fully reduced state ($FADH^-$) as the repair-active redox state (Adapted from Yamamoto et al., 2017)

1.6.2 Cyclobutane pyrimidine dimer (CPD) photolyases

About 70-80% of the UV-lesions are *cis,syn*-cyclobutane pyrimidine dimers. CPD photolyases break the cyclobutene ring between C5-C6 to restore the natural bases (Fig. 9). CPD photolyases are subdivided into three classes based on the level of homology in the amino acid sequence (Kanai et al., 1997). Class I comprises of photolyases found in unicellular microbes like *E.coli* and lower eukaryotes such as *Saccharomyces cerevisiae*. Class II includes CPD photolyases from higher eukaryotes like *Arabidopsis thaliana* and *Drosophila melanogaster* and Class III found only in few eubacteria species (K Hitomi et al., 2000; Landry et al., 1997; Y. F. Li et al., 1993; Ozturk, 2017; Sancar & Rupert, 1978; Yasui et al., 1994).

A strong homology exists between CPD photolyases and (6-4) photolyases indicating similarity in the photoreactivation mechanism. CPD lesions are flipped by CPD photolyases and bought in proximity to the FAD active site where fully reduced $FADH^-$, upon light activation, facilitates electron transfer to CPD lesions. Transfer of electron oxidize FAD to the semi-reduced $FADH^o$ radical while the CPD lesion is repaired and the excess electron later returned to restore the catalytic $FADH^-$ (Christine et al., 2002; Kao et al., 2005; Mees et al., 2004).

E.coli Class I CPD photolyase was the first CPF member to be structurally characterized (Park et al., 1995). Since then crystal structures of several Class I/II/III CPD photolyases from *M. mazei*, *A. nidulans*, *T. thermophilus, A.tumefaciens*, *O. sativa* etc. have been elucidated (Kenichi Hitomi et al., 2012; Kiontke et al., 2011; Komori et al., 2001; Scheerer et al., 2015; Tamada et al., 1997). The binding domains of the chromophores, for example MTHF and FAD in *E.coli*, have been characterized which illustrate the specific binding of pyrimidine dimers in active site (Park et al., 1995).

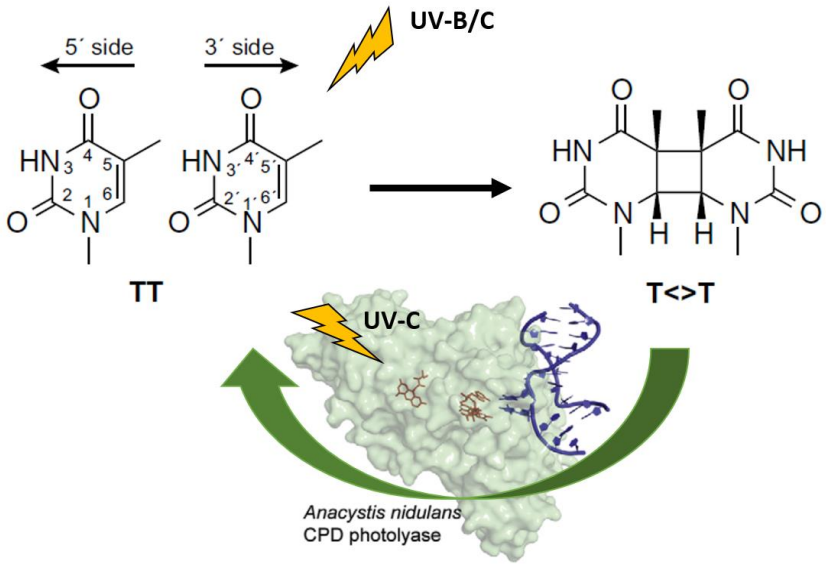

Fig 9: Formation and repair of CPD lesions. UV-B/C induce the formation of T<>T pyrimidine dimers at the TT site. These DNA lesions can be repaired by the CPD photolyases after photoexcitation.(Adapted from Yamamoto et al., 2017)

1.6.3 Cryptochromes

The term cryptochrome is derived from cryptogamic plants to define the cryptic nature of these proteins (Gressel, 1979). Cryptochromes are flavoproteins sensitive to blue light, which were first identified in *Arabidopsis* and later in *Drosophila* and mice (M Ahmad & Cashmore, 1993; K. Kobayashi et al., 1998; T Todo et al., 1996). Although structurally similar to photolyases, these proteins have several distinct functions in addition to their role in resetting the circadian clock such as magnetoreception, plant growth and development, regulation of metabolism and neuronal activity, and other signaling functions (Margaret Ahmad et al., 2007; Fogle et al., 2011, 2015; Müller & Carell, 2009; Ritz et al., 2010; Q. Wang & Lin, 2020; Xu et al., 2008; Yang et al., 2017). Some of these functions are attributed to the divergent C-terminal tail which are intrinsically disordered (Hemsley et al., 2007). The domain architecture

of cryptochromes is similar to that of photolyases; the PHR region binding the primary cofactor FAD and, in some cases, the additional cofactor of 5,10-methenyltetrahydrofolate (MTHF). The PHR region consist of an α/β domain comprising 5 parallel β strands flanked by α helices and a helical domain connected by a loop. The FAD binding cavity is formed by the two lobes of the helical domain. The non-covalent binding of FAD to the protein takes a U-shaped conformation (Chentao Lin & Todo, 2005).

1.6.3.1 CRY-DASH

DASH stands for *Drosophila*, *Arabidopsis*, *Synechocystis* and *Homo*. CRY-DASH are a novel group of cryptochromes closely related to animal CRYs rather than to plant CRYs or CPD photolyases but retain their DNA binding activity. They are considered to be the first cryptochromes found in bacteria. Since then, DASH CRYs have been identified in cyanobacteria, eubacteria, archaea, fungi, plants and vertebrates such as fishes and amphibians (Daiyasu et al., 2004). CRY-DASH bind to DNA in a sequence independent manner. This was seen for *Arabidopsis* and *Synechocystis* CRY-DASH binds to undamaged ss- and dsDNA. However, in both cases, no photolyase activity was detected. On the other hand, Xenopus, and zebrafish CRY-DASHs were capable of binding and repairing CPD lesions. Another study showed that CRY-DASHs are capable of repairing DNA lesions within ssDNA but not dsDNA (Selby & Sancar, 2006). It is also proposed that DNA binding of CRY-DASH may have a signaling function possibly as transcription regulators (Brudler et al., 2003; Kleine et al., 2003). In *O. tauri*, CRY-DASH protein OtCPF2 functions as a transcriptional repressor of mCLOCK:mBMAL in heterologous expression system (Heijde et al., 2010). However, this function was absent in the case of zebrafish and hence the role of CRY-DASH as a universal transcriptional repressor is debatable (Daiyasu et al., 2004). Interestingly, in *K.brevis*, CRY-DASH functions as a blue-light photoreceptor regulating the circadian entrainment of cell cycle (Brunelle et al., 2007). Thus, so far, no universal role of CRY-DASHs have been supported and their mechanism of action, signaling pathways and partners remain to be characterized.

The photoreduction of flavin bound to CRY-DASH in the process of light-mediated DNA-repair is similar to photolyases. Electron transfer within the protein facilities the conversion from FAD_{ox}/ $FADH^{o}$ to the fully reduced $FADH^{-}$ state. The structural features of this family of protein have been largely similar to class I CPD photolyases as seen for *Synechocystis* CRY-DASH and AtCRY3 (Brudler et al., 2003; Huang et al., 2006; Klar et al., 2007).

1.6.3.2 Animal cryptochromes

Animal cryptochromes are divided into two distinct groups, namely, type I cryptochromes such as *Drosophila* cryptochrome which are light sensitive/insect type functioning as photoreceptors and type II cryptochromes such as mammalian cryptochromes which are primarily light irresponsive functioning as negative regulators of transcription . There exist species which possess both types of cryptochromes such as the monarch butterfly and zebrafish (Kyriacou, 2009; C. Liu et al., 2015; Zhu et al., 2005).

1.6.3.2.1 Type I cryptochrome : Drosophila cryptochrome (dCRY)

Drosophila CRY is the primary photoreceptor involved in the photoentrainment of circadian clock by targeting TIMELESS (TIM) protein for degradation as described in section 1.4 (Emery et al., 1998; Ozturk et al., 2011; Peschel et al., 2009; Stanewsky et al., 1998). The structure of dCRY (Fig. 10) is similar to (6-4) photolyase differing mainly in the binding sites of FAD and MTHF and the C-terminal extension. The PHR comprises a N-terminal αβ domain and a C-terminal FAD binding region. The antenna recognition loop (Phe42 – Tyr54) in dCRY differs considerably from photolyases with different structure and amino acid composition. This also explains the lack of bound MTHF in recombinant dCRY preparations from insect cells and the absence of DNA repair activity in dCRY which is facilitated by the MTHF mediated sensitization of $FADH^{o-}$ state in photolyases. The phosphate binding loop (Glu246 – Met266), protrusion loop (Phe288 – Ala306), sulphur loop (Met331 – Cys337) and the C-terminal lid (Ser426 – Pro440) are characteristic of several CPF members. The C-terminal tail (Cys523 – Val542) is positioned as the DNA substrates of photolyases (Czarna et al., 2013; Kenichi Hitomi et al., 2009; Müller & Carell, 2009; Zoltowski et al., 2011). dCRY is a flavoprotein with oxidized flavin (FAD_{ox}) in the dark state which is converted to the anionic semiquinone state (FAD^{o-}) on light activation. FAD^{o-} decays back to FAD_{ox} in the dark (Berndt et al., 2007; Hoang et al., 2008). In the dark state, the C-terminal tail is sequestered within a cavity flanked by the phosphate binding loop, the protrusion loop, and the C-terminal lid. Photoactivation leads to a conformational change in the C-terminal tail of dCRY facilitating the interaction with TIM. Change in the electronic state of FAD in response to light may influence the interaction between the FAD binding pocket and C-terminal tail promoting conformational changes. (Czarna et al., 2013; Hemsley et al., 2007; Rosato et al., 2001; Vaidya et al., 2013; Zoltowski

et al., 2011). The electron transport facilitating the FAD photoreduction requires the conserved Trp triad (Trp342,Trp397 and Trp420) (Hoang et al., 2008; Kao, Tan, et al., 2008).

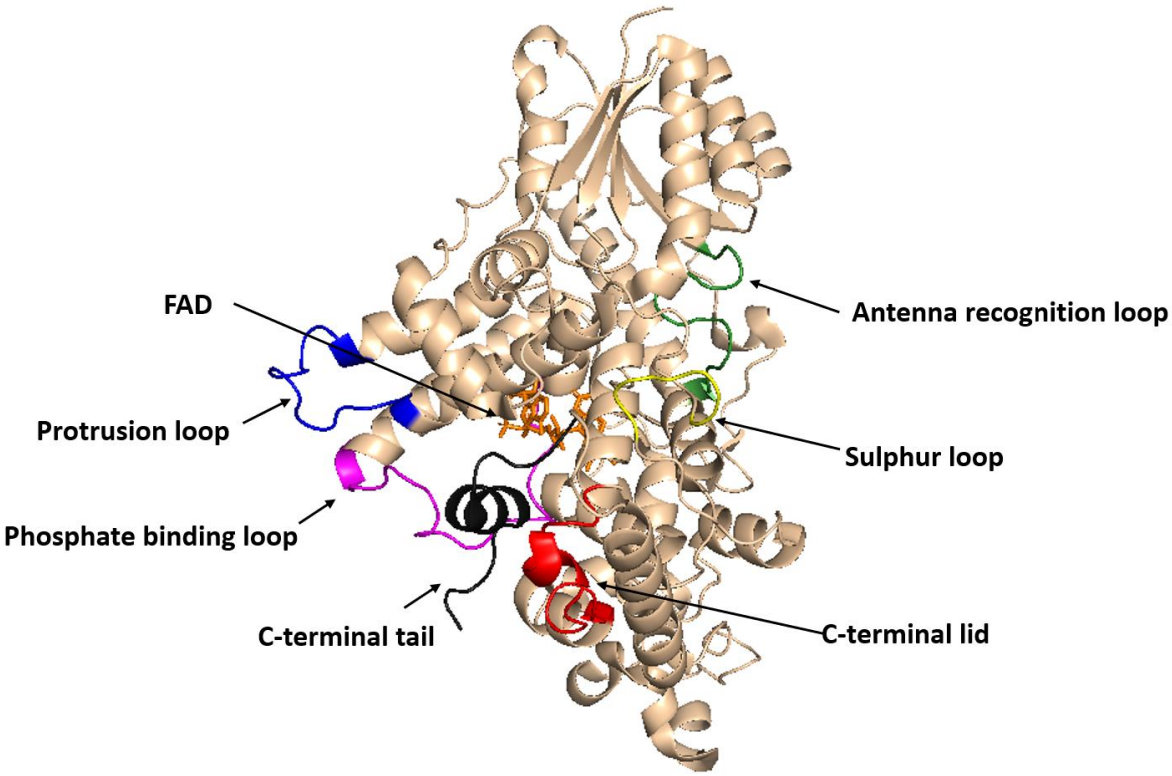

Fig. 10: Crystal structure of dCRY. A single subunit from the crystallographic dCRY dimer is depicted highlighting the antenna recognition loop (Phe42 – Tyr54) in green, phosphate binding loop (Glu246 – Met266) in magenta, protrusion loop (Phe288 – Ala306) in blue, sulphur loop (Met331 – Cys337) in yellow, C-terminal lid (Ser426 – Pro440) in red and the C-terminal tail (Cys523 – Val542) in black. The bound FAD molecule is represented in orange. PDB ID: 4JZY

dCRY was purified as a monomer in solution and the dimer observed in the crystal structure could be an artifact (Berndt et al., 2007; Czarna et al., 2013; Zoltowski et al., 2011). However, plant cryptochromes such as AtCRYs are known to form active homodimers, which is also required for their photoreceptor activity (Sang et al., 2005). Several studies established that cryptochrome dimerization is also essential for its biological functioning (Rosenfeldt et al., 2008). Photo-oligomerization of plant- and several photoactive animal CRYs such as dCRY, DpCRY and zCRY1aa was observed when HEK293 cells were transfected to co-express Flag- and Myc-tagged CRYs (Frøland Steindal & Whitmore, 2019; Q. Liu et al., 2020). The ability to homodimerize as a regulatory mechanism for photoreceptor activity would led to the

prediction that dCRY does so on photoactivation similar to plant CRYs (Q. Liu et al., 2020; Shao et al., 2020; Tamanini et al., 2007).

1.6.3.2.2 Type II cryptochrome : Mammalian cryptochromes

The search for mammalian homologs of photolyases led to the discovery of two genes in humans with 40-45% sequence similarity to *Drosophila* (6-4) photolyase. The proteins encoded by these genes, namely hCRY1 and hCRY2 bound chromophore flavin with low affinity *in vitro* however lacked DNA repair activity and are considered to be vestigial flavoproteins (Kutta et al., 2017). Functionally they were predicted to be similar to plant cryptochromes based on the presence of C-terminal extensions (Cashmore et al., 1999; Chaves, Pokorny, et al., 2011; D. S. Hsu et al., 1996; T Todo et al., 1997; Takeshi Todo, 1999). Mouse CRY1 is highly expressed in the SCN whereas CRY2 occurs in the central and peripheral retina (Miyamoto & Sancar, 1998). The type II cryptochromes are involved in the transcription/translation feedback loop described previously in section 1.3. The role of mammalian CRYs was further studied by *cry1* and *cry2* knockout mice. Single *mCry1* and *mCry2* knockout mice show antagonistic clock-adjusting behavior, while the double knockout mice are behaviorally arrhythmic (Tamanini et al., 2007). Thus, it was established that mammalian cryptochromes are involved in the circadian entrainment of behavior (Okamura et al., 1999; van der Horst et al., 1999; Vitaterna et al., 1999). Mammalian CRYs do not function as photoreceptors as was seen in retinally degenerate mice capable of showing circadian responses to light (R. G. Foster et al., 1991). In addition, the double knockout of *cry* genes in mice ($cry1^{-/-}/cry2^{-/-}$) did not impair the photic induction of *mPer1* and *mPer2*, further confirming that light-induced phase shifting is not dependent on mammalian CRYs (Okamura et al., 1999).

Interestingly, it was seen that chimeric proteins comprising *Arabidopsis* photolyase domain with the C-terminal domain of mCRY1 were capable of repressing the transcription of CLOCK:BMAL. The transcriptional repression by CRY proteins in mammals requires the C-terminal extension however only this extension is not sufficient. Together these results suggest that the transcriptional inhibition requires an interaction between the core domains and the C-terminal extension, however, the core domains of photolyases and cryptochromes can be functionally similar and interchangeable in certain cases (Chaves et al., 2006; van der Schalie et al., 2007).

Despite the identical folding of PHR among the CPF, functional homodimerization of mCRY proteins has so far not been detected unlike their plant homologs. One hypothesis is that the necessity of homo- or heterodimerization is connected to photoreceptor activity and hence absent in mammalian cryptochromes (Tamanini et al., 2007).

1.6.3.3 Plant cryptochromes

The cryptochrome from Arabidopsis AtCRY1 was the first cryptochrome discovered and to date the AtCRYs are most studied plant CRYs (M Ahmad & Cashmore, 1993). AtCRY1 mediates the inhibition of hypocotyl elongation in Arabidopsis in blue light (Koornneef et al., 1980). A second photoreceptor homolog AtCRY2 was identified in Arabidopsis and studied for its role in plant growth, photomorphogenesis and flowering time (El-Din El-Assal et al., 2003; Guo et al., 1998; Q.-H. Li & Yang, 2007; C Lin et al., 1998). AtCRY1 and AtCRY2 share considerable sequence homology however poorly conserved C-terminal domain. AtCRY1 has 190 amino acid C-terminal extension while AtCRY2 C-terminal tail consists of 120 amino acids. Both cryptochromes also differ in their sensitivity to blue-light; AtCRY1 being stable in bright light whereas AtCRY2 undergoes degradation on light activation (Cashmore et al., 1999; C Lin et al., 1998; X. Yu et al., 2007). AtCRYs contain both FAD and MTHF and lack the DNA repair activity (C Lin et al., 1995; Chentao Lin, 2000; Malhotra et al., 1995). In the dark state, AtCRY1 and AtCRY2 contain the fully oxidized FAD (FAD_{ox}) which on absorption of blue light leads to the formation of neutral FAD radical (Bouly et al., 2007; Giovani et al., 2003). This process is coupled to the conformational change of the C-terminal domain in AtCRY1, which is necessary for signal transduction (Cashmore, 2006; Cashmore et al., 1999; Giovani et al., 2003; C Lin et al., 1995; Partch et al., 2005; J. Wang et al., 2015). The FAD in plant CRYs is reoxidized in the dark to the fully oxidized FAD, leading to the deactivation of the protein (Banerjee et al., 2007; Bouly et al., 2007).

The plant circadian clock is regulated by both AtCRY1 and AtCRY2 which act redundantly by shortening the period length in response to light. Double mutants of *AtCry1* and *AtCry2* have longer period lengths in blue light. Plant CRYs are however not essential components of the circadian clock oscillator as rhythmicity is not lost in *AtCry* null mutants (Devlin & Kay, 2000; Somers et al., 1998; Yanovsky et al., 2000). AtCRY1 and AtCRY2 mediate gene expression of 10-20% of genes in response to blue-light (Chentao Lin & Todo, 2005). This process is mediated by cryptochrome interaction with chromatin in a sequence independent manner or

with other proteins regulating the stability and cellular localization of transcription regulators (Cutler et al., 2000; Valverde et al., 2004; H. Wang et al., 2001; W. Yu & Hardin, 2006).

1.7 Role of moonlight

Moonlight is reflected sunlight, albeit with relatively low intensity. Moonlight intensity varies largely on the lunar phase, however, even at the full moon phase, the light intensity is several orders of magnitude lower than that of sunlight (Kyba et al., 2017). Measurements of full moon light intensity off the coast of an island in Italy, Ischia have calculated an intensity of $1.79*10^{10}$ photons/cm^2/s at 5 m depth of water (natural habitat of *Platynereis*). Although the role of sunlight in the entrainment of endogenous circadian clocks is well established, recent data also suggest that moonlight is capable to affect nocturnal activity in several species (Chaput et al., 2016; Kronfeld-Schor et al., 2013; Lillywhite & Brischoux, 2012; Starr et al., 2012; Upham, 2008). In humans, studies indicate the impact of moonlight and artificial nocturnal light on sleep synchronization, onset of sleep and its duration (preprint Casiraghi et al., 2020). Several studies have shown that light from the moon has an impact on the sexual maturation and reproduction especially in marine organisms such as echinoderms, corals, oyster, fishes, turtles etc. (Bézy et al., 2020; Fukushiro et al., 2011; Hauenschild, 1960; Korringa, 1947; Payton & Tran, 2019; Raible et al., 2017; Sitter, 1932; Tessmar-Raible et al., 2011). Corals of the Great Barrier Reef exhibit annual synchronized spawning in late spring. The phenomenon is crucial as close to 30 diverse species coordinate the release of their gametes to increase their likelihood of fertilization and cross-fertilization. The gametes are viable for only a few hours and several environmental cues such a water temperature, solar irradiance, wind, tides, salinity levels, timing of sunset and the lunar phase control the precise timing. The moonlight cues the exact night and the spawning occurs several days after a full moon (Babcock et al., 1986; Boch et al., 2015; T. Foster et al., 2018; Kaniewska et al., 2015; Keith et al., 2016; Shlesinger & Loya, 2019; van Woesik et al., 2006). The cryptochrome CRY2 of the coral *Acropora millepora* has been reported to function as a moonlight receptor entraining the circalunar clock to the lunar phase. It was seen that the expression levels of *cry2* were significantly higher at midnight under full moon conditions versus new moon phase (Levy et al., 2007). In some species such as reef fish *Siganus guttatus*, moonlight was also seen to impact the circadian clock by increased expression of *per2* gene (Sugama et al., 2008).

1.8 Circadian and circalunar clock of the marine worm *Platynereis dumerilli*

Platynereis dumerilli belongs to the phylum Annelida (segmented worms), class Polychaeta. These worms are quite distinct from nematodes such as *Caenorhabditis elegans*. First studies with *Platynereis dumerilli* were published by zoologist Carl Hauenschild in 1951. Progeny of worms collected in the Gulf of Napoli, off the coast of Ischia are routinely used in laboratories. The marine bristle worm *Platynereis dumerilli* possess a circadian and a circalunar clock

The circadian clock of the worm controls the locomotion of the worm, with the activity being maximum during the night. Orthologs of core circadian clock genes, *pdp1*, *clock*, *Bmal1*, *vrille*, *period*, *timeless*, *timeout* and 2 *crys (l-cry and tr-cry)* were identified. It was seen that the clock genes exhibit circadian oscillations on the mRNA level which was also maintained in constant dark conditions. This provides evidence for the existence of an entrainable endogenous circadian clock within the worm as seen in mammals and *Drosophila*.

The moonlight functions as zeitgeber, entraining the circalunar clock, synchronizing the sexual maturity and reproduction of the worm to the lunar phase. Thus, being affected by the moon, *Platynereis* is referred to as a Moonstruck worm. In its natural habitat, 14 days after the full moon, around the new moon, four hours after sunset, the worms swim to the surface of the water and synchronously release their gametes. The average lifespan of worm is around 7 months and after reproduction, the worms burst and die. The circalunar clock governs the sexual maturation of the worms, which is minimum during the full moon (FM) phase and maximum shortly after new moon (NM) (Fig. 11A). It was also seen that worms grown in constant light conditions (day and night) or without nocturnal light cues, lost the synchrony of maturation indicating that moonlight alone was sufficient for the entertainment of the circalunar reproduction (Fig. 11B). The periodicity of reproduction is also maintained under free-running conditions (conditions with only sunlight cues but not moonlight cues) establishing the existence of endogenous circalunar clock. The circalunar clock of the worm is harbored in its forebrain, which persists even after the circadian clock is disrupted. On the other hand, the circalunar clock impacts the period and power of the circadian locomotive activity (Fig. 11C). Both clocks converge at the transcript level, wherein the transcript levels of circadian genes *period*, *clock*, *pdp1* and *timeless* are impacted by the lunar phase (Zantke et al., 2013).

Platynereis has 6 members of the CPF family, one each of CPD photolyase, (6-4) photolyase, CRY-DASH and 3 CRYs. Three different cryptochromes identified in the marine worm are namely L-CRY, TR-CRY and P-CRY (Fig. 12). L-CRY is orthologous to the light receptive dCRY. TR-CRY is similar to mammalian type repressor cryptochromes and P-CRY closely resembling *Arabidopsis* CRY1 (Oliveri et al., 2014a)

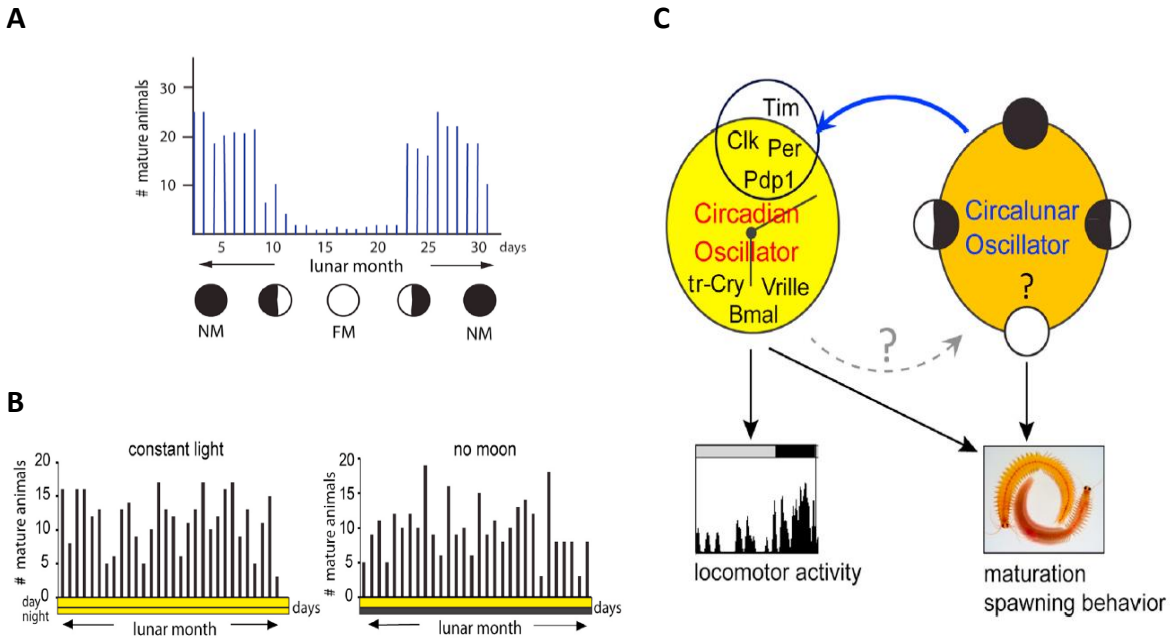

Fig 11: A) Synchronized spawning behavior of Platynereis in nature, wherein the worms exhibit maximal sexual maturity shortly after the new phase (NM). B) Loss or reproductive synchrony when worms are grown in the absence of proper nocturnal light cues, i.e., either in constant light or no moonlight conditions. C) Circadian/Circalunar model of Platynereis indicating the impact of circalunar clock (blue line) on the circadian clock causing increased transcription of clock genes period, clock, pdp1 and timeless (Zantke et al., 2013).

This is not surprising considering that several marine species have different types of cryptochromes such as the coral *Acropora millepora* with CRY1 (mammalian type) and CRY2 (similar to (6-4) photolyases) (Levy et al., 2007). L-cry transcript levels do not follow circadian rhythmicity. Studies in S2 cells showed that L-CRY is degraded after 6h of light exposure because of proteasome mediated degradation. This confirmed the function of L-CRY as a possible light receptor as seen in *Drosophila* and monarch butterfly. *Tr-cry* RNA levels were high during the day or during late evening/night. Together with levels of *period,* which were in antiphase with bmal1/clock expression, it was an indication that TR-CRY functions as a repressor in the transcription-translation feedback loop as seen in mammals. This was later

confirmed using luciferase reporter gene assays by the cotransfection of *tr-cry* leading to reduced activation of *bmal1* and *clock* in S2 cells (Zantke et al., 2013).

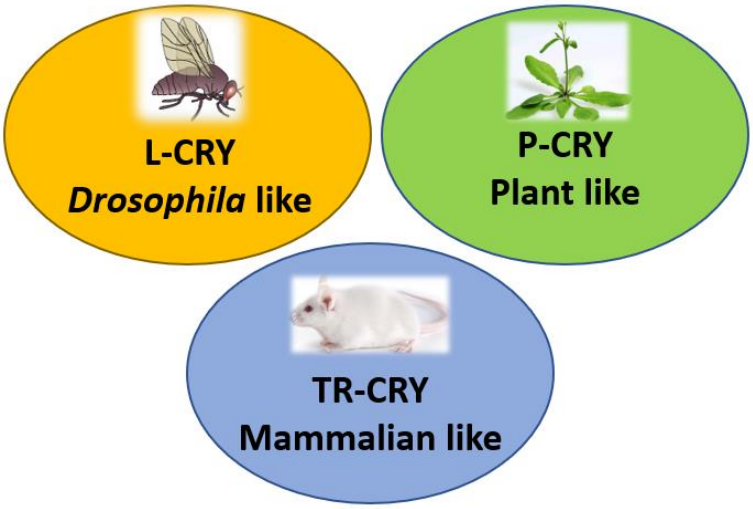

Fig 12: Cryptochromes of the marine worm. Platynereis dumerilli possess 3 kinds of cryptochromes: one each similar to Drosophila type (L-CRY), Plant like (P-CRY) and the mammalian repressor type (TR-CRY). These cryptochromes have postulated circadian and/or circalunar functions (Oliveri et al., 2014a; Zantke et al., 2013).

In an attempt to discern the downstream pathways where L-CRY might be involved, mass spectrometry was applied. Three putative interactors of L-CRY in the dark were identified during the course of this work and the following sections highlight the known information regarding these interactors namely, YTHDF, G3BP and PITHD1.

1.8 YTH domain-containing family protein (YTHDF)

The YTH domain-containing family of proteins is characterized by a RNA-binding domain (named YTH) (Fig. 13A, 13B). These proteins are present both in the nucleus and cytoplasm of the cells and have increased affinity to methylated RNA as compared to non-methylated (Roundtree & He, 2016; Shi et al., 2017; Tanabe et al., 2016; X. Wang et al., 2014). YT521-B/YTHDC1 from *Rattus norvegicus* was the first characterized YTH domain containing protein (Imai et al., 1998). YTHDC1 lacked previously known RNA-binding domains but was seen to influence alternative splicing. It was later shown that the YTH domain of YTHDC1 is a RNA-binding domain with degenerate sequence-specificity (Z. Zhang et al., 2010). A recent study showed that human YTHDC1 (localized in the nucleus) binds stronger to ssDNA containing N^6-methyladenosine (m^6A) in contrast to YTHDF1/2 which bind strongly to m^6A ssRNA instead

(Woodcock et al., 2020). The YTH domain is composed of 6 β strands flanked by 3 α helices. The domain has a positively charged surface facilitating the binding of the RNA in an extended conformation (Fig. 13C). Structural studies with YT512B revealed that the YTH fold adopts similar conformation in the free and RNA bound states (Theler et al., 2014).

One of the prominent post-transcriptional modification in eukaryotes is the N^6-methyladenosine (m^6A), which are dynamic and reversible (Jia et al., 2013; Perry et al., 1975; Wei et al., 1975). Studies show that inhibition of transmethylation by inhibiting methyltransferase *Mettl3* affects the circadian period of both the SCN as well as peripheral cell types. The circadian rhythm in peripheral liver cells is modulated by the mRNA export caused by m^6A modifications especially in the context of mammalian metabolism (Fustin et al., 2013; C.-Y. Wang et al., 2015). The other way around is also examined wherein metabolic signals affect methylation in turn impacting the circadian clock (X. Li et al., 2016).

A

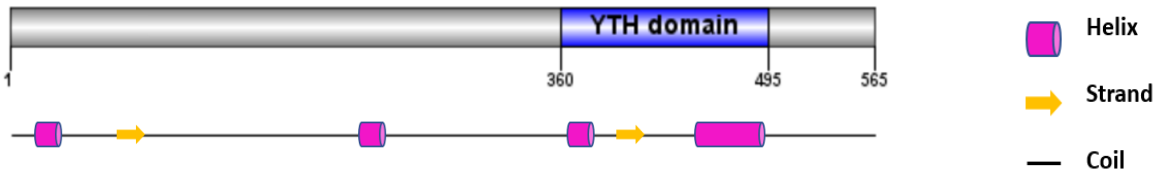

B

```
YTHDF  [P. dumerilli]  311 -GMPNN-ANNNSAP--L---VSTPS-HPVLERLKSANQYNPKDFNLNPKGVRFFIIKSYS
YTHDF1 [H.sapiens]     350 -SPGNV---QPNS---A---PSVES-HPVLEKLKAAHSYNPKEFEWNLKSGRVFIIKSYS
YTHDF2 [H.sapiens]     370 -GVGQS---QAGSG--S---TPSEP-HPVLEKLRSINNYNPKDFDWNLKHGRVFIIKSYS
YTHDF3 [H.sapiens]     376 -GLGVV---PVSAS--P---SSVEV-HPVLEKLKAINNYNPKDFDWNLKNGRVFIIKSYS
YTHDC1 [H.sapiens]     305 RGISPIVFDRSGSSASESYAGSEKKHEKLSSSVRAVRKDQTSKLKYVLQDARFFLIKSNN
                             .         .:              . : . ::: .. : ..:.   :  *.*:*** .

YTHDF  [P. dumerilli]  363 EDDIHRSIKYSIWCSTEHGNKRLDAAYRERERKGPVYLLFSVNGSGHFCGMAQMMSPLDY
YTHDF1 [H.sapiens]     399 EDDIHRSIKYSIWCSTEHGNKRLDSAFRCMSSKGPVYLLFSVNGSGHFCGVAEMKSPVDY
YTHDF2 [H.sapiens]     420 EDDIHRSIKYNIWCSTEHGNKRLDAAYRSMNGKGPVYLLFSVNGSGHFCGVAEMKSAVDY
YTHDF3 [H.sapiens]     426 EDDIHRSIKYSIWCSTEHGNKRLDAAYRSLNGKGPLYLLFSVNGSGHFCGVAEMKSVVDY
YTHDC1 [H.sapiens]     365 HENVSLAKAKGVWSTLPVNEKKLNLAFRSAR---SVILIFSVRESGKFQGFARLSSESHH
                             .:::  :   .:*.:   .:*:*: *:*       : *:***. **:* *.*.: *  .:

YTHDF  [P. dumerilli]  423 SATSSVWA------QDKWKGQMEVKWIYVKDVPNSQLRHIRLENNENKPVTNSRDTQEVP
YTHDF1 [H.sapiens]     459 GTSAGVWS------QDKWKGKFDVQWIFVKDVPNNQLRHIRLENNDNKPVTNSRDTQEVP
YTHDF2 [H.sapiens]     480 NTCAGVWS------QDKWKGRFDVRWIFVKDVPNSQLRHIRLENNENKPVTNSRDTQEVP
YTHDF3 [H.sapiens]     486 NAYAGVWS------QDKWKGKFEVKWIFVKDVPNNQLRHIRLENNDNKPVTNSRDTQEVP
YTHDC1 [H.sapiens]     422 GGSPIHWVLPAGMSAKMLGGVFKIDWICRRELPFTKSAHLTNPWNEHKPVKIGRDGQEIE
                             .    *        .   * :.: **  :::* .:  *:    *:.***. .** **:

YTHDF  [P. dumerilli]  477 PEKGKQVLKIIHNYRHTTSIFDDFVHYEKRQEEEAAKIQAMTQDGSGDQGPPPRDSGKSS
YTHDF1 [H.sapiens]     513 LEKAKQVLKIISSYKHTTSIFDDFAHYEKRQEEEEVVRKERQSRNKQ-------------
YTHDF2 [H.sapiens]     534 LEKAKQVLKIIASYKHTTSIFDDFSHYEKRQEEEESVKKERQGRGK--------------
YTHDF3 [H.sapiens]     540 LEKAKQVLKIIATFKHTTSIFDDFAHYEKRQEEEEAMRRERNRNKQ--------------
YTHDC1 [H.sapiens]     482 LECGTQLCLLFPPDES-IDLYQVIHKMR---HK-RRMHSQPRSRGRPSRREPVRDVGRRR
                             * ..*:  ::    .   .::: : : .   .:
```

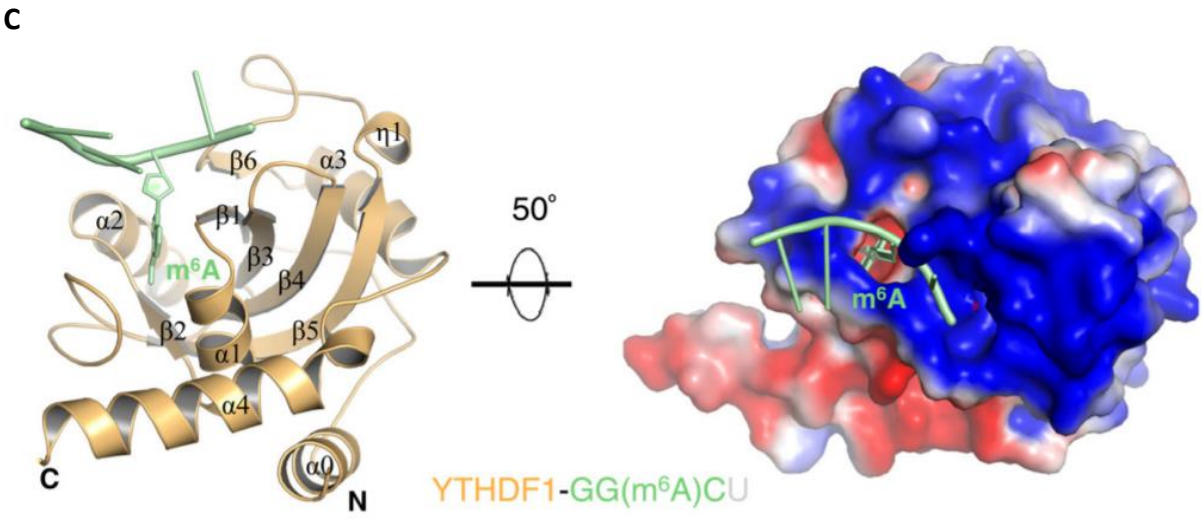

Fig 13: A) Schematic using Illustrator of biological sequences *(IBS) depicting the predicted secondary structure features of YTHDF based on the PSIPRED result shown in Appendix Fig. A1* (Buchan & Jones, 2019; W. Liu et al., 2015; McGuffin et al., 2000). *B) Sequence alignment of YTH domains of Platynereis YTHDF, human YTHDF1/2/3 and human YTHDC1. The alignment was generated with Clustal Omega and color coded based on degree of amino acid similarity depicted with high (*), medium (:) and low (.). C) Crystal structure of the YTH domain from human YTHDF1 (PDB 4RCJ) with a 5-mer GG(m6A)CU RNA (depicted in green). The positively charged electrostatic surface of the YTH domain is depicted on the right, which facilitates the binding of RNA.*

The proteins YTHDF1/2 act as m^{6}A-specific binding proteins post transcription (Dominissini et al., 2012; Theler et al., 2014). YTHDF2 is a mediator of lipid metabolism by regulating peroxisome proliferator-activator α (*PPaRα*) mRNA stability. Deletion of Bmal1 in mice liver cells, lead to significant increase of m^{6}A mRNA methylation of *PPaRα* (regulator of hepatic metabolism). On the other hand, YTHDF2 with its m^{6}A reader activity, binds to *PPaRα* methylated mRNA, leading to its degradation (Zhong et al., 2018).

YTHDF2 is necessary for early embryonic development in zebrafish (Zhao et al., 2017). In mice, YTHDF2 is present in the cytoplasm of both germ and somatic cells during the process of folliculogenesis and oocyte maturation. It was discovered that the expression of YTHDF2 is required for fertility in female mice but not in males. It functions by selectively degrading mRNA transcripts during meiotic maturation controlling the maternal transcript dosage (Ivanova et al., 2017). Another study showed the nuclear localization of YTHDF2 in cellular heat-shock response stabilizing stress-induced transcripts (Zhou et al., 2015). The potential

functions of YTHDF2 in response to physiological and environmental changes is yet to be explored.

1.9 Ras GTPase-activating protein-binding protein 1/2 (G3BP)

Ras is a family of GTPases, which activate serine/threonine kinases and initiate downstream signaling. Ras-GTPase activating protein (RasGAP) enhance the GTPase activity of Ras. The possible role of RasGAPs in the circadian clock was indicated by a study in the fungus *Phycomyces blakesleeanus* wherein a gene encoding a Ras GTPase activating protein when mutated affects the transcription of light regulated genes. A homolog found in *Neurospora crassa* is involved in circadian output affecting downstream signaling and photobiology (Polaino et al., 2017).

Ras-GTPase-activating protein-binding proteins (G3BPs/Rasputin in *Drosophila*) are proteins binding to the RasGAPs with the conserved SRC Homology 3 Domain (SH3) (Annibaldi et al., 2011; Gyurkó et al., 2015; Parker et al., 1996). SH3 domain containing proteins are involved in cell proliferation and differentiation, morphogenesis, cytoskeletal substrate, and p21 Ras signal transduction. (Khosravi-Far & Der, 1994; Musacchio et al., 1992; Wu et al., 1991). The domain is implied to be pivotal in protein-protein interactions necessary for function or subcellular localization.

The primary role of G3BPs is the regulation of mRNA stability and translation. They are part of several cellular functions and involved in diseases ranging from cancer, neurological diseases, and viral infections. The family of G3BPs comprise a N-terminal nuclear transport factor (NTF2) like domain, an RNA recognition motif (RRM), acidic and proline rich regions and the arginine-glycine rich box (RGG box) (Fig. 14A, 14B) (Burd & Dreyfuss, 1994; Nagai et al., 1995; Suyama et al., 2000). The NTF2 like domain is structurally and functionally like NTF2 protein regulating nuclear transport through nuclear pores. Studies have suggested the importance of this domain in the translocation of G3BPs to the nucleus or to their targeting to the nuclear envelope (Barnes et al., 2002; Prigent et al., 2000). The central proline-rich motif (PxxP) is vital for protein interactions facilitating the binding of aromatic acids to the SH3 domain (Kay et al., 2000). The RRM usually have $\beta_1\alpha_1\beta_2\beta_3\alpha_2\beta_4$ topology, composed of 4 beta strands packed against 2 alpha helices which interact with 2-8 nucleotide long RNA sequences. The RRM interaction with other protein has been shown to either inhibit or promote RNA binding (Cléry et al., 2008). Methylation of arginine residues of the RGG box

influences RNA binding, protein-RNA interactions and nuclear export (Bikkavilli & Malbon, 2011; Nichols et al., 2000; Shen et al., 1998; Tsai et al., 2016). Several crystal structures of the NTF2 domain of the G3BPs have been resolved till date (Fig. 14C) (Kristensen, 2015). However, no full-length structure or the structure of the RRM domain is determined.

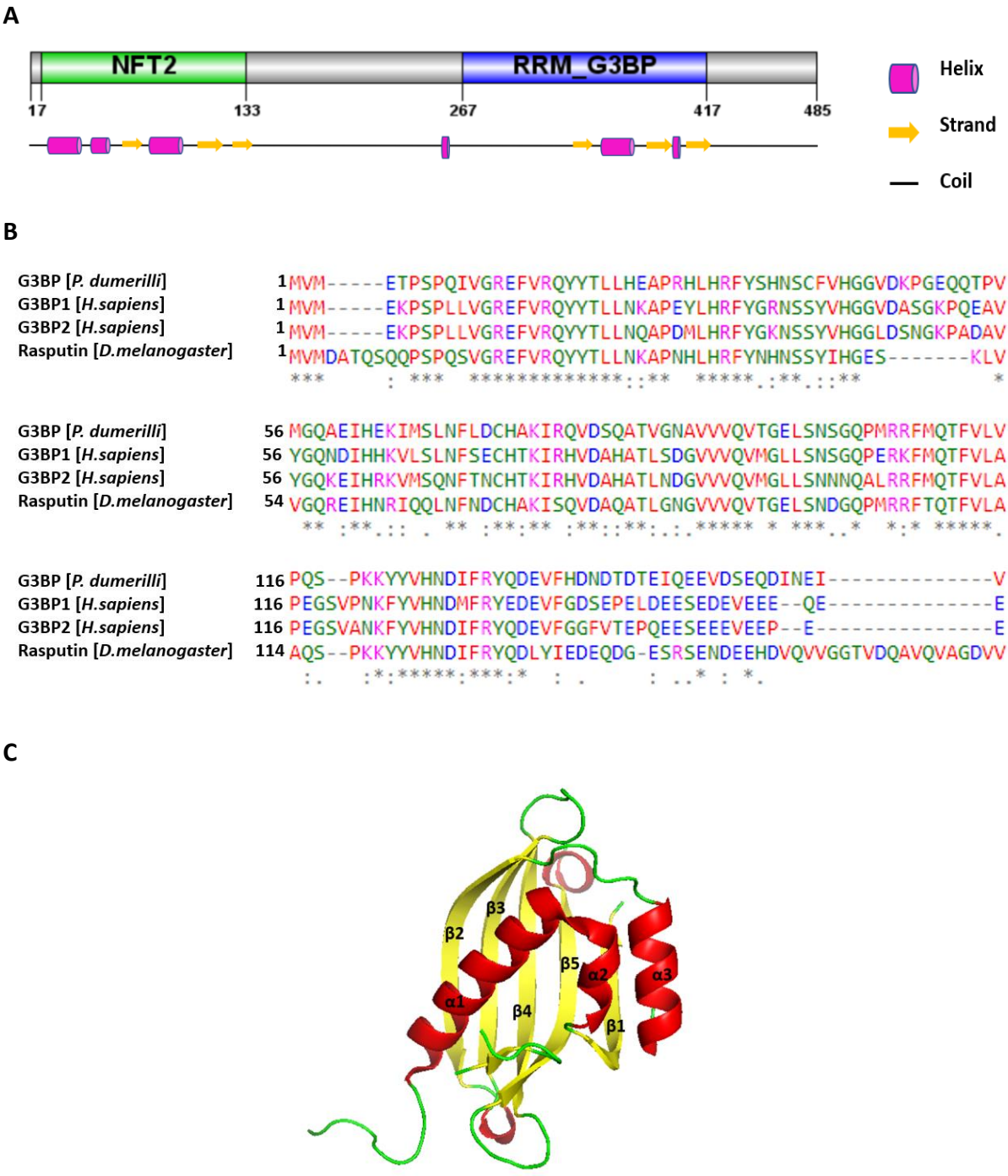

Fig 14: A) Schematic using IBS depicting the predicted secondary structure features of G3BP based on the PSIPRED result shown in Appendix Fig. A2 (Buchan & Jones, 2019; W. Liu et al.,

2015; McGuffin et al., 2000). NTF2: Nuclear transport factor 2 domain ; RRM-G3BP: RNA recognition motif in ras-GTPase-activating protein-binding protein G3BP1/2 and similar proteins. B) Sequence alignment of the NTF2 domains of Platynereis G3BP, Human G3BP2 Human G3BP1 and Drosophila Rasputin. The alignment was generated with Clustal Omega and color coded based on degree of amino acid similarity depicted with high (*), medium (:) and low (.). C) Crystal structure of NTF2 domain of human G3BP2 (PDB 5DRV) depicting the beta sheets in yellow (β1-β5) and alpha helices in red (α1-α3) and coils in green (Kristensen, 2015).

G3BP1's role in cancer metastasis in breast cancer, lung and oesophageal cancer has long been known. However, the precise mechanism is still a puzzle considering its involvement in several pathways such as stress granule formation, p53 regulation, Smad and Src/FAK signaling (H Zhang et al., 2013; Hao Zhang et al., 2015).

Studies with HeLa cells identified G3BP2 as an interactor of IκBα via its NTF2 and acidic domains. G3BP3 in the cytoplasm binds to the cytoplasmic retention sequence (CRS) of IκBα, retaining it in the cytoplasm and inhibiting the nuclear translocation of NF-κB. Thus, G3BP2 can indirectly regulate NF-κB signal transduction and impact several cellular functions (Prigent et al., 2000). G3BP2 is a known breast cancer initiating protein. So far only one target of G3BP2 has been identified, namely the squamous cell carcinoma antigen recognized by T cells 3 (SART3) mRNA. An anticancer drug , C108, inhibits G3BP2 activity by binding to its RRM, in turn leading to degradation of SART3 mRNA (Gupta et al., 2017).

1.10 PITH domain-containing protein 1-like (PITHD1)

PITH stands for proteasome-interacting thioredoxin domain. Proteins with this domain (Fig. 15A, 15B) are usually present in the cytoplasm with indications of its role in cell apoptosis and cancer (Miranda-Vizuete & Spyrou, 2000). PITH domain containing proteins are known to be associated with 26S proteasome. In humans, thioredoxin Txnl1 is involved in the targeting of proteins for degradation (Andersen et al., 2009). No crystal structure of this domain is available however a NMR structure of a closely related *Arabidopsis thaliana* protein (At3g04780.1) exists (Fig. 15C) (Song, 2005).

A

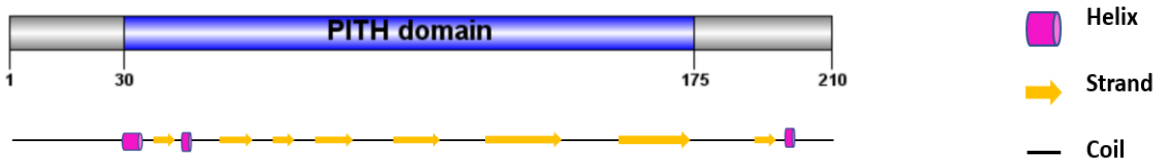

B

```
                    10        20        30        40        50        60        70        80
                    ....*....|....*....|....*....|....*....|....*....|....*....|....*....|....*....|
PITHD1 [P. dumerilli]  30 LYLKIDLERLQCLNEETEGSGKTVF-KPWDKRLDTTDFVESDADEELLFNIPFTGNVKLKGVIVIGG--EDDYHPSKMKL 106
CCD:pfam06201           1 LYSYIDLDKVECLNEDDPGSGKNVFeKPWDERLDESKYLESDADEQLLIHIPFTGPVKLHSILIRTGtsDGDSAPKTIKL 80

                    90       100       110       120       130       140       150
                    ....*....|....*....|....*....|....*....|....*....|....*....|....*....|.
PITHD1 [P. dumerilli] 107 YKNRPNM-TFDDTGAEADQEFDLNP-DHAGVLEYATKIARFNSVNHLSLFFPTN-FGADSTKIYYIGLKGD 174
CCD:pfam06201          81 FINRPDIlDFDDAEDTPTQEIELSEeDDEGVVEYPLRFVKFQNVSSLTLFFEDNnGGGETTRIDYIGLKGE 151
```

C

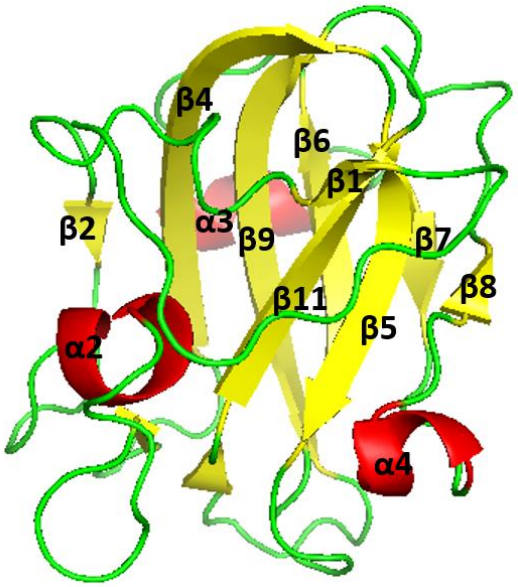

Fig 15: A) Schematic using IBS depicting the predicted secondary structure features of PITHD1 based on the PSIPRED result shown in Appendix Fig. A3 (Buchan & Jones, 2019; W. Liu et al., 2015; McGuffin et al., 2000). B) Sequence alignment of the PITH domain of PITHD1 from Platynereis with the conserved PITH domain of the protein family 06201 based on conserved domain analysis. (CDD: (S. Lu et al., 2020) C) Solution structure of At3g04780.1 (PDB 1XOY) depicting the beta sheets in yellow (β1-β11) and alpha helices in red (α1-α4) and coils in green (Song, 2005)

PITHD1 in humans was identified as a differential expression gene (Xue et al., 2011; Yi et al., 2010). It was later found to be an activator of internal ribosomal site enhancing translation in the context of megakaryocyte differentiation (B. Lu et al., 2015). Apart from these indications not much is known about this family of proteins.

1.11 Aim of the thesis

As not much was known about the *Platynereis* cryptochromes except for their phylogenetic similarity to the well-studied *Drosophila*, plant, and mammalian cryptochromes, the focus of the project was towards their characterization. Studies in S2 cells have established the role of TR-CRY in the circadian clock of *Platynereis* as a transcriptional repressor (Zantke et al., 2013). The proposed circadian/circalunar model does not include the role of cryptochromes L-CRY and P-CRY as their functions are still unclear. The initial aim was to establish the expression and purification of these cryptochromes to facilitate their characterization via spectroscopy and biophysical techniques. We wanted to determine if these cryptochromes could function as photoreceptors as is true for their respective homologs in *Drosophila and Arabidopsis. In-vivo* studies indicated the potential of L-CRY as a receptor for moonlight. Spectroscopic studies with light sources mimicking sunlight and moonlight were necessary to validate this observation.

In addition, the chromophores binding the cryptochromes were determined with the help of reverse-phase HPLC, UV/VIS and fluorescence spectroscopy to better elucidate the photocycle mechanism. Variability in the oligomeric state of purified L-CRY in solution as compared to dCRY, led to confirmational studies with MALS and SAXS. This was also the preliminary indication that L-CRY may possibly have a different conformation/oligomeric structure which was pursued with the help of crystallization and electron microscopy.

Another potential aim of the thesis was to provide functional insights into the role of these novel cryptochromes. With the help of pull-down approach coupled to mass spectrometry identification of novel interactors for L-CRY and P-CRY was attempted. The direct interaction between selected L-CRY candidates was later tested by establishing their recombinant expression, purification, and analytical SEC/pull-down studies. As the mechanisms involved in coexistence and regulation of circadian and circalunar clocks within an organism are largely unexplored, the correlation between *in-vitro* and *in-vivo* studies to provide functional insights continues to be the most intriguing aim of the work.

2 Materials and Methods

2.1 Materials

2.1.1 Agar plates

Agar plates with single antibiotic (Ampicillin/Kanamycin) selection for *E.coli* strains were supplied by the Media lab (IMB). Bacmid selection plates were prepared by dissolving LB-Agar supplied by Media Lab (IMB) and adding antibiotics Gentamicin, Kanamycin, Tetracycline, IPTG (40 µg/ml) and X-Gal (100 µg/ml dissolved in DMSO).

2.1.2 Antibiotics

Table 1: Antibiotics used in bacterial media

Antibiotic	Stock solution	Working concentration
Ampicillin	100 mg/ml	100 µg/ml
Chloramphenicol	34 mg/ml	34 µg/ml
Gentamicin	7 mg/ml	7 µg/ml
Kanamycin	30 mg/ml	30 µg/ml
Tetracycline	10 mg/ml	10 µg/ml

2.1.3 Cell lines and strains

Table 2: List of insect cell lines

Cell line	Organism	Purpose
Sf9	Ovarian cells from *Spodoptera frugiperda*	Transfection of Bacmid DNA, Virus generation and amplification. In this study, extensively used for protein expression as well.
High Five	Ovarian cells of *Trichoplusia ni*	High level expression of recombinant proteins.

Table 3: List of bacterial strains

E.coli strain	Genotype	Purpose
BL21 DE3	F^- *ompT gal dcm lon hsdS*$_B$(*rB*$^-$*mB*$^-$) λ(DE3 [*lacI lacUV5-T7p07 ind1 sam7 nin5*]) [*malB*$^+$]K-12(λ^S)	Recombinant protein expression
BL21(DE3)-RIL	*argU* (AGA, AGG), *ileY* (AUA), *leuW* (CUA), Camr	Recombinant protein expression

ccdB survival	F⁻*mcr*A Δ(*mrr-hsd*RMS-*mcr*BC) Φ80*lac*ZΔM15 Δ*lac*X74 *rec*A1 *ara*Δ139 Δ(*ara-leu*)7697 *gal*U *gal*K *rps*L (Str^R) *end*A1 *nup*G tonA::P_{trc}-ccdA	Amplification of pCoofy plasmids
DH5α	F⁻ *endA1 glnV44 thi-1 recA1 relA1 gyrA96 deoR nupG purB20* ϕ80d*lacZ*ΔM15 Δ(*lacZYA-argF*)U169, hsdR17(*rK⁻mK⁺*), λ⁻	Cloning and plasmid amplification
DH10Bac	F⁻, *mcrA*, Δ(*mrr-hsd*RMS-*mcr*BC), ϕ80*lac*ZΔM15, ΔlacX74, *deo*R, *rec*A1, *end*A1, *ara*D139, Δ(*ara*, *leu*)7697, *gal*U, *gal*Kλ-*rps*L, *nup*G/bMON14272/pMON7124	Recombinant Bacmid generation
Rosetta DE3	F⁻, *ompT*, *hsdSB*(rB⁻, mB⁻), *gal*, *dcm (DE3)*/ pRARE (C*am^R)*	Recombinant protein expression
Rosetta2 DE3	F⁻ *ompT hsdS*B (rB⁻ mB⁻) *gal dcm* (DE3) pRARE2 (Cam^R)	Recombinant protein expression

2.1.4 Chemicals and Consumables

Chemicals and consumables were purchased from Applichem (Darmstadt, Germany), Carl Roth GmbH & Co. KG (Karlsruhe, Germany), Corning GmbH (Karlsruhe, Germany), GE Healthcare (München, Germany), Hampton Research (Aliso Viejo, USA), Jena Bioscience GmbH (Jena, Germany), Qiagen (Hilden, Germany), Macherey-Nagel (Düren, Germany), Merck KGaA (Darmstadt, Germany), Molecular Dimensions (Suffolk, UK), Roche Diagnostics (Mannheim, Germany), Sartorius Stedim Biotech (Göttingen, Germany), Sarstedt AG (Nümbrecht, Germany), SERVA Electrophoresis (Heidelberg, Germany), Sigma Aldrich (München, Germany) and VWR International.

2.1.5 Chromatography columns and resin

Table 4: Columns used for different chromatographic methods

Method	**Column/Resin**
Affinity chromatography	HisTrap 1mL, 5 mL (GE Healthcare) GSTrap 1mL (GE Healthcare) MBPTrap 1mL (GE Healthcare) Glutathione-Sepharose 4 fast flow Ni NTA Resin
Ion-exchange chromatography	HiTrap QHP 5 mL

	HiTrap SPHP 5 mL
Size Exclusion chromatography	HiLoad Superdex200 16/60 pg Superdex200 10/300 GL Superdex200 Increase 10/300 GL

2.1.6 Equipments

Table 5: Technical equipment

Instrument	Type/Specification	Supplier
Äkta purification system	NGC Quest Äkta prime plus Äkta micro	Bio-Rad GE Healthcare GE Healthcare
Biological safety cabinet	Baker SterilGARD III Advance SG403 & SG603	GMI
CD spectrophotometer	JASCO J-815	JASCO Deutschland
Cell sorter	AriaII-SORP Cellsorter	Becton Dickinson
Centrifuges	Avanti J-HC, Rotor JS-5.0 Optima XE-100 (Ultracentrifuge) 5810 R RC 6+, Rotors F10S 6x500Y, F21S 8x50Y	Beckmann-Coulter Beckmann-Coulter Eppendorf Sorvall
Columns for affinity chromatography (batch)	Econo-Column 0.7 x 20 cm	Bio-Rad
Crystallization incubator	RUMED	Rubarth Apparate
Crystallization robot	Mosquito	TTP Labtech Ltd
Cryo electron microscope	Titan Krios G2	Thermo Fisher Scientific
Field Emission Electron microscope	JEM-2200 FS	JEOL
Gel electrophoresis		Bio-Rad
Gel Imaging system		Bio-Rad XRS+
Incubator shaker	Multitron Forma Steri-Cult 3308	Infors HT Thermo Fisher Scientific
Microfluidizer	LM10	Microfluidics Corp
Microscope	DM750	Leica
PCR cycler	TP professional standard Primus	Biometra MWG Biotech
Plate reader	Spark 20M	Tecan
Sonifier	Ultrasonics Sonifier 450	Branson

Spectrophotometer	Nanodrop 200c	Thermo Scientific
Spectrometer	LI 180	LI-COR

2.1.7 Enzymes

Table 6: List of enzymes

Enzyme	Source
Dpn-1	New England Biolabs (Ipswich, USA)
GST 3C Protease	Protein Production core facility (IMB)
HF DNA-Polymerase	Protein Production core facility (IMB)
His 3C Protease	Protein Production core facility (IMB)
RecA	New England Biolabs (Ipswich, USA)
Sm nuclease	Protein Production core facility (IMB)
Taq DNA-Polymerase	Protein Production core facility (IMB)

2.1.8 Gel electrophoresis

2.1.8.1 Agarose gel electrophoresis

Table 7: Components of agarose gel electrophoresis

Solution	Ingredients
1-2% agarose gel	1-2% (w/v) agarose 1x TAE buffer (40 mM Tris-HCl pH 7.6, 20 mM acetic acid, 1 mM Ethylenediaminetetraacetic acid (EDTA))
DNA gel stain	SYBR Safe DNA gel stain (Invitrogen, USA)
DNA marker	1 kb DNA Ladder (GeneCraft, Germany) 100 bp DNA Ladder (Invitrogen, USA)
6x DNA sample buffer	TrackIT (Thermo Fisher Scientific)

2.1.8.2 SDS gel electrophoresis

Table 8: Components of SDS gel electrophoresis

Solution	Ingredients
10% Separating gel solution	10% (v/v) Rotiphorese gel 30 (37.5:1), 300 mM BisTris pH 6.5, 0.06% (w/v) APS, 0.05% (v/v) TEMED
4% Stacking gel solution	4% (v/v) Rotiphorese gel 30 (37,5:1), 250 mM Tris-HCl pH 6.5, 0.08% (w/v) APS, 0.1% (v/v) TEMED
Running Buffer (1x MOPS)	50 mM MOPS, 50 mM Tris, 1 mM EDTA pH 7.5, 0.1% SDS (w/v), 5mM Sodium bisulfate ($NaHSO_4$) , final pH 7.7
Staining solution	0.1% Coomassie-Blue R250, 30 % Methanol, 10% Acetic acid
Destaining solution	30% Methanol, 10% Acetic acid
Protein size standards	Roti-Mark Standard 10-150 (Carl Roth, Germany)

	Roti-Mark Standard Protein Marker (Carl Roth, Germany)

2.1.8.3 Native gel electrophoresis

Table 9: Components of Native gel electrophoresis

Solution	Ingredients
Native gel 4-15%	Rotiphorese gel 30 (37.5:1), 300 mM BisTris pH 6.5, 0.06% (w/v) APS, 0.05% (v/v) TEMED
Sample buffer 4x	50 mM BisTris pH 7.2, 50 mM NaCl, 10% glycerol, 0.001% Ponceau
Running Buffer	50 mM BisTris, 50 mM Tricine pH 6.8
Running conditions	1h pre-run, followed by 2h running time at 150V at 4°C
Staining solution	0.1% Coomassie-Blue R250, 30 % Methanol, 10% Acetic acid
Protein size standards	NativMark Unstained Protein Standard (Life Technologies)

2.1.9 Media

Table 10: List of media and additives

Medium	Composition
LB Luria	10 g/L tryptone, 5g/L yeast extract, 10 g/L NaCl, pH 7.0
SF900II Serum Free Media	Commercially bought from Gibco (Life Technologies)
SOC Media	0.4% glucose, 2% (w/v) tryptone, 0.5% (w/v) yeast extract, 10 mM NaCl, 2.5 mM KCl, 10 mM $MgSO_4$, pH 7.2
TB Media	12 g/L tryptone, 24 g/L yeast extract, 4g/L glycerol, 0.017M KH_2PO_4, 0.072M K_2HPO_4

2.1.10 Oligonucleotides

Table 11: List of primers

	Name	Sequence 5‘ – 3‘
1	FP_lcry_K30	AAGTTCTGTTCCAGGGGCCCAAGGAGCACGTCTCCCTACAT
2	RP1_lcry	CCCCAGAACATCAGGTTAATGGCGTCAATACTTGATACAGGGTAGATC
3	RP2_lcry	CCCCAGAACATCAGGTTAATGGCGTCATCAGGCAGCCAGCAGAATTC
4	pCoofy6_pcry_FP200	GTGTTCCAGCAGCAGACCGGTGGAATGTCTAAGCCCGTGATCTTC
5	pCoofy6_pcry_RP697	CCCCAGAACATCAGGTTAATGGCGTCAGACCAGGTCGTTTCCGGT

6	pCoofy6_pcry_RP778	CCCCAGAACATCAGGTTAATGGCGTCACGAGAACACAATGCTGGACAT
7	pCoofy6_pcry_FP1	GTGTTCCAGCAGCAGACCGGTGGAATGGCTGGAAGGGGAATC
8	FP_YTHDF2_opt	AAGTTCTGTTCCAGGGGCCCATGTCGGCCTCGGTGGATCAGCGC
9	RP_YTHDF2_opt	CCCCAGAACATCAGGTTAATGGCGTCATTAATTGCTCTGGTTCGAGG
10	FP_G3BP2_opt	AAGTTCTGTTCCAGGGGCCCATGGTCATGGAGACCCCATCGCCG
11	RP_G3BP2_opt	CCCCAGAACATCAGGTTAATGGCGTCATTAGCGGCGCGGCACGCCGA
12	FP_PITHD1	AAGTTCTGTTCCAGGGGCCCATGTCGGGCCACGGAC
13	RP_PITHD1	CCCCAGAACATCAGGTTAATGGCGTCATTGTATTTGATGGTTCACTT

2.1.11 Vectors and Expression constructs

Table 12: List of vectors for *E.coli* and insect cell expression system

Vector	**Fusion Tag**	**Antibiotic Resistance**	**Cleavage site**	**Host**
pCoofy1	N-term 6xHis	Kanamycin	3C	*E.coli*
pCoofy3	N-term 6xHis-GST	Kanamycin	3C	*E.coli*
pCoofy4	N-term 6xHis-MBP	Kanamycin	3C	*E.coli*
pCoofy6	N-term 6xHis-SUMO	Kanamycin	Sumo	*E.coli*
pCoofy27	N-term 6xHis	Ampicillin	3C	Insect cells
pCoofy28	N-term 6xHis-GST	Ampicillin	3C	Insect cells
pCoofy29	N-term 6xHis-MBP	Ampicillin	3C	Insect cells
pFastBac HT B	N-term 6xHis	Ampicillin	TEV	Insect cells

Table 13: List of expression constructs

Expression construct	**Vector**	**Tag**	**Host**
L-CRY FL	pCoofy27	N-term 6xHis	Insect cells
L-CRY FL	pCoofy28	N-term 6xHis-GST	*E.coli*
L-CRY 30-567	pCoofy27	N-term 6xHis	Insect cells
L-CRY 30-553	pCoofy27	N-term 6xHis	Insect cells
P-CRY FL	pCoofy27	N-term 6xHis	Insect cells
P-CRY 1-697	pCoofy27	N-term 6xHis	Insect cells
P-CRY 200-697	pCoofy27	N-term 6xHis	Insect cells
P-CRY 200-778	pCoofy27	N-term 6xHis	Insect cells
P-CRY FL	pCoofy28	N-term 6xHis-GST	Insect cells

P-CRY 1-697	pCoofy28	N-term 6xHis-GST	Insect cells
P-CRY 200-697	pCoofy28	N-term 6xHis-GST	Insect cells
P-CRY 200-778	pCoofy28	N-term 6xHis-GST	Insect cells
L-CRY FL	pCoofy1	N-term 6xHis	*E.coli*
L-CRY FL	pCoofy3	N-term 6xHis-GST	*E.coli*
P-CRY FL OPT	pCoofy27	N-term 6xHis	Insect cells
P-CRY 200-697 OPT	pCoofy27	N-term 6xHis	Insect cells
P-CRY 200-778 OPT	pCoofy27	N-term 6xHis	Insect cells
P-CRY 1-697 OPT	pCoofy27	N-term 6xHis	Insect cells
P-CRY FL OPT	pCoofy28	N-term 6xHis-GST	Insect cells
P-CRY 200-697 OPT	pCoofy28	N-term 6xHis-GST	Insect cells
P-CRY 200-778 OPT	pCoofy28	N-term 6xHis-GST	Insect cells
P-CRY 1-697 OPT	pCoofy28	N-term 6xHis-GST	Insect cells
P-CRY 200-697 OPT	pCoofy1	N-term 6xHis	*E.coli*
P-CRY 200-697 OPT	pCoofy3	N-term 6xHis-GST	*E.coli*
P-CRY 200-697 OPT	pCoofy6	N-term 6xHis-SUMO	*E.coli*
P-CRY 200-778 OPT	pCoofy6	N-term 6xHis-SUMO	*E.coli*
PITHD1 FL	pCoofy1	N-term 6xHis	*E.coli*
YTHDF2 FL	pCoofy27	N-term 6xHis	Insect cells
YTHDF2 FL	pCoofy28	N-term 6xHis-GST	Insect cells
YTHDF2 FL	pCoofy4	N-term 6xHis-MBP	*E.coli*
G3BP2 FL	pCoofy27	N-term 6xHis	Insect cells
G3BP2 FL	pCoofy28	N-term 6xHis-GST	Insect cells
dCRY	pFastBac HT B	N-term 6xHis	Insect cells

2.2 Molecular Biology Methods

2.2.1 Agarose gel electrophoresis

Gel electrophoresis is used for the analysis and separation of macromolecules like DNA/RNA based on their size and charge. Negatively charged nuclei acid molecules move through the agarose matrix towards the positively charged anode during electrophoresis. This migration is affected by the size of the gel pores, size and conformation of the nuclei acids, the voltage applied as well as the buffer composition. In general, shorter nucleic acid fragments travel faster than longer ones. The percentage of agarose used depends on the size of the biomolecules required to be analyzed. The components required for agarose gel electrophoresis are as described in 2.1.8.1. The required amount of agarose is dissolved in 1x TAE buffer, 2 µl of SYBR safe DNA stain added per 30 ml and loaded into a gel casting tray with a comb. 5 µl of sample is mixed with 1 µl of 6xDNA loading dye and loaded into each well. 2.5

µl of appropriate marker is used per gel. The electrophoresis is carried out at 120V for 20 min. The gels were analyzed using an UV trans-illuminator and recorded with the Bio-Rad XRS+ gel imaging system.

2.2.2 Amplification and isolation of plasmids

100 ng of the plasmid for amplification was transformed into *E.coli* DH5α and a single colony picked for culturing in LB Luria with appropriate antibiotic. The cultures are grown at 37 ^{o}C overnight at 200 RPM. The cells are collected by centrifugation at 4000 RPM for 10 min at 4 ^{o}C. The plasmids were isolated for sequencing or transformation using Spin Miniprep (Qiagen, Venlo, Netherlands) or Nucleospin plasmid (Macherey & Nagel, Düren, Germamy).

2.2.3 Competent cell Preparation

Chemically competent cells were prepared using the Calcium chloride method. Cells from the glycerol stock were streaked out on LB agar plate and a single colony picked for pre-culture inoculation. 100 ml of LB culture was set with density OD_{600} = 0.1 and grown at 37 ^{o}C until OD_{600} of 0.6. The culture was shortly kept on ice and later centrifuged at 4000 RPM for 10 min at 4 ^{o}C. The supernatant was discarded, the cells resuspended and washed in 8 ml of chilled $CaCl_2$ Buffer I. A second round of centrifugation was carried out at the same settings as before, the pelleted cells were resuspended in 10 ml of cold $CaCl_2$ Buffer II and incubated for 15 min on ice. Aliquots 50 µl were prepared and snap frozen with liquid N_2. The chemical competent cells were stored at -80 ^{o}C.

Table 14: Composition of buffers used for competent cell preparation

Buffer	Composition
$CaCl_2$ Buffer I	100 mM $CaCl_2$
$CaCl_2$ Buffer II	100 mM $CaCl_2$, 10 % glycerol

2.2.4 Polymerase Chain Reaction (PCR)

PCR employs the ability of a thermostable DNA polymerase to synthesize new DNA strands complementary to the template strand, withstanding high temperatures. This requires thermal cycling, repeated cycles of heating and cooling for DNA denaturation and enzymatic polymerization. Both methods of cloning described in 2.2.5 require linearization of vector and amplification of insert DNA. The vector and insert should have overlapping ends to assist *in vitro* homologous recombination.

2.2.4.1 Vector linearization

The pCoofy vectors used for both SLIC and Gibson cloning were linearized using the forward and reverse linearization primers LP1 (binds to 3C protease site) and LP2 (C-terminal ccdB sequence). The ccdB gene is deleted in the process of linearization and later replaced by the insert DNA sequence. 50 µl PCR reactions were set up according to the scheme in Table 15. The PCR cycle is described in Table 16. The success of the PCR was analyzed by running 5 µl of the product an agarose gel electrophoresis of appropriate agarose percentage. The remaining PCR product was cleaned up using Nucleospin PCR cleanup kit by Macherey & Nagel (Düren, Germany).

Table 15: Pipetting scheme for vector linearization

Component	Stock concentration	Volume
Forward primer	10 µM	2 µl
Reverse primer	10 µM	2 µl
Phusion HF buffer	5x	10 µl
dNTP	2 mM	5 µl
Template		50-150 ng
HF DNA Polymerase		0.5 µl
ddH_20	Made up to final volume of 50 µl	

Table 16: PCR cycle scheme for vector linearization

Step	Temperature	Temperature and Time	Cycles
1.	Initialization	98 °C, 2 min	
2.	Denaturation	98 °C, 30 sec	30x
3.	Annealing	55 °C, 30 sec	
4.	Elongation	72 °C, 30 sec per kb	
5.	Final Extension	72 °C, 5 min	
6.	Hold	4 °C, ∞	

2.2.4.2 Insert Amplification

The appropriate primers from Table 11 were used for insert amplification so as to obtain complementary overhangs to the linearized vectors obtained from. The PCR scheme and cycle are as described in Table 17 and 18. Further steps followed were as stated above in vector linearization.

Table 17: Pipetting scheme for insert amplification

Component	Stock concentration	Volume
Forward primer	10 µM	2 µl
Reverse primer	10 µM	2 µl
Phusion HF buffer	5x	10 µl
dNTP	2 mM	5 µl
Template		50-150 ng
HF DNA Polymerase		0.5 µl
ddH_20	Made up to final volume of 50 µl	

Table 18: PCR cycle scheme for insert amplification

Step	Temperature	Temperature and Time	Cycles
1.	Initialization	98 ^oC, 2 min	
2.	Denaturation	98 ^oC, 30 sec	30x
3.	Annealing	50 ^oC, 30 sec	
4.	Elongation	72 ^oC, 30 sec per kb	
5.	Final Extension	72 ^oC, 5 min	
6.	Hold	4 ^oC, ∞	

2.2.5 Cloning

The plasmids with full length *Platynereis dumerilli* genes were kindly provided by collaborator lab. Cloning for all constructs into pCoofy vectors was carried out using either sequence ligation-independent cloning (SLIC) or Gibson cloning (Gibson et al., 2009; Scholz et al., 2013). Both methods utilize the principle of *in vitro* homologous recombination which facilitates annealing of single-stranded DNA overhangs. The vectors and inserts were digested with Dpn1 when necessary to remove methylated template DNA followed by PCR cleanup. Following this either one of the below cloning methods was employed.

2.2.5.1 Sequence Ligation-Independent Cloning (SLIC)

For SLIC reaction, vector to insert ratios varying from 1:1, 1:2, 1:3, 1:5 or 1:7 was tested depending on the size of the insert DNA. The reaction scheme was set up according to Table 19. The insert amount was calculated using NEBiocalculator. Vector/Insert only controls were included when necessary. The reaction was incubated for 1-2 h at 37 ^oC or left overnight at room temperature. The ligation mixture was later transformed into competent DH5α or NEB Turbo cells and plated on agar plates with appropriate antibiotics. The colonies obtained were

tested using colony PCR as described in 2.2.6 and amplified as per 2.2.2. The plasmid was isolated using commercial kit (Qiagen, Hilden, Germany) and sent for sequencing as mentioned in 2.2.7.

Table 19: Pipetting scheme for SLIC reaction

Component	Stock concentration	Amount
Linearized vector		100 ng
Amplified insert		Acc to vector: insert ratio
RecA buffer	10 x	1 µl
RecA	2 µg/ml	1 µl
ddH_20	Made up to final volume of 10 µl	

2.2.5.2 Gibson Cloning

Gibson assembly is a versatile method to anneal DNA fragments independent of restriction enzymes. It is a three-enzyme reaction wherein the T5 exonuclease digests one strand of double stranded DNA from the 5' end leading to a 3' overhang. The reaction is terminated at 50 ^{o}C. The DNA fragments are designed with significant overlap (at least 20-25 bp, >=60 ^{o}C), so as to anneal well at 50 ^{o}C. The Phusion DNA Polymerase fills in the gaps generated by the T5 exonuclease. Finally, Taq ligase ligates the nicks in the fragments. The ligated recombinant DNA is transformed into *E.coli*.

The linearized vector and amplified inserts obtained from 2.2.4 are used to setup 20 µl reaction mix. 10 µl of 2xGibson master mix (supplied by Protein Production core facility, IMB) along with appropriate volume of vector and insert according to desired vector: insert ratio is setup on ice in 0.2 ml PCR tube. The reaction is incubated at 50 ^{o}C for 30 - 60 min. The entire reaction volume is used for transformation into 100 µl NEB Turbo or DH5α cells as per protocol in 2.2.8.

2.2.6 Colony PCR

Colony PCR is used to detect positive bacterial colonies that have taken up the desired plasmid. DNA sequence of interest is amplified using appropriate primers and the PCR products are run on agarose gel to verify the length of the desired insert as described in 2.2.1. The pipetting scheme and PCR cycle is mentioned below in Table 20 and 21. The colonies with correct insert size are picked for amplification as described in 2.2.2 and sent for DNA sequencing as per 2.2.7.

Table 20: Pipetting scheme for Colony PCR

Component	Stock concentration	Amount
ThermoPol Buffer	10x	5 µl
dNTP	10 mM	1 µl
Forward primer	10 µM	1 µl
Reverse primer	10 µM	1 µl
Taq DNA Polymerase		1 µl
Template		Single colony
ddH20	Made upto final volume of 50 µl	

Table 21: PCR cycle scheme for Colony PCR

Step	Temperature	Temperature and Time	Cycles
1.	Initialization	95 ^{o}C , 5 min	
2.	Denaturation	95 ^{o}C , 30 sec	30x
3.	Annealing	Melting temperature of primer pair, 30 sec	
4.	Elongation	68 ^{o}C, 1 min per kb	
5.	Final Extension	68 ^{o}C, 5 min	
6.	Hold	4 ^{o}C , ∞	

2.2.7 DNA Sequencing

5-7µl of 80-100 ng/µl of plasmid DNA was mixed with 1µl of 10 µM primer in PCR tubes and sent for sequencing. Sequencing of DNA was done by GATC (Eurofins Genomics, Germany) or StarSEQ GmbH (Mainz, Germany).

2.2.8 Transformation

Bacterial transformation is the process by which cells take up and incorporate exogenous genetic material. The cell membrane of chemically competent cells is made permeable to DNA uptake by heat shock. Antibiotic selection marker present on the exogenous plasmid DNA helps in the positive selection of transformed cells. Chemically competent cells as prepared in 2.2.3 were thawed on ice and 100 ng of plasmid of interest was added. The cells are incubated for 20 min on ice followed by heat shock at 42 ^{o}C for 1 min and later kept on ice for 5 min. 800 - 1000 µl of SOC/LB media was added and the cells grown at 37 ^{o}C, 200 RPM.

2.2.9 Insect cell culture

2.2.9.1 Insect cell stock generation

Frozen cells were thawed at room temperature and added into 20 ml of SF900II SFM media without antibiotics to start a fresh suspension culture. The cells were allowed to adapt for a couple of days by growing them at 27 ^{o}C, 90 RPM before splitting and generating a working culture. A cell density of 0.5 x10^{6} – 0.8x10^{6} was routinely maintained for stocks of 30 mL Cells were diluted 1:1 with trypan blue solution (0.4% trypan blue in PBS buffer) and counted using a hemocytometer to distinguish between live and dead cells. Alternatively, automated cell counting using Luna cell counter (Labtech, USA) was used.

To freeze cells for future stock generation, cells were grown to a density of 5x106 cells/mL in SF900II media and 10 % DMSO was added. Cryogenic vials were aliquoted with 1 mL of culture and snap frozen in liquid N2 and transferred to -150 ^{o}C freezer for long term storage.

2.2.9.2 Bacmid preparation

Bac-to-Bac baculovirus expression system (Invitrogen, USA) was used for rapid, efficient generation of recombinant baculoviruses. The method allows the site-specific transposition of gene of interest into shuttle vector (bacmid). The bacmid bMON14272 is about 136 kb and contains the attachment site for Tn7 (mini-attTn7) bacterial transposon inserted into the LacZα gene with kanamycin resistance. A helper plasmid such as pMON7124 (13.2 kb) is also needed as it encodes for the transposase and provides tetracycline resistance. *E.coli* strain DH10Bac contains both a bacmid and helper plasmid. The pCoofys for insect cell expression contain polyhedron promoter and mini-Tn7 transposable element. The transposition of the mini-Tn7 from pCoofys into the bacmid DNA disrupts the expression of LacZα gene which enables in blue/white recombinant selection in the presence of chromogenic substrate X-gal and inducer IPTG. The recombinants thus appear as white colonies on bacmid selection plates.

1000 ng of pCoofy plasmid were transformed into chemically competent E.coli DH10Bac as described in 2.2.8. 400 µl of LB (without antibiotics) is added and the cultures grown overnight at 37 ^{o}C, 200 RPM. The cells are centrifuged and dilution series of 1:1, 1:10, 1:100 and 1:1000 is setup in LB. The transformed cells are streaked out on bacmid selection plates (LB Agar supplemented with 50 µg/ml kanamycin, 7 µg/ml gentamicin, 10 µg/ml tetracycline, 150

µg/ml X-gal in DMSO and 40 µg/ml IPTG). The blue/white colonies can be distinguished after 48 h. All white colonies and one negative control blue colony are restreaked on a fresh bacmid selection plate and incubated overnight. Simultaneously, 5ml LB media with appropriate antibiotics was inoculated with the picked colonies and cultured overnight at 37 ^{o}C, 200 RPM.

The cultures from the positive restreaked clones were centrifuged for 10 min at 2900 rcf. The supernatant was discarded, and the pellet stored at -20 ^{o}C if bacmid preparation was scheduled for later. The bacmid is isolated by isopropanol precipitation using buffers from the Spin Miniprep kit (Qiagen, Netherlands).

The pellet is resuspended gently with 300 µl of P1 buffer and pipetted into 1.5 mL Eppendorf tubes. 300 µl of P2 buffer containing lysis blue was added and the tubes gently inverted until blue colour was homogenous. The incubation was limited to less than 5 min and 300 µl of N3 buffer was added to neutralize the lysis. Gentle inversion of tubes was carried out until blue colour disappeared and a white precipitate was formed. The tubes were centrifuged for 10 min at 13000 RPM and the supernatant transferred into fresh Eppendorf. This step was done twice and finally 700 µl of 100% isopropanol was added and mixed to obtain a homogeneous solution. The tubes were centrifuged for 10 min at 13000 RPM. A clear bacmid pellet should be seen which is subsequently washed with 200 µl of 70% ethanol. A final centrifugation step is carried out for 5 min at 13000 RPM. Finally, the bacmid pellet was washed with 50 µl cold 70% ethanol.

2.2.9.3 Virus generation and amplification

The following steps were carried out in a sterile hood. The bacmid pellet prepared in 2.2.9.2 was air dried under the hood after the removal of residual ethanol. 20 µl of autoclaved dd$H_2$0 was added to the pellet and resuspending by tapping gently on the hood bench. 200 µl of SF900II media was added.

A six-well plate was used for bacmid transfection. 5 wells were filled with *Sf9* cells with a density of 0.5x10^6 – 1.0x10^6 cells/well in a total of 3 mL volume. The last well was used as a medium only control. The cells are allowed to adhere to the surface of the well by incubating the plate for 20 min at 27 ^{o}C. Two clones per construct were transfected and each of them was duplicated. 10 µl of Cellfectin II (Invitrogen, USA) diluted in 100 µl of SF900II media was added per clone. 150 µl of this cocktail was used to transfect each well. The cells were

incubated at 27 ^{o}C for 3-6 days. The success of transfection is assessed by the increase in the size of cells in comparison to the non-transfected control and their reduced cell numbers. In case of transfection with bacmid containing YFP gene, fluorescence under microscope was used to judge the transfection success. The supernatant containing the virus was pipetted from the wells and stored in 15 mL falcon tubes wrapped with aluminum foil as P_0 virus.

Amplification of the virus to increase the virus titer was carried out by infecting pre-adapted 50 mL *Sf9* cultures at a density of 0.5x106 cells/mL with 500 µl of P_0 virus. The cells are grown for 3-4 days until the viability dropped to 70% and the cell size increased considerably. The culture was later centrifuged, and the supernatant stored in falcon tubes in the dark at 4 ^{o}C until required for protein expression.

2.2.10 Protein expression

Recombinant DNA with the gene of interest generated by one of the cloning approaches described in 2.2.5 is used for recombinant protein expression. The target protein under the control of a promoter leads to the high-level protein expression within a selected expression system. Two expression systems namely, bacterial expression in *E.coli* and insect cell expression were extensively used in this study. The choice of the expression system largely depends on several factors such as posttranslational modifications necessary, protein solubility and functionality, protein yield, time required for protein production and cost. Bacterial expression systems are easy to scale, low cost with simple culture conditions and suitable for faster protein production. The protein solubility may sometimes be an issue which may require gene optimization. Also, some mammalian cell proteins and membrane proteins may be difficult to express. The main advantages of insect cells are provision for glycosylation, posttranslational modifications, and suitability to express intracellular proteins and multi-protein complexes. Baculovirus system also enables better protein folding in some cases. However, the process of baculovirus generation is time consuming and laborious.

2.2.10.1 Protein expression in E.coli

Recombinant plasmid for the desired protein expression was transfected into E.coli expression system and plated. There is a possibility to test several strains and culturing conditions in parallel. For most test expressions, both LB and TB media were tested. A single colony was picked to start a starter culture which is grown at 37 ^{o}C, 200 RPM overnight. Large

scale culture in 5L baffled Erlenmeyer flasks was inoculated at OD_{600} of 0.1 and grown at 37 ^{o}C, 180 RPM until OD_{600} reaches 0.6. The culture was cooled to the appropriate temperature for expression (18 ^{o}C for most cases) and induced with 0.1 mM IPTG. The expression conditions for various constructs was as described in Table 22. The cells were harvested after overnight expression by centrifugation at 4000 RPM for 15 min. The cells were washed once with lysis buffer and stored at -80 ^{o}C until further use.

Table 22: Expression conditions for constructs in *E.coli*

Construct	Vector	Strain	Medium	Temperature	IPTG (mM)
P-CRY PHR	pCoofy6	Rosetta	LB Luria	18 ^{o}C	0.1 mM
P-CRY 200-778	pCoofy6	Rosetta	LB Luria	18 ^{o}C	0.1 mM
PITHD1 FL	pCoofy1	Rosetta/BL21	TB	18 ^{o}C	0.1 mM
YTHDF2 FL	pCoofy4	Rosetta	TB	18 ^{o}C	0.1 mM

2.2.10.2 Protein expression in insect cells

Test expression in insect cells was carried out with 50 – 500 µl of P1 virus added to 50 mL of High Five cells at 0.5x10^6 cells/mL. Cells are counted every day and if they continue to divide, they are further diluted to < 1x10^6 cells/mL. Sampling was started day after proliferation arrest (DPA) and continued upto 72 h. A sample of 1x10^6 cells/mL was taken every day, centrifuged for 2 min at 13000 RPM. The pellet was suspended in appropriate lysis buffer, sonicated, and checked on SDS-PAGE for protein expression and solubility.

Once the appropriate expression conditions were established, 1 L of insect cells at a density of 1x10^6 cells/mL were infected with tested volume of P1 virus and harvested after predetermined expression duration by centrifugation at 7000 RPM for 15 min. The pellet was stored at -80 ^{o}C. In some cases, addition of 2 mM Glutamine (Life Technologies, USA) to the media was essential to improve expression.

Table 23: Expression conditions for constructs in insect cells

Construct	Vector	Cell line	Expression duration (days)
L-CRY	pCoofy27	*Sf9*	3
L-CRY 30-567	pCoofy27	*Sf9*	2
L-CRY 30-553	pCoofy27	*Sf9*	2
Tr-CRY FL	pCoofy27/28/29	*Sf9*/High Five	3
Tr-CRY	pCoofy27/28/29	*Sf9*/High Five	3

YTHDF2 FL	pCoofy27	*Sf9*	2
YTHDF2 FL	pCoofy28	*Sf9*	2
G3BP2 FL	pCoofy27	*Sf9*	2
G3BP2 FL	pCoody28	*Sf9*	2

2.3 Biochemical Methods

2.3.1 Gel electrophoresis

2.3.1.1 SDS-PAGE

Polyacrylamide gels are used to separate proteins electrophoretically. In a protein mixture, smaller proteins migrate faster than larger proteins through the gel when an electric current is applied. The rate of movement is influenced by the pore size of the gel and the strength of the applied current. Sodium dodecyl sulfate polyacrylamide gel electrophoresis (SDS-PAGE) is a method used to validate the presence and purity of proteins after protein expression or each purification step. SDS is a negatively charged ionic detergent that denatures proteins and imparts a similar charge: mass ratio. Thus, the separation is governed only by the chain length , i.e., mass of the protein. The molecular weight is estimated by comparing the migration of the sample with migration of a protein standard on the gel. In this work, Bis-Tris gels were predominantly used. The composition of the gels, sample and running buffers, staining and destaining solutions are listed in Table 8. A gel casting device was used to cast 10 gels together using 60 mL of resolving solution and 20 mL of stacking solution.

40 µl of protein sample was mixed with 10 µl of 5x sample buffer. The sample is denatured at 95 ^{o}C for 5 min and 15 µl was loaded onto a 10 lane SDS-PAGE. 5 µl of protein marker was added in lane for every gel. Electrophoresis was carried out for 30 min at constant current of 130 mAU . The gel was later boiled in water, stained and subsequently destained. Each step was carried out by heating the gel for 1 min in microwave. The gel was destained in destaining solution for 30 min to clear up the background so as to visualize the protein bands and later transferred into water for overnight destaining on a shaker.

2.3.1.2 Native PAGE

Native gel electrophoresis is carried out to determine the polymeric state of protein under non-denaturing conditions in the absence of reducing agents. The mobility of the protein is

dependent on the size of the protein, quaternary state, and the charge-to-mass ratio. The oligomeric state of L-CRY was checked by running the protein under dark and blue-light conditions. For the light activated state, the protein was illuminated for 110s and loaded on the gel which was constantly illuminated using a blue-light plate (410 nm, 1mW/cm^2 at 10 cm) kept close to the electrophoresis unit (approximate distance 5-6 cm). The molecular weight is estimated by comparing the migration of the sample with the migration of a NativMark unstained protein marker. 4-15% BisTris gradient gels were used which were pre-run for 1h before sample loading under same conditions. The composition of the gels, sample and running buffers, and the staining solutions are listed in Table 9.

2.3.2 Protein purification

All the below mentioned steps were carried out in dark/red light whenever possible for all light sensitive proteins. The cold room and other working area were equipped with red light LEDs. In other cases, the protein containers were wrapped with aluminum foil.

2.3.2.1 Cell lysis in *E.coli*

Frozen pellets were thawed on ice and resuspended in appropriate lysis buffer with 1 tablet of complete EDTA-free protease inhibitor, 1mM PMSF, 0.5 mM AEBSF, few flakes of lysozyme, 5 mM $MgCl_2$ and 30 µl benzonase. The cells were stirred continuously at 4 ^oC until complete dissolved. The resuspension was lysed by 3 passages through a microfluidizer with setting 1 x 15000 psi and 2 x 12000 psi . The lysate was centrifuged at 19000 RPM for 45 min at 4 ^oC.

2.3.2.2 Cell lysis in insect cells

10-20 g of frozen insect cell pellets were thawed on ice and resuspended in 200 ml of appropriate lysis buffer supplemented with 1 tablet of complete EDTA-free protease inhibitor, 1mM PMSF, 0.5 mM AEBSF, 5 mM $MgCl_2$ and 30 µl benzonase. The cells were suspended by continuous stirring at 4 ^oC for 20 -30 min. Lysis was carried out by sonication using a 9 mm tip. The settings for lysis were output 6, duty cycle: 20 % and 3 cycles of 2 min. The cells were constantly stirred on ice during sonication and a gap of 2 min between each cycle was observed to avoid overheating. After 3 sonication cycles, the lysate was centrifuged using an ultracentrifuge at 50000 RPM for 45 min at 4 ^oC

2.3.2.3 Affinity chromatography

Affinity chromatography selectively binds proteins by a reversible interaction to a specific ligand bound to a chromatography column. The ligand used can range from enzymes, antibodies, lectins, metal ions, hormones, etc. Affinity chromatography is used for initial capture or intermediate purification of proteins.

Purification of histidine-tagged proteins

Histidine tags are commonly used in the purification of recombinant proteins as they are relatively smaller compared to other used tags and do not affect the properties of a protein considerably. Hence, it is not always essential to cleave the tag during or after purification. Metals ions such as Ni^{2+}, Co^{2+} and Zn^{2+} have high selective affinity to poly-histidine tagged proteins. Undesired endogenous proteins in the lysate will pass through or weakly bind to metal-ion-charged media which can be washed off. The protein of interest is eluted with a high concentration of imidazole in general. Alternatively, lowering the pH or use of strong chelating agents such as EDTA can also be used. The technique is known as immobilized metal ion chromatography (IMAC). All histidine-tagged constructs in this study contain N-terminal hexa-histidine tag. Longer histidine tags may be used for stronger binding to the column. HisTrap FF crude nickel columns (GE Healthcare) or beads were used for all metal affinity chromatographic steps. The purification scheme used for different constructs in this study was as mentioned below.

Table 24: Affinity chromatography for purification of L-CRY FL and its variants

Protein	L-CRY FL and variants
Column	5ml HisTrap FF
Buffer	Lysis/Binding Buffer: 20 mM Tris pH 7.5, 150 mM NaCl, 20 mM imidazole, 5% glycerol, 5 mM β-mercaptoethanol Elution Buffer: 20 mM Tris pH 7.5, 150 mM NaCl, 1 M imidazole, 5% glycerol, 5 mM β-mercaptoethanol
Column Equilibration	10 CV binding buffer
Sample Application	Load with sample pump 3ml/min (max)
Wash unbound sample	6 CV binding buffer
Wash steps	WI 6 CV 5% elution buffer WII 6 CV 10% elution buffer
Elution steps	EI 6 CV 25% elution buffer EII 6 CV 50% elution buffer EIII 2 CV 100% elution buffer

Table 25: Affinity chromatography for purification of P-CRY variants

Protein	P-CRY variants
Column	5ml HisTrap FF
Buffer	Lysis/Binding Buffer: 50 mM Bis Tris propane , 300 mM NaCl,5% glycerol, 1 mM DTT, pH set according to pI of the construct Elution Buffer: 50 mM Bis Tris propane , 300 mM NaCl,5% glycerol, 1 M Imidazole, 1 mM DTT, pH set according to pI of the construct
Column Equilibration	10 CV binding buffer
Sample Application	Load with sample pump 3ml/min (max)
Wash unbound sample	6 CV binding buffer
Wash steps	WI 15 CV ATP wash buffer (50 mM Tris pH 7.4, 150mM NaCl, 2mM ATP, 50 mM KCl, 10 mM $MgSO_4$) WII 15 CV High salt buffer (Lysis Buffer + 1.5M NaCl)
Elution steps	EI 10 CV 0-100% elution buffer

Table 26: Affinity chromatography for purification of L-CRY ligands

Protein	L-CRY ligands - YTHDF/G3BP/PITHD1
Column	5ml HisTrap FF
Buffer	Lysis/Binding Buffer: 20 mM Tris, 300 mM NaCl, 20 mM imidazole, 5% glycerol, 5 mM β-mercaptoethanol Elution Buffer: 20 mM Tris , 300 mM NaCl, 1 M imidazole, 5% glycerol, 5 mM β-mercaptoethanol pH adjusted as per pI
Column Equilibration	10 CV binding buffer
Sample Application	Load with sample pump 3ml/min (max)
Wash unbound sample	6 CV binding buffer
Elution steps	EI 10 CV 0-100% elution buffer

Table 27: Affinity chromatography for purification of dCRY

Protein	dCRY
Column	5ml HisTrap FF
Buffer	Lysis/Binding Buffer: 25 mM Tris pH 8.0, 300 mM NaCl, 20 mM imidazole, 5% glycerol, 5 mM β-mercaptoethanol Elution Buffer: 25 mM Tris pH 8.0, 300 mM NaCl, 1 M imidazole, 5% glycerol, 5 mM β-mercaptoethanol
Column Equilibration	10 CV binding buffer
Sample Application	Load with sample pump 3ml/min (max)
Wash unbound sample	6 CV binding buffer
Wash steps	WI 6 CV 5% elution buffer WII 6 CV 10% elution buffer
Elution steps	EI 10 CV 10-100% elution buffer

Purification of GST-tagged proteins

Glutathione S-transferase (GST) is a 26 kDa protein which is used as fusion tag in recombinant protein expression and purification. Inclusion of this tag promotes greater expression and solubility. GST has high affinity to glutathione ligand coupled to a column. The reversible binding enables elution of desired protein under mild conditions using reduced glutathione in elution buffer. GST has the tendency to dimerize and hence it is better to cleave the tag if solubility of the protein is not affected and further use in GST pull-down experiments is not needed. L-CRY ligands were expressed and purified as GST fusions for further protein-protein interaction studies. The purification scheme was as described below in Table 28.

Table 28: Affinity chromatography for purification of L-CRY ligands with GST tag

Protein	L-CRY ligands - YTHDF/G3BP
Column	2ml GSH beads self-packed
Buffer	Lysis/Binding Buffer: 50 mM Tris, 200 mM NaCl, 2.7 mM KCl, 5% glycerol, 1 mM DTT Elution Buffer: 50 mM Tris, 200 mM NaCl, 10 mM Glutathione, 5% glycerol, 1 mM DTT pH adjusted as per pI
Column Equilibration	10 CV binding buffer
Sample Application	Load with sample pump 2ml/min (max)
Wash unbound sample	6 CV binding buffer
Wash steps	WI 6 CV binding buffer
Elution steps	EI 4 CV elution buffer EII 4 CV elution buffer (incubated 10 min) EIII 4 CV elution buffer

Purification of MBP-tagged proteins

Maltose binding protein (MBP) is used as a fusion tag to increase expression and solubility of target proteins. In addition, MBP functions as an affinity tag for purification by binding to amylose columns . MBP has a molecular mass of 42.5 kDa. Elution is carried out with mild elution buffers containing maltose. Eluted protein can later be cleaved with specific protease to remove the MBP-tag and the tag separated by a reverse affinity chromatography step.

Table 29: Affinity chromatography for purification of L-CRY ligand YTHDF from *E.coli*

Protein	L-CRY ligand YTHDF
Column	1ml MBPTrap HP
Buffer	Lysis/Binding Buffer: 50 mM Tris pH 7.4, 200 mM NaCl, 5% glycerol, 1 mM DTT, 1 mM EDTA

	Elution Buffer: 50 mM Tris pH 7.4, 200 mM NaCl, 5% glycerol, 1 mM DTT, 1 mM EDTA ,10 mM Maltose
Column Equilibration	10 CV binding buffer
Sample Application	Load with sample pump 1ml/min (max)
Wash unbound sample	6 CV binding buffer
Wash steps	WI 15 CV ATP wash buffer (50 mM Tris pH 7.4, 150mM NaCl, 2mM ATP, 50 mM KCl, 10 mM $MgSO_4$) WII 15 CV High salt buffer (Lysis Buffer + 1.5M NaCl)
Elution steps	EI 20 CV 100% elution buffer

2.3.2.4 Ion-exchange chromatography

Proteins are amphoteric and the net charge changes with changes in the surrounding pH. Ion exchange chromatography separates proteins based on differences in their net surface charges. At isoelectric point (pI), proteins have no net charge. At pH above pI, proteins are negatively charged and bind to anion exchangers while at pH below pI, they are positively charged and bind strongly to cation exchangers. In general, a pH = pI ± 1.5 was used in this study. Bound proteins are eluted by increasing the ionic strength (salt concentration) of the surrounding environment. Salt ions compete with bound proteins leading to the release of low net charged proteins first. Alternatively, it is also possible to elute proteins with change in pH of the buffer. Anion-exchange chromatography was mainly used in this study as a second step for most purifications. Cation-exchange chromatography was used only for P-CRY cctail construct. The conditions used were as mentioned in Table 30-32. The fractions containing the protein from affinity chromatography step were pooled, concentrated and the buffer exchanged during the concentration process. The protein was diluted 1:10 in low salt buffer before loading on the column.

Table 30: Anion-exchange chromatography for purification of L-CRY, P-CRY PHR and PITHD1

Protein	L-CRY and variants
Column	5 mL HiTrap QHP (GE Healthcare)
Column cleaning before use	2 CV 2M NaCl 4 CV 0.5M NaOH 2 CV 2M NaCl 2 CV ddH_2O
Buffer	Low salt buffer : 50 mM Tris HCl, 50 mM NaCl, 1mM DTT, 5% glycerol High salt buffer : 50 mM Tris HCl, 1 M NaCl, 1mM DTT, 5% glycerol pH adjusted as per pI
Column equilibration	6 CV low salt buffer
Sample Application	Load with sample pump 3ml/min (max)
Wash unbound sample	8 CV low salt buffer

Fraction size	2 ml
Gradient	20 CV (0-100% high salt buffer)

Table 31: Anion-exchange chromatography for purification of dCRY

Protein	dCRY
Column	5 mL HiTrap DEAE Sepharose (GE Healthcare)
Column cleaning before use	2 CV 2M NaCl 4 CV 0.5M NaOH 2 CV 2M NaCl 2 CV ddH_2O
Buffer	Low salt buffer : 50 mM Tris HCl pH 8.0, 1mM DTT, 5% glycerol High salt buffer : 50 mM Tris HCl pH 8.0, 500 mM NaCl, 1mM DTT, 5% glycerol
Column equilibration	6 CV low salt buffer
Sample Application	Load with sample pump 3ml/min (max)
Wash unbound sample	8 CV low salt buffer
Fraction size	2 ml
Gradient	20 CV (0-100% high salt buffer)

Table 32: Cation-exchange chromatography for purification of P-CRY cctail

Protein	P-CRY cctail
Column	5 mL HiTrap SP HP (GE Healthcare)
Column cleaning before use	2 CV 2M NaCl 4 CV 0.5M NaOH 2 CV 2M NaCl 2 CV ddH_2O
Buffer	Low salt buffer : 50 mM Tris HCl, 50 mM NaCl, 1mM DTT, 5% glycerol High salt buffer : 50 mM Tris HCl, 1 M NaCl, 1mM DTT, 5% glycerol pH adjusted as per pI
Column equilibration	6 CV low salt buffer
Sample Application	Load with sample pump 3ml/min (max)
Wash unbound sample	8 CV low salt buffer
Fraction size	2 ml
Gradient	20 CV (0-100% high salt buffer)

2.3.2.5 Size exclusion chromatography

Size exclusion chromatography or gel filtration is a polishing technique widely used as a last step in protein purification. It fractionates proteins according to their hydrodynamic radius. Large sized proteins are unable to enter into the matrix pores and hence elute first. On the other hand, smaller proteins tend to have later elution times. The total volume (V_T) of a SEC column is characterized as:

$$V_T = V_0 + V_i + V_g$$

where V_0 - void volume, i.e., volume external to the packing material , V_i - internal volume, i.e., volume within the porous beads accessible to small molecules and V_g - bed volume, i.e., volume of the packing material.

The volume of the solvent required to elute a molecule given by its elution volume (V_e) is

$$V_e = V_0 + \sigma V_i$$

where σ - partition coefficient, which when compared to the values measured for protein standards, provides information about the size of an unknown protein. A linear relationship in the form a calibration curve between the partition coefficient and the molecular size is used for this purpose. The method can be beneficial in the determination of approximate molecular weight/oligomeric state of a protein. The shape of the peaks under the elution conditions provides information about the homogeneity or aggregation of proteins. All proteins purified in this study were of suitable molecular weight to be separated by a prep grade Superdex 200 column (Mr 10000 – 600000) (GE Healthcare).

The protein sample was concentrated upto 3 ml for injection with a 5 ml capillary loop. The samples were filtered with 0.2 µm filter and centrifuged at 14000 RPM for 10 min prior to injection. After elution, the purity of protein checked with a SDS-PAGE and the fractions containing pure protein were pooled and concentrated using cellulose membrane protein concentrators of appropriate molecular weight cutoff by centrifugation. The concentration was measured using NanoDrop 2000c at 280 nm using theoretical extinction coefficient obtained from Protparam for L-CRY ligands. The extinction coefficient at 280nm of L-CRY (bound FAD) used was 230920 M^{-1} cm^{-1}. The extinction coefficients used for P-CRY PHR and PHR cctail are 224690 M^{-1} cm^{-1} and 227670 M^{-1} cm^{-1} respectively. The A260/A280 ratio was also considered to estimate nuclei acid contamination for L-CRY ligands.

Table 33: Size exclusion chromatography for purification

Protein	L-CRY , P-CRY, dCRY and L-CRY ligands
Column	120 ml HiLoad 16/60 Superdex 200 pg
Column cleaning before use	4 CV 0.5M NaOH 2 CV ddH_2O
Buffer	25mM Bis Tris propane pH 8.0, 150 mM NaCl, 5% glycerol, 1 mM TCEP (L-CRY) 50mM Bis Tris propane pH 8.0, 300 mM NaCl, 5% glycerol, 1 mM DTT (P-CRY variants), pH adjusted as per pI 25 mM Tris pH 8.0, 5% glycerol, 150 mM NaCl, 1 mM TCEP (dCRY)

	25mM HEPES, 150 mM NaCl, 5% glycerol, 1mM DTT (L-CRY ligands), pH adjusted as per pI
Column equilibration	1 CV size exclusion buffer
Sample Application	5 ml capillary loop
Fraction size	1 ml
Elution	Isocratic elution over 1CV size exclusion buffer
Flow rate	0.6 ml/min

2.3.2.6 Analytical Size exclusion chromatography

The analytical S200 10/300 column was used to study change in oligomeric state in dark as compared to light. For dark runs, the procedure was carried out in red light/complete darkness. The protein was light-activated prior to injection and the run was carried out in light.

In addition, initial interaction studies of L-CRY with their ligands was tested using the same column. For interaction studies, proteins were pre-incubated on ice for 1 h prior to injection. 1 ml capillary loop was used for injection. The column was calibrated using Gel filtration protein standard (Bio-Rad, USA). The calibration standard includes Thyroglobulin (670 kDa), γ-globulin (158 kDa), ovalbumin (44 kDa), myoglobin (17 kDa) and vitamin B12 (1350 Da).A calibration curve was prepared and used for all comparisons in this study.

2.3.3 Size Exclusion Chromatography coupled Multiangle Light Scattering (SEC-MALS)

Static light scattering (SLS) is a method used to obtain average molecular weight (M_w) of a protein by measuring the intensity of the scattered light. Multiangle light scattering (MALS) measures light scattering at multiple angles relative to the angle of incidence simultaneously. SEC-MALS is a combination of size exclusion chromatography coupled to an MALS device, wherein the absolute molar mass of sample fractions eluting from the SEC column can be calculated. In this study SEC-MALS was carried out to determine the exact molecular weight and oligomeric state of purified L-CRY. L-CRY was loaded onto a Superose 6 10/300 SEC column (Mr 5000 – 5 x 10^6) (GE Healthcare) and run at flowrate 0.4 ml/min. The SEC buffer for L-CRY (25 mM Bis-Tris propane pH 8.0, 150 mM NaCl) was applied for the run. For P-CRY variants, respective SEC buffer without glycerol and DTT was used for the run. MALS data were obtained from the DAWN DSP instrument (Wyatt Tech, Germany) and processed using ASTRA 4.90.07. The standard run for comparison was Bovine pancreas ribonuclease. The extinction coefficient at 280nm of L-CRY (bound FAD) used for molecular weight

determination was 230920 M^{-1} cm^{-1}. The extinction coefficients used for P-CRY PHR and PHR cctail are 224690 M^{-1} cm^{-1} and 227670 M^{-1} cm^{-1} respectively.

2.3.4 UV/VIS Absorbance spectroscopy

Ultraviolet-Visible (UV/VIS) absorbance spectroscopy is an analytical technique wherein, light in the UV-VIS range (300 – 700 nm) is passed through a sample for absorption. A detector records the transmitted light through the sample. On incidence of light, molecules in the sample are excited by the photon and transit from the ground state to the excited state crossing over the band gap (energy difference between the two states). The energy of the photon must match the energy of the band gap for the transition to takes place, i.e., for the photon to be absorbed. The band gap is determined by the molecular structure of compounds and hence is a unique identity of each compound. Thus, this technique helps to identify compounds as they differ in their absorbance spectrum.

The absorbance of a sample is given by Beer-lambert law:

$$A = \varepsilon Cl$$

Where A - Absorption of the sample , ε - molar attenuation coefficient , C - concentration of the sample and l - optical path length.

In this study, UV-VIS absorption was used for the determination of protein concentrations by considering the absorbance at 280 nm and using the extinctions coefficients. For L-CRY and P-CRY constructs, absorbance at 280 nm due to chromophores was accounted for in the extinction coefficient values (mentioned under sections 2.3.2.5 and 2.3.3). The absorbance spectra were used to analyze bound ligands to cryptochromes and monitor changes in light activated state. The spectra were plotted and analyzed using the software Origin (Version 7.5/10.5 (trial), Origin Lab Corporation, Northampton, MA, USA)

Blue light illumination and dark recovery

The UV-Visible absorption spectra (300 to 700 nm) of purified L-CRY were recorded using the Tecan Spark 20M plate reader. The light-state spectrum was collected after illuminating L-CRY with a 445 nm light-emitting diode (19 milliwatts/cm^2) for 110 s. Dark recovery kinetics of L-CRY were measured at around 18°C by recording the absorption changes at 450 nm after initial 110 s blue light illumination. The UV-VIS Spectrophotometer Jasco V-550 was used for

kinetic measurements at 6°C. The time constant was calculated by fitting a single exponential curve to the experimental data.

Moon light illumination and dark recovery

A light source mimicking the moonlight spectrum (NELIS devices) was used for moonlight UV-visible spectroscopy experiments. The light source provides an intensity of 2.56*10-8 W/cm2 at the sample (7cm from light source). To analyze moonlight-dependent photoreduction of L-CRY, dark-adapted L-CRY (kept on ice) was illuminated with moonlight continuously for 6 h and UV-VIS spectra (300 – 700 nm) were collected at different time points using the Tecan Spark 20M plate reader. For measuring the dark recovery time constant, L-CRY was illuminated with 6 h full moonlight on ice. UV-VIS spectra (300 – 700 nm) were measured at 18 °C. The absorbances at 450 nm were taken from these complete spectra, plotted against time, and fitted to obtain the time constant after moonlight illumination. To assess if moonlight can maintain the light state, L-CRY was initially illuminated with a 445 nm blue light LED for 110 sec, followed by continuous moonlight illumination at full moon intensity (2.56*10-8 W/cm2). UV-VIS spectra were collected at different time points as before. The sample was kept on ice and illuminated with moonlight in between measurements. Absorbances at 450 nm were taken from the complete spectra for time points (10 min to 2h 30 min) and used to determine the time constant after blue-light illumination in presence of moonlight.

Sunlight illumination and dark recovery

A light source mimicking the sunlight spectrum was used for UV-visible spectroscopy experiments. The light source provides an intensity of 5.9*10-4 W/cm2 at the sample (7cm from light source). To analyze sunlight-dependent photoreduction of L-CRY, dark-adapted L-CRY (kept on ice) was illuminated with sunlight continuously and UV-VIS spectra (300 – 700 nm) were collected using the Tecan Spark 20M plate reader. For measuring the dark recovery time constant, absorbances at 450 nm were monitored continuously at 18 °C. For measuring the dark recovery time constant on ice, L-CRY was illuminated with sunlight on ice for 20 min and UV-VIS spectra (300 – 700 nm) were measured at 18 °C. The absorbances at 450 nm were taken from these complete spectra, plotted against time, and fitted to obtain the time constant after sunlight illumination.

To assess if sunlight source could further increase the photoreduction from the moonlight activated state, L-CRY was initially illuminated with continuous moonlight at full moon intensity (2.56*10-8 W/cm2) for 6 h, followed by 20 min of sunlight illumination and later allowed to dark recover. Complete UV-VIS spectrum from 300 – 700 nm was measured in each case.

2.3.5 Fluorescence spectroscopy

Several substances emit light on absorbance of light or electromagnetic radiation. The emitted light has a longer wavelength than absorbed light. Fluorescence spectroscopy is a complementary technique to the absorption spectroscopy wherein the transitions from the excited state to the ground state are monitored. Fluorescence emission is sensitive to the changes in the environment of the chromophore. In a fluorescence spectroscopy experiment, the excitation wavelength is fixed to record the emission spectrum and the emission wavelength is fixed to record the excitation spectrum.

The Flavin fluorescence spectra was recorded with 10 nm bandwidth using 450 nm excitation wavelength for emission spectra and 530 nm emission wavelength for excitation spectra. The detection of MTHF was done by recording emission spectra at an excitation wavelength of 380 nm and excitation spectra at an emission wavelength of 460 nm.

2.3.6 CD spectroscopy

Biomolecules such as proteins are optically active and able to rotate both plane and circularly polarized light. Circularly polarized light is the superimposition of two plane polarized light of same wavelength and amplitude in two perpendicular planes with a phase difference of 90^{o}. Circular dichroism (CD) spectroscopy enables to detect secondary structure of proteins in solution such as alpha-helix, beta- sheet or random coil and the changes in the conformation of the protein under different conditions.

CD spectroscopy detects the differential absorption of left- and right- handed light. The delta absorbance is given as:

$$\Delta A = A_L - A_R$$

where ΔA - delta absorbance , A_L - absorbance of left circularly polarized light , A_R - absorbance of right circularly polarized light. Applying Beer-Lamberts law, delta absorbance can be rewritten in terms of molar extinction coefficient(ε) as

$$\Delta A = \Delta \varepsilon C l$$

where $\Delta\varepsilon = \varepsilon_L - \varepsilon_R$, C - concentration , l - path length.

CD is usually represented in terms of ellipticity. The relationship between CD and ellipticity (θ) is given as:

$$\theta = 2.303\ (A_L - A_R)\ 180/4\pi = 33\ (A_L - A_R) = 33\ \Delta A \text{ degree}$$

Ellipticity when corrected for concentration is represented as molar ellipticity [θ]. Pre-purified L-CRY (0.1 mg/ml) was dialyzed into 10 mM sodium phosphate buffer overnight. The sample was centrifuged at 14000 RPM for 10 min at 4°C to remove any aggregates. The spectra was recorded from 190nm to 250 nm. For the light state spectra, the protein was illuminated with blue light 445 nm LED bulb for 110 s and the CD spectra recorded immediately. 10 scans for each measurement were carried out at 4°C and accumulated to analyze the spectra with cdnn spectra deconvolution software (Böhm et al., 1992).

2.3.7 Reverse phase HPLC

Chromatography is a technique that helps to separate compounds based on their distribution in two different immiscible phases. This is defined by the partition or the distribution coefficient, K_d. The two immiscible phases namely the stationary and the mobile phase determine the type of chromatographic technique suitable for use. Reverse phase high performance liquid chromatography (Reverse phase HPLC) is an adsorption-based column chromatography technique wherein stationary phase in the column is a solid and the mobile phase used is a aqueous polar solvent. The column is packed with silica, modified by attachment of long hydrocarbon chains, which functions as a non-polar stationary phase. The mobile phase is a mixture of water and an alcohol such as methanol. When a sample is applied to such a column, the non-polar molecules strongly adhere to the stationary phase due to strong vander waals dispersion forces and the polar molecules move along with the mobile phase. In this study, this technique provided a means to distinguish the individual cofactors bound to cryptochromes based on their relative mobility with a polar solvent.

Commercially synthesized Flavin Mononucleotide (FMN), Flavin Adenine Dinucleotide (FAD) and Methenyltetrahydrofolate (MTHF) were dissolved in buffer (25 mM Bis-Tris propane pH 8.0, 150 mM NaCl, 5% glycerol) and run at 1ml/min (20 °C) over a Macherey-Nagel C18 Gravity-SB (150/4/5 µm) column to separate the chromophores by reverse phase (RP) HPLC analyses. A gradient from 20-100% of methanol against water (+0.1% Trifluoroacetic acid) was used for optimal separation. To analyse the chromophore content, 10 µl of purified L-CRY (2 mg/ml)/P-CRY PHR (0.5 mg/ml) was heat-denatured for 5 min at 97°C and centrifuged at 14000 RPM for 10 min at 4°C to separate the released chromophores from the denatured protein. The supernatant containing the released chromophores was subjected to RP-HPLC analysis. The chromophores were monitored by absorption at 370 nm. A similar protocol was also applied to study P-CRY bound cofactors.

2.3.8 Small angle X-ray scattering (SAXS)

SAXS is a small-angle scattering technique for the structural analysis of molecules in solution. Biological SAXS helps determine the size and shape of macromolecules such as proteins in solution without the need for crystallization. In addition, it is possible to test the change of environmental parameters such as pH, salt and temperature on the structural aspects of macromolecules (Kikhney & Svergun, 2015). Advances in the technique have made time-resolved conformational analysis possible. SAXS experiments can be carried out in batch mode or coupled to a SEC run. The SAXS studies with L-CRY were done in a batch mode to facilitate light illumination of the sample.

Sample in a quartz capillary is illuminated by collimated monochromatic X-ray beam (λ - 0.10 to 0.15 nm) and the intensity of the scattered X-rays is recorded by the detector. The scattering from the pure solvent/buffer is recorded as well and subtracted from the sample scattering to obtain the signal from the sample molecules only. The intensity (I) of the scattered X-ray is represented as a function of momentum transfer (s).

$$s = 4\pi\sin\theta / \lambda$$

where 2θ - scattering angle and λ - beam wavelength. Particles in solution are randomly oriented and hence the scattering pattern is isotropic in nature. The data is ,thus, plotted as radially averaged one-dimensional curves I(s) vs s.

SAXS experiments were carried out at beamline P12, DESY, Hamburg. Frozen aliquots of purified L-CRY at 4.9 mg/ml (in buffer 25 mM Bis-Tris propane pH 8.0, 150 mM NaCl, 5% glycerol and 1mM TCEP) were thawed and a concentration series of approximately 1, 2 and 3 mg/ml was prepared for data collection. As scattering intensity (I) is proportional to the concentration, it is advisable to make a compulsory concentration series for better signal-to-noise ratio. Samples at high concentration also provide indications about inter-particle interactions such as aggregation or repulsive interactions. For dark state measurement, a red-light filter was used to illuminate the sample capillary and the sample was handled in dark/dark adapted prior to use. The data was merged and processed using the ATSAS 2.8.4 package (D. Franke et al., 2017). For light state measurement, the sample was loaded and held in the capillary (illuminated by blue light by changing the filter) for 110 s. The data was later collected and processed as for the dark state.

Guinier approximation is the first step to characterize the sample by SAXS. The Guinier plot obtained by plotting log I(s) vs s, provides the radius of gyration (R_g) which is the slope of the linear region of the plot. The nonlinear part of the Guinier plot is an indicator of the sample quality, i.e., sample polydispersity, improper background subtraction or attractive/repulsive inter-particle effects. The program AUTORG statistically optimizes the range of s to determine Rg values. The porod distribution, p(r), is obtained by indirect Fourier transform methods to yield the distance distribution curve. Particle shapes such as globular, elongated or multidomain units can be easily visualized by such a curve (Mertens & Svergun, 2010; Petoukhov et al., 2007). The maximum dimension of the molecule D_{max} was reliably calculated with the help of GNOM (D. I. Svergun, 1992). The Kratky plot ($I*s^2$ vs s) indicates the flexibility in other words the folded/unfolded state of proteins (Doniach, 2001). These three plots essentially help to characterize the sample and extract relevant parameters from the scattering data.

In addition, the scattering curve can also be used to reconstruct a 3D structure of the protein using *ab initio* methods. DAMMIN (Dummy Atom Model Minimization) is the most popular method currently used wherein the molecule is represented as a collection of densely packed beads within spherical volume of diameter equal to D_{max} (D. Svergun, 1999). A fitting procedure is carried out to generate a final compact, connected dummy bead model which fits to the experimental data. DAMMIF (F refers to fast) is the new implementation of

DAMMIN (Daniel Franke & Svergun, 2009). The models generated were averaged using DAMAVER (Volkov & Svergun, 2003) .

2.3.9 X-ray crystallography

X-ray crystallography determines the unique arrangement of atoms within a crystal using a technique called X-ray diffraction. A X-ray beam is diffracted by a crystal and measuring the intensities of diffracted beams at different angles, it is possible to derive the 3-dimensional structure of the molecules within the crystal. Objects diffract electromagnetic radiation with a wavelength in the same order of magnitude as the distance between them. The distance between carbon atoms is 1.5 Å. Hence, X-rays with a wavelength of 0.1 nm (1 Å) are used to visualize protein structures. The diffraction pattern obtained is an array of spots due to constructive and destructive interference. Bragg's law describes the angle at which a X-ray beam of particular wavelength is diffracted from a crystalline surface as

$$n \times \lambda = 2d\sin\theta$$

where n - integer number , λ - wavelength of X-ray , d - distance between lattice planes and θ - incidence angle of the X-ray beam.

2.3.9.1 Conventional crystallization setups

For crystallization success, the concentration of the protein must be slightly higher than its solubility limit. This varies with the salt concentration, amount of polyethylene glycols and other precipitants in the crystallization condition. Vapor diffusion is widely used for initial crystallization trials and hit optimization. A protein-precipitant mixture (varying ratios can be employed, in general 1:1 for initial trials) in either hanging drop or sitting drop position is equilibrated with a reservoir containing the precipitant agent. Ideally , the protein transitions into the supersaturated state as an equilibrium between the reservoir solution and drop is established. Moderate supersaturation enables spontaneous nucleation to take place. As the protein transitions into the metastable zone of the phase diagram, pre-formed crystal nuclei continue to grow stably. High supersaturation leads to precipitate formation and whereas undersaturation keeps the protein in soluble state. Both these conditions are undesirable and provide indications to vary protein concentration for future crystallization trials.

Freshly purified protein or aliquots of frozen protein thawed on ice were centrifuged at 16100 g for 15 min at 4^{o}C to remove protein aggregates or dust particles. 100 nl of protein was used in 1:1 ratio with the reservoir solution. Initial crystallization trials were performed with homemade substitutes of commercially available screens in a 96-well format using the Mosquito robot (TTP Labtech, UK). To ensure a closed system for vapor diffusion, the plates were sealed with adhesive foil and incubated at 20^{o}C and 4^{o}C. The setups were evaluated with stereo microscope at regular intervals to identify hits.

The hits identified after initial screening were further optimized to obtain larger or better diffracting crystals by fine screening the amount of precipitant, pH of the buffer or addition of additives in incremental steps. The optimization was carried out in 24-well format with 1 µl of protein in 1:1 with the reservoir solution. Other ratios such as 2:1 was also tested. The plates incubated at appropriate temperatures and monitored regularly to record clear drops, precipitates, phase separation, microcrystals , crystals etc.

2.3.9.2 *In-vivo* crystallization in insect cells

Protein crystallization occurs naturally when heterologously expressed proteins are produced in high enough concentrations to facilitate crystal formation *in vivo.* Several studies previously have utilized this occurrence and coupled it with techniques like serial femtosecond X-ray crystallography (SFX) to obtain structural insights (Jakobi et al., 2016; Koopmann et al., 2012; Sawaya et al., 2014). As wide range of proteins were reported to crystallize *in vivo*, a pipeline to use this method coupled with *in cellulo* diffraction for structure determination alongside conventional crystallographic approaches has been established (Boudes et al., 2016). The two commonly used approaches vary primarily on how the diffraction images are collected from *in vivo*-grown crystals. In some cases, it is feasible to isolate and purify the crystals from the cell and proceed further with conventional mounting with cryoprotection for data collection. This is however a challenge in case of microcrystals or delicate crystals that potentially degrade on cell lysis. To overcome these challenges, the entire cell containing the crystals are mounted on grid meshes and exposed to the X-ray beam.

During the expression of L-CRY in *Sf9* cells it was observed that the cells produced crystals. These crystals were however not very stable outside the cell environment and hence difficult to isolate. In order to optimize this approach and segregate cells with potential crystals from

the rest, a flow cytometry sorting was employed. FACS was carried out at the IMB Cytometry Core facility with the help of Dr. Stefanie Möckel. *Sf9* cells infected with baculovirus producing L-CRY full length protein were cultured for 48-72 h. The cells were centrifuged at 4000 RPM for 5 min and resuspended in SF900II media supplemented with 1% FCS and 2 mM EDTA (filtered). A total cell concentration of 5-7.5 x 10^6 cells/ml was recommended for sorting cells with a 85-100 µm nozzle on the AriaII-SORP Cellsorter (Becton Dickinson). The cells were filtered and stained with DAPI to facilitate live and dead cell sorting. Cells containing crystals have higher side light scattering pattern and this was used as a gating constraint to sort them from the crystal free *Sf9* cells. Cells were sorted into 15 ml falcon tubes containing SF900II media and stained with tryphan blue to enable visualization in subsequent steps. Cells were concentrated by centrifugation to 10^7 cells/ml and 0.5 µl was directly pipetted onto MiTeGen micromeshes (700/25). Excess liquid was blotted, and the grids were flash-cooled in liquid nitrogen and later mounted at synchrotron beamline (SLS, PSI) to collect diffraction *in cellulo*. Some grids were also prepared with 50% ethylene glycol as cryoprotectant.

2.3.10 Electron Microscopy

Electron microscopy uses electromagnetic lenses to focus high-velocity electron beam to provide a high-resolution 3D structural model of biological macromolecular complexes. In Transmission electron microscopy (TEM), the beam of electrons emitted from a filament are accelerated in an electric field, focused by condenser lens onto the specimen under a high vacuum system. EM images are 2D projections which are combined along different directions to construct a 3D structure. Biological samples are inherently complicated as they are composed of aqueous media which is not suitable for vacuum conditions and weakly diffracting elements (C, N, O, H) providing low contrast (Y. Wang & Wang, 2015). The vacuum system causes dehydration of biological samples affecting their structural integrity (Yifan, 2018). To overcome these difficulties, two methods are commonly used namely negative staining and cryo electron microscopy.

2.3.10.1 Negative staining

Heavy metal salts such uranyl formate or uranyl acetate are used to preserve and improve contrast for biological samples. The resolution obtained from the method is on the lower range around 20 Å (Y. Wang & Wang, 2015). In order to achieve a high-resolution structure, cryoEM is the method of choice currently employed. Negative staining is usually employed as

the first step to examine the sample quality at room temperature. This is crucial in case of protein samples to detect heterogeneity or aggregation. In addition, it provides an estimate of the possible concentration/dilution needed to prepare cryoEM grids in the next step and in certain cases, also be used to optimize buffer conditions.

Negative stain grids for L-CRY, P-CRY PHR and P-CRY cctail were prepared by applying 4.5 µl of the sample on glow discharged Quantifoil holey carbon grids (Cu R2/1 + 2nm carbon, 200 mesh). The hole size on the grid is 2 µm with 1 µm spacing. The sample was incubated for 1 min blotted with the help of Whatman paper. The grids were washed thrice with 20 µl sample buffer and blotted to remove excess liquid. Staining was carried out by briefly dipping the grids in two droplets of 20 µl uranyl formate (stock solution 0.75% (w/v) in water). Excess stain was carefully removed using Whatman filter paper, and the grids were air-dried and stored in the grid box for measurement. The entire fixation was done under red light conditions for all constructs. The dilutions prepared and screened for each construct is as described in Table 34.

Table 34: Samples prepared for negative stain screening

Sample	Concentration	Buffer	Dilution	No of grids prepared
L-CRY	7 mg/ml	25 mM Bis Tris propane pH 8.0, 150 mM NaCl, 1mM TCEP	1:100 1:250 1:500 1:1000 1:2000	1 1 1 1 4
P-CRY PHR	5 mg/ml	25 mM Bis Tris propane pH 9.0, 150 mM NaCl, 1mM TCEP	1:100 1:250 1:500	1 1 4
P-CRY cctail	7 mg/ml	25 mM Bis Tris propane pH 8.0, 150 mM NaCl, 1mM TCEP	1:100 1:250 1:500 1:2000	1 1 1 3

JEOL JEM-2200 FS electron microscope operating at 200 kV was used for screening and data collection. Specimen quartet holder EM-01070SQH (JEOL) was used for inserting the sample grid and the images were recorded manually with a 4k x 4k CMOS F416 (TVIPS) detector. The

software EMMENU-2 (TVIPS) was used to control the camera. The sample grid was placed on high tilt specimen retainer EM-21311HTR (JEOL) inserted with a side-entry EM-21010 SCSH holder (JEOL) for data acquisition. The software SerialEM was used for sample screening and acquisition (Mastronarde, 2005).

2.3.10.2 Transmission electron cryo-microscopy (cryoEM)

Sample is applied to grid covered with a thin layer of carbon holey film, blotted to remove excess liquid, and rapidly embedded in a layer of vitreous ice using liquid ethane cooled by liquid nitrogen. This causes the freezing of the molecules into a thin layer of amorphous ice embedded in random orientations. The measurement is done at low temperatures (~90 K) using liquid nitrogen to keep the sample intact in a hydrated state. Low doses of electron exposure are used to prevent radiation damage of the sample. A large number of micrographs are collected to improve the signal-to-noise ratio and to provide different views for 3D reconstruction. This method is now commonly known as single-particle cryoEM (Jonic & Vénien-Bryan, 2009).

CryoEM grids were prepared by applying the protein sample on freshly glow-discharged carbon/gold grids (Quantifoil R1.2/1.3 , 400 or UltrAufoil R1.2/R1.3 400 mesh grids). The grids were glow-discharged for 30s using Baltec MED-020. The Leica EM GP2 plunge freezer was used. The chamber for the ethane pot was cooled with liquid nitrogen at -180 ^{o}C and filled with liquid ethane. The blotting chamber was maintained at 6 ^{o}C with close to 90% humidity (set value 99%). 4.5 µl of sample (L-CRY 7 mg/ml, diluted 1:10) was applied on the grid and blotted using Whatman No 2 filter (fresh for every 4 grids) . Different blotting times as described in Table 35 were tested. The grids were later plunge-frozen in liquid ethane and stored in 4-slot grid boxes for future screening and measurement.

Table 35: Grids prepared for cryoEM of L-CRY

Grid type	Concentration	Buffer	Blotting time	No of grids prepared
Quantifoil R1.2/R1.3	7 mg/ml	25 mM Bis Tris propane pH 8.0, 150 mM NaCl, 1mM TCEP	0.5 s 1.0 s 1.5 s 2.0 s	1 1 1 1
UltrAufoil R1.2/R1.3	7 mg/ml	25 mM Bis Tris propane pH 8.0,	0.5 s 1.0 s	1 1

		150 mM NaCl, 1mM TCEP	1.5 s 2.0 s	1 1

The grids were screened at low-dose conditions using Titan Krios G2 operating at 300 kV equipped with a field emission gun (FEG). Images were recorded with a 4k x 4k Falcon II direct detection camera. The software Leginon was used for sample screening (Suloway et al., 2005). In-house grid screening and data collection was carried out to determine the overall ice thickness and to ascertain the quality of different blotting conditions used as mentioned in Table 35. Promising grids were used to acquire preliminary dataset for high-resolution measurements and preserved for further high-quality data acquisition at ESRF.

2.3.11 Protein pull-down

Protein pull-down assays are an *in vitro* technique for determining the physical interaction between proteins. They are in principle similar to immunoprecipitation experiments, however, lacking antibodies. In this study, protein pull-downs were used for initial identification of previously unknown protein-protein interactions. Pull-down with recombinantly purified protein was later done to test for the direct interaction between the identified candidates and L-CRY described in 2.3.14. The method is an extension of an affinity-based purification, wherein a tagged bait coupled to beads is used to draw out putative prey interactors from a mixture of potential candidates. The protein-protein complexes thus formed are eventually eluted by appropriate buffers, visualized on a polyacrylamide gels and identified/confirmed with mass spectrometry.

2.3.11.1 Pull-down of L-CRY interactors for mass spectrometry

L-CRY was studied as a potential moonlight receptor and hence to explore into the possible interactors for this receptor, a pull-down approach coupled with mass spectrometry was employed. Pre-purified L-CRY with N-terminal His_6 tag was bound to magnetic nickel beads. 20 frozen worm heads (ZT20) from new moon phase were resuspended in buffer (50mM Tris pH 7.5, 150 mM NaCl, 2.5 mM $MgCl_2$, 1% Triton X, 1mM phenylmethylsulfonyl fluoride, benzonase and cOmplete™ EDTA-free protease inhibitor cocktail tablets) and lysed by sonication. The tubes were wrapped with aluminum foil and the pull-down experiment was done under red light (for dark state interactors). The light state pull-down was done with worm heads from ZT8. The tubes were constantly illuminated with blue-light LED plate (410

nm, 1 mW/cm^2 at 10 cm) at approximate distance 5-6 cm (for light state interactors). L-CRY bound to magnetic nickel beads was used as bait (sample) and empty nickel beads as control. The worm head lysate was incubated with magnetic nickel beads (sample and control) for 3 h at 4°C on rotation. The beads were washed thrice with resuspension buffer (without 1% Triton X) and finally eluted with Lithium Dodecyl Sulfate (LDS) buffer at 70°C for 10 min.

2.3.11.2 Pull-down of P-CRY interactors for mass spectrometry

For identifying P-CRY interactors, P-CRY cctail (200-778) was coupled with nickel beads and used a bait while P-CRY PHR coupled beads were considered as control. Lysate from 20 frozen worm heads of the new moon phase (ZT20) were used and the same protocol as in 2.3.11.2 for dark state interactors was carried out in natural light conditions/dark with the tubes covered with aluminum foil.

2.3.12 Sample preparation for mass spectrometry

Quantitative mass spectrometry is useful when two or more conditions are studied for comparison. Most methods are based on stable isotope labelling wherein specific mass tags are added to proteins that provides the basis for quantification (Bantscheff et al., 2007). In this study quantitative mass-spectrometry was carried out with dimethyl labelling as metabolic labelling was not feasible with marine worms. The samples from protein pull down experiments were processed as described below. The elutions from 2.3.11.1 and 2.3.11.2 were loaded on NuPAGE 4-12% Bis-Tris commercial gels, excised and prepared for in-gel digestion and dimethyl labelling.

2.3.12.1 In-gel digestion

Each sample gel lane was cut into 1 x 1 mm pieces, transferred into 96 well plate placed on deep well plate to collect flow through . 200 µl of destaining solution (25 mM ammonium bi-carbonate , 50% ethanol) was used for destaining at 37 ^{o}C, 15 min shaking at 300 RPM for several times until the gel was destained. The liquid was spun down at 300 x g , 1 min after every exchange. The gel was dehydrated in 2x 170 µl of 100% acetonitrile (ACN) solution for 10 min at 25 ^{o}C on a shaker. The liquid was spun down at 300 x g , 2 min. The gel pieces were covered in 150 µl reduction buffer (10 mM DTT in 50 mM ammonium bi-carbonate) and incubated for 60 min at 56 ^{o}C (without the deep well plate and with lid put on top) for rehydration and reduction. Centrifuge with the deep well plate at 300 x g , 2 min. 150 µl of

alkylation buffer (50 mM iodoacetamide in 50 mM ammonium bi-carbonate) was added and the plate incubated in dark for 45 min at RT. The liquid was spun down, and the gel pieces washed with 180 µl of digestion buffer (50 mM Triethylammonium bicarbonate pH 8.0) for 20 min, 300 RPM at 25 ^{o}C. Liquid was spun down and dehydration was carried out twice with 170 µl of 100% ACN for 10 min at 25 ^{o}C on a shaker until the gel pieces were hard and white. The plate was centrifuged, and the samples dried ay 37 ^{o}C until the membrane turned white. Rehydration was done with 160 µl trypsin solution (1000 ng/sample). The 96 well plate was kept on a fresh deep well block to be used for peptide extraction the next day. The plates were incubated overnight at 37 ^{o}C in an incubator. The supernatant of the trypsin digest was recovered by centrifugation at 300 x g, 2 min. The peptides were extracted thrice with 150 µl extraction buffer (30% ACN) for 15 min at 25 ^{o}C, shaking at 300 RPM. The supernatant was spun down after each extraction. The gel pieces were dehydrated twice with 100 µl 100% ACN for 10 min, 25 ^{o}C, shaking at 300 RPM. Supernatant was spun down, and all peptide solution was transferred into labelled Eppendorf tubes to be dried using a Speed-vac until 100 - 200 µl final volume.

2.3.12.2 Dimethyl labelling

The experiment in 2.3.11.1/2.3.11.2 were done in 2 replicates. Each sample and control elution are then used for labelling the digested peptides with a heavy and light label (forward experiment) and with switching the label (reverse experiment). After extraction of peptides in 2.3.12.1, the pipetting scheme mentioned in table 36 was used.

Table 36: Pipetting scheme for dimethyl labelling

Labelling	Solution A	Solution B	Reaction scheme
LIGHT	**4 µL of 4% formaldehyde**	**4 µL of 0.6 M $NaBH_3CN$**	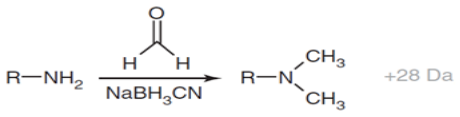
HEAVY	**4 µL of 4% formaldehyde-d2**	**4 µL of 0.6 M $NaBH_3CN$**	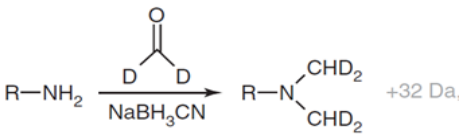

The samples were incubated for 2 h at 20 ^{o}C on a shaker (200 – 300 RPM) in the fume hood. Quenching was done with 16 µl of 1% ammonia solution. The samples were mixed briefly, spun down, and put-on ice. 4 µl of formic acid was added to further quench and acidify the sample. The light and heavy labelled samples were mixed 1:1 and finally stage tipped.

2 layers of Empore C18 material were used to prepare desalting tips. 50 µl of methanol was used to activate the material by spinning it at 500 x g, 5 min. 50 µl of buffer B (80% ACN, 0.1% formic acid) was added and spun down at 500 x g, 5 min. A second wash with 50 µl of buffer A (0.1% formic acid), 500 x g , 5 min was carried out. The samples after dimethyl labelling were added to the tips and centrifuged 500 x g, 10 min. 50 µl of buffer A used as wash with 500 x g , 2 min. Finally, the peptides were eluted with 30 µl of buffer B and carried out by the IMB Proteomics core facility before applying the samples on the mass spectrometer.

2.3.13 Mass spectrometry

Mass spectrometry (MS) is a high-throughput method used for protein characterization. The proteins are digested into peptides, separated, fragmented, ionized and analyzed to determine the identity and molecular mass of proteins. This is done by measuring the mass-to-charge ratio of peptide fragment ions. Protein identification is carried out by database search approaches (P. Wang & Wilson, 2013). The proteins in the sample solution are ionized using the electrospray ionization method and passed through a mass analyzer such as quadrupole-orbitrap to obtain the peptide mass fingerprint. In case of protein identification, MS/MS approach is applied to further fragment specific peptide ions along peptide bonds to obtain sequence level information. All samples were processed by the IMB Proteomics core facility.

Q Exactive Plus (ThermoFisher Scientific, Germany) was used for all mass spectrometry experiments. Stable-isotope dimethyl labeling was used for quantitative proteomics. The MaxQuant (Version 1.5.2.8) (Cox & Mann, 2008; J. L. Hsu et al., 2003; Team, 2016) was used for data analysis with default settings, except re-quantify was activated against the Uniport database Platynereis_dumerilli_(CLAMWORM)_Uniport_20190116.fasta and the in-house generated worm head database Pdu_HeadRef_Prot_v4.fasta (Schenk et al., 2019). The output was further filtered by removing known contaminants, reverse data base binders and proteins

only identified by site modification. We also filtered for minimum 2 peptides (minimum 1 unique) per protein group.

2.3.14 Confirmation of direct protein interaction

The potential candidates identified and selected from 2.3.11.1 were recombinantly expressed and purified to confirm for direct interaction with L-CRY. For this purpose, the tag on the ligands was kept whereas the N-terminal His_6 tag of L-CRY was cleaved. Magnetic nickel/GST beads were used to bind the ligand, extensively washed with appropriate buffers, and later incubated with L-CRY for 1 h on rotation at 4^oC. The beads were washed thrice to remove excess unbound protein and eluted in LDS buffer by heating at 70°C for 10 min.

3 Results

3.1 L-CRY

L-CRY, one of the three known cryptochromes in *Platynereis,* is 45% identical to dCRY at the sequence level and most of this homology lies within the photolyase homology region. A sequence alignment of the two cryptochromes highlights the regions of differences amongst them (Fig. 16). Notably, the N-terminal and C-terminal extensions present in L-CRY are of about 27 and 14 amino acids, respectively. In addition, several residues present in the protrusion loop of dCRY (F288-A306) are missing in L-CRY. The protrusion loop together with the phosphate binding loop is known to constrict FAD access and are in the environment of FAD (Czarna et al., 2013; Kenichi Hitomi et al., 2009; N. Liu & Zhang, 2016). This already provides an initial indication towards a possibly different functional specialization of L-CRY. Another striking distinction is the abundance of cysteine residues in L-CRY. L-CRY contains 22 cysteines which is double the number present in dCRY. Since *Platynereis* aligns its maturation and spawning behavior with low intensity moonlight, it was intriguing to notice the presence of tyrosine residue (Y353) corresponding to Y319 in CRY4 of pigeon. This surface tyrosine is thought to impart low-light sensitivity in night migratory animals (Zoltowski et al., 2019). Several other similarities and differences are mentioned in Table 37.

Table 37: Notable similarities and distinctions between dCRY and L-CRY at sequence level

FEATURE	dCRY	L-CRY	CONSENSUS
TRP TRIAD	W342 W397 W420	W351 W405 W428	CONSERVED
SURFACE TYROSINE CORRESPONDING PIGEON CRY4(Y319)	ABSENT	Y352	A343 in dCRY
ANTENNA RECOGNITION LOOP	F42-Y54	W66-Y78	SIMILAR
PHOSPHATE BINDING LOOP	E246-M266	K263-M283	SIMILAR
PROTRUSION LOOP	F288-A306	Y305-G315	SEVERAL MISSING RESIDUES IN L-CRY
SULFUR LOOP	M331-C337	M340-C346	CONSERVED
C-TERMINAL LID	S426-P440	S434-P448	SIMILAR
PHOTLYASE HOMOLOGY REGION	R4-K510	S34-K523	
FAD BINDING REGION	G310-K510	A319-K523	
Residues in vicinity to FAD in dCRY structure and corresponding residues in L-CRY	H378 R381 D410 C416 N419 W420 W536	H386 R389 D418 C424 N427 W428 W547	
TAIL	C523-V542	C534-Y566	L-CRY HAS EXTENDED TAIL

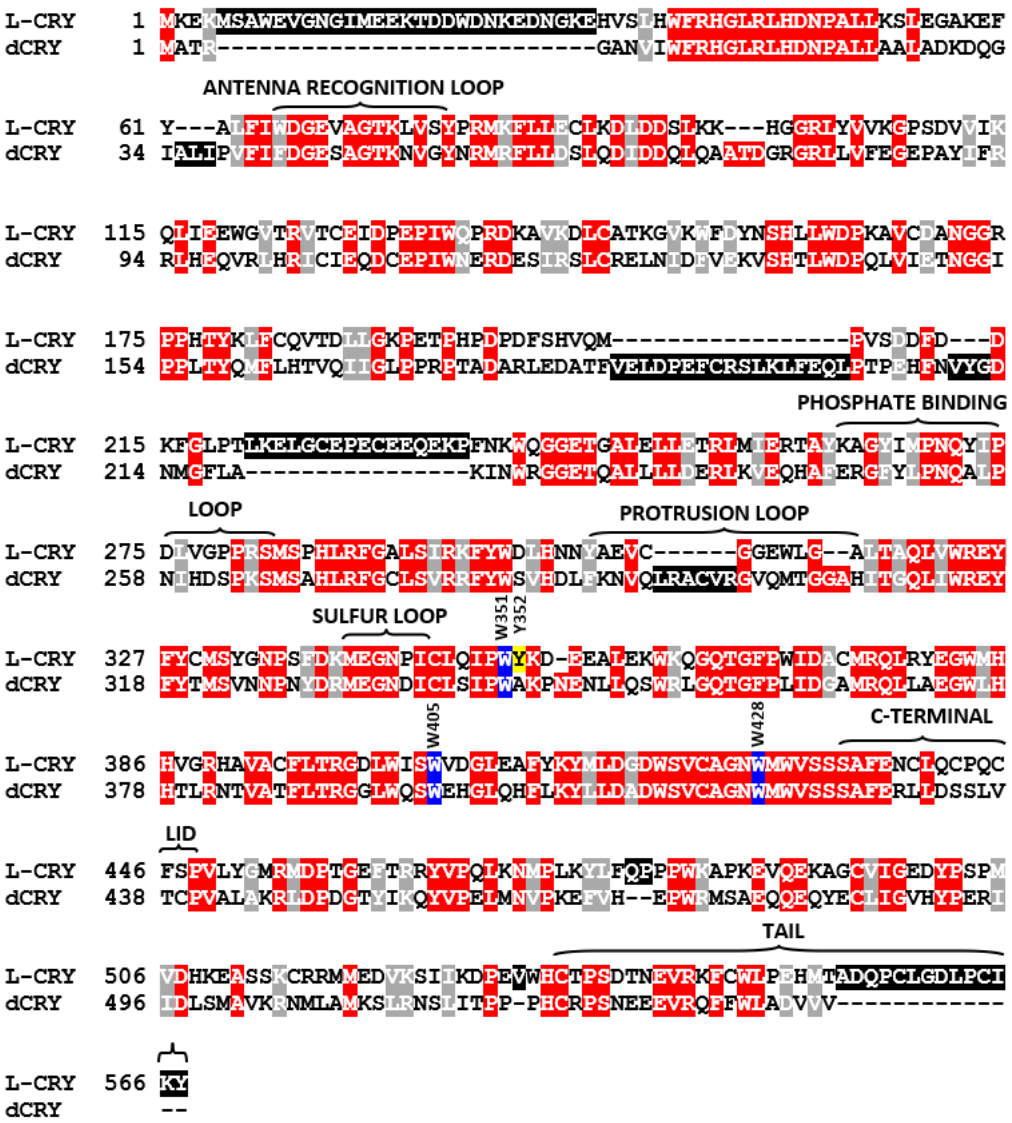

Figure 16: Sequence alignment between dCRY and homologous L-CRY generated using multiple sequence alignment tool T-Coffee (Notredame et al., 2000)*. Conserved residues are highlighted in red, similar residues in grey and the additional residues in black respectively. The tryptophan triad is marked in blue. The Tyrosine (Y352) corresponding to the pigeon CRY4 Y319 contributing to low-light sensitivity is marked in yellow.*

3.1.1 Recombinant expression and purification of L-CRY and L-CRY truncations in insect cells

L-CRY full length was cloned into pCoofy27 vector and thus expressed and purified from insect cells as a N-terminal His_6-tagged fusion protein. The P1 virus obtained after bacmid transfection and virus amplification was used to infect 1.2 L of 1 x 10^6 *Sf9* cells for 72 h. L-CRY was purified by a 3-step purification protocol. To maintain the dark state of the cryptochrome throughout the purification, all steps were carried out with minimum light exposure or in red

light. The first step after cell lysis (2.3.2.2) was an IMAC with nickel column wherein step elution was carried out (Table 24). The wash steps with 5-10% imidazole was necessary to get rid of several contaminants. The theoretical molecular weight of L-CRY is 67.7 kDa and L-CRY eluted with 250 mM imidazole. The elution fractions were pooled and concentrated to 10 ml volume. This was diluted 10-fold with low salt buffer and applied to an anion-exchange chromatography column (Table 30). Fractions eluting with 240-300 mM NaCl contained the L-CRY. All fractions containing the protein were pooled and applied to a S200 16/60 size exclusion column for a final polishing step (Table 33). No peak with 450 nm absorbance corresponding to free flavin was observed at later elution volumes indicating all flavin was bound to L-CRY. The SDS-PAGE analysis indicated that the purity of purified L-CRY was greater than 90% (Fig. 17A). Using band identification by trypsin digestion followed by mass spectrometry, it was confirmed that the indicated band was indeed L-CRY. The absorbance at 450 nm corresponding the L-CRY peak and yellow elution fractions indicated the presence of flavin (Fig. 17C). The 450 nm absorbance was used in later purifications for the selection of L-CRY containing fractions after IMAC and anion-exchange chromatographic steps. Thus, avoiding the need to carry out SDS-PAGE analysis after every purification step. 20 g of *Sf9* cells yielded 2 mg of pure L-CRY. Purified L-CRY run on an analytical S200 10/300 elutes at a volume of 13.9 ml (Fig. 17B). Thus, L-CRY was purified as a dimer in solution based on the molecular weight calibration for the column. On a 4-15% native gel, it was observed that L-CRY ran between the protein markers of 66 kDa and 146 kDa indicating a dimeric state. The protein when activated by blue-light and run under similar conditions was seen to form additional bands indicating the occurrence of photo-oligomerization (Fig. 17D).

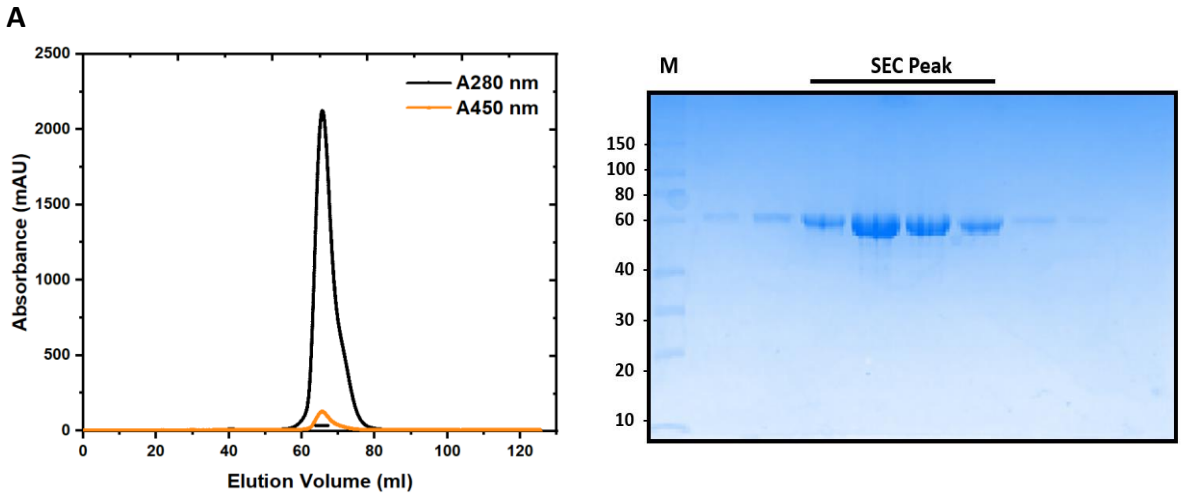

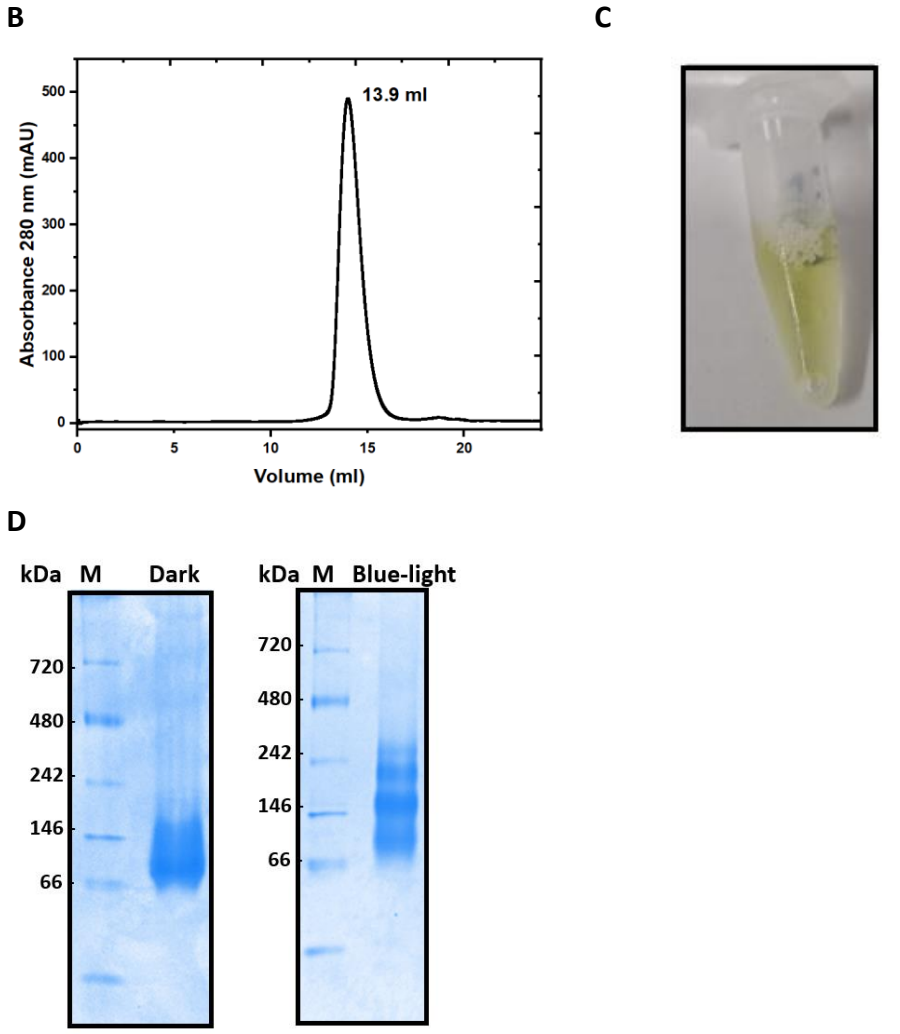

Figure 17: Size exclusion chromatography of L-CRY FL purified from Sf9 cells. A) SEC profile and corresponding 10% Bis-Tris gel depicting His_6-tagged L-CRY purified using S200 16/60 column B) The elution profile of L-CRY on S200 10/300 column in dark/red light conditions. Elution volumes and corresponding molecular weight of calibration standards: 10.3 ml – 670 kDa (Thyroglobulin), 13.67 ml – 158 kDa (γ-globulin), 15.71 ml – 44 kDa (ovalbumin), 17.42 ml – 17 kDa (myoglobin) and 20.11 ml – 1350 Da (vitamin B12). C) Purified L-CRY with bound FAD which imparts yellow color to the protein. D) Native gel electrophoresis of L-CRY in dark and blue-light conditions depicts the running behavior of L-CRY as a dimer in the dark and the formation of oligomers under blue light conditions.

In contrast to L-CRY, dCRY was purified as a monomer in solution (Berndt et al., 2007). However, plant cryptochromes such as *At*CRYs are known to form active homodimers, which is also required for their photoreceptor activity (Sang et al., 2005). Several studies established that cryptochrome dimerization is also essential for its biological functioning (Rosenfeldt et al., 2008). It was shown before for AtCRY2 using SEC-MALS that light stimulation led to robust

homo-oligomerization (Hallett et al., 2016). L-CRY was activated with blue-light for 110s and immediately injected onto a S200 10/300 column. To avoid or reduce the reversal back to the dark state, the analytical SEC was carried out in light conditions. The photo oligomerization seen on the native gels was not observed and a similar AtCRY2 blue-light induced shift in the elution volume was not observed for L-CRY in our setup (Fig. 18). Neither did the dimeric state of L-CRY fall apart.

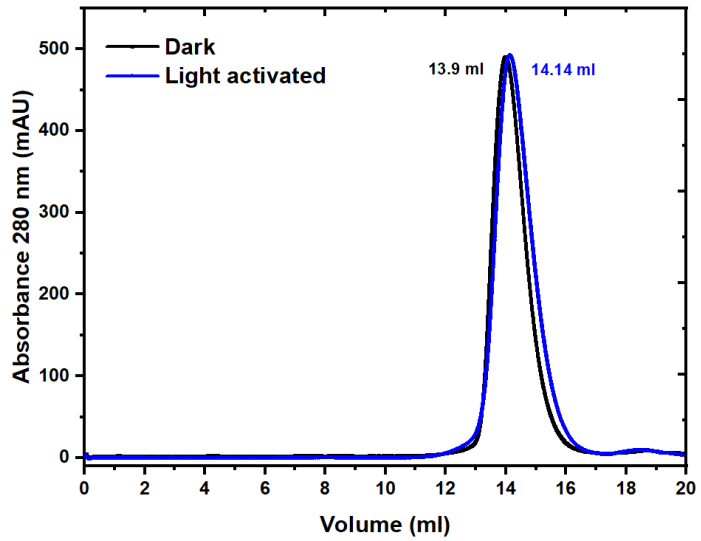

Figure 18 : The elution profile of L-CRY on S200 10/300 column in dark and light conditions. Elution volumes and corresponding molecular weight of calibration standards: 10.3 ml – 670 kDa (Thyroglobulin), 13.67 ml – 158 kDa (γ-globulin), 15.71 ml – 44 kDa (ovalbumin), 17.42 ml – 17 kDa (myoglobin) and 20.11 ml – 1350 Da (vitamin B12).

To facilitate crystallization attempts, the two truncations of L-CRY, namely, L-CRY (K30-Y567) and L-CRY (K30-T553) were designed based on the comparative dCRY alignment in Fig 16. These constructs were also purified using the same protocol as L-CRY FL. In general, the full-length construct behaved much better on the SEC column. Also, L-CRY full length was of higher quality in terms of purity as seen on the SDS-PAGE (Fig. 19A, 19B).

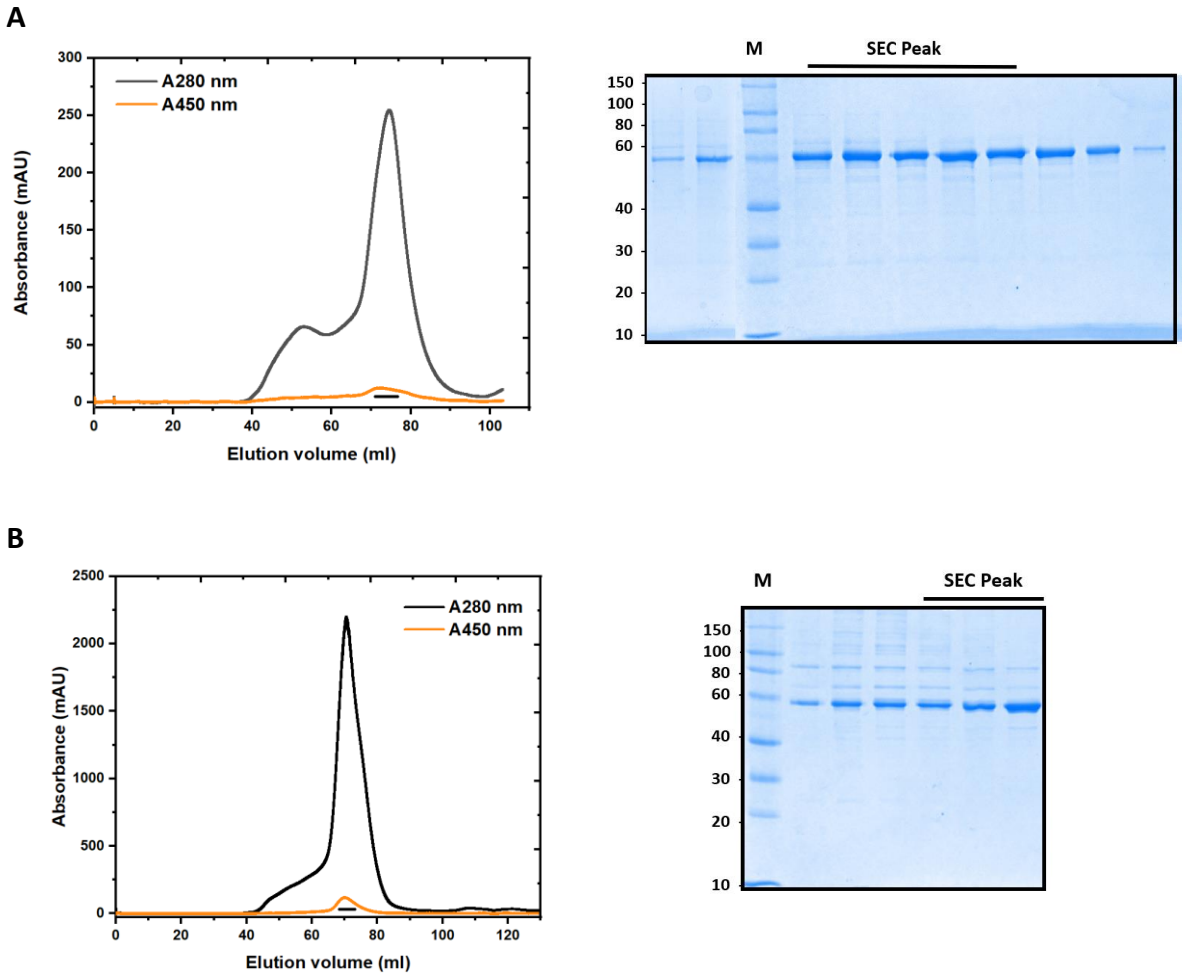

Figure 19 : Size exclusion chromatography of L-CRY variants from Sf9 cells. A) SEC profile and corresponding 10% Bis-Tris gel depicting His_6-tagged L-CRY (K30-Y567) purified using S200 column 16/60 column B) SEC profile and corresponding 10% Bis-Tris gel depicting His_6-tagged L-CRY (K30-T553) purified using S200 column 16/60 column. Bar at the bottom of peak corresponds to the fractions on the SDS-PAGE labelled as SEC peak. M: protein marker in kDa.

3.1.2 Chromophore content of L-CRY using HPLC

Cryptochromes are long known to be flavoproteins that can bind additional photoactive molecules. They belong to a superfamily of proteins grouped together with DNA photolyases, which non-covalently bind two cofactors. A N-terminally located chromophore (antenna chromophore) and a C-terminally located flavin adenine dinucleotide (FAD) molecule. Nucleotide-like compounds such as FMN, FAD, 8-hydroxydeazaflavin or a folate such as MTHF are known antenna chromophores that act as the main light-harvesting chromophore (Chaves, Pokorny, et al., 2011; Klar et al., 2006, 2007). Most known cryptochromes share a domain that is highly similar to the chromophore binding domain found in photolyases called

the photolyase homology region (PHR). L-CRY shares 40% sequence identity with dCRY and most of this identity lies within the FAD binding region. To characterize the chromophores bound to L-CRY, the protein was denatured, and the released supernatant was analyzed by RP-HPLC (2.3.7). The chromatogram revealed peak at an elution volume of 4.67 ml when absorbance at 370 nm was monitored (Fig. 20A). For comparison, chromophore standards were run under same conditions (Fig. 20B). From the elution profile based on the distribution behavior of chromophores in the sample, it was evident that FAD was the sole cofactor bound to L-CRY. There were no traces of MTHF or FMN found in the sample.

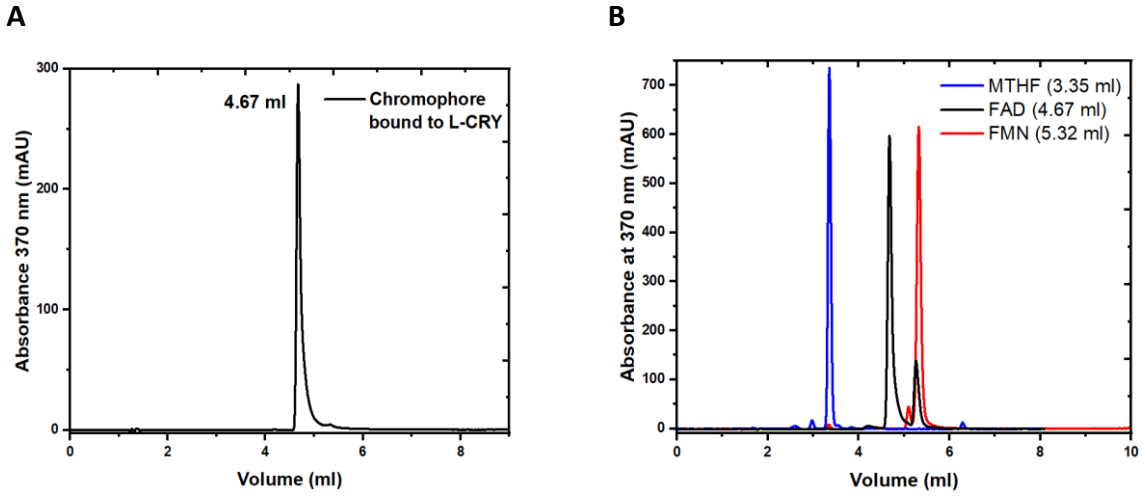

Figure 20: Reverse phase HPLC analysis to identify L-CRY bound chromophore. A) L-CRY bound chromophore obtained after heat denaturation run on Macherey-Nagel C18 Gravity-SB (150/4/5 µm) column. B) Elution profile of standard chromophores FMN, MTHF and FAD run on the same column under similar conditions for comparison.

3.1.3 Spectroscopic characterization of L-CRY

3.1.3.1 UV/VIS Absorbance spectroscopy

With the help of UV/VIS absorbance spectroscopy, it was observed that L-CRY contained bound flavin (Fig. 21A) as seen when compared to the spectrum of free flavin (Fig. 21B). The obtained spectrum is a characteristic of flavoproteins binding either FMN as in the case of LOV/LOV proteins (Kasahara et al., 2010) or FAD as in the dCRY (Berndt et al., 2007; Kutta et al., 2017) . The absorption spectrum of dark-state L-CRY showed several peaks in the UV-A and blue regions with maxima at 359nm, 371nm, 451nm and 475nm (Fig. 21A). On comparison with the absorption spectra of various FAD redox states, the dark spectrum of L-

CRY is consistent with the presence of oxidized FAD (Fig. 21C) (Evans et al., 2013; Worthington et al., 2003). The presence of any secondary chromophore such as MTHF is also negated since the characteristic folate absorbance at 380 nm is not observed (Sancar, 2003).

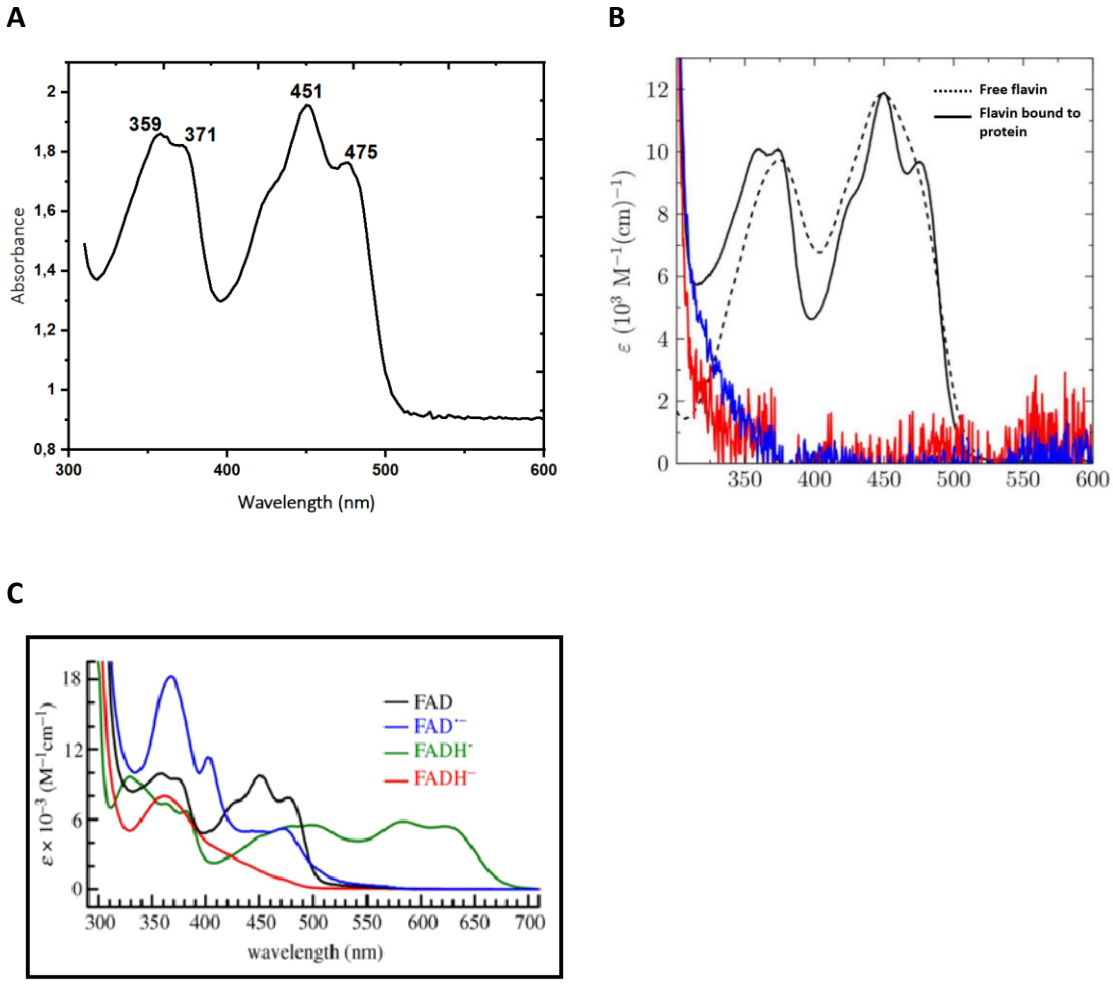

Figure 21: UV-VIS absorption spectroscopy with L-CRY. A) Dark spectrum of L-CRY indicating the presence of bound FAD. B) UV-VIS spectra of free flavin and flavin bound to protein. Figure adapted from Kutta et al. 2017. C) Absorption spectra of different FAD redox states. Figure from Evans et al. 2013.

3.1.3.2 Fluorescence spectroscopy

Fluorescence spectroscopy also confirmed the presence of flavin in purified L-CRY. Flavin chromophores exhibit characteristic emission maxima between 500 - 525 nm and excitation maxima between 370 – 450 nm. L-CRY excitation spectra was recorded with emission at 530 nm and emission spectra with excitation at 450 nm. The presence of flavin was confirmed as excitation maxima at 370 nm and around 450 nm and emission maxima at 530 nm consistent

with FAD were observed in the spectra (Fig. 22). For MTHF detection, emission spectra with excitation at 380 nm was recorded. The emission spectra have a prominent peak at 520 nm. A small peak like feature is observed around 450 – 460 nm, however, this is not as prominent as seen in Vibrio cholerae CRY2 (Worthington et al., 2003). This would also be in line with the lack of any bound MTHF as seen before from RP-HPLC analysis.

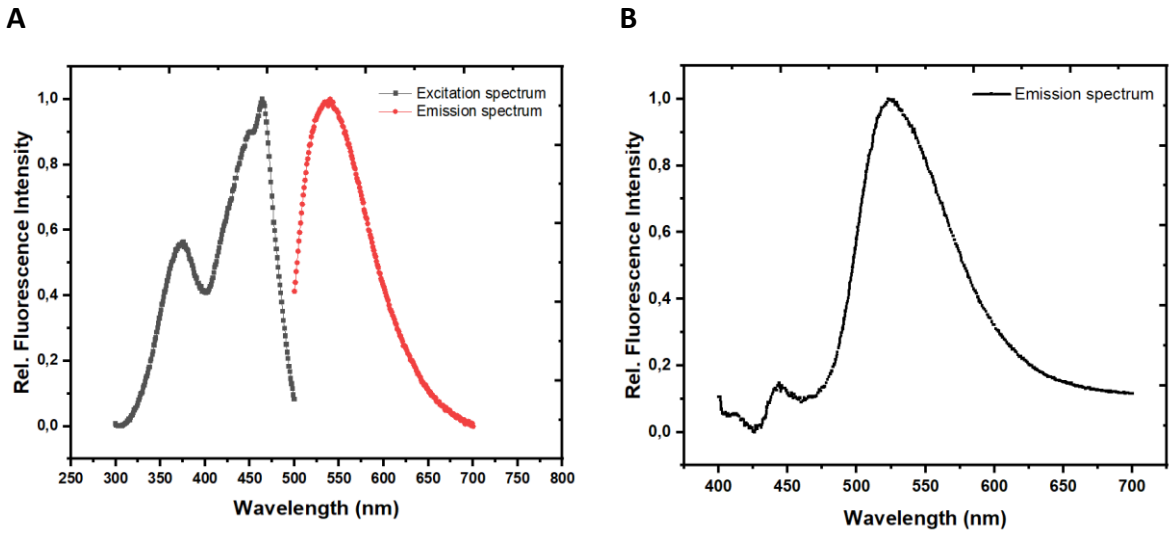

Figure 22: Fluorescence spectroscopic characterization of L-CRY A) Excitation and emission of flavin as seen by the 370 nm and 450 nm peaks in the excitation spectrum and the 520 nm peak in the emission spectrum. B) Emission spectrum of MTHF obtained with excitation at 380 nm shows maxima at 520 nm which is again a confirmation of presence of FAD.

3.1.3.3 CD spectroscopy

Secondary structure prediction with SOPMA (Combet C., Blanchet C., 2000), predicts L-CRY contains 36.58% alpha helix, 12.14% extended strand, 5.64% beta turn and 45.64% random coil. CD spectroscopic measurements and analysis with cdnn software revealed the presence of defined secondary structures 31% helix, 20% beta sheets, 18% beta turns and 30% random coils. This is also reflected in the spectrum (Fig. 23) as α-helical proteins show positive band at 193 nm and negative bands at 208 nm and 222nm (Greenfield, 2007). In comparison to dCRY (45% helix, 37% beta sheet and 18% disordered regions) (Thesis Alexander Berndt), the α-helical content of L-CRY is much lower. No significant secondary structure change was observed in the CD spectrum of light activated L-CRY (not shown). The overall secondary structure content remained the same as well.

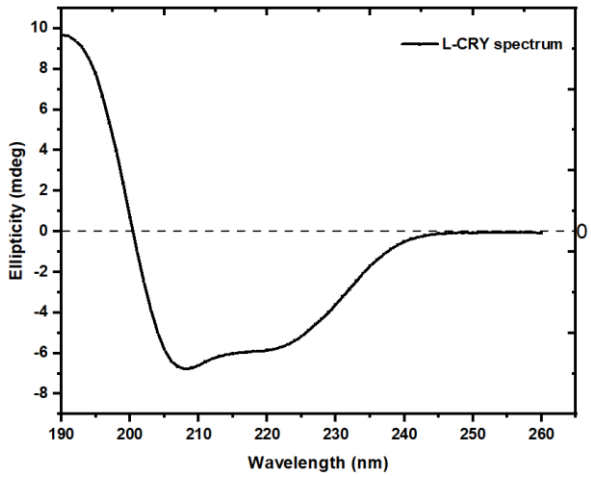

Figure 23: CD spectrum of dark-state L-CRY. The spectrum is buffer subtracted and obtained from combining individual spectra.

3.1.3.4 Photocycle of L-CRY

To analyze its photocycle, L-CRY was photoreduced with a 445 nm emitting blue light LED for 110 s. The light activated spectrum showed that blue-light irradiation of L-CRY leads to the conversion of oxidized FAD into an anionic FAD radical (FAD^{o-}) with characteristic FAD^{o-} absorption maxima at 370 nm and 404 nm and reduced absorbance at 450 nm (Fig. 24A). The reaction scheme for the conversion of oxidized FAD into an anionic FAD radical is represented (Fig. 24B). The absence of prominent features between 550 nm and 700 nm indicates that no neutral $FADH^{o}$ radical is formed. The dark recovery kinetics of oxidized FAD from FAD^{o-} were measured as absorption changes at 450 nm. Fitting a single exponential curve to the experimental data resulted in a time constant of approximately 4 min at 6 ^{o}C (Fig. 24C), which is the time until 1/e (approximately 37%) of the molecules recover back to the dark state. The transition from light activated state back to the dark state was nicely seen with the help of spectra taken at several timepoints using the Tecan plate reader at 18 ^{o}C (Fig. 24D). The time constant of dark recovery for L-CRY was estimated to be about 2 min at 18^{o}C (Fig. 24E). Dark recovery time constant of 4.7 min after blue-light stimulation was calculated for sample kept on ice (Fig. 24F, 24G) for further comparison to recovery constants measured with sample on ice. Altogether, the FAD-dependent photoreaction of L-CRY is similar to that of *Drosophila* cryptochrome (dCRY), suggesting that L-CRY could be a blue-light sensitive photoreceptor regulating the circadian or circalunar clock of *Platynereis dumerilli.*

A

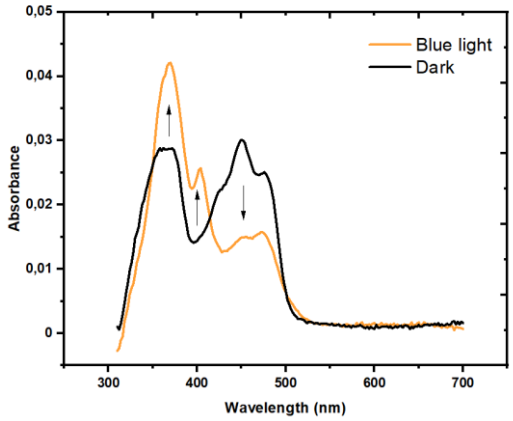
Blue light
Dark
Absorbance
Wavelength (nm)

B

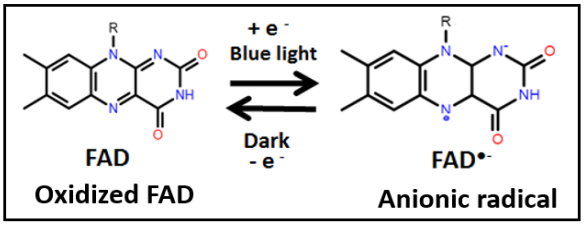
+ e -
Blue light
Dark
- e -
FAD
Oxidized FAD
FAD•-
Anionic radical

C

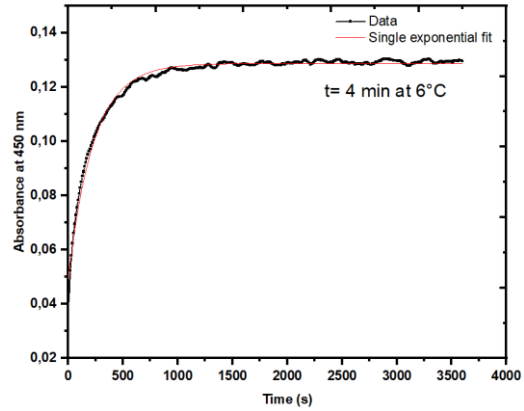
Data
Single exponential fit
t= 4 min at 6°C
Absorbance at 450 nm
Time (s)

D

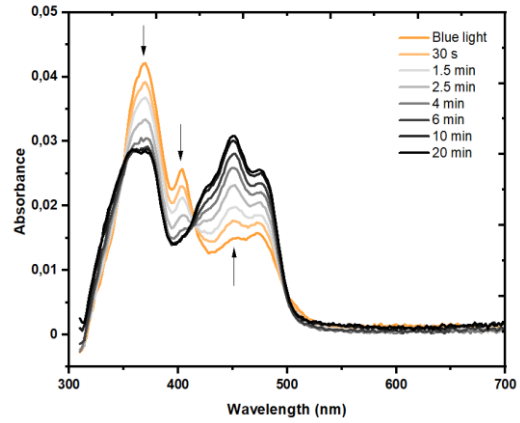
Blue light
30 s
1.5 min
2.5 min
4 min
6 min
10 min
20 min
Absorbance
Wavelength (nm)

E

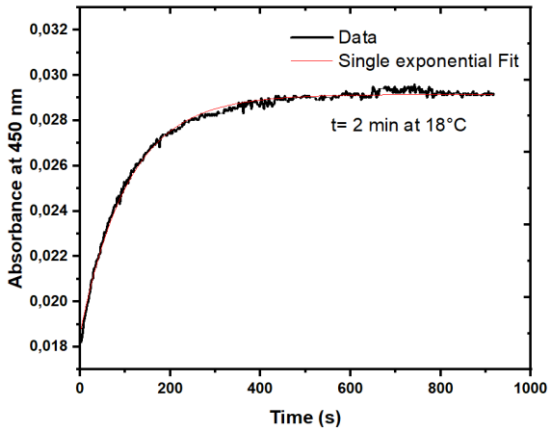
Data
Single exponential Fit
t= 2 min at 18°C
Absorbance at 450 nm
Time (s)

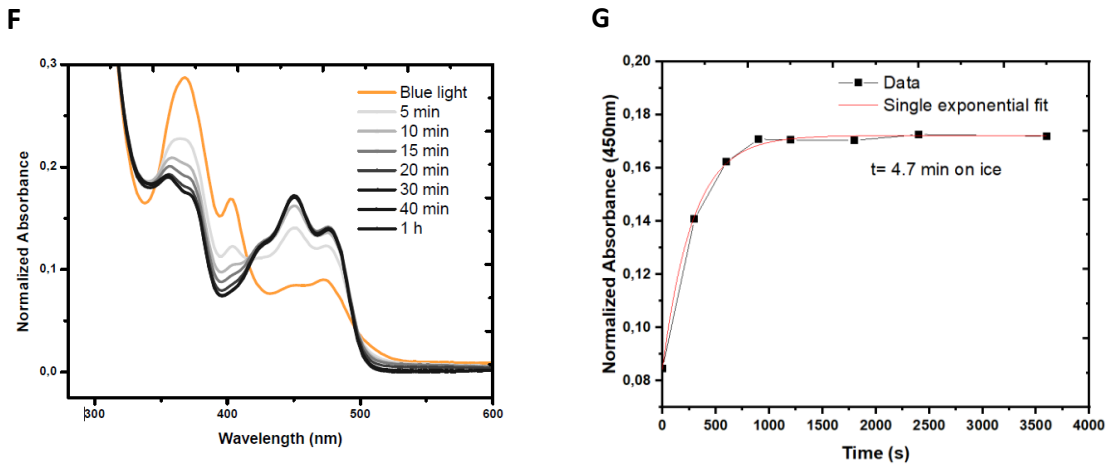

Figure 24: Blue-light response of L-CRY and dark recovery. A) Absorption spectrum of L-CRY in dark and after 110 sec blue-light illumination (λ = 445 nm). Arrows indicate the change in absorbance at 370 nm, 402 nm, and 451 nm between oxidized FAD (dark) and anionic FAD radical (FAD°-) (after blue-light). The blue-light activated spectrum is depicted in orange to indicate that this light source is representative of daylight. The same convention is followed throughout. B) Reaction scheme of conversion from oxidized FAD to anionic FAD radical on blue-light illumination. C) Dark recovery of L-CRY after blue-light illumination monitored by changing absorbance at 450 nm over time at 6°C. A time constant of 4 min was obtained by single exponential decay fit to the data. D) Full spectra of L-CRY at different time points after blue light activation depicting the dark recovery. E) Dark recovery kinetics after blue light illumination monitoring change in absorbance at 450 nm. A time constant of approx. 2 min at 18 ^{o}C was calculated by single exponential fit. F) Full spectra of L-CRY at different time points after blue light activation depicting the dark recovery on ice. G) Dark recovery kinetics on ice following blue-light stimulation obtained from absorbances at 450 nm taken from the full spectra shown in F. A time constant of 4.7 min was calculated.

3.1.3.5 Moonlight response of L-CRY

The absorbance spectrum of L-CRY overlaps with the moonlight spectrum in the habitat of *Platynereis dumerilli* (Fig. 25A). Thus, L-CRY has the spectral sensitivity to sense moonlight. To ascertain if L-CRY would be a potential moonlight receptor, a light source mimicking moonlight (full moon intensity of 2.56*10-8 W/cm2) was used to illuminate L-CRY. Notably, short durations of moonlight exposure did not photoreduce L-CRY and the spectra were similar to the dark state oxidized FAD spectrum (Fig. 25B).

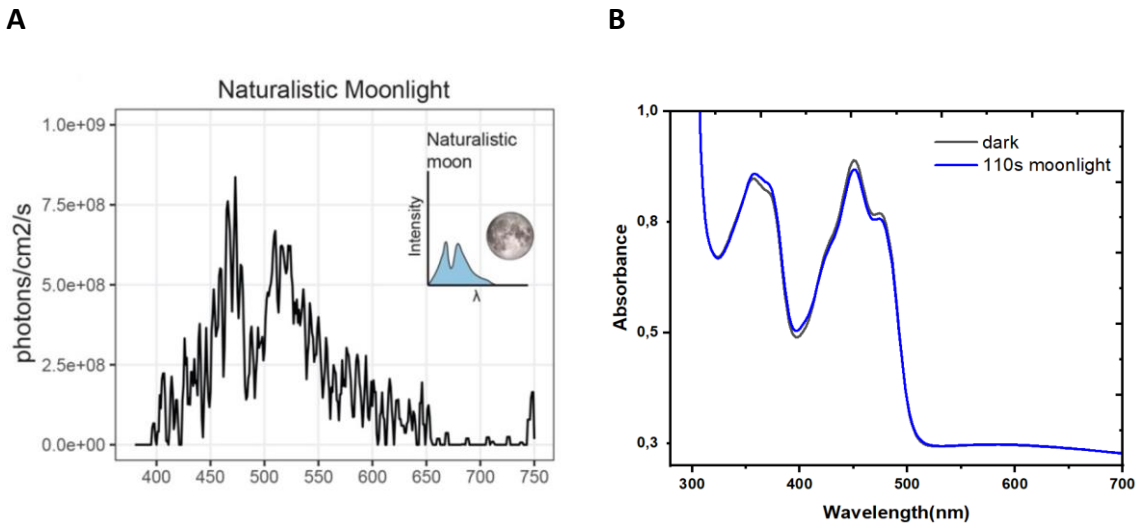

Figure 25: Naturalistic moonlight and response of L-CRY. A) The moonlight source was constructed and supplied by collaborator group. The spectrum shown is provided by them and represents the full moonlight under water in the natural habitat of Platynereis dumerilli. B) Exposure to naturalistic moonlight for short duration of 110s does not lead to photoreduction as seen before with blue-light (Fig. 24A).

Only after continuous moonlight illumination for approximately 3 h, spectral changes begin to appear. Subsequent spectra taken from 4 h to 6 h time intervals indicate the build-up of the moonlight activated state of $FAD^{\circ -}$, as documented by the appearance of a peak at 402 nm and reduction of absorbance at 450 nm (Fig. 26A). L-CRY does not attain the full light activated $FAD^{\circ -}$ state as was observed with blue-light illumination. However, the presence of isosbestic points at 415 nm and 495 nm suggests that the moonlight-induced photoreaction occurs only between two species, i.e., between oxidized FAD (dark) and the anionic $FAD^{\circ -}$ radical (moonlight). L-CRY is able to recover back to the dark state after 6h moonlight activation (Fig. 26B). The dark recovery of L-CRY after 6 h moonlight exposure (full spectra shown in Fig. 26C) resulted in a time constant of 6.7 min at 18°C (Fig. 26D).

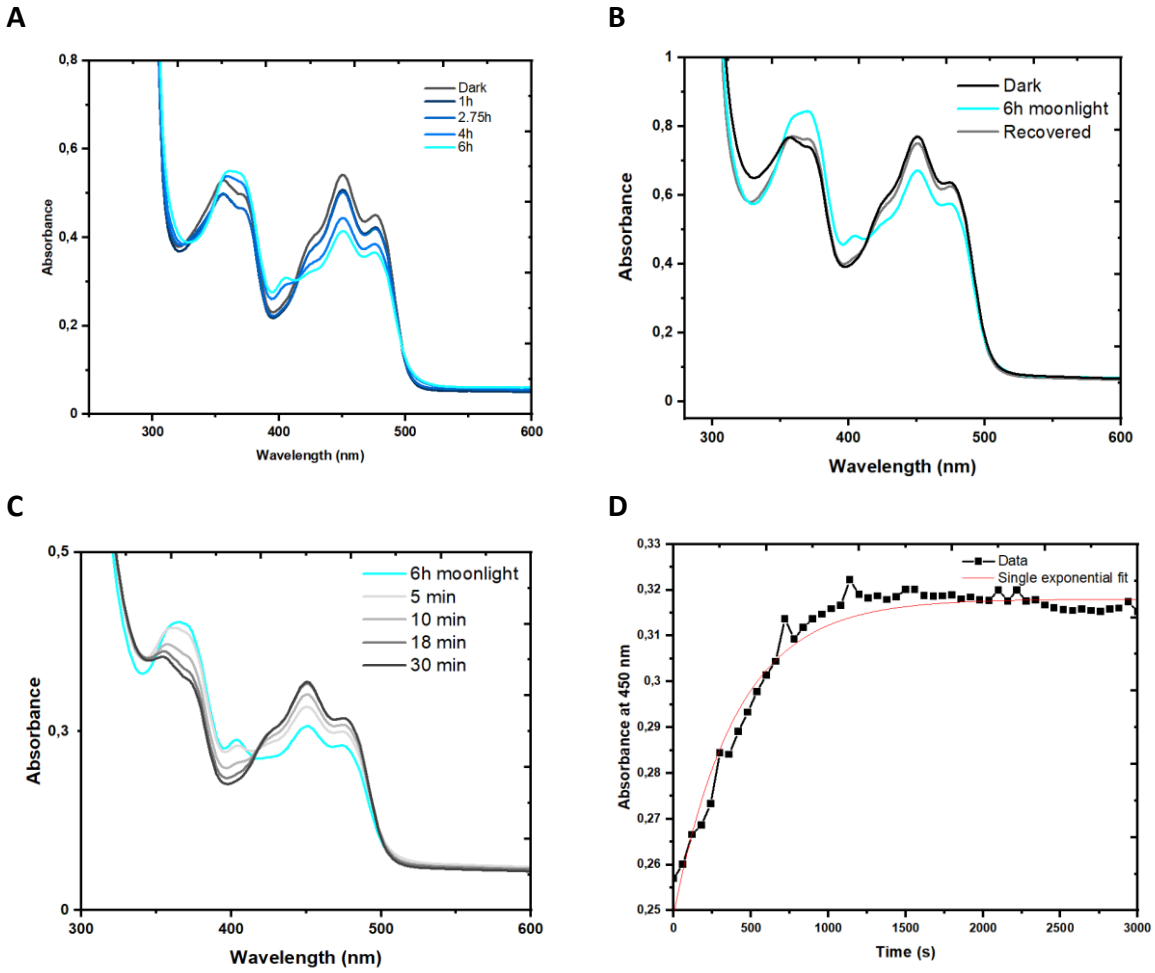

Figure 26: Moonlight response of L-CRY and dark recovery. A) Absorption spectra of L-CRY on continuous illumination with full moon intensity obtained at different time points. The L-CRY spectrum transitions from the dark state (oxidized FAD) towards the light activated FAD°⁻ radical state starting from approximately 3h up to 6h. B) Moonlight activated L-CRY recovers back to the dark state with oxidized FAD ("Dark": dark-adapted L-CRY before 6h moonlight exposure; "Recovered": spectrum after 1 h dark incubation following moonlight exposure). C) Full spectra of L-CRY at different time points taken in dark at 18 °C following activation with 6 h of full moonlight. D) Dark recovery of L-CRY after 6h full moon intensity illumination. Absorbance at 450 nm was obtained from full spectra shown in C. L-CRY recovers with a time constant of 6.7 min at 18°C

Prolonged moonlight illumination up to 9 h did not alter the photoreduced state considerably (Fig. 27). This was also the same after 12h of illumination (not shown).This indicates that partial anionic radical state attained after 6h of moonlight does not proceed further and this state is more or less maintained with prolonged illumination time. The moon is visible in the

sky for theoretically 12 h or more. However, on a full moon day, the moon is visible only at night and duration on an average would be between 8-9h. Thus, L-CRY present in the partial anionic state for prolonged duration of time, would possibly relay a downstream functional signal along with/without other possible factors.

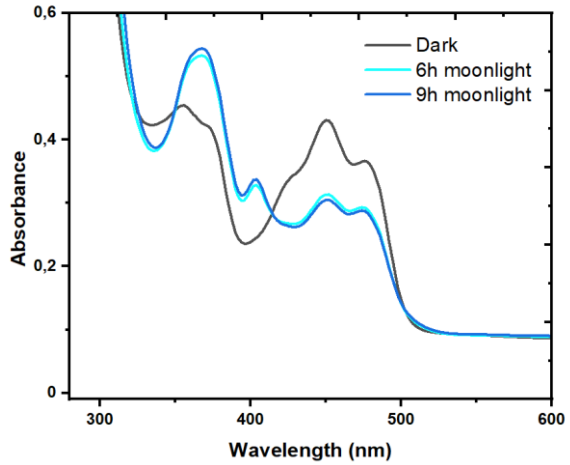

Figure 27: The final moonlight state of L-CRY is maintained upon prolonged moonlight exposure. Continuous illumination of L-CRY with moonlight beyond 6 h up to 9 h did not alter the photoreduced state considerably.

To mimic a day to full-moon night scenario, L-CRY was first photoreduced with blue light for 110 sec, followed by continuous moonlight exposure for 6h (L-CRY protein kept on ice) (Fig. 28A). Interestingly, light-activated L-CRY first returns to the oxidized FAD dark-state within about 30 min of moonlight irradiation with a time constant of approximately 9 min (Fig. 28B, 28C). Hence, the presence of moonlight delays (compared to 4 min time constant for recovery in complete darkness) but does not prevent recovery of the L-CRY dark-state. Subsequently continued moonlight illumination led to the partial conversion of dark-state L-CRY to the intermittent $FAD^{\circ -}$ light state, starting from approximately 3h up to 6h (Fig. 28A), as previously observed (Fig. 26A).

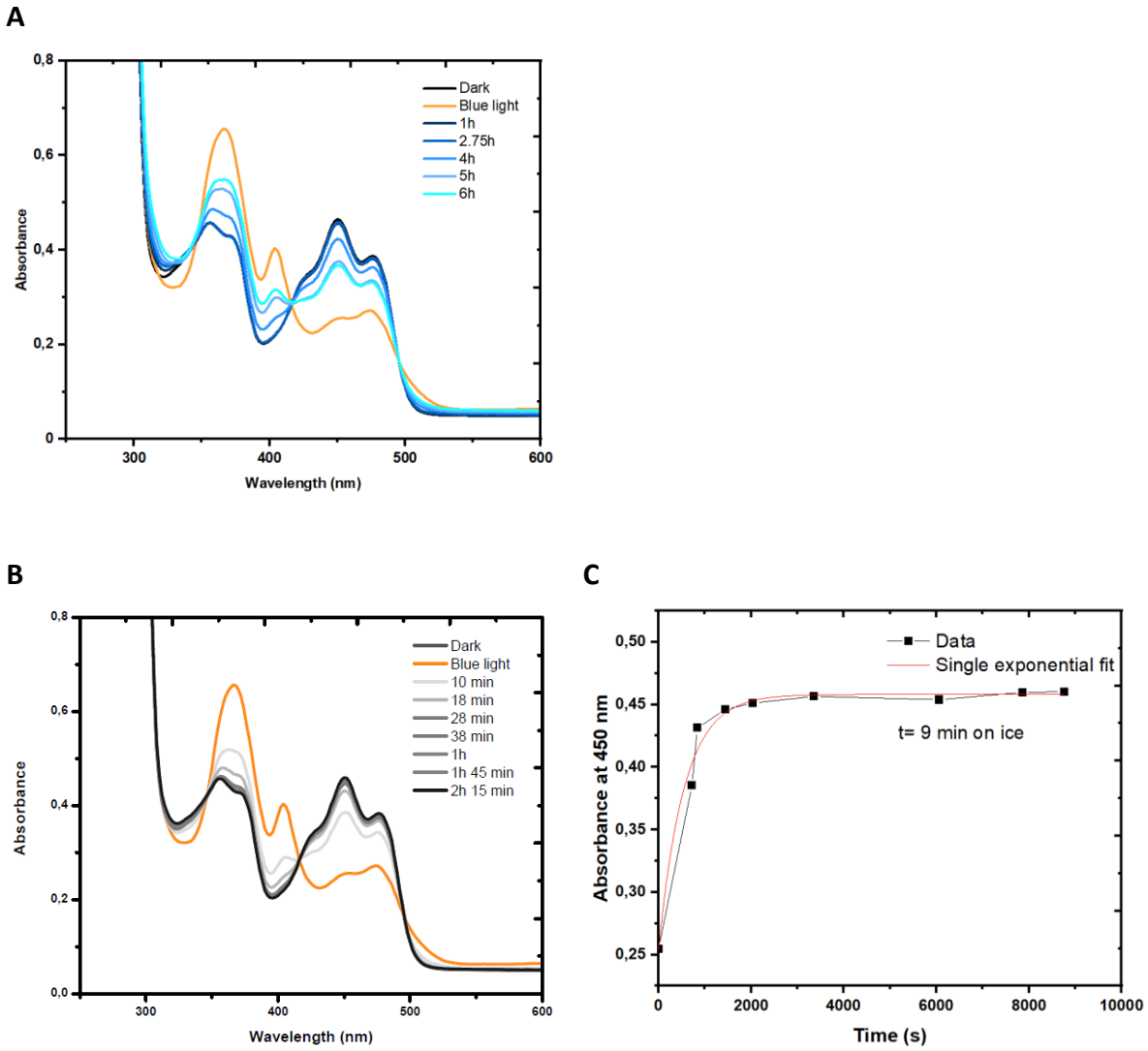

Figure 28: Spectroscopy mimicking daylight to full-moonlight transition (sunset) and recovery kinetics in presence of moonlight A) Dark-adapted L-CRY (dark) was illuminated for 110 sec with blue-light and subsequently exposed to continuous full moonlight for 6 h (1h to 6h spectra). Blue-light activated L-CRY first returns to the dark state (1h, 2:45 h) and then partially transitions to the FAD°⁻ radical state from 4 h up to 6 h moon light exposure. B) Blue-light activated L-CRY first returns to the dark state as seen here. Absorbance values at 450 nm from these full spectra were used for the recovery kinetics shown in C. Continued moonlight illumination beyond 2h 15 min resulted in the moonlight activated state as shown in A. C) Recovery kinetics (time constant approximately 9 min, sample on ice) of oxidized FAD from the blue-light induced anionic FAD°⁻ radical in presence of full-moon irradiation.

To probe if moonlight activated L-CRY could in turn be completely photoreduced mimicking a full-moon night to day scenario, L-CRY was first illuminated with moonlight for 6 h followed by 110 s of blue-light activated. It was observed that L-CRY was indeed photoreduced to the

full light activated anionic FAD°⁻ radical (Fig. 29) as was seen previously with blue-light illumination. L-CRY was also able to recover back to the dark state.

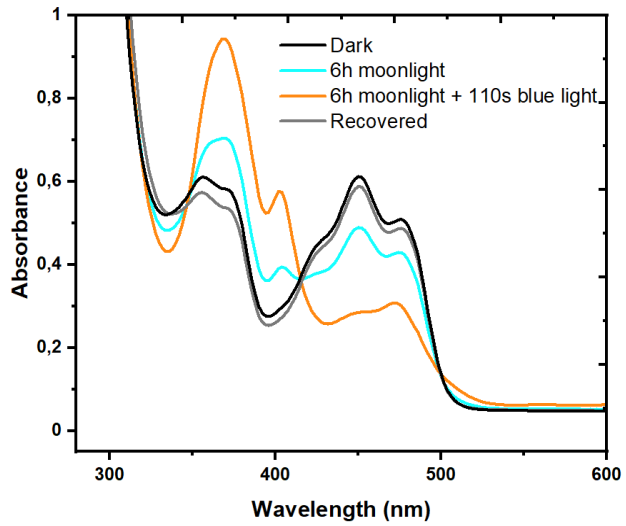

Figure 29: Spectroscopy mimicking full-moonlight to daylight transition (sunrise). Dark-adapted L-CRY (spectrum "dark" taken before moonlight exposure) was illuminated with 6 h moonlight followed by 110s of blue light illumination. The moonlight activated state is converted to the full light activated FAD°⁻ state with blue light and recovers back to the dark-state with oxidized FAD (spectrum "recovered" taken after 1h dark recovery).

We also investigated the dependence of L-CRY photoreduction on moonlight intensity by exposing L-CRY to namely one-third, half, one and twice the full moonlight intensity for 4 h. Interestingly, a higher degree of photoreduction was observed when L-CRY was illuminated with increased moonlight intensity for the same duration of time (Fig. 30A). Hence, L-CRY can differentiate between different moonlight intensities. This provides insights into L-CRY's ability to sense changing moonlight intensities during waning and waxing moon phases as well as its ability to distinguish the moonlight (partial activation) from daylight (full activation). Increasing the intensity to twice that of full moon intensity photoreduces L-CRY to a state within 2h similar to the state achieved with FM at 4h (Fig. 30B). 8h with 1/3FM does not achieve a similar state, implying that there must exist a minimum threshold intensity required to illicit the response seen at FM. However, the moonlight FAD°⁻ light state attained after 6 h with full moon and twice full moon intensities were similar. The final moonlight activated state, thus, was not impacted significantly with increased moonlight intensity (Fig. 30C). This

is ecologically relevant as worms inhabit generally between 1-5m below the water surface and the response of L-CRY to moonlight must be similar within a range of intensities.

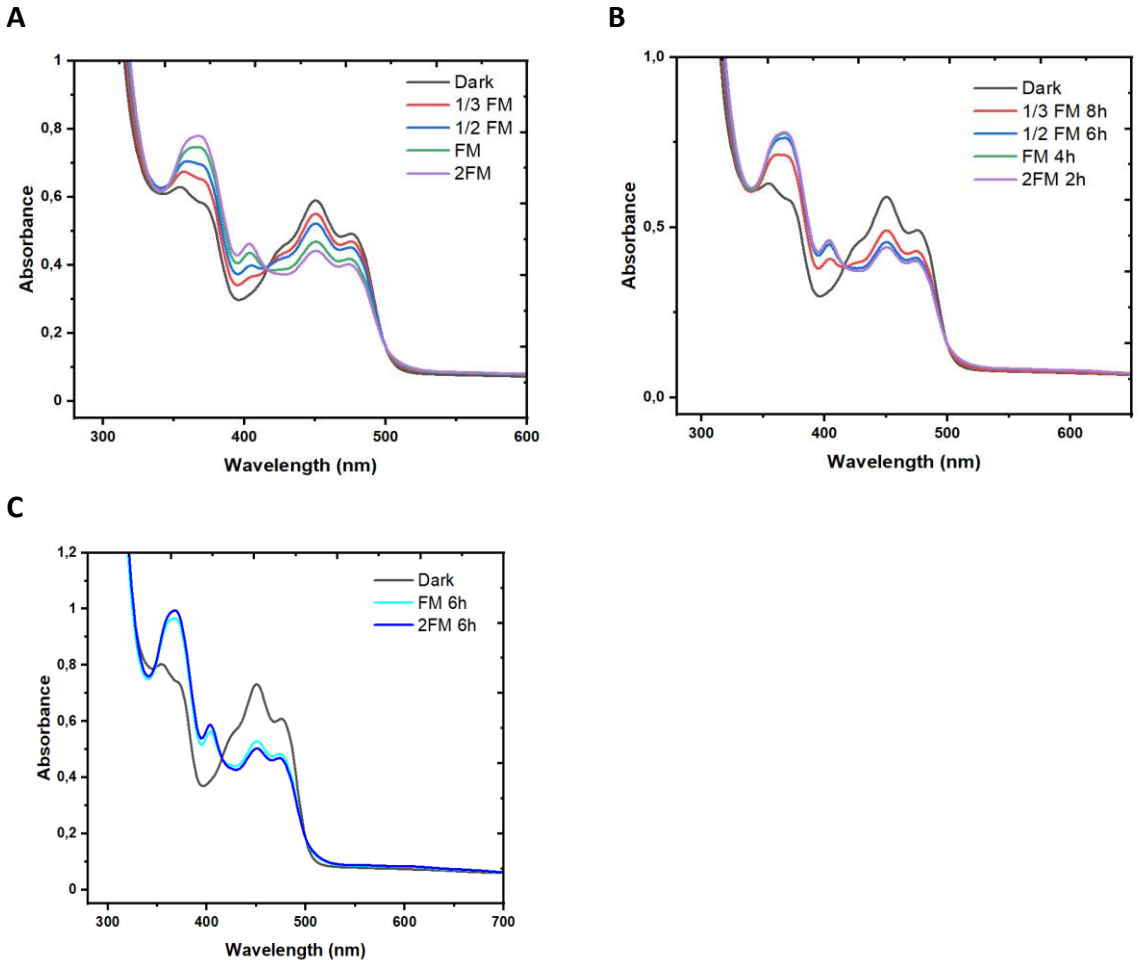

Figure 30: A) L-CRY illuminated with different moon light intensities (1/3 FM, 1/2 FM, 1 FM, 2 FM) for 4 h showed that the degree of photoreduction was dependent on moonlight intensity. B) Response of L-CRY to different moonlight intensities when illuminated for increased time intervals indicates that the state achieved with 1/2FM 6h, FM 4h and 2FM 2h were similar. C) The moonlight activated state after 6 h illumination with full moon and twice full moonlight intensities were similar.

3.1.3.6 Sunlight response of L-CRY

When purified L-CRY was illuminated with a light source mimicking naturalistic sunlight, oxidized FAD (FAD_{ox}) was photoreduced to the anionic FAD radical ($FAD°^-$), as observed before with a blue light LED. This can be seen as changes in the absorbance at 368 nm, 404 nm, 450 nm and in the range of 550 to 700 nm. While 110s blue-light illumination led to a nearly complete photoreduction to $FAD°^-$, a sunlight pulse of 110 s partially induced the anionic radical state, consistent with the 40 times lower intensity of the naturalistic sunlight

compared to the blue light LED (Fig. 31A). Sunlight-induced photoreduction to $FAD^{\circ -}$ was nearly complete after 20 min. Exposure to sunlight upto 2h did not further increase the extent of photoreduction (Fig 31B). The dark recovery constant at 18°C after 20 min of sunlight illumination was determined from the absorbance at 450 nm. A time constant of approximately 3.2 min was calculated after using a single exponential fit which is in the range of the dark recovery observed after blue-light illumination , which was 2 min (Fig. 31C). For comparison, we also measured dark recovery of L-CRY after 20 min of sunlight illumination on ice. This resulted in a time constant of 5 min (Fig. 31D,31E) . As blue-light LEDs are routinely used in circadian studies (Gomes & Preto, 2015; Tosini et al., 2016; Wahl et al., 2019), this validates the similar photoreduction observed with blue light LED and naturalistic sunlight source, reaffirming that these two light sources are good representatives to daylight.

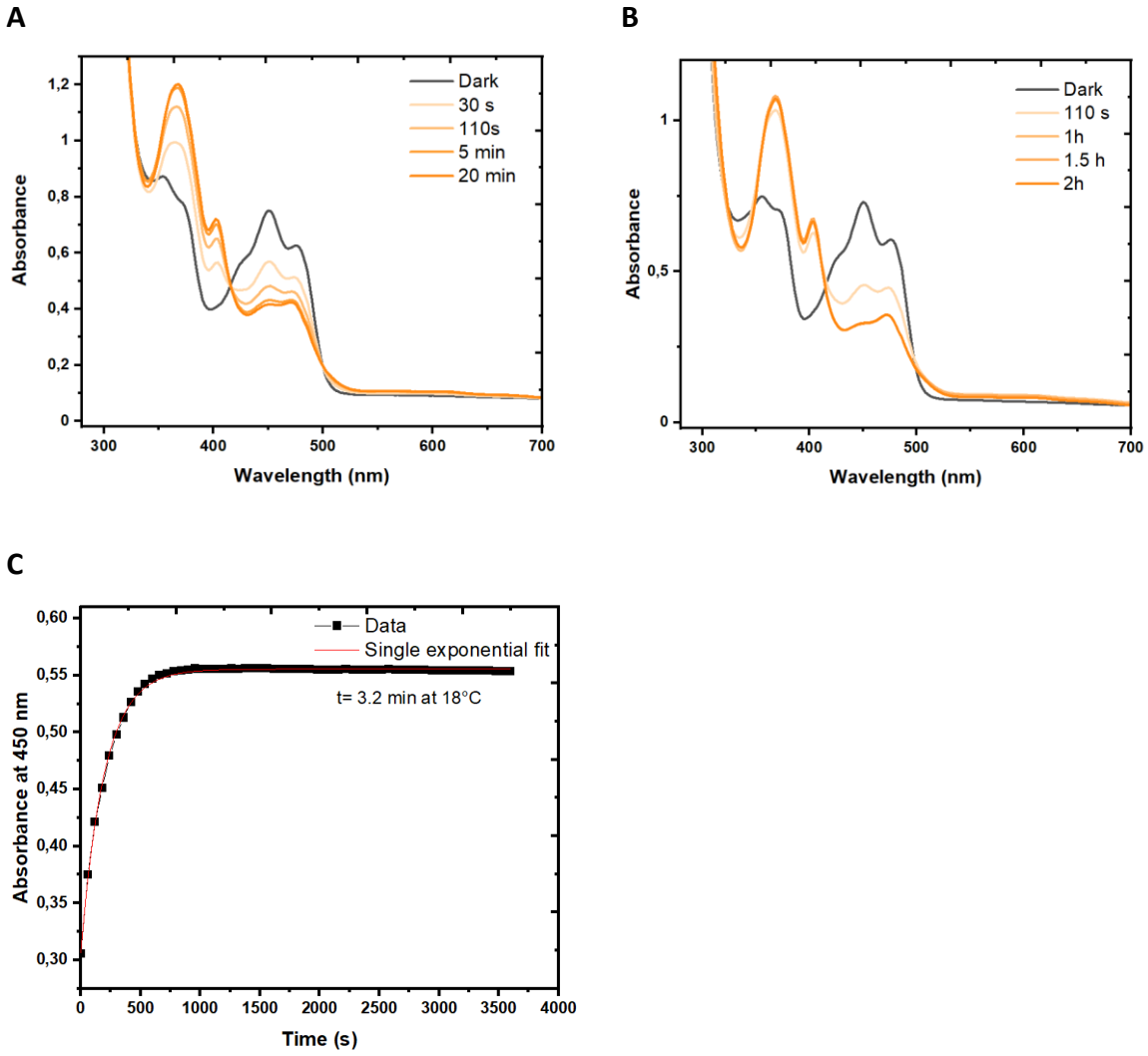

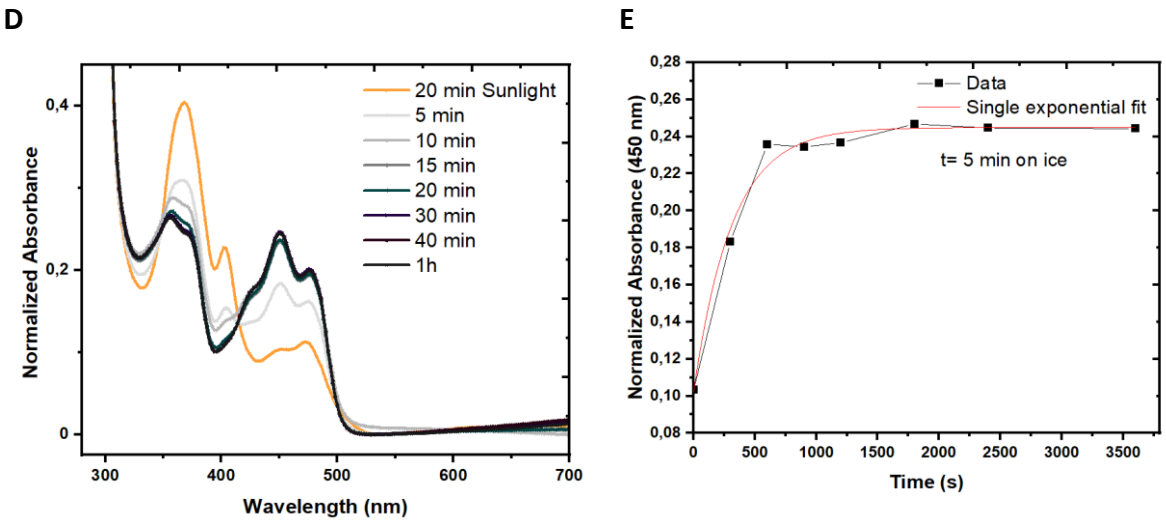

Figure 31: Response of L-CRY to sunlight. A) L-CRY was illuminated with sunlight for different time intervals leading to the increased formation of anionic FAD°⁻ radical. The extent of conversion from oxidized FAD (dark) to the anionic FAD radical increases with increased sunlight exposure from 110s to 20 min B) The anionic FAD radical state (FAD°⁻) is obtained on illumination with sunlight. Prolonged exposure upto 2h does not lead to further photoreduction. C) Dark recovery kinetics after sunlight illumination monitoring change in absorbance at 450 nm every 1 min. A time constant of approx. 3.2 min at 18 °C was calculated by single exponential fit. D) Monitoring dark recovery of L-CRY on ice after 20 min sunlight illumination. E) The normalized 450 nm absorbances were extracted from the full spectra depicted in D. A time constant of approx. 5 min was calculated by single exponential fit .

Mimicking the sunrise scenario, L-CRY was first illuminated with naturalistic full moonlight intensity for 6 h as done previously followed by a 110s and 20 min of sunlight exposure. This resulted in the enrichment of the anionic FAD radical (FAD°⁻) state (Fig. 32). The sunlight source is potentially able to further photoreduce moonlight activated L-CRY to a complete light-activated state.

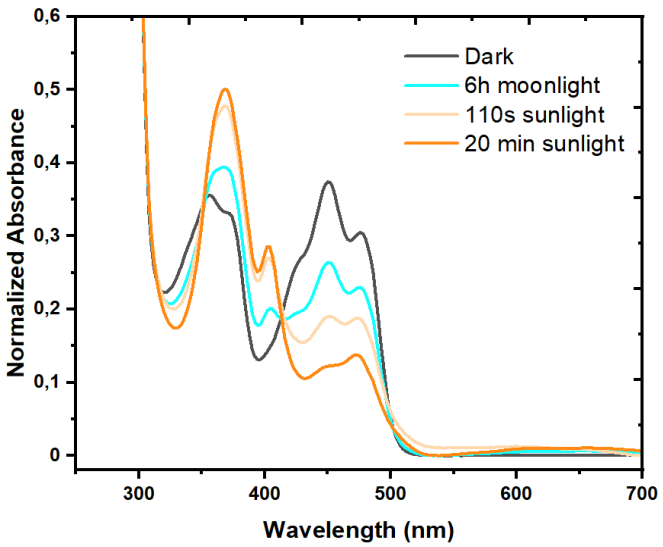

Figure 32: Response of L-CRY to full-moonlight followed by daylight. Dark adapted L-CRY illuminated for 6h moonlight leads to the formation of partial anionic FAD radical which is further converted to complete anionic FAD radical on 20 min sunlight illumination.

Following the light pattern during sunset, we illuminated L-CRY first with 20 min sunlight and followed recovery in the presence of naturalistic full moonlight illumination. We observed that L-CRY recovered back to the dark state with a time constant of 7 min when monitored on ice (Fig. 33A, 33B). Hence moonlight somewhat delays but does not prevent recovery of the sunlight-activated state of L-CRY as seen before with moonlight effect after blue-light illumination.

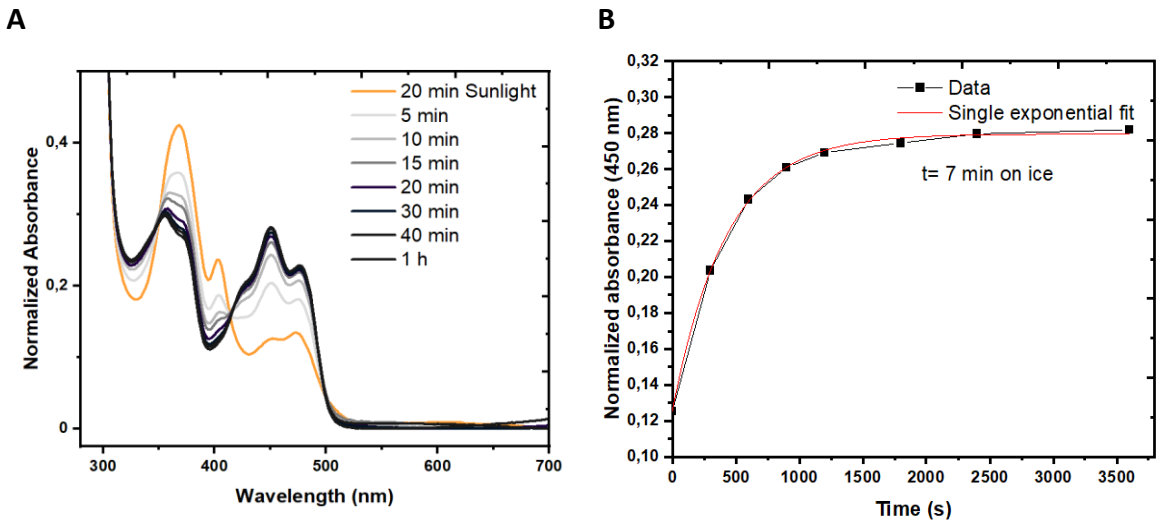

Figure 33: Recovery of L-CRY in moonlight after sunlight illumination. A) Monitoring recovery of L-CRY on ice after 20 min sunlight illumination in the presence of naturalistic full moon. The

normalized 450 nm absorbances were extracted from the full spectra. B) A time constant of approx. 7 min was calculated by single exponential fit.

Upon prolonged moolight exposure for up to 6 h following 20 min sunlight, oxidized FAD from the dark state is first converted to the complete anionic FAD radical as seen before in Fig 31A. On subsequent naturalisic moonlight illumination, L-CRY returns back to the dark state as shown in Fig. 31D (time point not depicted in Fig 34) and later the partial FAD radical is formed due to moonlight illumination (Fig. 34). Thus, L-CRY is able to transition between different states in response to sunlight and moonlight.

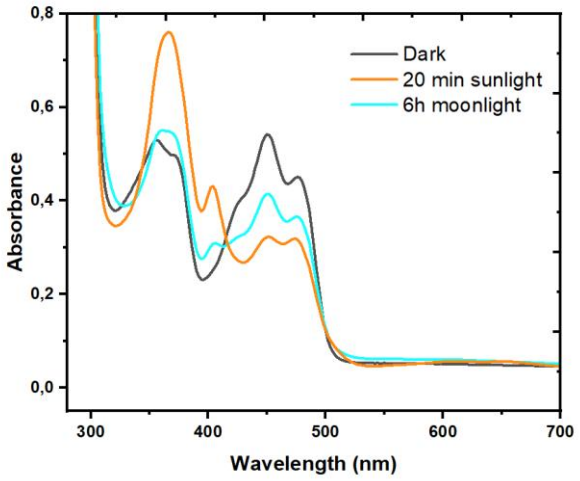

Figure 34: Response of L-CRY to daylight followed by full-moonlight. L-CRY activated with 20 min sunlight forms the complete anionic FAD radical which on continuous naturalistic moonlight illumination upto 6h transitions to the partial anionic FAD radical.

3.1.4 Crystallization of L-CRY

Full length L-CRY with N-terminal His_6-tag was initially screened for crystallization conditions. Setups with different protein concentration from 5-20 mg/ml in sitting drop conditions were screened. Two different temperatures namely 20 ^{o}C and 4 ^{o}C were tested. Initial hit conditions were reproduced in the hanging drop condition, varying the protein: buffer volumes, drop size and protein concentration. However, the trials were not successful. Buffer optimization was carried out with thermofluor experiments. It was found that Bis-Tris buffer pH 8 was the most promising. In addition, two different truncated constructs of L-CRY (K30-Y567) and (K30-T553) were tested for purification and crystallization. Of them construct (K30-Y567) was also tested for crystallization trials with no success. All prior crystallization attempts were carried

out with His-tagged protein. To exclude the effect of tag hampering crystallization, trials were also pursued after cleavage of N-terminal His_6-tag. However, the results remained the same.

Overexpression of L-CRY led to crystallization of the protein within *Sf9* insect cells after 3 days of transfection. When spontaneously lysed cells were observed under the microscope, yellow-colored crystals as seen in Fig. 35 were observed. The crystals were, however, very unstable. It was not possible to purify the crystals or to find an appropriate cryoprotectant without damaging the crystals. The crystals appeared most stable in the SF900II insect cell media, the composition of which is not publicly disclosed.

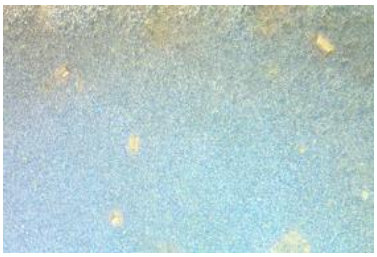

Figure 35: Crystals of L-CRY formed within Sf9 insect cells. Yellow colored crystals were observed under the microscope from L-CRY expressing insect cell culture.

Spontaneous crystallization of protein on overexpression within living cells and particularly *Sf9* cells is not unheard of (Schönherr et al., 2018). To be certain that the structures seen within the cells were indeed crystals, the cells were observed under a confocal microscope with a polarizer (Fig. 36). It was necessary to separate crystal containing cells from the rest and this was done by adapting a published cell-sorting approach described in 2.3.9.2 (Boudes et al., 2016).

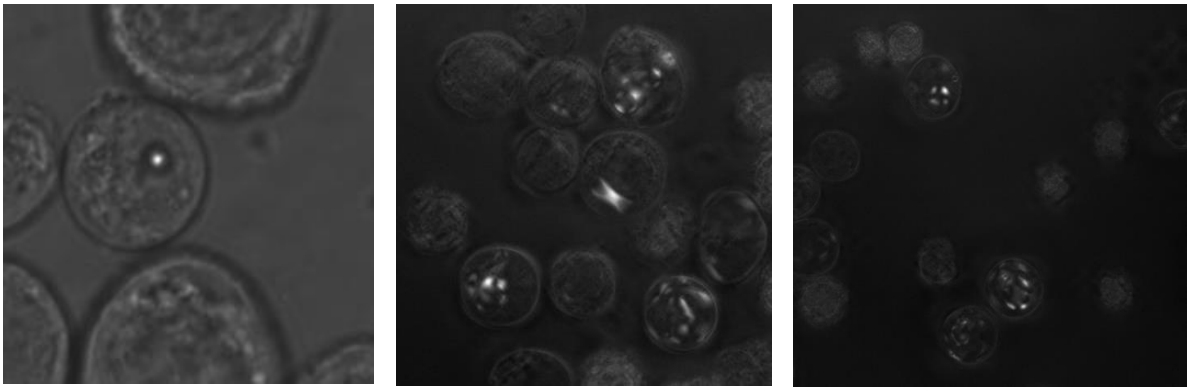

Figure 36: Sf9 insect cells overexpressing L-CRY FL led to the formation of crystals after 3 days of transfected depending on the amount of virus added. Not all infected cells carry crystals.

For comparison non-infected *Sf9* cells were also sorted. The gating was done to separate live cells from dead ones using DAPI staining and also to have single cells and not clusters. The cells containing crystals would exhibit higher side light scattering (SSC) as seen for infected *Sf9* culture making it possible to separate crystal containing cells from the rest of the population (Fig. 37, 38). The cells successfully sorted were stained with tryphan blue, concentrated, and applied to MiTeGen micromeshes (Fig. 39).

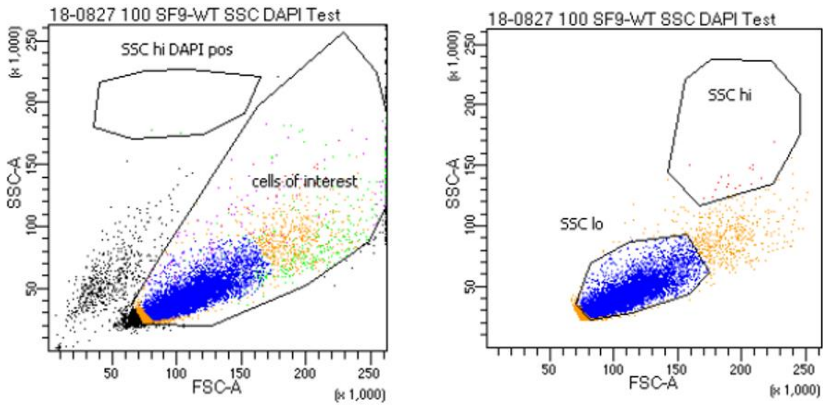

Figure 37: Representative FACS scatter plots from non-infected Sf9 cells which do not express L-CRY. The gating was adjusted to sort populations of cells based on viability (DAPI staining) and side light scattering (SSC). FSC: Forward light scattering.

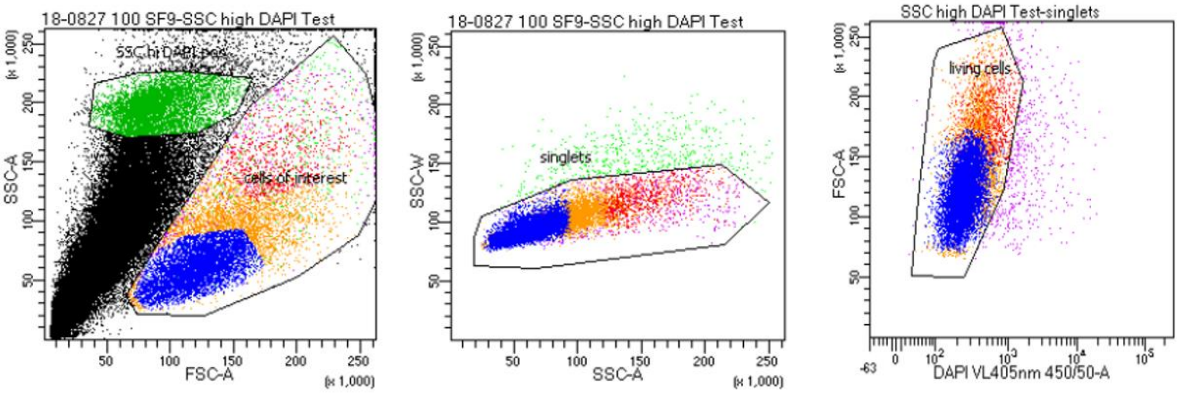

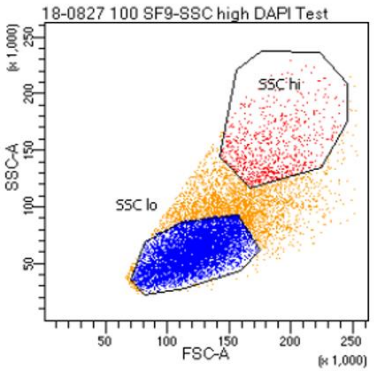

Figure 38: Representative FACS scatter plots from Sf9 cells overexpressing L-CRY FL infected by recombinant baculovirus. The gating was adjusted to sort populations of cells based on viability (DAPI staining), single cell occurrence and high side light scattering (SSC). High SSC, single living cells containing crystals were sorted from the culture. FSC: Forward light scattering.

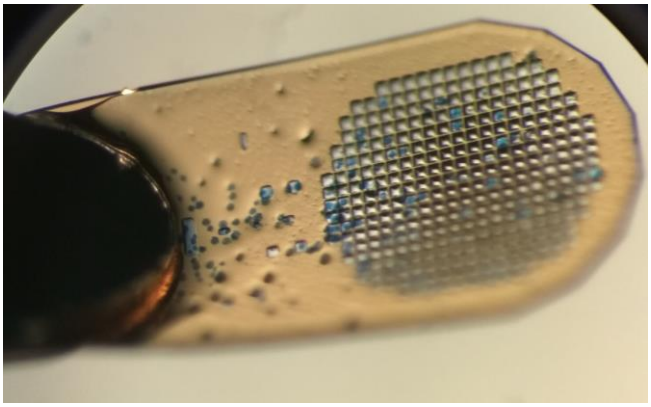

Figure 39: Crystal containing cells sorted by FACS were stained with Tryphan blue and loaded on MiTeGen micromeshes (700/25). Cryoprotection was provided with the addition of 50% ethylene glycol.

The micromeshes were screened at Swiss Light Source (SLS). The ice content on the meshes was considerable and it was not possible to collect a diffraction data set. Several factors such as the orientation of the cells on the mesh in comparison to the crystal position within the cell, the size of the crystals and the cryoprotectant used are required to be optimized for further trials.

3.1.5 Multiangle light scattering of L-CRY

L-CRY elutes as a dimer after size-exclusion chromatography, unlike dCRY, an additional technique was employed to validate this. The SLS measurement as described in 2.3.3 was

carried out by Prof. Elmar Jaenicke (JGU Mainz). Static light scattering measurements helped to confirm the indication from size-exclusion chromatography that indeed L-CRY is purified as a dimer of approximately 133 kDa. The obtained molecular weight was in accordance with the theoretical molecular weight. Apart from minor aggregation observed by the light scattering between 7-8 ml (light scattering depicted in black in Fig. 40), no additional oligomeric forms of L-CRY were detected.

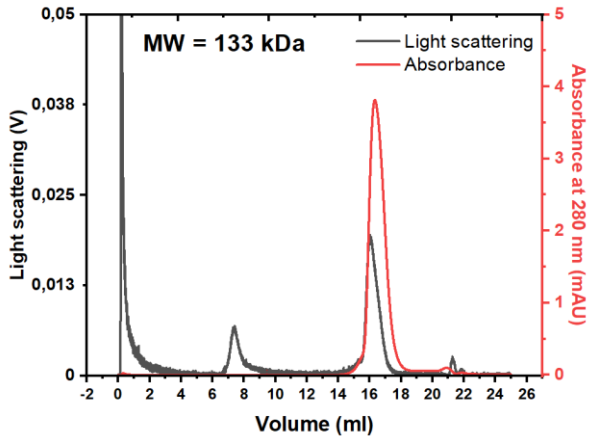

Figure 40: Multi-Angle Light Scattering (MALS) analyses of dark-state L-CRY confirms that L-CRY forms a homodimer (theoretical MW 135 kDa) in solution. The elution of L-CRY was monitored by the absorbance at 280 nm (red) and the light scattering (black).

3.1.6 L-CRY structural analysis by SAXS

In parallel to crystallization trials, SAXS analysis was carried out in order to determine structural attributes of L-CRY in solution and generate a low-resolution envelope. As it was necessary to maintain the dark/light state of the protein, SAXS experiments were carried out in the batch mode. The SAXS analysis revealed that L-CRY is a relatively extended protein. CRYSOL was used to simulate the scattering from the dCRY crystal structure (PDB 4JZY) and compare it with the L-CRY SAXS scattering. It was seen that L-CRY scattering from solution does not fit the dCRY simulated solution scattering. A Chi-square of 55.90 was calculated and the fitting of the curves were inherently different (Fig 41A). This indicates that the measured data is quite different from dCRY. The Guinier plot of ln(I) vs s^2 shows a linear fit in the low q-region (Fig 41B). This indicates that the sample was homogenous with no considerable aggregates at the measured concentrations. The R_g of L-CRY was calculated to be 5.75 nm as compared to 3.5 nm for dCRY crystal structure. Kratky plot helps to identify unfolded samples.

Globular proteins exhibit bell-shaped curves following Porod's law. Extended molecules, on the other hand, lack this feature and show a plateau or increasing $I*s^2$ in the larger s region. Thus, the Kratky plot indicate that L-CRY is partially folded when compared to the curves for compact, folded proteins (Fig 41C). The distance distribution analysis using GNOM determined the maximum particle dimension (D_{max}) as 19.56 nm (Fig. 41D). Comparing the distance distribution p (r) of L-CRY with those of typical geometric shapes, led to the conclusion that L-CRY exhibits a prolate ellipsoid shape in solution (Mertens & Svergun, 2010) . An ab initio envelope of L-CRY was modelled using the output file from GNOM with the help of DAMMIF/N and GASBOR. The envelope indicates an extended shape for L-CRY (Fig. 42A). The fit of the model to the scattering data indicates a good fit (Fig. 42B). The models were clustered using DAMCLUST and the SASRES resolution of the ensemble was computed as 41 +/- 3 Å (Petoukhov et al., 2012; Tuukkanen et al., 2016). The fitting of dCRY structure into L-CRY envelope was not possible due to the difference in shape and the inherent mismatch of the scattering pattern.

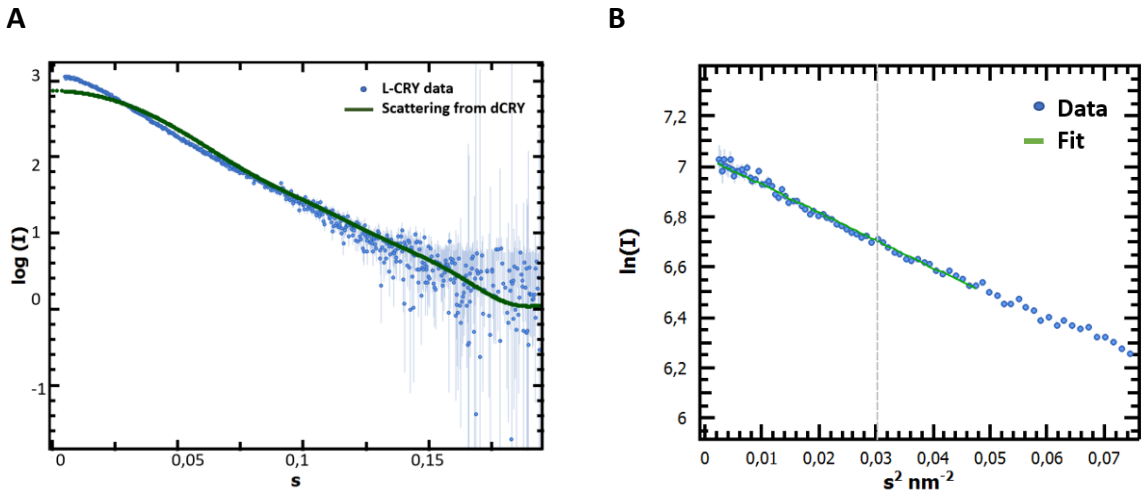

C

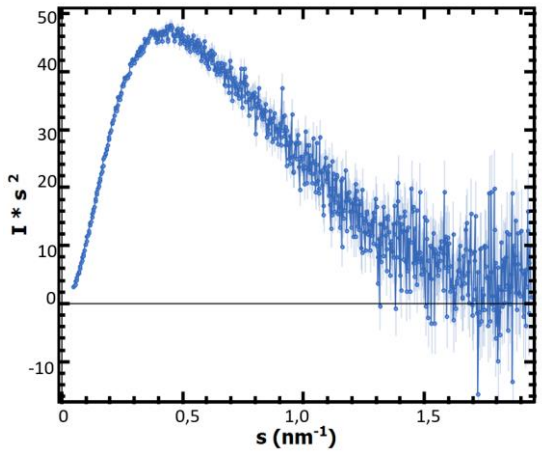

D

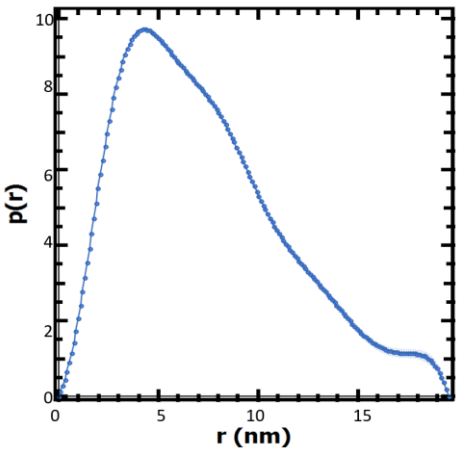

Figure 41: SAXS analysis of L-CRY A) Overlay of L-CRY SAXS scattering (dark blue) with solution scattering from dCRY crystal structure (4JZY) (olive green). B) Guinier plot of L-CRY depicting the region used for linear approximation and the fit to the data. C) Kratky plot depicts the compactness of L-CRY. D) Distance distribution analysis using GNOM calculated a Dmax of 19.56 nm.

A

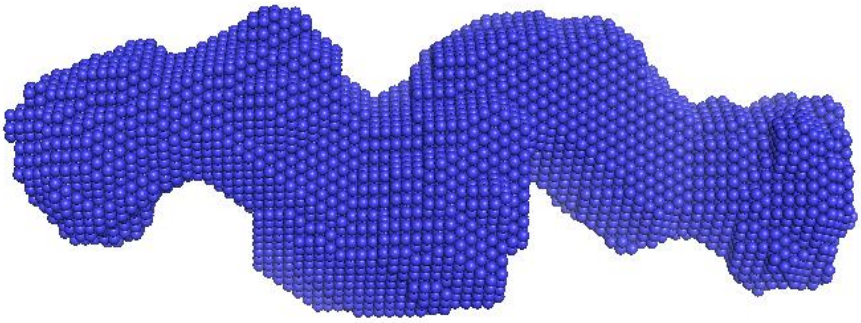

B

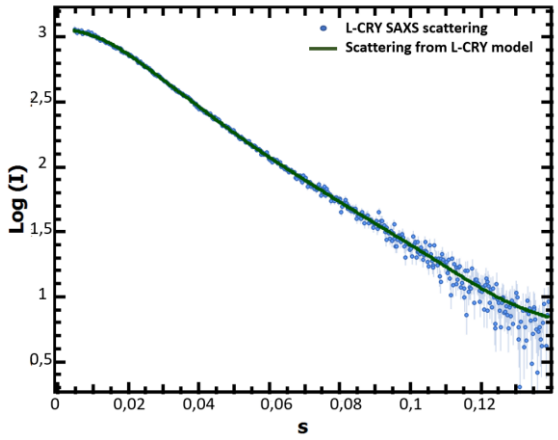

Figure 42: SAXS model of L-CRY. A)Ab-initio model generated with DAMMIF shows the extended structure of L-CRY. B) Overlay of L-CRY SAXS scattering (dark blue) with scattering of the modelled L-CRY structure (olive green) indicating the goodness of fit.

3.1.7 Single molecule electron microscopy of L-CRY

The dimer of L-CRY as a potential functional oligomeric state was intriguing and to explore this from a structural standpoint would be interesting. As previous crystallization attempts were not successful, single molecule electron microscopy was employed. With advancements in the field, CRYO-EM can now solve structures in a wide range of molecular weights, ranging from hundreds of kilo Daltons for protein complexes to hundreds of mega Daltons. Structures for proteins below 100 kDa are now also being successfully determined (Murata & Wolf, 2018). Hence, the L-CRY dimer of around 133 kDa was a promising for structural characterization.

3.1.7.1 Negative stain model of L-CRY

Negative staining is relatively less time consuming and cost effective and hence an important prerequisite before proceeding to cryo electron microscopy. The negative stain dataset recorded helped to verify the quality of the sample. In addition, it was possible to visualize different conformations and/or oligomeric states. An initial three-dimensional model of the protein at low-resolution was constructed which can later help in the refinement of the cryo-EM dataset.

A dilution of 1:500 was suitable to observe L-CRY particles without regions of clustering. L-CRY sample stained well and exhibited no signs of aggregation on the grid (Fig. 43A). The 2D

classes generated depicted that L-CRY did not exhibit particle ambiguity or oligomerization (Fig. 43B). This was essential as an important quality check of the sample. With this initial information, a low-resolution negative stain model of L-CRY was generated (Fig. 44). The resolution of this model is around 25 Å.

A

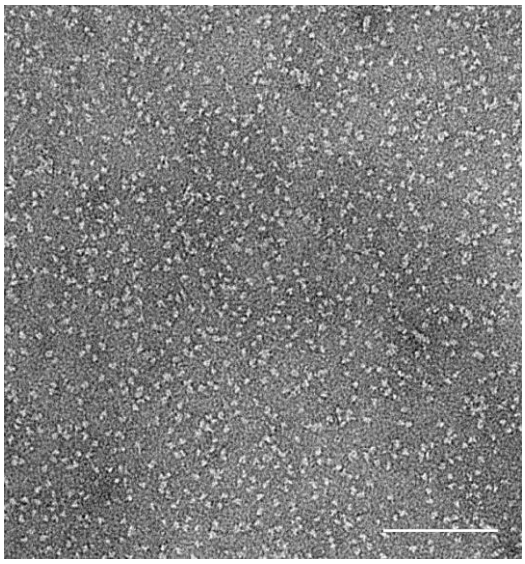

B

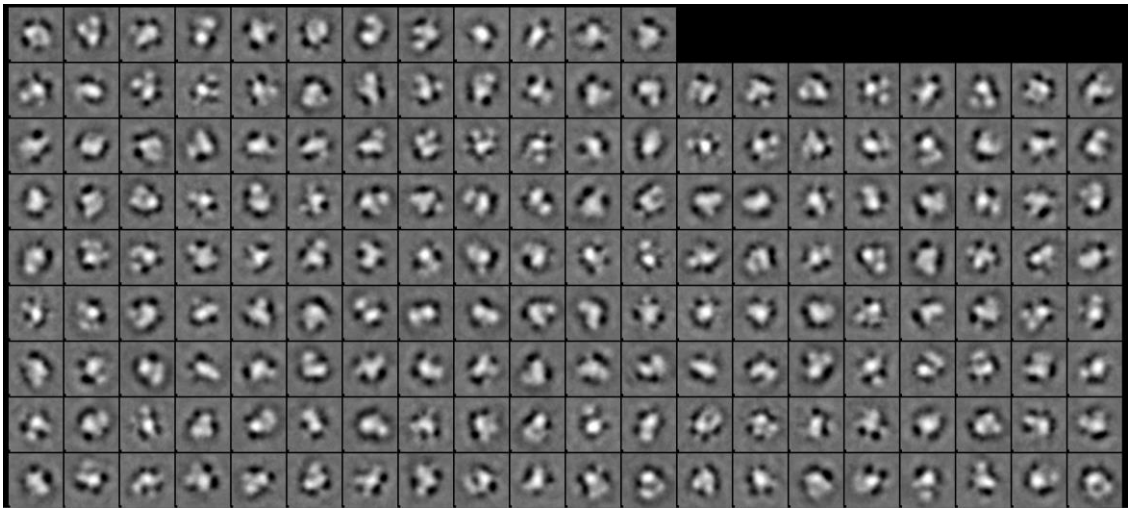

Figure 43: Negative stain of L-CRY. A) Representative exposure image of L-CRY (10 mg/ml) diluted 1:500. The scale bar for the image is 100 nm. B) 2D classes generated for L-CRY by processing negative stain micrographs.

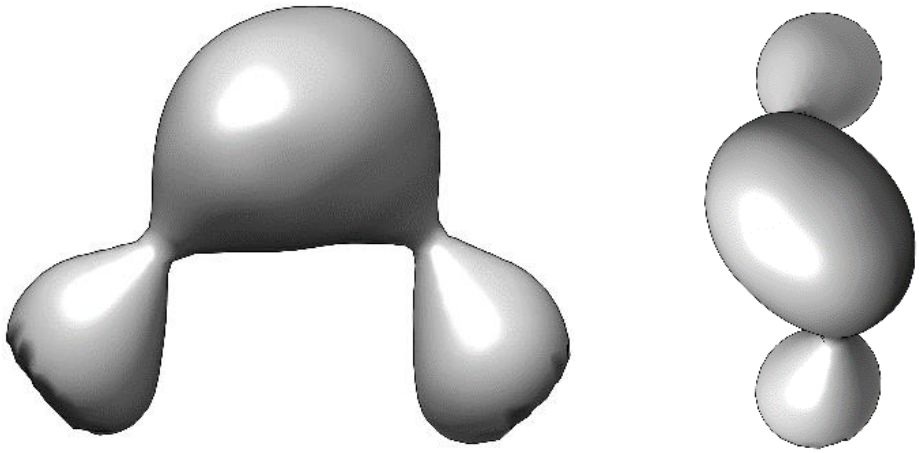

Side view **Top view**

Figure 44: Negative stain 3D model of L-CRY. The dimeric model of L-CRY was resolved to 25Å. The model indicates the symmetric orientation of the dimer.

3.1.7.2 CRYO-EM structure of L-CRY

Initial cryo dataset was collected in-house at the Caesar Institute using the acquisition parameters described in Table 38. The screening of grids and preliminary data collection confirmed the favorability towards high-resolution measurements in future (Fig. 45A). 5030 movie frames were collected and processed with MotionCor2 to correct for sample drifts. A total of 453,824 particles were identified. 22 2D classes were generated using Relion3.0 accounting for 277,192 particles (Fig. 45B). 3D classification with a subset of 107,317 particles was used to generate the final CRYO-EM structure of 5.7 Å (Fig. 46). The homogeneous local resolution and the 3D density map depict uniform structural features. The limitation to the resolution is now rather the hardware employed for data acquisition. Hence, future data acquisition at ESRF is planned to obtain high resolution structure.

Table 38: Acquisition parameters used for L-CRY CRYO data collection in-house (Caesar Institute, Bonn)

Software	Leginon
Microscope	TITAN Krios
Camera	Falcon II
Pixelsize	1.06
Magnification	59kX
Microscope Voltage	300 kV
Cs	0.001 mm
Binning	1
# Frames	40
Defocus Range	-1.5 to -2.5 µm
No. of Micrographs acquired	5030
No. of Micrographs after quality control	3345

A

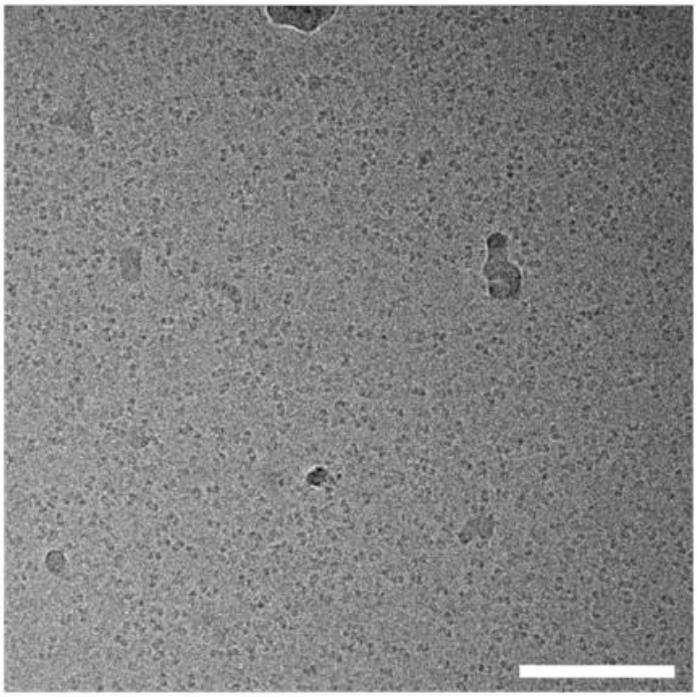

B

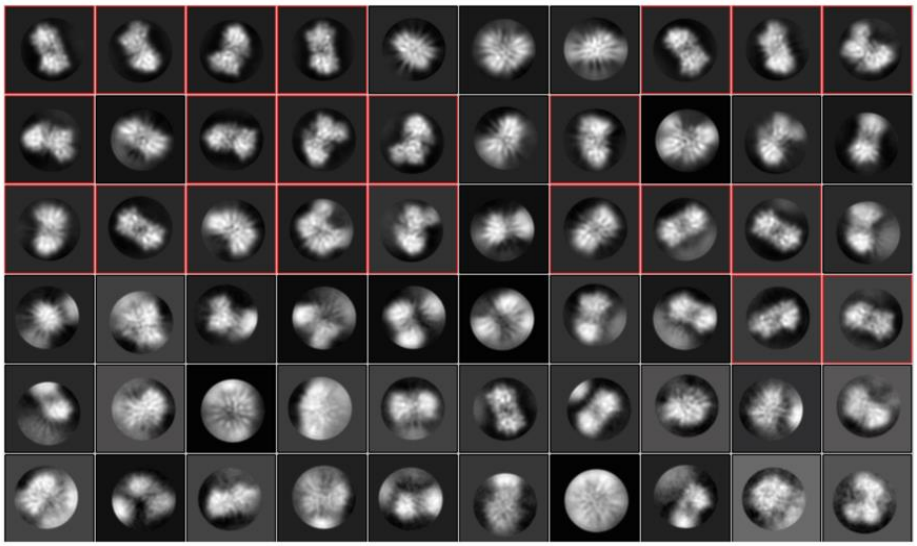

Figure 45: CRYO EM of L-CRY. A) Representative exposure image of L-CRY (7 mg/ml) diluted 1:10 . The scale bar for the image is 100 nm. B) 2D classes generated for L-CRY by processing CRYO-EM micrographs. The classes marked in red indicate particles of high resolution which account for 40% of all particles.

A

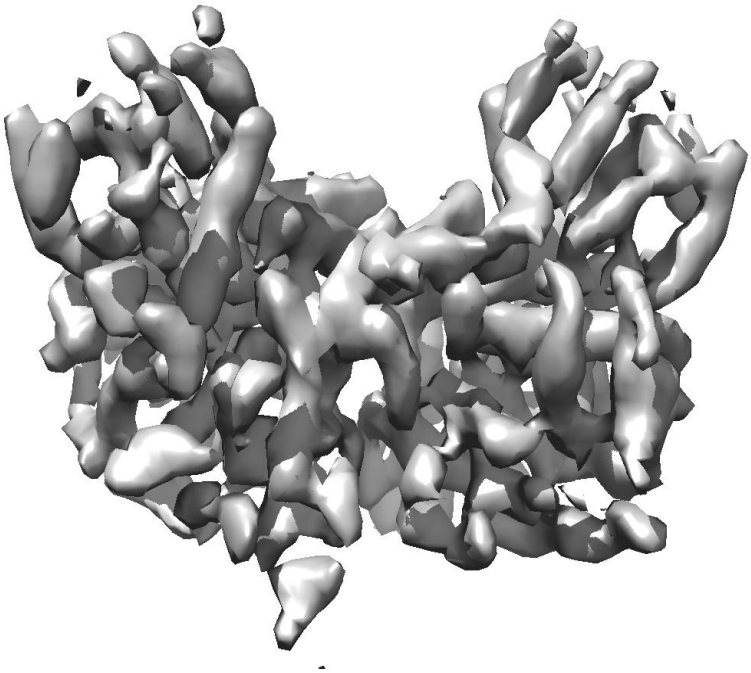

B

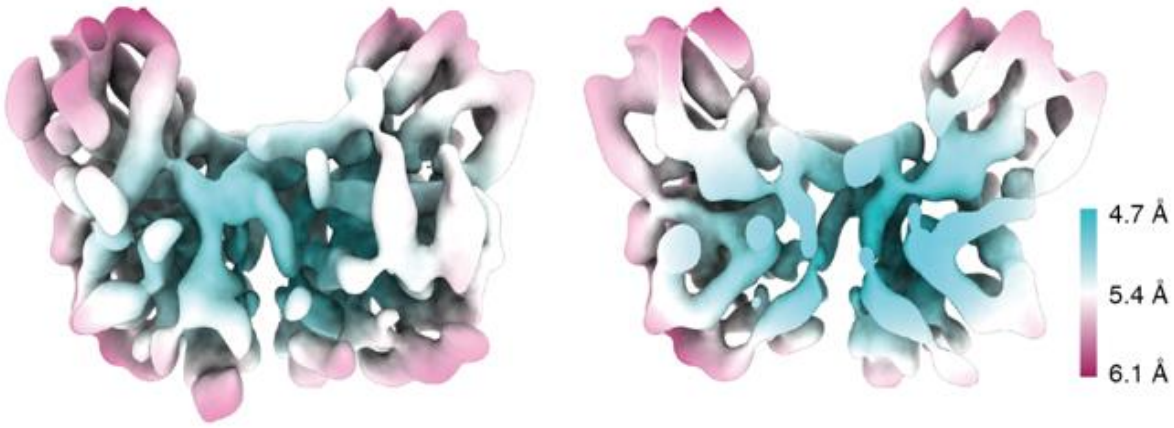

Figure 46: CRYO-EM map of L-CRY. A) 3D density map of L-CRY dimer shows well connected densities for alpha helices. B) Color coded map of L-CRY based on local resolution from 4.7 Å (cyan) to 6.1 Å (maroon). The dimer interface lies in the high-resolution region of the map depicted in cyan.

3.1.8 Pull down and mass spectrometry with L-CRY

With the help of pull down coupled with mass spectrometry, we could identify putative interactors of L-CRY. As nothing regarding the downstream pathways wherein LCRY is a player was known prior, this study was a potential lead to follow-up. Dark interactors of L-CRY were obtained from proteins pulled down from the new moon phase (ZT20) of the lysed worm heads using pre-purified L-CRY as bait under dark/red-light conditions. The light pull-down was carried with worm heads from new moon phase (ZT8) under blue-light conditions (samples constantly illuminated with blue-light LED plate at maximum intensity, distance 5-6 cm). The pull-down experiment was done with L-CRY bound to nickel beads as bait (sample) and just nickel beads (control). Each experiment was done in 2 replicates. Each sample and control elution are then used for labelling the digested peptides with a heavy and light label (forward experiment) and with switching the label (reverse experiment).

The scatter plot of the log2 converted normalized ratio data for the individual label pairs for the potential dark and light interactors is shown in Fig. 47 and Fig. 48. The cloud of points (on the top left) are all proteins that were identified in both the sample and control pulldowns indicating non-specific binding to beads. The points close to L-CRY (on the right bottom,

numbered) are proteins that were pulled down specifically with L-CRY. The potential dark and light interactors are enlisted in Table 39 and Table 40 respectively. Stringent selection of interactors was carried out as the control with just nickel beads is not ideal.

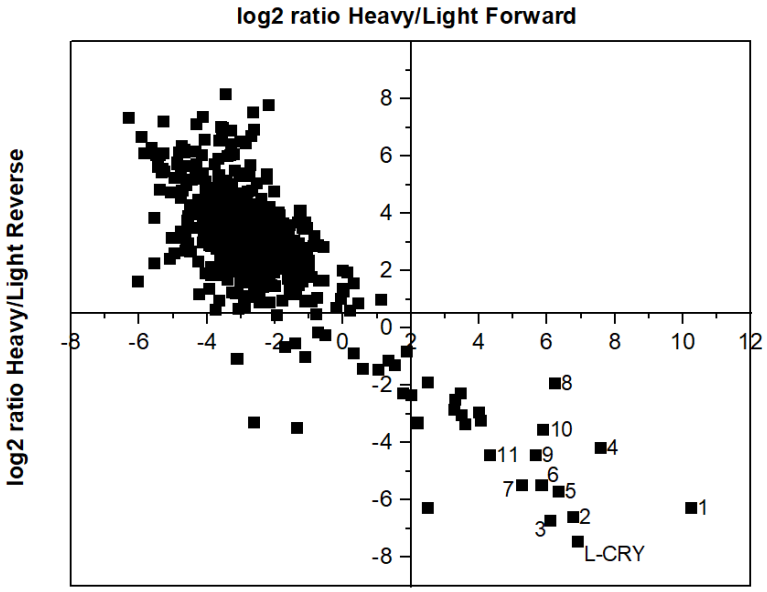

Figure 47: Dark state interactors of L-CRY. Scatter plot depicting the potential dark state interactors of L-CRY listed in Table 40. The non-specific proteins pulled down in the experiment are not numbered.

Two of the candidates namely Ras GTPase-activating protein-binding protein (G3BP) and YTH domain-containing family protein 2-like isoform X2 (YTHDF) were identified in an independent mass spectrometry study as circalunarly regulated (Ayers et al., 2018). This was a strong indication towards the possible link between L-CRY and the ligands being involved in circalunar entrainment pathway. With this initial evidence, these two candidates were selected for further validation of direct interaction. In addition, we also tested the PITH domain-containing protein 1-like ligand.

Table 39: List of dark state L-CRY interactors numbered in Figure 33.

Hit	Protein ID	Annotation
1.	comp2275698_c0_seq5	Cleavage and polyadenylation specificity factor subunit 6, partial [Stegodyphus mimosarum]
2.	**comp2259230_c0_seq1**	**Ras GTPase-activating protein-binding protein 2 [Crassostrea gigas]**
3.	comp2055425_c0_seq1	PREDICTED: PITH domain-containing protein 1-like [Lingula anatina]
4.	comp2277227_c0_seq5	hypothetical protein BRAFLDRAFT_283402 [Branchiostoma floridae]
5.	**comp2276668_c0_seq1**	**PREDICTED: YTH domain-containing family protein 2-like isoform X2 [Octopus bimaculoides]**
6.	comp2277172_c1_seq24	PREDICTED: proto-oncogene vav-like isoform X6 [Lingula anatina]
7.	comp2272795_c0_seq4	PREDICTED: DNA topoisomerase I, mitochondrial-like isoform X2 [Lingula anatina]
8.	comp2277522_c1_seq2	CREB-binding protein [Zootermopsis nevadensis]
9.	comp2276070_c0_seq2	prospero [Leptochiton asellus]
10.	comp2269702_c0_seq2	TFG beta signaling pathway factor [Pinctada fucata]
11.	comp2278582_c0_seq1	PREDICTED: E3 ubiquitin-protein ligase TRIP12-like isoform X3 [Lingula anatina]

The dark pull-down for interactors was performed twice and the above three selected candidates were found in atleast three of the four replicates generated. The candidates obtained for light pull-down are from one set of the experiment. A repetition of this is essential before further selection. However, it was interesting to note that G3BP was also one of the potential light state interactors.

A similar pulldown was carried out with wildtype versus mutant worm heads to see if the presence of any of the interactors was strongly dependent on L-CRY. However, we did not find any significant difference between the wildtype and mutant. The limitation of this approach is that in both cases, recombinantly purified full-length L-CRY was used as bait to pull down interactors. With this regard, it would be worth to do IP with L-CRY antibody.

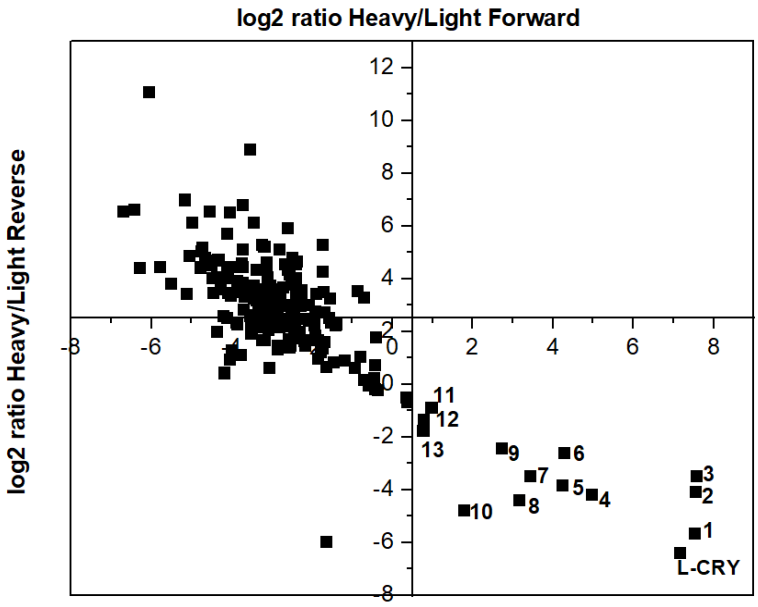

Figure 48: Light state interactors of L-CRY. Scatter plot depicting the potential dark state interactors of L-CRY listed in Table 41. The non-specific proteins pulled down in the experiment are not numbered.

Table 40: List of light state L-CRY interactors numbered in Figure 34

Hit	Protein ID	Annotation
1.	comp2259230_c0_seq1	Ras GTPase-activating protein-binding protein 1 [Pongo abelii]
2.	comp2233247_c0_seq2	Putative ATP-dependent RNA helicase me31b [Drosophila melanogaster]
3.	comp2270491_c0_seq1	GTP-binding protein 1 [Homo sapiens]
4.	comp2269702_c0_seq2	Mothers against decapentaplegic homolog 2 [Rattus norvegicus]
5.	comp2275155_c0_seq1	DDB1- and CUL4-associated factor 7 [Mus musculus]
6.	comp1198037_c0_seq1	Transcriptional repressor IclR [Escherichia coli (strain K12)]
7.	comp2265690_c0_seq3	Probable ATP-dependent RNA helicase DDX17 [Mus musculus]
8.	comp2277227_c0_seq5	ATP-dependent RNA helicase DDX55 [Gallus gallus]
9.	comp2278140_c0_seq40	Casein kinase I isoform gamma-1 [Bos taurus]
10.	comp2262145_c0_seq1	TRPL translocation defect protein 14 [Drosophila melanogaster]
11.	comp2254677_c0_seq1	O-phosphoserine--tRNA(Cys) ligase [Methanococcus aeolicus (strain ATCC BAA-1280 / DSM 17508 / OCM 812 / Nankai-3)]
12.	comp2272124_c0_seq1	Scavenger receptor cysteine-rich type 1 protein M130 [Bos taurus]
13.	A0A1C6ZZX0	Fibrinogen-like protein 1 [Bos taurus]

3.2 L-CRY ligands

Three ligands from the novel dark interactor list namely, YTHDF, Ras-GAP binding protein 2 and PITHD1 were selected for in-vitro validation of direct interaction. To do so, these proteins were recombinantly expressed in either *E.coli*/insect cells.

3.2.1 Expression and purification of L-CRY ligands

3.2.2.1 YTH domain-containing family protein 2-like isoform X2 (YTHDF)

Purification from *E.coli*

The YTHDF protein is largely unstructured except for the C-terminal region which comprises the YTH domain (Fig. 13A, Fig. A1) The full-length protein was cloned into several pCoofy vectors to test for *E.coli* expression and solubility. The protein exhibits low solubility in general. N-terminally His_6-tagged YTHDF was expressed in Rosetta using TB media induced with 0.1mM IPTG and cultured overnight at 18 °C. The cells were lysed in lysis buffer mentioned in Table 26 (supplemented with 0.1% NP-40 and 0.05% Triton X 100) and the supernatant after centrifugation was loaded onto a nickel column. ATP wash was carried to get rid of chaperones. YTHDF was eluted with step elution of 1M imidazole and the eluate has high 260/280 ratio indicating nucleic acid-binding. Subsequent step to get rid of nucleic acid by heparin column was not successful as the protein degraded rapidly while still being bound to nucleic acids. A sample of the elution was run on a 1% agarose gel and stained with SYBR safe (dsDNA) and SYBR Gold (for ssDNA/ssRNA). It was seen that the protein binds single-stranded nucleic acids, most likely RNA, as known from YTHDF proteins in other organisms. Purification trial with His_6-SUMO tagged YTHDF, led to the protein eluting with the high salt buffer and precipitating.

YTHDF fused to His_6-MBP tag was relatively well expressed. The protein was purified following an affinity and size exclusion chromatography. It was possible to obtain clean protein. However, after overnight tag cleavage with Prescission protease, the protein degraded and aggregated on the S200 16/60 size-exclusion chromatography column. Cleavage of the tag was not suitable for the construct and hence this step was omitted. The aggregation of MBP-fused YTHDF persisted. Nevertheless, a small fraction of the protein eluted as a monomer after size exclusion (Fig. 49A, 49B). These fractions were concentrated and later used for initial pull-down experiments.

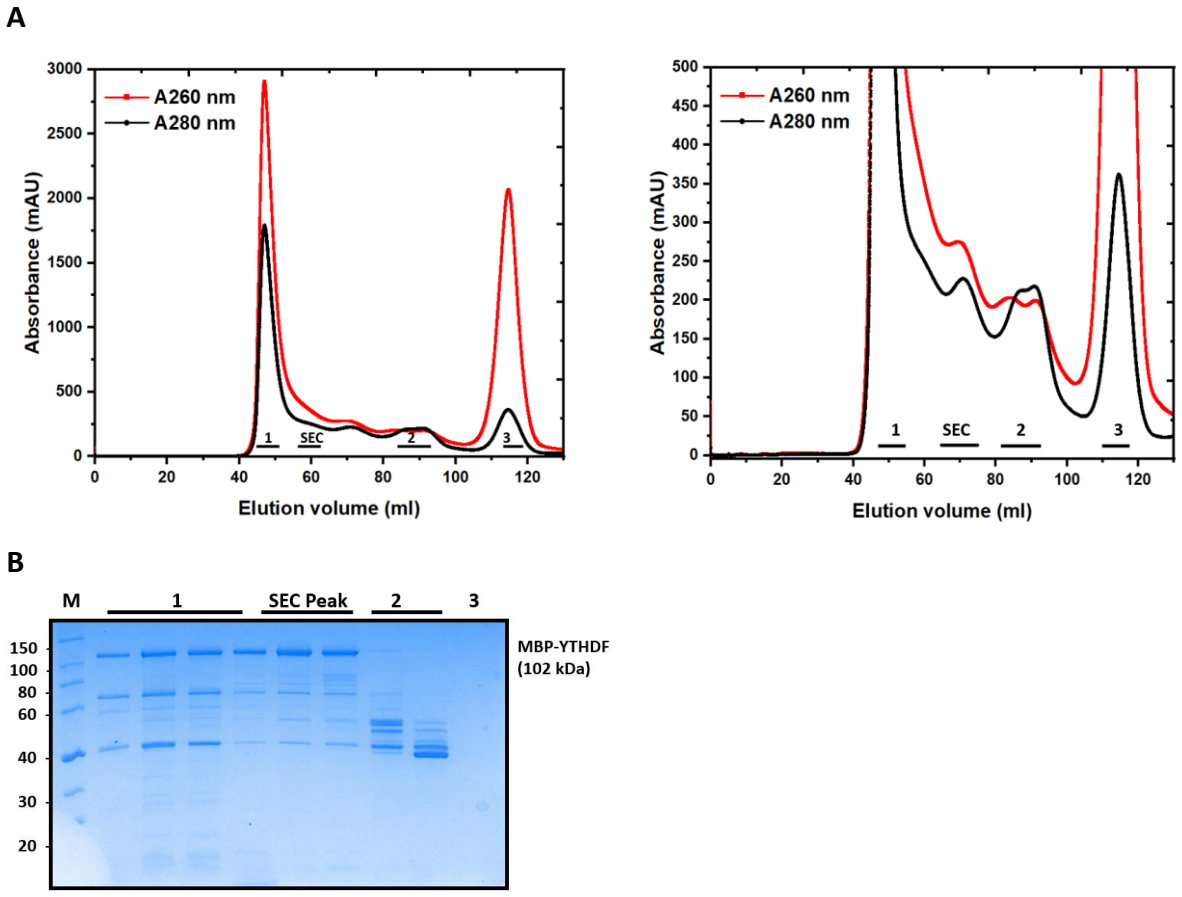

Figure 49: Size exclusion chromatography of YTHDF from E.coli. A) SEC profile of His_6-MBP YTHDF on S200 column 16/60 column. The zoomed profile (right) with bar at the bottom of peak corresponds to the fractions labelled on the SDS-PAGE. B) Corresponding SDS-PAGE of His_6-MBP tagged YTHDF purified using S200 column 16/60 column. M - protein marker in kDa. The fractions labelled SEC Peak were pooled and used for interaction studies.

Purification of YTHDF from insect cells

The full-length construct of YTHDF was codon optimized for insect cells and cloned into pCoofy27 (N-terminal His_6 tag) and pCoofy28 (N-terminal His_6-GST tag) for purification and pull-down validation. Protein was expressed as described in 2.2.10.2. Both proteins were purified using IMAC followed by size exclusion chromatography with conditions described in Tables 26 and 33. The fractions from IMAC elution consisting the protein of expected molecular weight were pooled, concentrated and applied to the SEC column. It was observed that the binding of His_6-GST tagged YTHDF to GSH beads was limited due to the competitive binding from endogenous glutathione-binding proteins from insect cells (Bichet et al., 2000). Therefore, His_6-GST tagged protein was also purified with a nickel affinity column. Fractions

containing the protein from nickel affinity were pooled together and run over S200 16/60 column. SDS-PAGE analysis of the SEC fractions showed the presence of few impurities and/or degradation products conforming with the multiple peaks seen in the chromatogram (Fig. 50A, 50B). In comparison to YTHDF purified from *E.coli*, the amount of nuclei acid/ssRNA was limited as seen from the A280 nm and A260 nm in the chromatogram.

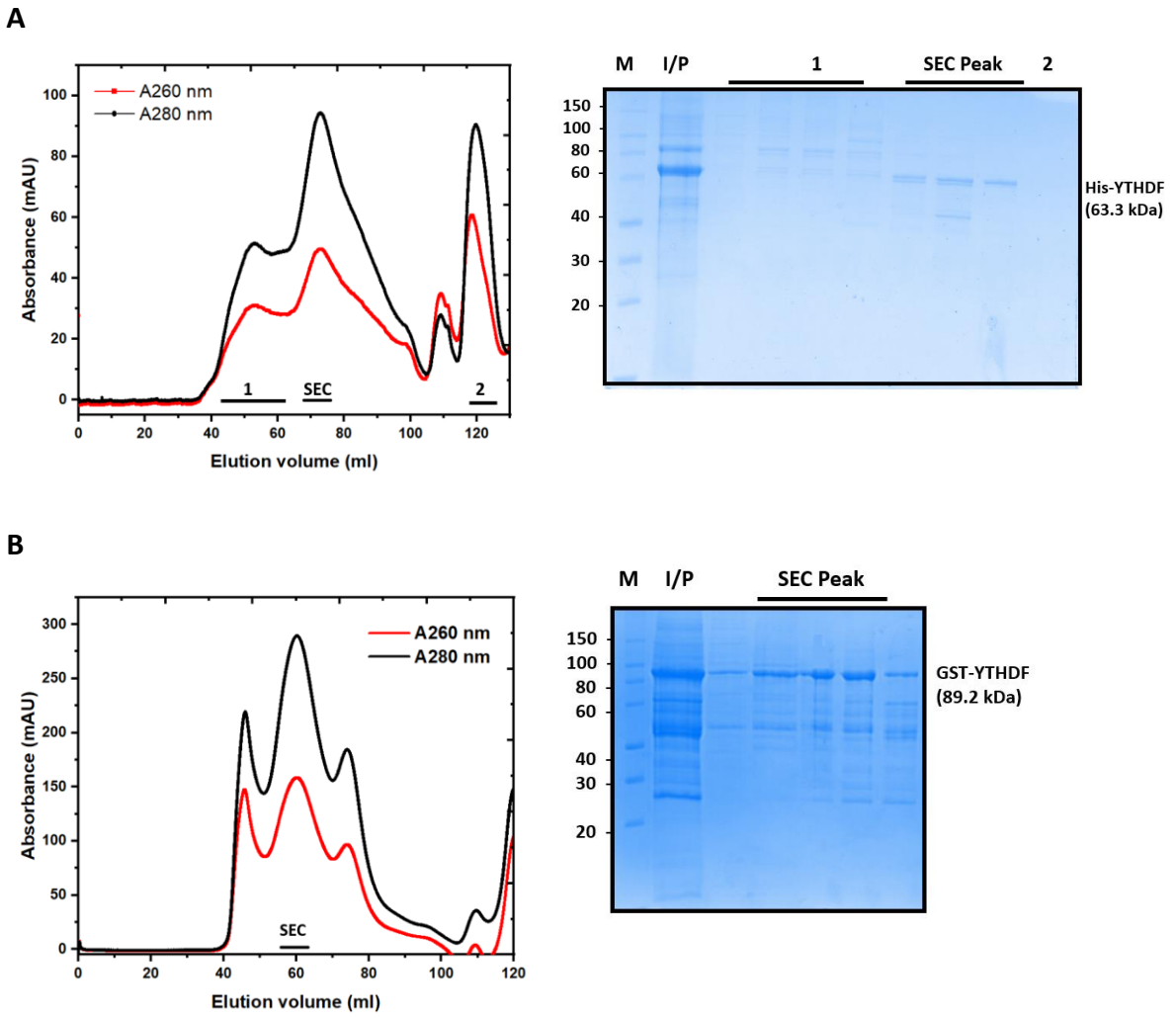

Figure 50 : Size exclusion chromatography of YTHDF from Sf9 cells. A) SEC profile and corresponding SDS-PAGE of His_6-tagged construct purified using S200 column 16/60 column B) SEC profile and corresponding SDS-PAGE of His_6-GST tagged construct purified using S200 column 16/60 column. Bar at the bottom of peak corresponds to the fractions labelled on the SDS-PAGE. I/P: Input to the SEC column ; M: protein marker in kDa. The fractions labelled SEC Peak were pooled and used for interaction studies.

3.2.2.2 Ras-GAP binding protein 1/2 (G3BP)

Ras-GAP binding protein 2 , codon optimized for insect cells was cloned and purified with both N-terminal His_6 tag and His_6-GST tag. The tagged constructs were purified using a IMAC followed by size exclusion chromatography described in Tables 26 and 33. The fractions from IMAC elution consisting the protein of expected molecular weight on the SDS-gel were pooled, concentrated and applied to the SEC column. The SEC run for the His_6-tagged construct depicts multiple peaks due to the presence of contaminants that eluted adjacent to the main peak (Fig. 51A). Additional anion-exchange step was included in the purification of His_6-GST tagged construct. However, this did not improve the purity of the protein. Furthermore, the stability of the His_6-tagged construct was better than the His_6-GST tagged construct. This can be seen from the SDS page analysis of the SEC runs wherein the His_6-GST tagged protein shows degradation bands (Fig. 51B).

A

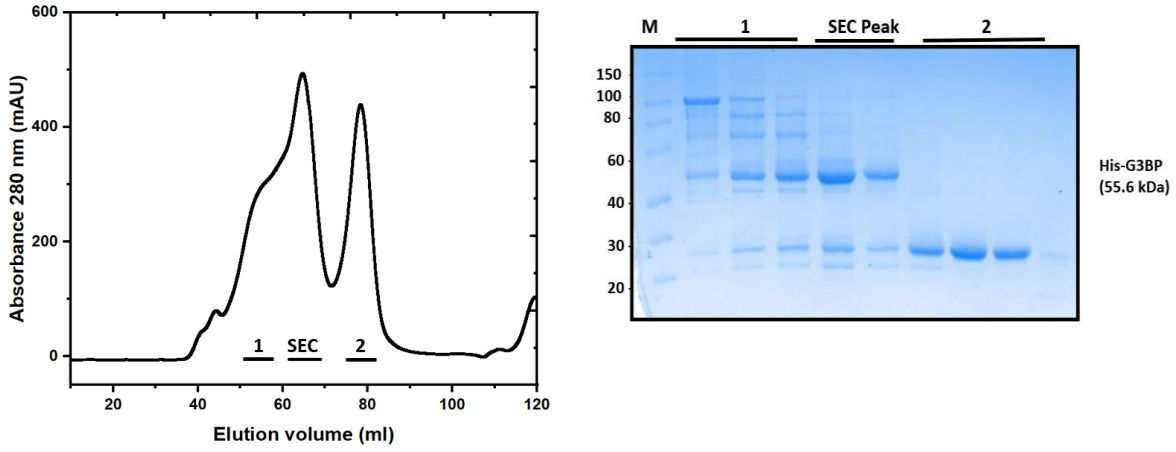

B

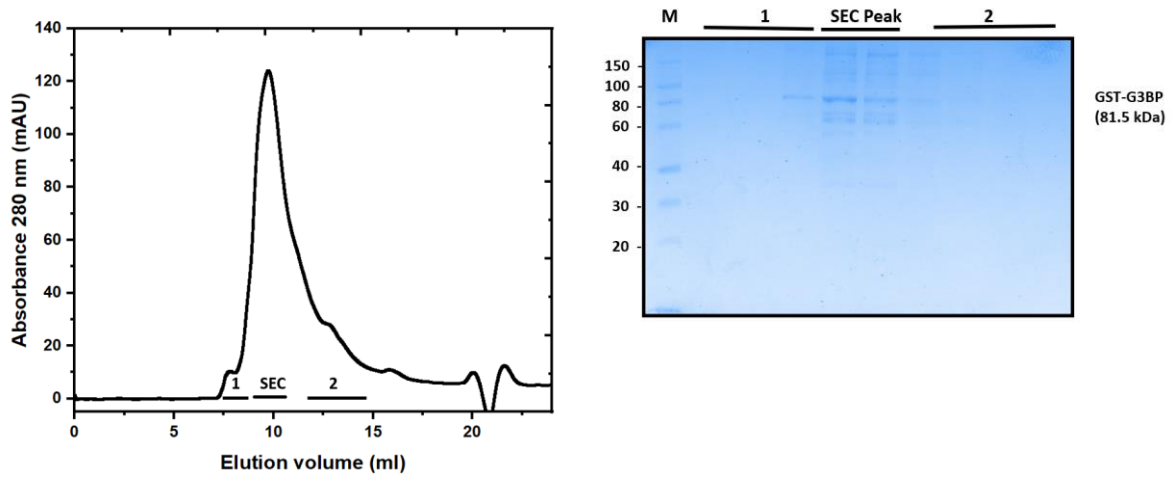

Figure 51 : Size exclusion chromatography of Ras-GAP binding protein 2. A) SEC profile and corresponding SDS-PAGE of His_6-tagged construct purified using S200 column 16/60 column B) SEC profile and corresponding SDS-PAGE of His_6-GST tagged construct purified using S200 column 10/300 column . Bar at the bottom of peak corresponds to the fractions on the SDS-PAGE labelled as SEC peak. M - protein marker in kDa. The fractions labelled SEC Peak were pooled and used for interaction studies.

3.2.2.3 PITH domain-containing protein 1-like (PITHD1)

PITHD1 was cloned and expressed using pCoofy1. Two different *E.coli* strains namely BL21 and Rosetta were tested. Expression conditions were as described in 2.2.10.1. Pellet obtained from 3L of culture was used for purification. The sequence of purification steps included an IMAC, anion-exchange, and finally size exclusion as described in Tables 26, 30 and 33. The fractions from IMAC and anion-exchange elution consisting the protein of expected molecular weight on the SDS-gel were pooled, concentrated and applied to the SEC column. The expression and solubility of the construct was adequate to obtain 10 mg of protein from 3L of culture. Chaperone around 70 kDa was the only other considerable contaminant binding to the affinity column. This was prominently seen in the expression from Rosetta strain. The additional anion-exchange did not succeed in getting rid of the chaperone which was later excluded to a larger extent during SEC. The SEC chromatogram of the protein purified from BL21 depicts predominantly a single symmetrical peak (Fig. 52B) as opposed to the SEC elution profile from the Rosetta purified protein (Fig. 52A). For this reason, the PITH domain containing protein 1 purified from BL21 was used for all further studies. The elution volume of the PITHD1 was 89.87 ml. Purified PITHD1 with expected molecular weight of 26 kDa was of relatively pure quality as seen in the gels (Fig. 52).

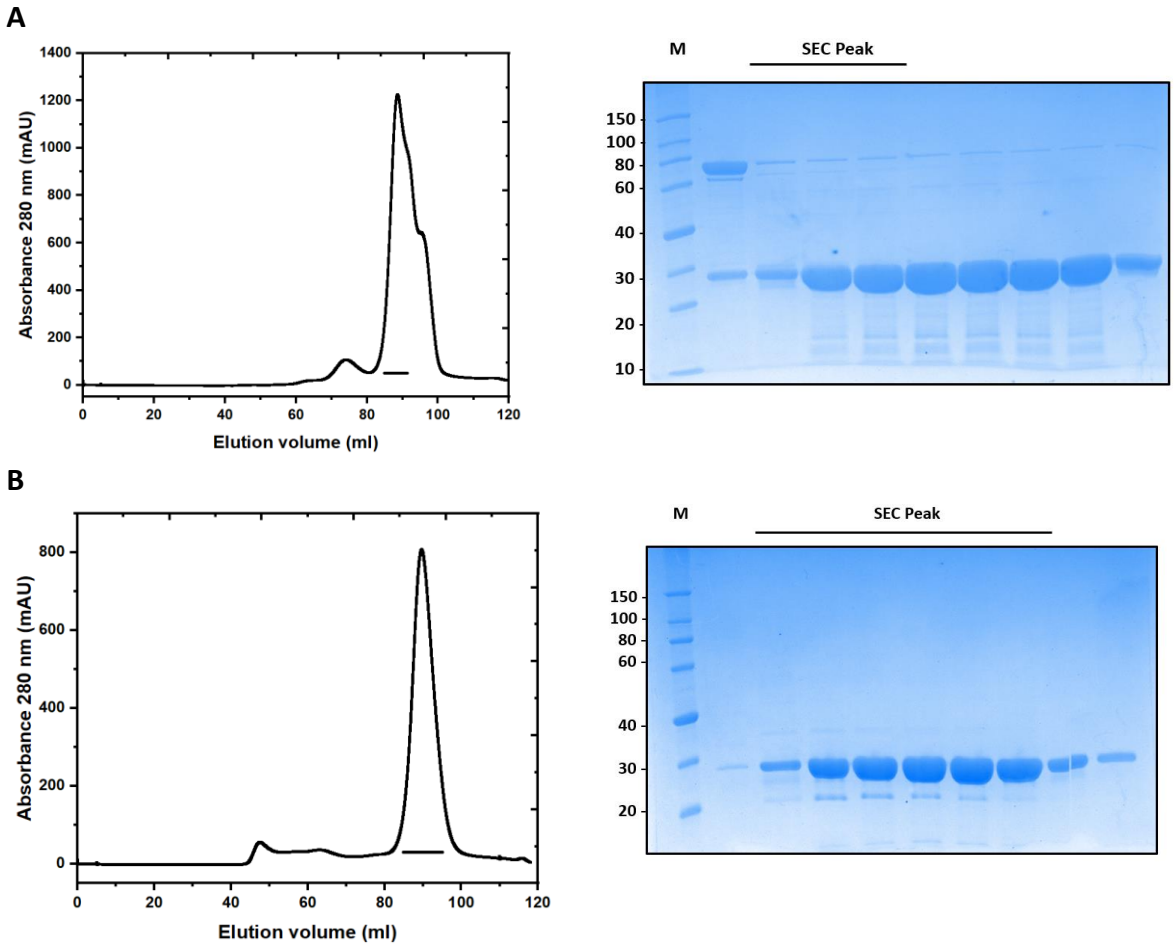

Figure 52: Size exclusion chromatography of PITH domain containing protein 1 using S200 16/60 column. A) SEC profile and corresponding SDS-PAGE of protein purified from Rosetta B) SEC profile and corresponding SDS-PAGE of protein purified from BL21. Bar at the bottom of peak corresponds to the fractions on the SDS-PAGE labelled as SEC peak. M - protein marker in kDa. The fractions labelled SEC Peak were pooled and used for interaction studies.

3.2.3 In-vitro confirmation of direct interaction between L-CRY and interactors

PITHD1 purified from *E.coli* as stated in 3.2.2.3 was tested for direct interaction with L-CRY. The proteins were mixed in 1:1 ratio and incubated overnight and run on an analytical S200 10/300 column. Due to baseline variation, normalized absorbance at 280 nm was used to overlay the SEC runs. The peak seen in Fig. 53A corresponds mainly to L-CRY which is in accordance with the independent L-CRY elution volume. The shoulder numbered 3 is likely the overlap of trailing L-CRY and the front end of PITHD1 peak. This is also evident from the gel, which indicates the reducing L-CRY amounts corresponding to increasing PITHD1 amounts in lanes marked 3 (Fig. 53B). Thus, no direct interaction could be established between the two proteins.

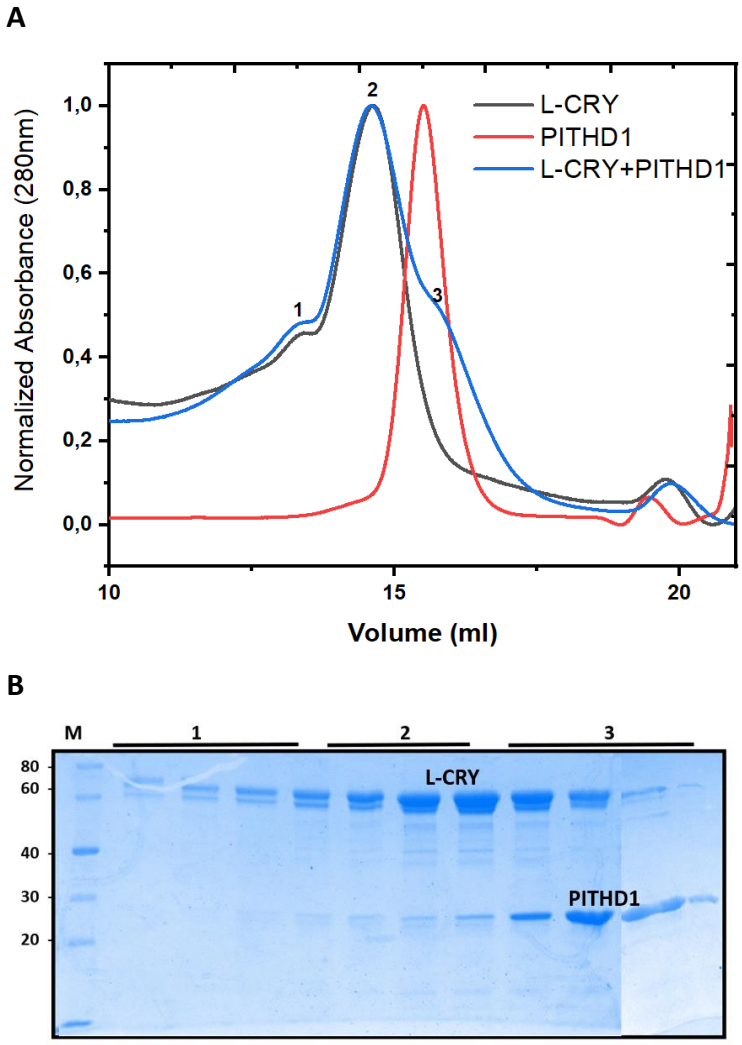

Figure 53: Analytical size-exclusion chromatography of complex between L-CRY and PITHD1. A) SEC profile on a S200 10/300 column of L-CRY (black), PITHD1 (red) and 1:1 preincubated L-CRY and PITHD1 (blue). The peak and shoulders of the L-CRY+PITHD1 run used for SDS-PAGE are numbered (1-3). B) Corresponding SDS-PAGE analyzing the fractions indicated in the chromatogram as 1-3. M: Marker in kDa.

The full-length constructs of YTHDF and G3BP were codon optimized for insect cells and cloned into pCoofy27 (N-terminal His_6 tag) and pCoofy28 (N-terminal His_6-GST tag) for purification and pull-down validation. Both proteins were purified using affinity and size exclusion chromatography. The N-terminal His_6 tag of L-CRY was cleaved and magnetic nickel/GSH beads were used for pull-down. Pre-purified bait (His-GST YTHDF/His Ras-GAP-BP) was incubated with the beads for 1h followed by 2-3 wash steps. L-CRY was later incubated with YTHDF/G3BP bound beads for 1.5-2 h and the beads washed multiple times. The elution fraction with the bound proteins was obtained by heating the beads at 70°C for 10 min with

1x lithium dodecyl sulfate buffer (LDS) buffer. Suitable L-CRY and ligand controls were also carried out in parallel.

The elution fraction "E" from G3BP+L-CRY pull down with magnetic nickel beads shows no band corresponding to L-CRY on the gel (Fig. 54A). The controls carried out in parallel indicate the binding of G3BP to nickel beads and not of L-CRY as expected (Fig. 54B, 54C). The elution fraction from YTHDF+L-CRY pull down with magnetic GST beads shows faint band corresponding to L-CRY on the gel (Fig. 55A). The L-CRY control carried out in parallel indicates low non-specific binding to beads (Fig. 55B). The elution from YTHDF control shows the expected binding (Fig. 55C). The results from the pull down indicated the absence of direct interaction between L-CRY and either of the ligands YTHDF or G3BP. Possibly the interaction with L-CRY requires other mediators which are yet to be discovered.

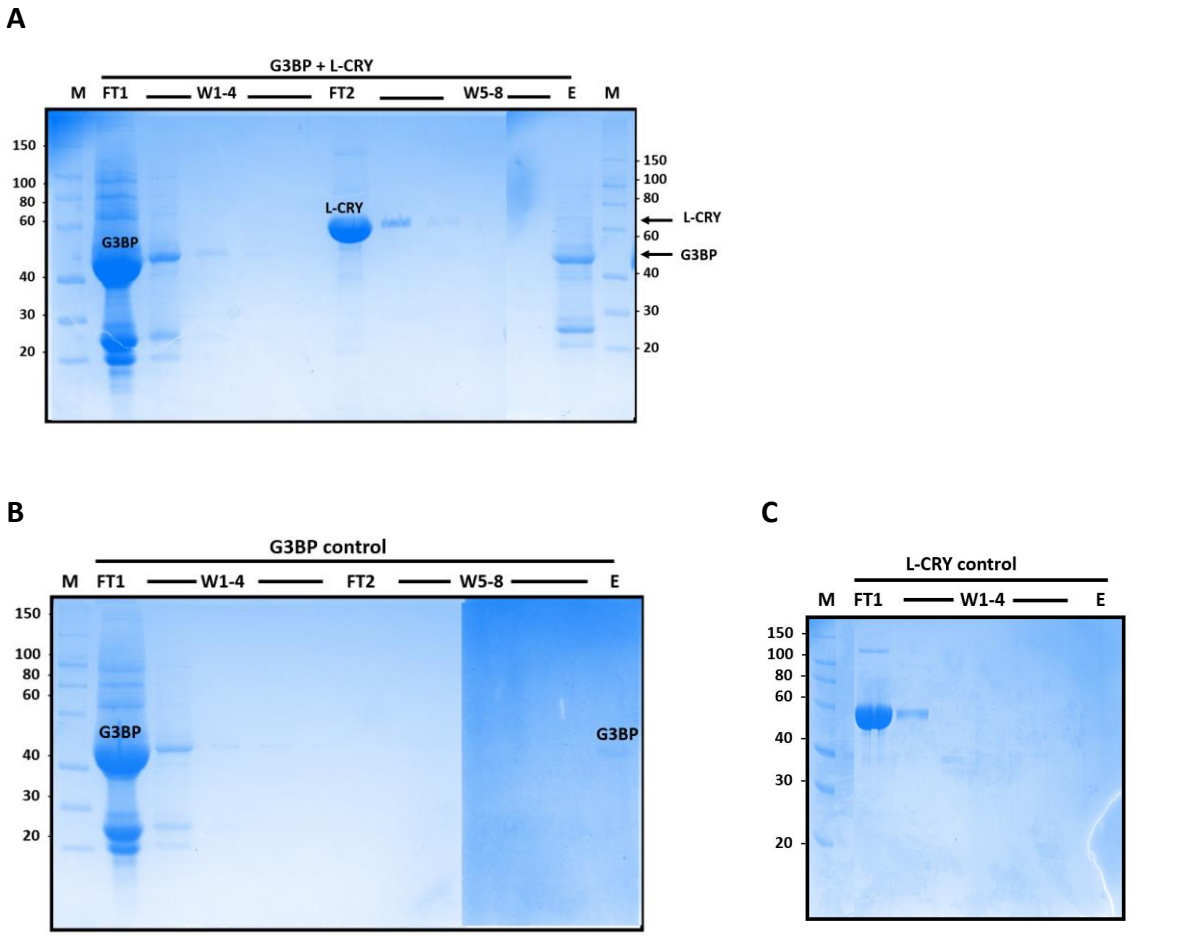

Figure 54: Pull-down of G3BP with L-CRY using magnetic nickel-beads. A) Nickel beads saturated with G3BP were incubated with L-CRY and washed thoroughly. The elution fraction indicates no binding of L-CRY to G3BP. B) G3BP control wherein beads were incubated,

washed, and eluted. C) L-CRY control wherein beads were saturated with L-CRY, washed and eluted. M: Marker; FT1, FT2 : flow through of excess protein ; W1-W8: Wash ; E: Elution.

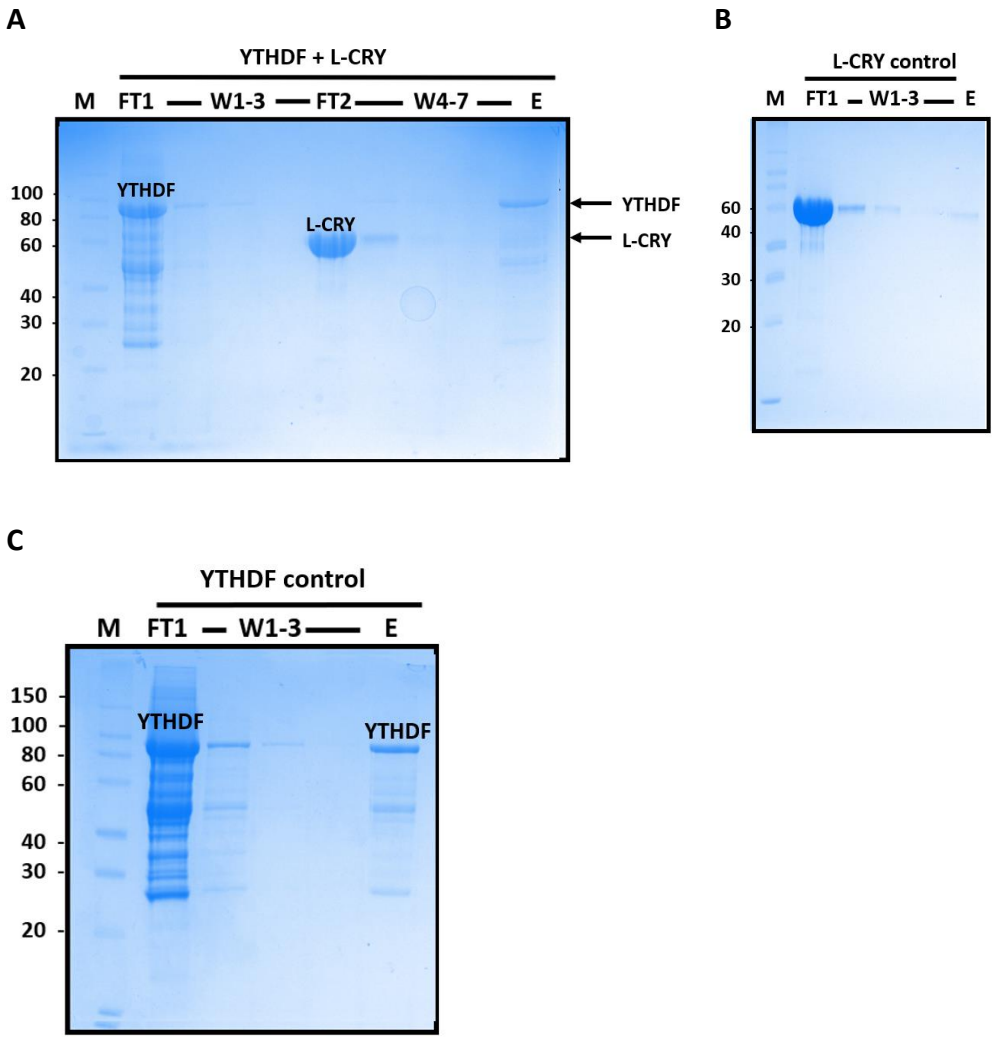

Figure 55: Pull-down of YTHDF with L-CRY using magnetic GSH beads. A) Nickel beads saturated with YTHDF were incubated with L-CRY and washed thoroughly. The elution fraction indicates no binding of L-CRY to YTHDF. B) YTHDF control wherein beads were incubated, washed, and eluted. C) L-CRY control wherein beads were saturated with L-CRY, washed and eluted. M: Marker; FT1, FT2 : flow through of excess protein ; W1-W8: Wash ; E: Elution.

3.3 P-CRY

3.3.1 Expression and purification of P-CRY variants

Several constructs of P-CRY full length and variants were tested in insect cells and *E.coli*. However, no expression was observed. Finally, genes were optimized for insect cell expression. This led to expression of the proteins in Sf9 cells however, they remained insoluble. Hence, these optimized genes were recloned into pCoofy6 vector with N-terminal

His-SUMO tag to facilitate solubility. Two constructs of P-CRY namely, P-CRY PHR (200-697) and P-CRY PHR with cctail (200-778) were expressed in *E.coli* with conditions stated in Table 22. Pellet from 6L expression culture were used for each purification as the solubility was low despite the N-terminal His_6-SUMO tag. Of the two constructs, P-CRY PHR with cctail was more soluble. P-CRY variants were purified with an IMAC, anion-exchange, and size-exclusion chromatography. as described in Tables 26, 30, 32 and 33. Anion-exchange was used for P-CRY PHR and cation-exchange for P-CRY cctail. The fractions from IMAC and ion-exchange elution consisting the protein of expected molecular weight on the SDS-gel were pooled, concentrated and applied to the SEC column. All steps were carried out with minimum exposure to red light or dark conditions were maintained wherever feasible. The ion-exchange step was essential to get rid of *E.coli* chaperone (not shown). The elution volume of P-CRY PHR and P-CRY PHR with cctail from the S200 16/60 was 83.9 ml and 82.5 ml. The determination of the oligomeric state of P-CRY variants was done with SLS as the molecular weight calculations from SEC elution volumes were not in accordance with theoretical molecular weights. The absorption with 380 nm was higher as compared to 450 nm indicating the presence of additional chromophore such as MTHF. The purified protein was pale yellowish-green color (Fig. 56).

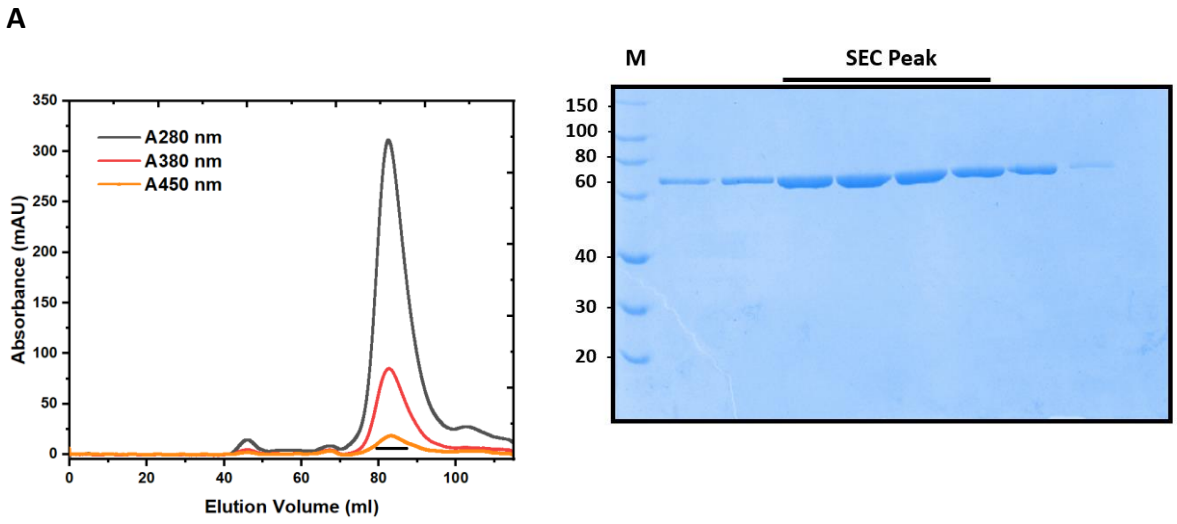

B

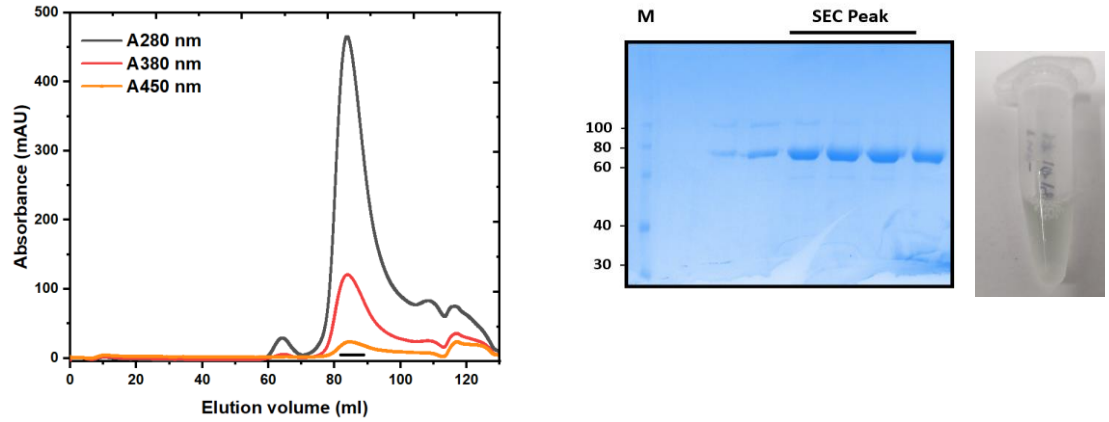

Figure 56 : Size exclusion chromatography of P-CRY variants using S200 16/60 column. A) SEC profile and corresponding SDS-PAGE of P-CRY PHR. B) SEC profile and corresponding SDS-PAGE of P-CRY cctail . Bar at the bottom of peak corresponds to the fractions on the SDS-PAGE labelled as SEC peak. M - protein marker in kDa. Concentrated P-CRY cctail binding chromophores depicted by the pale bluish-green color.

3.3.2 Chromophore content of P-CRY using HPLC

Purified P-CRY variants were pale greenish-blue in color and monitoring absorbances at 450 nm and 380 nm gave initial indications that P-CRY might have a secondary chromophore bound to it, in addition to FAD. To characterize the chromophores bound to P-CRY, the protein was denatured, and the released supernatant was analyzed by RP-HPLC (2.3.7). The chromatogram revealed 2 elution peaks when absorbance at 370 nm was monitored (Fig. 57). For comparison, chromophore standards were run under same conditions (Fig. 20B). Initial peak between 3.4-3.7 ml is distorted, however, the elution volume corresponds to that of MTHF. The MTHF standard elutes at 3.35 ml. It is probable that heat denaturation of MTHF leads to thermal degradation of the folate (Thuy Nguyen et al., 2003). The peak eluting at 4.67 ml corresponds to FAD as seen with standard FAD elution. These results provide good evidence that P-CRY binds two chromophores, namely MTHF and FAD.

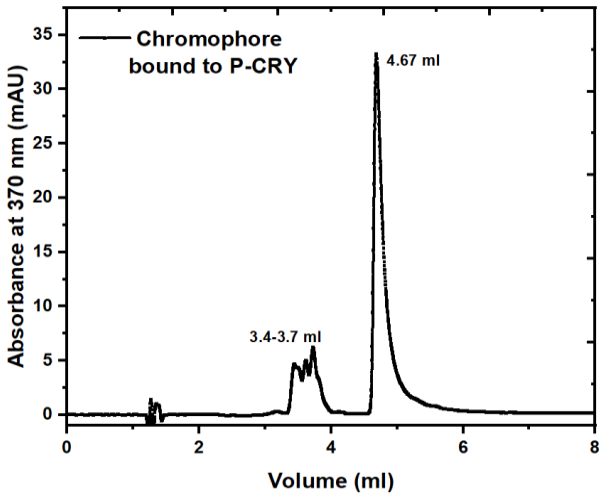

Figure 57: Reverse phase HPLC analysis to identify P-CRY bound chromophore. A) Elution profile of P-CRY bound chromophore obtained after heat denaturation run on Macherey-Nagel C18 Gravity-SB (150/4/5 µm) column.

3.3.3 UV/VIS Absorbance spectroscopy of P-CRY

After establishing that FAD is one of the chromophores bound to P-CRY, a UV-VIS dark spectrum of P-CRY was taken to ascertain the oxidation state of FAD. The spectrum shows maxima at 398 nm, 582 nm, and 628 nm (Fig. 58A). The spectral absorption in the yellow-red region is an indication of flavin neutral radical (refer Fig. 21C). Also, the peak around 380-390 nm is an indication of pterin-like chromophore such as MTHF as seen before e.g. in rice CPD photolyases (Teranishi et al., 2008) and CryP in diatom *Phaeodactylum tricornutum* (Juhas et al., 2014).

On illumination with red light (λ = 635 nm), the peaks at the 580-630 nm range are lost. This could indicate the transition towards the fully reduced FAD state ($FADH^-$) (Fig. 58B). However, the transition is not complete as seen for *Xenopus laevis* (6-4) photolyase (Okafuji et al., 2010) or CryP of diatom and the increase in the absorption at 340 nm could indicate possible aggregation effects. The absorption peak at 398 nm is not lost, which was observed in Arabidopsis DASH cryptochrome (Cry3) as an indication of MTHF photoreduction (Moldt et al., 2009). No dark recovery was observed. For further characterization of P-CRY photocycle, a better quality of sample would be essential.

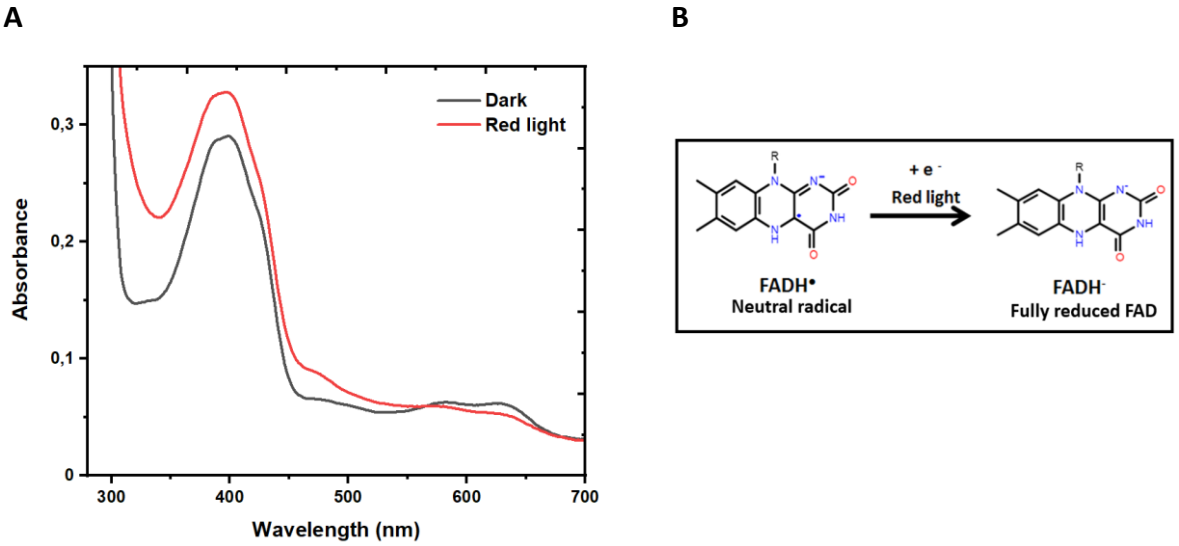

Figure 58: UV-VIS absorption spectra of P-CRY in dark and after red-light illumination. A) Absorption spectrum of P-CRY in dark and after 12 min of red-light illumination (λ = 635 nm). Absorbance at 370 nm and around 580-650 nm vary between neutral radical (FADH°) and fully reduced FAD ($FADH^-$) (after red-light). Spectra for different FAD redox states is depicted in Fig. 6C for reference. B) Reaction scheme for the conversion of neutral radical to fully reduced FAD on red-light illumination.

3.3.4 Multiangle light scattering of P-CRY

The oligomeric state of P-CRY variants was confirmed with the help of MALS measurements carried out by Prof. Elmar Jaenicke (JGU Mainz). The calculated molecular weight for P-CRY PHR was 141 kDa ($MW_{theoretical}$ dimer = 136 kDa) and that of P-CRY cctail was 156 kDa ($MW_{theoretical}$ dimer = 156 kDa) (Fig. 59). The obtained molecular weight was in accordance with the theoretical molecular weight of the dimers. No additional oligomeric states were detected. Considerable aggregation was observed for the P-CRY cctail construct by the light scattering pattern between 7-8 ml (Fig. 59B).

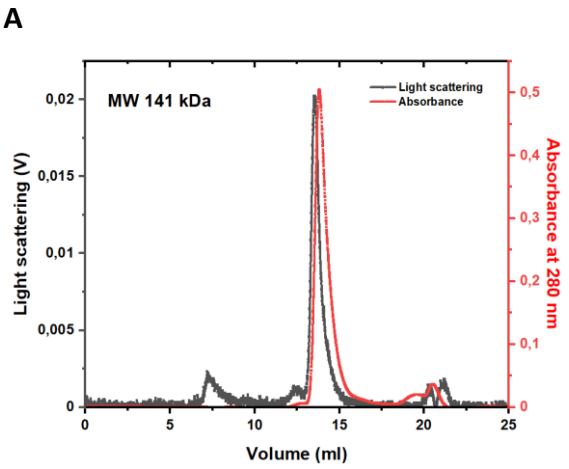

B

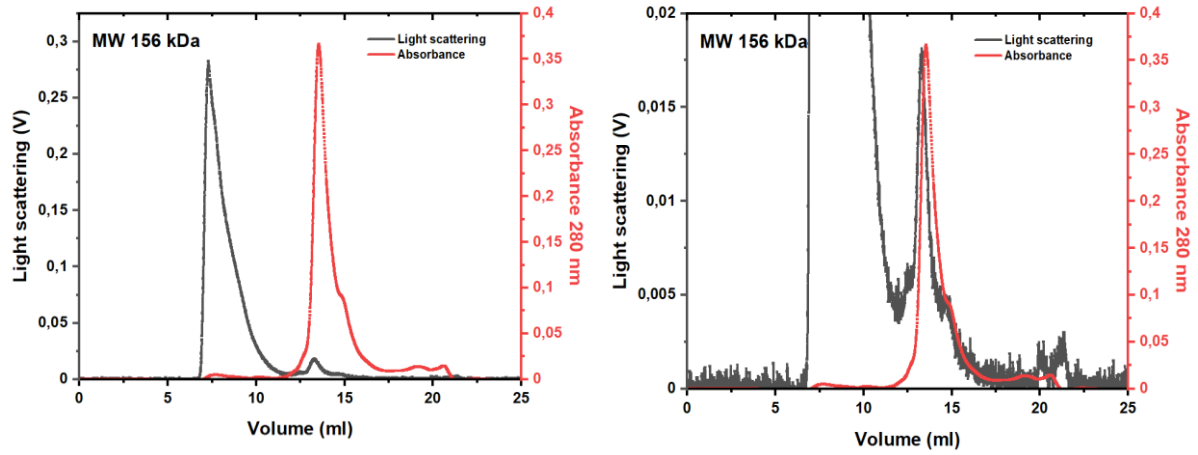

Figure 59:Multi-Angle Light Scattering (MALS) analyses of dark-state P-CRY variants confirms that P-CRY forms a homodimer in solution. The elution of P-CRY variants was monitored by the absorbance at 280 nm (red) and the light scattering (black). A)P-CRY PHR construct monitored for scattering and absorbance indicates minor aggregation and a single dimer peak of 141 kDa. B) P-CRY cctail monitored for scattering and absorbance. The light scattering peak around 7 ml indicates aggregation. Zoomed figure depicting the overlay of the absorbance and light scattering corresponding to the dimer peak of 156 kDa.

3.3.5 Crystallization of P-CRY

P-CRY cctail was concentrated to 5 mg/ml and crystallization screens were carried out. Some hit conditions showed microcrystals formation after 24 h of setting up the drop at 20 ^{o}C. Reproductions were carried out at both 20 ^{o}C and 4 ^{o}C. The quality of the crystals could not be improved. It would be essential to improve the protein quality and buffer conditions before further crystallization trials.

3.3.6 Single molecule electron microscopy of P-CRY

Negative stain

P-CRY PHR (5 mg/ml) and P-CRY cctail (7 mg/ml) were diluted and negative stained with uranyl formate. Representative micrograph for P-CRY cctail is shown in Fig. 60A. The protein was stained well with minor aggregation or clumping on the grids. The 2D classes P-CRY cctail were generated and indicate several similar class orientations (Fig. 60). However, based on the initial negative stain results, it appears possible to proceed with cryo grid preparation and resolve a model for the P-CRY variants in the future.

A

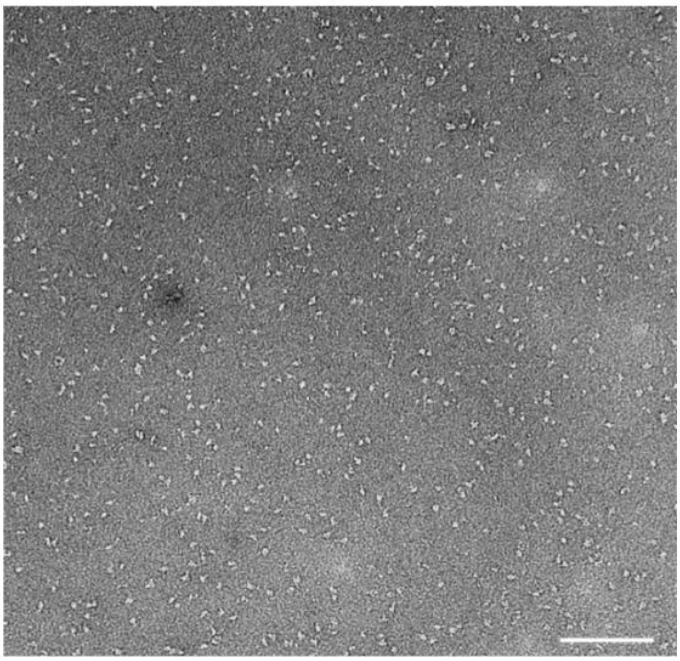

B

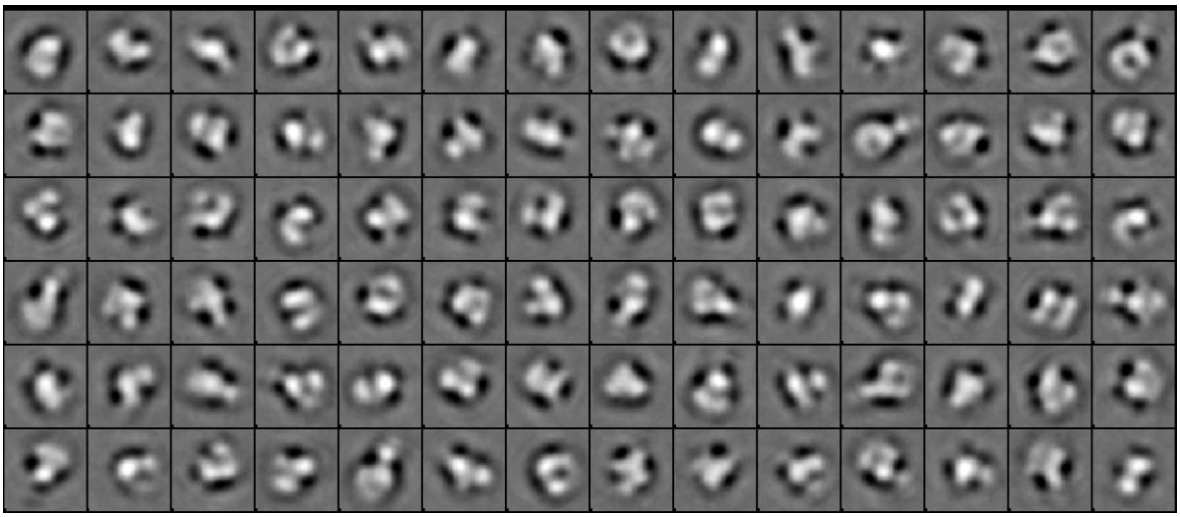

Figure 60 : Negative stain of P-CRY cctail. A) Representative exposure image of P-CRY (7 mg/ml) diluted 1:2000. The scale bar for the image is 100 nm. B) 2D classes generated for P-CRY cctail by processing negative stain micrographs.

3.3.7 Pull down and mass spectrometry with P-CRY variants

A similar pull-down approach as done before with L-CRY was tested with P-CRY in order to gain functional insights. P-CRY cctail (200-778) was coupled with nickel beads and used a bait while P-CRY PHR coupled beads were considered as control. This was done in order to avoid the issue of non-specific bead binding seen before with L-CRY due to lack of proper control. Lysate from 20 frozen worm heads of the new moon phase (ZT20) were used for dark pull

down. As seen in the scatter plot in Fig. 61, most of the candidates were common to both P-CRY PHR and P-CRY cctail. Few interactors specific to the tail construct were discovered mentioned in Table 41. Most of them were transcription-translation regulators. It was also seen that several *E.coli* homologous proteins were present in the list. As P-CRY variants were purified from *E.coli,* there exists the possibility of residual carry over from purification steps. It was later discovered by our collaborators that P-CRY is predominant in the trunk part of the worm and not so much in the head by preliminary in situ studies. Protein extraction from *Platynereis* trunks has so far not been successful due to extensive degradation also in presence of protease inhibitors. Considering this information, it is first necessary to establish extraction protocol from trunk lysates and repeat the pull-down studies in order to obtain potential interaction partners for P-CRY.

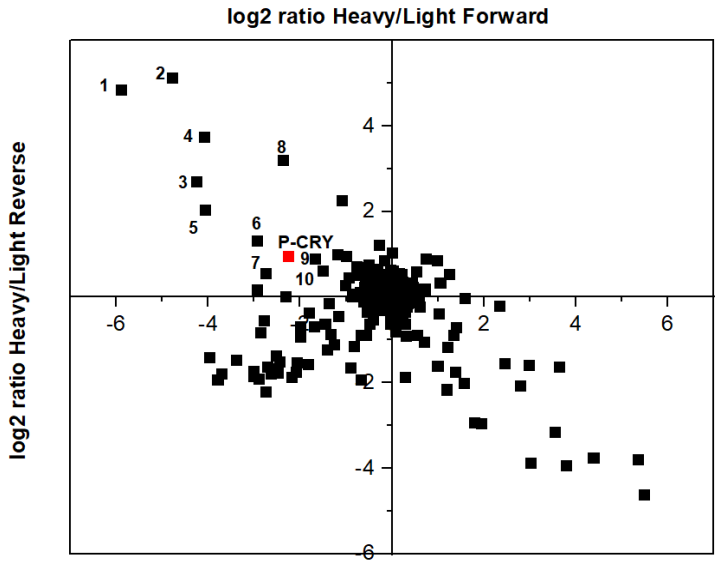

Figure 61 : Dark state interactors of P-CRY cctail (marked in red) versus P-CRY PHR as control. Scatter plot depicting the potential dark state interactors listed in Table 42. The non-specific proteins pulled down in the experiment are not numbered.

Table 41: List of light state P-CRY cctail interactors numbered in Figure 51

Hit	Protein ID	Annotation
1.	comp2260289_c1_seq5	ref|WP_008334097.1| MULTISPECIES: elongation factor Tu [Herbaspirillum] emb|CAM32590.1| GTPase translation elongation factor TU (E [Herbaspirillum seropedicae] gb|ADJ61624.1| EF-Tu elongation factor p
2.	comp2219690_c0_seq1	gb|ACY86044.1| hypothetical protein ETAE_3213 [Edwardsiella tarda EIB202]

		50S ribosomal protein L15 [Escherichia coli]
3.	comp1286416_c0_seq1	gb|EDX33388.1| PTS IIA-like nitrogen-regulatory protein PtsN [Shigella dysenteriae 1012] gb|EGI09597.1| nitrogen regulatory protein (Enzyme IIA-NTR)(Phosphotransferase enzyme IIA component) (PTS system)
4.	comp2028508_c0_seq1	gb|KFZ99738.1| hypothetical protein DP20_3417 [Shigella flexneri]
5.	comp2232304_c1_seq4	ref|WP_000018003.1| MULTISPECIES: transcriptional regulator [Proteobacteria] ref|NP_417542.1| PadR family putative transcriptional regulator [Escherichia coli str. K-12 substr. MG1655] ref|NP_708879.1
6.	comp1667713_c1_seq1	emb|CSE66591.1| sensory box-containing diguanylate cyclase [Shigella sonnei]
7.	comp2030991_c0_seq1	emb|CSR66986.1| alpha-galactosidase [Shigella sonnei]
8.	comp2065367_c0_seq1	pir||Q3ECS7 hypothetical 77K protein (spoT 3' region) - Escherichia coli tRNA (guanosine-2'-O)-methyltransferase [Escherichia coli]
9.	comp2155138_c0_seq2	emb|CTT92577.1| AraC family transcriptional regulator [Escherichia coli]
10.	comp2096703_c0_seq1	gb|EYY51009.1| hypothetical protein BX81_18085, partial [Escherichia coli O165:H25 str. 2010C-4874] selenocysteine-specific translation elongation factor, partial [Shigella flexneri]

3.4 dCRY

3.4.1 Purification of dCRY

Full length dCRY cloned in pFastBac HT B vector was used for the expression and purification from insect cells as a N-terminal His_6-tagged fusion protein. The P1 virus obtained after bacmid transfection and virus amplification was used to infect 1.2 L of 1 x 10^6 *Sf9* cells for 72 h. dCRY was purified by a 3-step purification protocol. To maintain the dark state of the cryptochrome throughout the purification, all steps were carried out with minimum light exposure or in red light. The conditions for nickel affinity were as mentioned in Table 27. dCRY eluted with 100 mM imidazole. The elution fractions were pooled and concentrated to 10 ml volume. This was diluted 10-fold with low salt buffer and applied to an anion-exchange chromatographic DEAE Sepharose column (Table 31). dCRY was eluted with a gradient from 0-500 mM NaCl and all fractions containing the protein were pooled, concentrated and applied to a S200 16/60 for a final polishing step with SEC buffer (25 mM Tris pH 8.0, 150 mM

NaCl, 5% glycerol, 1 mM TCEP). The SDS-PAGE analysis indicated that purified dCRY was pure with minimal contaminants (Fig. 62). The absorbance at 450 nm corresponding the dCRY peak and yellow elution fractions indicated the presence of oxidized flavin. 10 g of *Sf9* cells yielded 5 mg of pure dCRY. Fractions containing pure dCRY were pooled, concentrated, and stored at -80°C until further use.

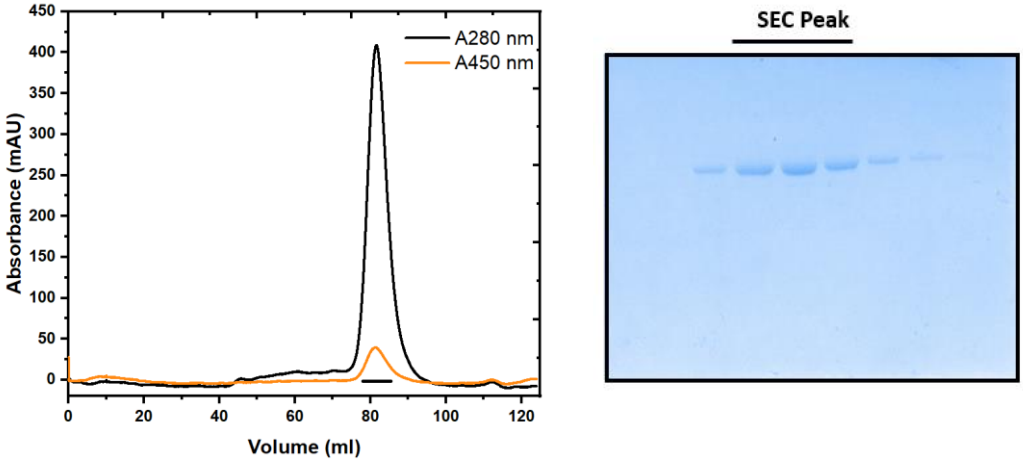

Figure 62: Size exclusion chromatography of dCRY from Sf9 insect cells. SEC profile and corresponding 10% Bis-Tris gel depicting His_6-tagged dCRY purified using S200 column 16/60 column. Bar at the bottom of peak corresponds to the fractions on the SDS-PAGE labelled as SEC peak.

3.4.2 Moonlight and sunlight response of dCRY

The response of dCRY to moonlight illumination was studied using absorption spectroscopy as done previously with L-CRY. It is known that dCRY in the dark state consists of oxidized flavin which on blue light illumination is converted to the anionic radical (Berndt et al., 2007). Continuous illumination with full moon intensity does not photoreduce L-CRY to the light activated state (Fig. 63A). A 20 min sunlight exposure converted the oxidized flavin to the light activated anionic radical as seen with blue-light illumination. Thus, dCRY sensitivity to sunlight and photoreduction is comparable to its response to blue-light.

Increasing the moonlight intensity to twice the full moon intensity did not alter the response of dCRY (Fig. 63B). Thus, dCRY is less sensitive *in vitro* to naturalistic moonlight conditions but possibly can play a role *in vivo* impacting the circadian clock in *Drosophila* (collaborator lab).

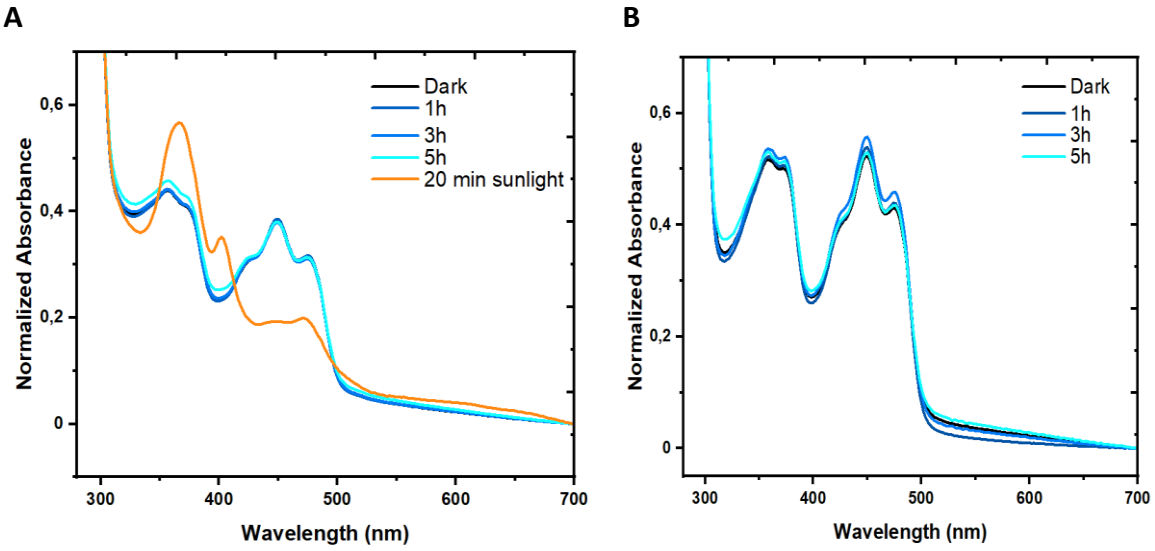

Figure 63: Moonlight and sunlight response of dCRY. A) Absorption spectra of dCRY on continuous illumination with full moon intensity obtained at different time points followed by 20 min of sunlight illumination. The dCRY spectrum transitions from the dark state (oxidized FAD) to the light activated $FAD^{\bullet-}$ radical state in response to sunlight. B) Absorption spectra of dCRY on continuous illumination with 2xfull moon intensity obtained at different time points. dCRY does not show transition towards light state in response to moonlight.

4 Discussion

4.1 L-CRY: The dCRY orthologous cryptochrome

Platynereis dumerilli possess three different cryptochrome types of which L-CRY is an ortholog of the *Drosophila* cryptochrome dCRY. dCRY has been well characterized as the circadian blue light photoreceptor (Emery et al., 2000; Ishikawa et al., 1999). At a sequence level, L-CRY is 45% identical to dCRY and most of the homology lies within the photolyase homology region (PHR), which contains the FAD binding region (Fig. 16). This provided an early indication of the possible photochemistry of L-CRY. To confirm our hypothesis, we expressed and purified full length L-CRY from insect cells. Purified L-CRY contained bound FAD (Fig. 17A,C). Reverse phase HPLC analysis of bound chromophores also confirmed the absence of any secondary light-harvesting chromophores such as methenyltetrahydrofolate (MTHF) (Fig. 20A). We could validate a photoreaction mechanism for L-CRY similar to dCRY. L-CRY possessed oxidized FAD in the dark state which on photoreduction with blue-light led to the formation of the anionic FAD radical. Based on our absorption spectra, we exclude the possibility of other flavin redox states such as the neutral $FADH^{o}$ radical or fully reduced FADH. The presence of three isosbestic points around 352 nm, 414 nm and 502 nm confirms the presence of two flavin states (Fig. 24). L-CRY reverted back to the dark state with a time constant between 2 min (at 18 ^{o}C) to 4.7 min (on ice) based on the monitored temperature.

4.2 L-CRY dimer in the dark state

Our purified L-CRY behaved as a dimer in solution (Fig. 17B) in contrast to the monomer of dCRY (Berndt et al., 2007). However, plant cryptochromes such as *At*CRYs are known to form active homodimers, which is also required for their photoreceptor activity (Sang et al., 2005). Several studies established that cryptochrome dimerization is also essential for its biological functioning (Rosenfeldt et al., 2008). These results prompt us to speculate that L-CRY in its dimeric state could be the signaling state. The dimeric dark state of L-CRY was additionally corroborated with the help of MALS (Fig. 40) and CRYO-EM (Fig. 46). The dimer interface of L-CRY suggested by CRYO-EM includes residues that are not conserved in dCRY. This could be one of the explanations for the differences in the oligomeric state of both these cryptochromes. The physiological role of this dark state dimer has to be investigated further.

4.3 L-CRY response to moonlight and sunlight

Based on the blue-light spectrum of L-CRY, it was evident that L-CRY exhibits absorbance between 420-500 nm which are also a part of the moonlight range. These results along with the observation that l-cry wildtype worms sense artificial light conditions leading to higher asynchrony compared to l-cry mutants (collaborator Lab), hinted towards a possibility of a novel lunar photoreceptor. To test this, purified L-CRY was subjected to illumination with naturalistic moonlight source. Photoreduction of FAD_{ox} to the anionic radical state with 110s of moonlight as seen previously with blue-light illumination was not observed (Fig. 25B). Prolonged activation with moonlight led to the slow build-up of a partial light activated state/anionic $FAD^{\circ-}$ radical. The observed photoactivation with moonlight did not attain the complete light-activated state even on prolonged illumination. Based on the observed spectra, it was seen that moonlight induced partial activation was variable leading to FAD reduction between 35-50% (Fig. 64) and in some cases also beyond 50% (Fig. 27, 30C). The partial photoreduction could mean that one monomer of the L-CRY homodimer contains the moonlight-photoreduced $FAD^{\circ-}$ radical, while the other monomer is in a conformation wherein the FAD molecule is still in the FAD_{ox} state leading to an asymmetric dimer (Fig. 65). This is speculative and needs to be confirmed. The variability in the degree of photoreduction can be attributed to the technical setup wherein the protein is illuminated on ice for several hours and the spectrum taken using a Tecan plate reader in the dark. This shift in the light conditions would lead to some extent of dark recovery. In addition, the setup on ice is not controlled in terms of humidity and the surrounding temperature. The experiments are carried out in aerobic environment and the loss in effectiveness of reducing agents over time is not monitored. Any sort of aggregation which might occur due to loss of reducing agents or prolonged illumination are difficult to monitor spectroscopically as an increase in absorbance around 340-370 nm is also a characteristic of anionic $FAD^{\circ-}$ radical formation. A well-designed setup under controlled conditions would be essential in order to simultaneously illuminate with moonlight source and record the spectrum of the sample without disturbing the sample.

The response of L-CRY to sunlight was similar to that observed with blue-light illumination which was in accordance with the expectation as blue-light (around 450 nm) is routinely used in circadian spectroscopic studies as a substitute for daylight (Fig. 24, 31A, 31B). The recovery in dark after sunlight illumination was also within minutes as after blue-light illumination (Fig.

31C, 31E). The delay in the recovery of blue-light/sunlight activated L-CRY in presence of moonlight could be an interplay between dark recovery kinetics and low efficiency of moonlight to alter the FAD redox state (Fig. 28C, 33B).

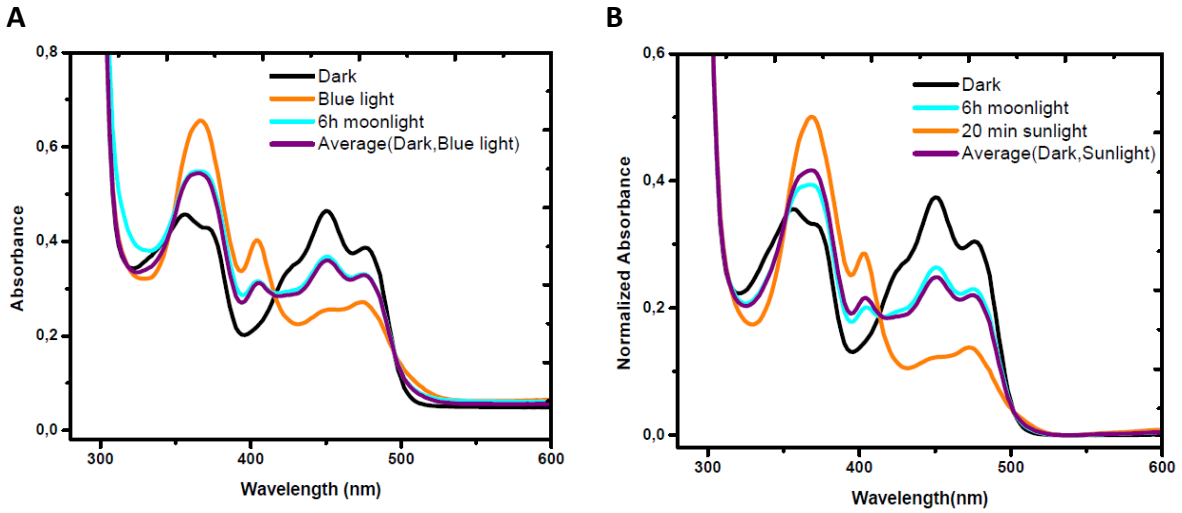

Figure 64: Moonlight induced partial anionic radical. A) The 6h moonlight illumination led to a spectrum (cyan) corresponding to the calculated 52.6% accumulation of anionic FAD°⁻ radical. B) The 6h moonlight illumination in another experiment led to a spectrum (cyan) corresponding to the calculated 39% accumulation of anionic FAD°⁻ radical. The average spectra (violet) in both A and B is obtained by averaging the blue-light/sunlight (orange) and dark (black) spectra respectively. The accumulation of anionic FAD°⁻ radical was calculated using the absorbances at 404 nm with the ratio ΔA(Moonlight - Dark) / ΔA(Blue light/sunlight - Dark).

Mimicking the transitions during the day such as sunrise and sunset scenarios with the naturalistic moonlight and sunlight, led to the observation that moonlight was not sufficient to maintain the sunlight state, which first recovered back to the dark state. This could likely be due to the fast dark recovery kinetics and the low fluence rate of moonlight or possibly the absence of some key stabilizing partners which might occur in *in vivo*. L-CRY is speculated to integrate photon information over long periods of time. This is based on previous studies wherein Drosophila CRY and vertebrate melanopsin were shown to exhibit high light sensitivity by using dim-light integration mechanism. This photon integration process was active up to at least 6 hours in Drosophila flies. Furthermore, it has been shown that the probability of photon capture per CRY molecule is low in Drosophila and hence temporal integration to increase light sensitivity physiologically is essential (Vinayak et al., 2013). Considering the habitat of the *Platynereis dumerilli* and the low intensities of light at water depths, this principle could well be true for the marine worms. We observed that one-third

of full moonlight intensity supplied for 8 h was still not sufficient to attain a similar photoreduction as 6 h full moon intensity (Fig. 30B), which indicates a threshold for minimum intensity that is essential for moon-light activation of L-CRY. Moreover, our spectroscopic data suggest, that L-CRY is able to dose-dependently react to moonlight intensity changes (Fig. 30 A). We speculate this could physiologically relate to detecting moon waxing and waning phases and naturally not stimulate worm spawning behavior. Furthermore, our observation, that L-CRY remains in the moonlight-state with partial $FAD^{\circ-}$ accumulation also upon prolonged full moonlight exposure beyond 6 h, while even a short 110 s high-intensity blue-light exposure fully photoreduces L-CRY suggests, that L-CRY is able to distinguish between and to differentially react to moonlight and the much higher intensity day-light.

Previous studies speculated the possibility of dCRY homologues functioning as a moonlight receptor in marine animals due to its sensitivity to dim light (Oliveri et al., 2014a; Vinayak et al., 2013). However, naturalistic full moonlight did not lead to photoreduction of dCRY *in vitro* (Fig. 63A). This was true even at intensities twice that of naturalistic moonlight indicating that dCRY sensitivity to moonlight is not similar to L-CRY (Fig. 63B). However, we cannot exclude the cellular sensitivity of dCRY in response to dim light as observed in Drosophila flies. In addition, it was previously observed that dCRY and AtCRY when expressed in *Sf*21 insect cells when irradiated with blue-light exhibited much higher efficiency of photoreduction as compared to purified proteins. This increased sensitivity *in vivo* was also dependent on the fluence rate. It was reasoned that occurrence of suitable electron donors/acceptors and the redox environment *in vivo* could be responsible for this phenomenon. It was also hypothesized that the pathway of cryptochrome photoreduction *in vivo* is possibly different from that in *in vitro* conditions with purified proteins (Hoang et al., 2008). 20 min sunlight illumination led to the formation of anionic FAD radical as seen by the spectral changes, which once again confirmed the role of dCRY as a circadian photoreceptor (Fig. 63A).

4.4 Interplay between dark and light states of L-CRY

CRYs are known to undergo light-induced conformational changes (Berntsson et al., 2019; Czarna et al., 2013; Kondoh et al., 2011; Vaidya et al., 2013; Zoltowski et al., 2019). For Drosophila CRY (dCRY), it has been validated that there exist several structural intermediates as compared to the two defined spectroscopic states in the transition from the dark state to the light activated signaling state (Berntsson et al., 2019; Vaidya et al., 2013). It was also

established that the protein structural changes are a result of the change in the FAD oxidation state (Berntsson et al., 2019). Together, this could explain the observation of slow build-up of the light activated state due to moonlight. Considering L-CRY is a dimer in the dark state, it would require long periods of exposure to low intensity moonlight to bring about the required oxidation change in each of the FAD molecules within the dimer. The partial activated state of L-CRY could perhaps be the dimer of L-CRY wherein one molecule of FAD is reduced to the anionic radical and the other FAD molecule remains in the FAD_{ox} state. A different conformational change within the L-CRY dimer as compared to the blue-light conformation may possibly lead to one monomer being trapped with the FAD_{ox} state (Fig. 65). The proteolytic cleavage of dCRY in dark compared to light indicated that light-induced conformational changes in dCRY are not only limited to the release of the C-terminal tail and the connecting helix but rather a more complex global rearrangement in the protein (Ozturk et al., 2011; Vaidya et al., 2013). As L-CRY exhibits distinct spectral attributes in response to moonlight versus sunlight, it can be perceived that the possibly the conformational changes underlying as a response to these different light regimes might also be distinct.

Light sensitive and accessible positions identified in dCRY by limited proteolysis and mass spectrometry include Arg354, Arg368, Arg430, Arg494, Lys503 and Arg532 (Vaidya et al., 2013). The corresponding residues in L-CRY are namely Lys363, Arg377, Asn437, Pro504 , Ser513 and Arg543. Except for Lys363, Arg377 close to the sulphur loop and Arg543 in the C-terminal tail region, the other residues are not conserved. In addition, these residues are not within the identified L-CRY dimer interface, which leads to the speculation that the dimer of L-CRY would be stable, and light protected.

The technical considerations for carrying out SAXS in complete darkness and short blue-light illumination have been difficult to address. Nevertheless, so far SAXS analysis of L-CRY in dark and light did not yield any considerable differences in the scattering curve and the observed oligomeric state. Also, no monomeric subunits were observed during the blue-light illuminated native gel electrophoresis (Fig. 17D). Hence, the dimer of L-CRY is considered to be stable also under bright light conditions.

We cannot exclude the possibility of L-CRY photo-oligomerization as seen in plant- and several photoactive animal CRYs such as dCRY, DpCRY and zCRY1aa (Frøland Steindal & Whitmore, 2019; Q. Wang & Lin, 2020). Native gel electrophoresis of L-CRY in dark and blue-light

conditions showed L-CRY as a dimer running slightly below the 146 kDa marker and the formation of higher order L-CRY oligomers in the presence of blue-light. In Arabidopsis CRY2, oligomerization increased with increased fluence rates of blue light (Q. Wang & Lin, 2020) indicating that a possible L-CRY oligomerization to a tetramer or higher order oligomers by naturalistic moonlight would be slower in comparison to blue-light. This hypothesis needs to be tested.

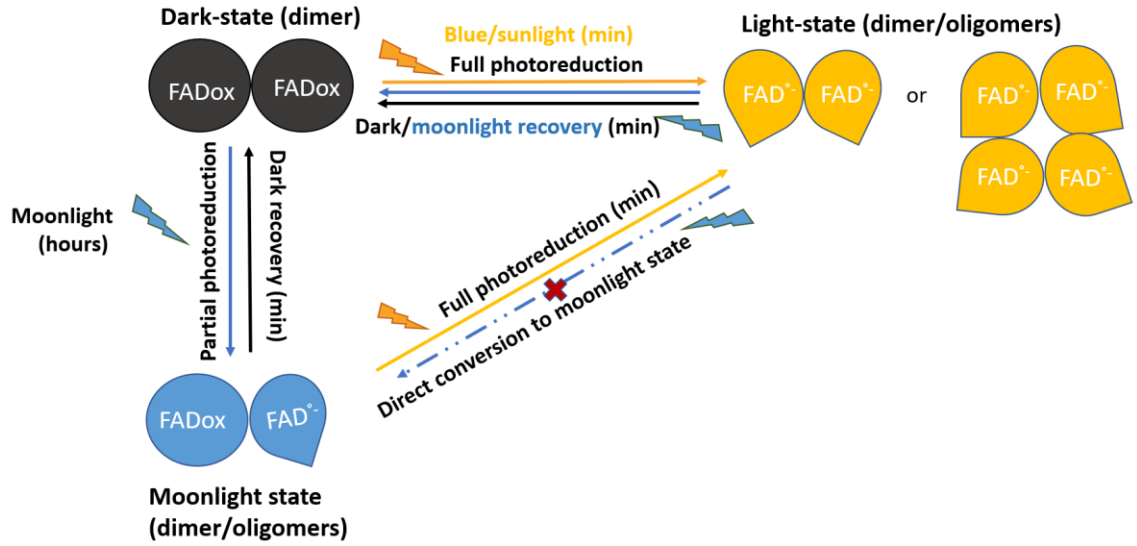

Figure 65: Hypothetical model of L-CRY dark and light oligomeric state. L-CRY exists as a dimer in the dark state (confirmed with MALS, CRYO-EM) with FAD_{ox} which on blue/sunlight illumination are photoreduced to the anionic radical FAD^{o-}. L-CRY may exist as a dimer or undergo photo-oligomerization in response to light as seen for other related cryptochromes in vivo. Illumination with moonlight leads to only partial photoreduction of L-CRY which may be attributed to an asymmetric dimer consisting of one molecule each of FAD_{ox} and FAD^{o-}, trapped in this state due to some conformational changes. The moonlight state may also either be a dimer or a higher order oligomer. Both the sunlight and moonlight activated states are able to recovery back in the dark. Direct conversion of the partial photoactivated moonlight state to the fully photoreduced sunlight state was observed, however, the converse was not seen. The sunlight state recovers back to the dark state before attaining the moonlight activated state.

4.5 Structure of L-CRY

Conventional crystallization attempts with L-CRY were so far unsuccessful. The ability of insect cells to produce *in vivo* crystals can still be exploited after further optimization of virus titer, expression time to yield larger crystals which might be more stable outside the cell environment. Techniques for the isolation of *in vivo* crystals may provide the possibility to obtain L-CRY structure with the help of X-ray Free-Electron Laser (XFEL) technique.

An extended envelope of L-CRY was computed using the SAXS scattering pattern (Fig. 42). The fitting of the dCRY crystal structure into the envelope was not ideal with an exceedingly high chi square value (Fig. 41A). The SAXS data presented in this suffer from the ambiguity to confidently distinguish between a true dark state and an light activated state due to complications in experimental setup. A more reliable measurement would be necessary to confidently discern this issue.

The dark state dimer structure of L-CRY obtained with the help of CRYO-EM provides the first insight into the L-CRY dimer interface. While the current resolution of 5.7 Å helped to identify L-CRY regions involved in homodimer formation, a higher resolution dark state structure in the near future would help resolve residues in the dimer interface.

It would be interesting to next obtain the light activated structure of L-CRY which would answer the current question with regards to the dimeric or oligomeric state of L-CRY in response to light activation and the positioning of the C-terminal tail. As is speculated with the SAXS analysis of dCRY that light-induced conformational changes in the light accessible motifs provide the switch to facilitate dCRY-TIM interactions (Vaidya et al., 2013), a similar mechanism may exist in L-CRY which could lead to interaction with downstream signalling partners.

4.6 L-CRY and its interaction partners

The identification of YTHDF and G3BP as potential dark state interactors of L-CRY provides the first glimpse towards the functional pathways wherein L-CRY could exert downstream regulation. In addition, the discovery that these two ligands are also circalunarly regulated themselves at the protein level adds additional complexity to their functional characterization. Although the mRNA localization of these ligands overlaps with the L-CRY expression pattern (collaborator Lab), so far, we could not prove a direct *in vitro* interaction between L-CRY and the ligands with the help of purified proteins. The stability of ligands without N-terminal tags was low and the expression and purification from insect cells was not optimal. In order to further optimize this approach, co-expression of both L-CRY and the ligands can be explored after cloning them into SmartBac expression system (Zhai et al., 2019).

Both G3BPs and YTHDFs are known mRNA binding proteins influencing their stability, degradation, and transport. In a study, YTHDF paralogs were enzymatically biotinylated with *E.coli* biotin ligase (BirA) and interacting proteins were detected based on their proximity induced biotinylation. The analysis indicated G3BP1/2 as one of the top 25 interactors of YTHDF paralogs (Zaccara & Jaffrey, 2020), leading to the speculation that they might be involved in a mega kDa complex with L-CRY and possibly other yet unknown factors. Interestingly, G3BP was also found as a light state interactor in the one trial of blue-light activated pull-down. It is possible that the recombinantly expressed ligands lack some post-translational modifications that might be essential for their binding to L-CRY. In this context, it might be worth to verify these interactors and reveal additional factors by carrying out immunoprecipitation (IP) coupled with mass spectrometry using worm head lysates from appropriate lunar phase using the L-CRY antibody. This would also provide the additional possibility to detect interactors specific to the moonlight activated state of L-CRY as currently pursuing this with purified protein is a challenge considering the variability in partial photoreduction state and the long durations of moonlight illumination required.

4.7 Complementary photoreceptor - P-CRY?

The plant-like cryptochrome in *Platynereis* namely P-CRY was identified by Oliveri *et al,* but its function remains unknown. It was recently discovered that *Crassostrea gigas* has a similar plant like cryptochrome with a sequence identity of 56.7% to the *Platynereis* P-CRY (Perrigault & Tran, 2017). Homolog of P-CRY in *Danio rerio* and *Crassostrea gigas* exhibited similar circadian change of expression. It is suggested that the last common eukaryotic marine ancestor should possess P-CRY class cryptochrome which is lost in metazoans (Oliveri et al., 2014b; Perrigault & Tran, 2017). In this study, *Platynereis* P-CRY was purified from *E.coli* as two variants, P-CRY PHR (200-697) and P-CRY PHR with cctail (200-778). The strong absorption at 380 nm and the identification of chromophore MTHF in addition to FAD with the help of HPLC corroborate the finding that P-CRY contains both FAD and MTHF as seen in AtCRYs (Fig. 56,57). The dark state spectrum of P-CRY depicts the neutral radical (FADH°) which on illumination with red light is converted to the fully reduced FAD ($FADH^-$) (Fig. 58). Recovery in the dark did not lead to the reoxidation of FAD. Thus, we identified a red-light photoreceptor with absorption beyond 600 nm. Initial spectroscopic measurements indicate that P-CRY might be closely related to DASH cryptochromes which function in the repair of

photodamaged DNA. Does the initial finding of several transcription and translational factors as potential interactors based on the pull-down approach have other implications?

The quality of the P-CRY variants so far purified from *E.coli* is still suboptimal as they are prone to aggregation on concentration. Although initial characterization of chromophores and 2D classes with negative staining have been obtained from this sample, further studies for the purpose of structural investigation would warranty the need for sample optimization to improve yields by gene optimization for *E.coli* expression system, cloning into different vectors and extensive test expression to use techniques such as dynamic light scattering and thermal shift assay to improve the buffer conditions and protein stability.

The MALS analysis of P-CRY variants so far indicates that P-CRY is a dimer in the dark state (Fig. 59). However further analysis with SAXS, native PAGE or cell based photo-oligomerization assays might shed light into the light state oligomeric state of P-CRY and indicate if P-CRY forms higher order oligomers as seen for plant cryptochromes on photoactivation (Palayam et al., 2020; Shao et al., 2020). Elucidation of structure with the help of CRYO-EM after further sample optimization could be pursued in order to compare this novel cryptochrome with known plant cryptochrome structures.

The finding that the l-cry -/- mutants were still able to maintain high maturation synchrony under artificial light conditions (collaborator lab) indicates that L-CRY might not be the sole photoreceptor in *Platynereis* responsible for moonlight reception and downstream regulation. Is it possible that the plant-like cryptochrome, P-CRY, compensates for the loss of L-CRY to some extent or if these cryptochromes have certain degree redundant functionality? Although the preliminary in-situ results indicate that abundance of P-CRY in the worm trunk rather than in the worm heads as it is seen for L-CRY (collaborator Lab), further confirmatory studies such as immunohistochemistry with antibodies against both L-CRY and P-CRY would help to ascertain this. In addition, what could be the signaling role of the neutral radical and the fully reduced FAD in the worm? What exactly is the functional relevance of red light in the context of worm circadian and circalunar clocks as both naturalistic moonlight and sunlight exhibit considerable components between 550-750 nm? How do the p-cry -/- mutants respond to different light entrainment cycles? Several of these questions must be explored in future to better understand the role of P-CRY.

5 Conclusion and Outlook

Two novel photoreceptors from the marine worm, the *Drosophila* homolog L-CRY, and the plant-like P-CRY were recombinantly expressed and purified from *E.coli* or *Sf9* insect cells. The chromophores bound to both the cryptochromes, FAD and MTHF were identified using HPLC which was a key finding for further photocycle characterization. L-CRY is a blue-light receptor while P-CRY responds to red light. With the help of custom-made light sources that mimic moonlight/sunlight, the photoreduction and recovery of L-CRY was studied. This provided initial indications of the transition between the dark and light activated states of L-CRY. Detailed characterization following the different transition states of the photocycle can be better studied using for example EPR spectroscopy.

Attempts to obtain the crystal structure of L-CRY and P-CRY were so far unsuccessful. However, a 5.7 Å structure of L-CRY dimer in the dark has been resolved with the help of cryo electron microscopy which showed a dimer interface not known for other cryptochromes. The dimer interface will have to be confirmed by mutational analyses. The next question is to elucidate conformational/structural changes that may occur on blue-light/moonlight activation. A high-resolution structure with the help of CRYO EM would help to gain further insights.

The pull-down based mass spectrometry approach to identify novel interactors of L-CRY led to the identification of two potential candidates. So far, no direct interaction has been confirmed *in vitro* with the help of recombinantly purified proteins from insect cells. However, a likely *in vivo* macro-complex comprising L-CRY, YTHDF/G3BP and other yet to be identified components cannot be excluded. Pull-down from worm head lysates using the generated antibodies against L-CRY/YTHDF/G3BP will be useful in confirming the interactors as well as identifying additional components of a macro-complex. As P-CRY constructs were purified from *E.coli*, it would be best to carry out pull-down approaches with worm trunk lysates using a P-CRY antibody to provide insights into the pathways involving this cryptochrome. Whether the downstream regulated components of L-CRY and P-CRY are overlapping or complementary would also be an interesting finding, divulging unknown aspects of these novel cryptochromes.

6 References

Ahmad, M, & Cashmore, A. R. (1993). HY4 gene of A. thaliana encodes a protein with characteristics of a blue-light photoreceptor. *Nature*, *366*(6451), 162–166. https://doi.org/10.1038/366162a0

Ahmad, Margaret, Galland, P., Ritz, T., Wiltschko, R., & Wiltschko, W. (2007). Magnetic intensity affects cryptochrome-dependent responses in Arabidopsis thaliana. *Planta*, *225*(3), 615–624. https://doi.org/10.1007/s00425-006-0383-0

Akashi, M., & Takumi, T. (2005). The orphan nuclear receptor RORalpha regulates circadian transcription of the mammalian core-clock Bmal1. *Nature Structural & Molecular Biology*, *12*(5), 441–448. https://doi.org/10.1038/nsmb925

Allada, R., & Chung, B. Y. (2010). Circadian Organization of Behavior and Physiology in Drosophila. *Annual Review of Physiology*, *72*(1), 605–624. https://doi.org/10.1146/annurev-physiol-021909-135815

Andersen, K. M., Madsen, L., Prag, S. øoren, Johnsen, A. H., Semple, C. A., Hendil, K. B., & Hartmann-Petersen, R. (2009). Thioredoxin Txnl1/TRP32 is a redox-active cofactor of the 26 S proteasome. *Journal of Biological Chemistry*, *284*(22), 15246–15254. https://doi.org/10.1074/jbc.M900016200

Annibaldi, A., Dousse, A., Martin, S., Tazi, J., & Widmann, C. (2011). Revisiting G3BP1 as a RasGAP binding protein: Sensitization of tumor cells to chemotherapy by the RasGAP 317-326 sequence does not involve G3BP1. *PLoS ONE*, *6*(12). https://doi.org/10.1371/journal.pone.0029024

Aschoff, J., & Pohl, H. (1978). Phase relations between a circadian rhythm and its zeitgeber within the range of entrainment. *Naturwissenschaften*, *65*(2), 80–84. https://doi.org/10.1007/BF00440545

Asher, G., & Sassone-Corsi, P. (2015). Time for food: The intimate interplay between nutrition, metabolism, and the circadian clock. *Cell*, *161*(1), 84–92. https://doi.org/10.1016/j.cell.2015.03.015

Ayers, T., Tsukamoto, H., Gühmann, M., Veedin Rajan, V. B., & Tessmar-Raible, K. (2018). A Go-type opsin mediates the shadow reflex in the annelid Platynereis dumerilii. *BMC Biology*, *16*(1), 1–9. https://doi.org/10.1186/s12915-018-0505-8

Babcock, R. C., Bull, G. D., Harrison, P. L., Heyward, A. J., Oliver, J. K., Wallace, C. C., & Willis, B. L. (1986). Synchronous spawnings of 105 scleractinian coral species on the Great Barrier Reef. *Marine Biology*, *90*(3), 379–394. https://doi.org/10.1007/BF00428562

Baik, L. S., Au, D. D., Nave, C., Foden, A. J., Enrriquez-Villalva, W. K., & Holmes, T. C. (2019). Distinct mechanisms of Drosophila CRYPTOCHROME-mediated light-evoked membrane depolarization and in vivo clock resetting. *Proceedings of the National Academy of Sciences of the United States of America*, *116*(46), 23339–23344. https://doi.org/10.1073/pnas.1905023116

Banerjee, R., Schleicher, E., Meier, S., Viana, R. M., Pokorny, R., Ahmad, M., Bittl, R., & Batschauer, A. (2007). The signaling state of Arabidopsis cryptochrome 2 contains flavin semiquinone. *Journal of Biological Chemistry*, *282*(20), 14916–14922. https://doi.org/10.1074/jbc.M700616200

Bantscheff, M., Schirle, M., Sweetman, G., Rick, J., & Kuster, B. (2007). Quantitative mass spectrometry in proteomics: A critical review. *Analytical and Bioanalytical Chemistry*, *389*(4), 1017–1031. https://doi.org/10.1007/s00216-007-1486-6

Barnes, C. J., Li, F., Mandal, M., Yang, Z., Sahin, A. A., & Kumar, R. (2002). Heregulin induces expression, ATPase activity, and nuclear localization of G3BP, a Ras signaling component, in human breast tumors. *Cancer Research*, *62*(5), 1251–1255.

Bell-Pedersen, D., Cassone, V. M., Earnest, D. J., Golden, S. S., Hardin, P. E., Thomas, T. L., & Zoran, M. J. (2005). Circadian rhythms from multiple oscillators: lessons from diverse organisms. *Nature Reviews Genetics*, *6*(7), 544–556. https://doi.org/10.1038/nrg1633

Bernard, S., Gonze, D., Čajavec, B., Herzel, H., & Kramer, A. (2007). Synchronization-induced rhythmicity of circadian oscillators in the suprachiasmatic nucleus. *PLoS Computational Biology*, *3*(4), 667–679. https://doi.org/10.1371/journal.pcbi.0030068

Berndt, A., Kottke, T., Breitkreuz, H., Dvorsky, R., Hennig, S., Alexander, M., & Wolf, E. (2007). A novel photoreaction mechanism for the circadian blue light photoreceptor Drosophila cryptochrome. *Journal of Biological Chemistry*, *282*(17), 13011–13021. https://doi.org/10.1074/jbc.M608872200

Berntsson, O., Rodriguez, R., Henry, L., Panman, M. R., Hughes, A. J., Einholz,

C., Weber, S., Ihalainen, J. A., Henning, R., Kosheleva, I., Schleicher, E., & Westenhoff, S. (2019). Photoactivation of Drosophila melanogaster cryptochrome through sequential conformational transitions. *Science Advances*, *5*(7). https://doi.org/10.1126/sciadv.aaw1531

Berson, D. M. (2003). Strange vision: ganglion cells as circadian photoreceptors. *Trends in Neurosciences*, *26*(6), 314–320. https://doi.org/10.1016/S0166-2236(03)00130-9

Bézy, V. S., Putman, N. F., Umbanhowar, J. A., Orrego, C. M., Fonseca, L. G., Quirós-Pereira, W. M., Valverde, R. A., & Lohmann, K. J. (2020). Mass-nesting events in olive ridley sea turtles: environmental predictors of timing and size. *Animal Behaviour*, *163*(April), 85–94. https://doi.org/10.1016/j.anbehav.2020.03.002

Bichet, P., Mollat, P., Capdevila, C., & Sarubbi, E. (2000). Endogenous glutathione-binding proteins of insect cell lines: Characterization and removal from glutathione S-transferase (GST) fusion proteins. *Protein Expression and Purification*, *19*(1), 197–201. https://doi.org/10.1006/prep.2000.1239

Bikkavilli, R. K., & Malbon, C. C. (2011). Arginine methylation of G3BP1 in response to Wnt3a regulates β-catenin mRNA. *Journal of Cell Science*, *124*(Pt 13), 2310–2320. https://doi.org/10.1242/jcs.084046

Boch, C. A., Ananthasubramaniam, B., Sweeney, A. M., Iii, F. J. D., Morse, D. E., Boch, A., & Doyle, J. (2015). *Linked references are available on JSTOR for this article : Effects of Light Dynamics on Coral Spawning Synchrony*. *220*(3), 161–173.

Böhm, G. (n.d.). *No Title*.

Bonmati-Carrion, M. A., Arguelles-Prieto, R., Martinez-Madrid, M. J., Reiter, R., Hardeland, R., Rol, M. A., & Madrid, J. A. (2014). Protecting the melatonin rhythm through circadian healthy light exposure. *International Journal of Molecular Sciences*, *15*(12), 23448–23500. https://doi.org/10.3390/ijms151223448

Boudes, M., Garriga, D., Fryga, A., Caradoc-Davies, T., & Coulibaly, F. (2016). A pipeline for structure determination of in vivo-grown crystals using in cellulo diffraction. *Acta Crystallographica Section D: Structural Biology*, *72*(4), 576–585. https://doi.org/10.1107/S2059798316002369

Bouly, J.-P., Schleicher, E., Dionisio-Sese, M., Vandenbussche, F., Van Der Straeten, D., Bakrim, N., Meier, S., Batschauer, A., Galland, P., Bittl, R., &

Ahmad, M. (2007). Cryptochrome blue light photoreceptors are activated through interconversion of flavin redox states. *The Journal of Biological Chemistry*, *282*(13), 9383–9391. https://doi.org/10.1074/jbc.M609842200

Brettel, K., & Byrdin, M. (2010). Reaction mechanisms of DNA photolyase. *Current Opinion in Structural Biology*, *20*(6), 693–701. https://doi.org/10.1016/j.sbi.2010.07.003

Brown, S. A., Zumbrunn, G., Fleury-Olela, F., Preitner, N., & Schibler, U. (2002). Rhythms of mammalian body temperature can sustain peripheral circadian clocks. *Current Biology : CB*, *12*(18), 1574–1583. https://doi.org/10.1016/s0960-9822(02)01145-4

Brudler, R., Hitomi, K., Daiyasu, H., Toh, H., Kucho, K., Ishiura, M., Kanehisa, M., Roberts, V. A., Todo, T., Tainer, J. A., & Getzoff, E. D. (2003). Identification of a New Cryptochrome Class: Structure, Function, and Evolution. *Molecular Cell*, *11*(1), 59–67. https://doi.org/https://doi.org/10.1016/S1097-2765(03)00008-X

Brunelle, S. A., Hazard, E. S., Sotka, E. E., & Van Dolah, F. M. (2007). Characterization of a dinoflagellate cryptochrome blue-light receptor with a possible role in circadian control of the cell cycle. *Journal of Phycology*, *43*(3), 509–518. https://doi.org/10.1111/j.1529-8817.2007.00339.x

Buchan, D. W. A., & Jones, D. T. (2019). The PSIPRED Protein Analysis Workbench: 20 years on. *Nucleic Acids Research*, *47*(W1), W402–W407. https://doi.org/10.1093/nar/gkz297

Burd, C. G., & Dreyfuss, G. (1994). Conserved structures and diversity of functions of RNA-binding proteins. *Science*, *265*(5172), 615 LP – 621. https://doi.org/10.1126/science.8036511

Byrdin, M., Sartor, V., Eker, A. P. M., Vos, M. H., Aubert, C., Brettel, K., & Mathis, P. (2004). Intraprotein electron transfer and proton dynamics during photoactivation of DNA photolyase from E. coli: review and new insights from an “inverse” deuterium isotope effect. *Biochimica et Biophysica Acta*, *1655*(1–3), 64–70. https://doi.org/10.1016/j.bbabio.2003.07.001

Cadet, J., Sage, E., & Douki, T. (2005). Ultraviolet radiation-mediated damage to cellular DNA. *Mutation Research*, *571*(1–2), 3–17. https://doi.org/10.1016/j.mrfmmm.2004.09.012

Cajochen, C., Altanay-Ekici, S., Münch, M., Frey, S., Knoblauch, V., & Wirz-Justice, A. (2013). Evidence that the lunar cycle influences human sleep.

Current Biology, *23*(15), 1485–1488. https://doi.org/10.1016/j.cub.2013.06.029

Cashmore, A. R. (2006). Cryptochromes. *Photomorphogenesis in Plants and Bacteria*, *114*, 199–221. https://doi.org/10.1007/1-4020-3811-9_11

Cashmore, A. R., Jarillo, J. A., Wu, Y.-J., & Liu, D. (1999). Cryptochromes: Blue Light Receptors for Plants and Animals. *Science*, *284*(5415), 760 LP – 765. https://doi.org/10.1126/science.284.5415.760

Casiraghi, L., Spiousas, I., Dunster, G., McGlothlen, K., Fernández-Duque, E., Valeggia, C., & de la Iglesia, H. (2020). *Moonstruck sleep: Synchronization of Human Sleep with the Moon Cycle under Natural Conditions*. bioRxiv. https://doi.org/10.1101/2020.06.01.128728

Chaput, J. P., Weippert, M., LeBlanc, A. G., Hjorth, M. F., Michaelsen, K. F., Katzmarzyk, P. T., Tremblay, M. S., Barreira, T. V., Broyles, S. T., Fogelholm, M., Hu, G., Kuriyan, R., Kurpad, A., Lambert, E. V., Maher, C., Maia, J., Matsudo, V., Olds, T., Onywera, V., … Pietrobelli, A. (2016). Are children like werewolves? Full moon and its association with sleep and activity behaviors in an international sample of children. *Frontiers in Pediatrics*, *4*(MAR), 1–6. https://doi.org/10.3389/fped.2016.00024

Chaves, I., Nijman, R. M., Biernat, M. A., Bajek, M. I., Brand, K., da Silva, A. C., Saito, S., Yagita, K., Eker, A. P. M., & van der Horst, G. T. J. (2011). The potorous cpd photolyase rescues a cryptochrome-deficient mammalian circadian clock. *PLoS ONE*, *6*(8). https://doi.org/10.1371/journal.pone.0023447

Chaves, I., Pokorny, R., Byrdin, M., Hoang, N., Ritz, T., Brettel, K., Essen, L.-O., van der Horst, G. T. J., Batschauer, A., & Ahmad, M. (2011). The Cryptochromes: Blue Light Photoreceptors in Plants and Animals. *Annual Review of Plant Biology*, *62*(1), 335–364. https://doi.org/10.1146/annurev-arplant-042110-103759

Chaves, I., Yagita, K., Barnhoorn, S., Okamura, H., van der Horst, G. T. J., & Tamanini, F. (2006). Functional evolution of the photolyase/cryptochrome protein family: importance of the C terminus of mammalian CRY1 for circadian core oscillator performance. *Molecular and Cellular Biology*, *26*(5), 1743–1753. https://doi.org/10.1128/MCB.26.5.1743-1753.2006

Chiu, J. C., Ko, H. W., & Edery, I. (2011). Erratum: NEMO/NLK phosphorylates PERIOD to initiate a time-delay phosphorylation circuit that sets circadian clock speed (Cell (2011) 145 (357-370)). *Cell*, *145*(4), 635. https://doi.org/10.1016/j.cell.2011.04.023

Chiu, J. C., Vanselow, J. T., Kramer, A., & Edery, I. (2008). The phospho-occupancy of an atypical SLIMB-binding site on PERIOD that is phosphorylated by DOUBLETIME controls the pace of the clock. *Genes and Development*, *22*(13), 1758–1772. https://doi.org/10.1101/gad.1682708

Christine, K. S., MacFarlane, A. W. 4th, Yang, K., & Stanley, R. J. (2002). Cyclobutylpyrimidine dimer base flipping by DNA photolyase. *The Journal of Biological Chemistry*, *277*(41), 38339–38344. https://doi.org/10.1074/jbc.M206531200

Cléry, A., Blatter, M., & Allain, F. H.-T. (2008). RNA recognition motifs: boring? Not quite. *Current Opinion in Structural Biology*, *18*(3), 290–298. https://doi.org/10.1016/j.sbi.2008.04.002

Combet C., Blanchet C., G. C. and D. G. (2000). NPS@: Network Protein Sequence Analysise. *Trends in Biochemical Sciences*, *25*(3), 147–150.

Cox, J., & Mann, M. (2008). MaxQuant enables high peptide identification rates, individualized p.p.b.-range mass accuracies and proteome-wide protein quantification. *Nature Biotechnology*, *26*(12), 1367–1372. https://doi.org/10.1038/nbt.1511

Crane, B. R., & Young, M. W. (2014). Interactive Features of Proteins Composing Eukaryotic Circadian Clocks. *Annual Review of Biochemistry*, *83*(1), 191–219. https://doi.org/10.1146/annurev-biochem-060713-035644

Cutler, S. R., Ehrhardt, D. W., Griffitts, J. S., & Somerville, C. R. (2000). Random GFP::cDNA fusions enable visualization of subcellular structures in cells of Arabidopsis at a high frequency. *Proceedings of the National Academy of Sciences*, *97*(7), 3718 LP – 3723. https://doi.org/10.1073/pnas.97.7.3718

Czarna, A., Berndt, A., Singh, H. R., Grudziecki, A., Ladurner, A. G., Timinszky, G., Kramer, A., & Wolf, E. (2013). XStructures of drosophila cryptochrome and mouse cryptochrome1 provide insight into circadian function. *Cell*, *153*(6), 1394. https://doi.org/10.1016/j.cell.2013.05.011

Daiyasu, H., Ishikawa, T., Kuma, K., Iwai, S., Todo, T., & Toh, H. (2004). Identification of cryptochrome DASH from vertebrates. *Genes to Cells : Devoted to Molecular & Cellular Mechanisms*, *9*(5), 479–495. https://doi.org/10.1111/j.1356-9597.2004.00738.x

Darlington, T. K., Wager-Smith, K., Ceriani, M. F., Staknis, D., Gekakis, N., Steeves, T. D. L., Weitz, C. J., Takahashi, J. S., & Kay, S. A. (1998). Closing

the circadian loop: CLOCK-induced transcription of its own inhibitors per and tim. *Science*, *280*(5369), 1599–1603. https://doi.org/10.1126/science.280.5369.1599

De La Iglesia, H. O., & Hsu, Y. W. A. (2010). Biological clocks and rhythms in intertidal crustaceans. *Frontiers in Bioscience - Elite*, *2 E*(4), 1394–1404. https://doi.org/10.2741/e200

de la Iglesia, H. O., & Johnson, C. H. (2013). Biological Clocks: Riding the Tides Horacio. *Current Biology*, *23*(20), R921–R923. https://doi.org/10.1016/j.jneumeth.2010.08.011.Autogenic

Devlin, P. F., & Kay, S. A. (2000). Cryptochromes are required for phytochrome signaling to the circadian clock but not for rhythmicity. *The Plant Cell*, *12*(12), 2499–2510. https://doi.org/10.1105/tpc.12.12.2499

Dibner, C., Schibler, U., & Albrecht, U. (2009). The mammalian circadian timing system: Organization and coordination of central and peripheral clocks. In *Annual Review of Physiology* (Vol. 72). https://doi.org/10.1146/annurev-physiol-021909-135821

Dominissini, D., Moshitch-Moshkovitz, S., Schwartz, S., Salmon-Divon, M., Ungar, L., Osenberg, S., Cesarkas, K., Jacob-Hirsch, J., Amariglio, N., Kupiec, M., Sorek, R., & Rechavi, G. (2012). Topology of the human and mouse m6A RNA methylomes revealed by m6A-seq. *Nature*, *485*(7397), 201–206. https://doi.org/10.1038/nature11112

Domratcheva, T., & Schlichting, I. (2009). Electronic Structure of (6−4) DNA Photoproduct Repair Involving a Non-Oxetane Pathway. *Journal of the American Chemical Society*, *131*(49), 17793–17799. https://doi.org/10.1021/ja904550d

Doniach, S. (2001). Changes in biomolecular conformation seen by small angle X-ray scattering. *Chemical Reviews*, *101*(6), 1763–1778. https://doi.org/10.1021/cr990071k

Douki, T, Court, M., Sauvaigo, S., Odin, F., & Cadet, J. (2000). Formation of the main UV-induced thymine dimeric lesions within isolated and cellular DNA as measured by high performance liquid chromatography-tandem mass spectrometry. *The Journal of Biological Chemistry*, *275*(16), 11678–11685. https://doi.org/10.1074/jbc.275.16.11678

Douki, Thierry, & Cadet, J. (2001). Individual Determination of the Yield of the Main UV-Induced Dimeric Pyrimidine Photoproducts in DNA Suggests a High Mutagenicity of CC Photolesions. *Biochemistry*, *40*(8), 2495–2501.

https://doi.org/10.1021/bi0022543

DULBECCO, R. (1949). Reactivation of Ultra-Violet-Inactivated Bacteriophage by Visible Light. *Nature*, *163*(4155), 949–950. https://doi.org/10.1038/163949b0

Dunlap, J C. (1999). Molecular bases for circadian clocks. *Cell*, *96*(2), 271–290. https://doi.org/10.1016/s0092-8674(00)80566-8

Dunlap, Jay C, Loros, J. J., Decoursey, P. J., & Decoursey, P. J. (2004). *Chronobiology Overview of Biological Timing from Unicells to Humans 3 of Biological Timing Systems 27*. 406.

Ehlers, C. L., Frank, E., & Kupfer, D. J. (1988). Social Zeitgebers and Biological Rhythms: A Unified Approach to Understanding the Etiology of Depression. *Archives of General Psychiatry*, *45*(10), 948–952. https://doi.org/10.1001/archpsyc.1988.01800340076012

El-Din El-Assal, S., Alonso-Blanco, C., Peeters, A. J. M., Wagemaker, C., Weller, J. L., & Koornneef, M. (2003). The Role of Cryptochrome 2 in Flowering in Arabidopsis. *Plant Physiology*, *133*(4), 1504 LP – 1516. https://doi.org/10.1104/pp.103.029819

Emery, P., So, W. V., Kaneko, M., Hall, J. C., & Rosbash, M. (1998). Cry, a Drosophila clock and light-regulated cryptochrome, is a major contributor to circadian rhythm resetting and photosensitivity. *Cell*, *95*(5), 669–679. https://doi.org/10.1016/S0092-8674(00)81637-2

Emery, P., Stanewsky, R., Helfrich-Förster, C., Emery-Le, M., Hall, J. C., & Rosbash, M. (2000). Drosophila CRY Is a Deep Brain Circadian Photoreceptor. *Neuron*, *26*(2), 493–504. https://doi.org/https://doi.org/10.1016/S0896-6273(00)81181-2

Evans, E. W., Dodson, C. A., Maeda, K., Biskup, T., Wedge, C. J., & Timme, C. R. (2013). Magnetic field effects in flavoproteins and related systems. *Interface Focus*, *3*(5). https://doi.org/10.1098/rsfs.2013.0037

Faraji, S., & Dreuw, A. (2012). Proton-Transfer-Steered Mechanism of Photolesion Repair by (6–4)-Photolyases. *The Journal of Physical Chemistry Letters*, *3*(2), 227–230. https://doi.org/10.1021/jz201587v

Faraji, S., Zhong, D., & Dreuw, A. (2016). Characterization of the Intermediate in and Identification of the Repair Mechanism of (6-4) Photolesions by Photolyases. *Angewandte Chemie (International Ed. in English)*, *55*(17), 5175–5178. https://doi.org/10.1002/anie.201511950

Fogle, K. J., Baik, L. S., Houl, J. H., Tran, T. T., Roberts, L., Dahm, N. A., Cao, Y., Zhou, M., & Holmes, T. C. (2015). CRYPTOCHROME-mediated phototransduction by modulation of the potassium ion channel β-subunit redox sensor. *Proceedings of the National Academy of Sciences of the United States of America*, *112*(7), 2245–2250. https://doi.org/10.1073/pnas.1416586112

Fogle, K. J., Parson, K. G., Dahm, N. A., & Holmes, T. C. (2011). CRYPTOCHROME is a blue-light sensor that regulates neuronal firing rate. *Science (New York, N.Y.)*, *331*(6023), 1409–1413. https://doi.org/10.1126/science.1199702

Foster, R. G., Provencio, I., Hudson, D., Fiske, S., De Grip, W., & Menaker, M. (1991). Circadian photoreception in the retinally degenerate mouse (rd/rd). *Journal of Comparative Physiology. A, Sensory, Neural, and Behavioral Physiology*, *169*(1), 39–50. https://doi.org/10.1007/BF00198171

Foster, T., Heyward, A. J., & Gilmour, J. P. (2018). Split spawning realigns coral reproduction with optimal environmental windows. *Nature Communications*, *9*(1), 1–8. https://doi.org/10.1038/s41467-018-03175-2

Franke, D., Petoukhov, M. V., Konarev, P. V., Panjkovich, A., Tuukkanen, A., Mertens, H. D. T., Kikhney, A. G., Hajizadeh, N. R., Franklin, J. M., Jeffries, C. M., & Svergun, D. I. (2017). ATSAS 2.8: A comprehensive data analysis suite for small-angle scattering from macromolecular solutions. *Journal of Applied Crystallography*, *50*, 1212–1225. https://doi.org/10.1107/S1600576717007786

Franke, Daniel, & Svergun, D. I. (2009). DAMMIF, a program for rapid ab-initio shape determination in small-angle scattering. *Journal of Applied Crystallography*, *42*(2), 342–346. https://doi.org/10.1107/S0021889809000338

Franke, H.-D. (1985). On a clocklike mechanism timing lunar-rhythmic reproduction inTyposyllis prolifera (Polychaeta). *Journal of Comparative Physiology A*, *156*(4), 553–561. https://doi.org/10.1007/BF00613979

Frøland Steindal, I. A., & Whitmore, D. (2019). Circadian clocks in fish-what have we learned so far? *Biology*, *8*(1). https://doi.org/10.3390/biology8010017

Fukushiro, M., Takeuchi, T., Takeuchi, Y., Hur, S.-P., Sugama, N., Takemura, A., Kubo, Y., Okano, K., & Okano, T. (2011). Lunar phase-dependent expression of cryptochrome and a photoperiodic mechanism for lunar phase-recognition in a reef fish, goldlined spinefoot. *PloS One*, *6*(12),

e28643. https://doi.org/10.1371/journal.pone.0028643

Fustin, J. M., Doi, M., Yamaguchi, Y., Hida, H., Nishimura, S., Yoshida, M., Isagawa, T., Morioka, M. S., Kakeya, H., Manabe, I., & Okamura, H. (2013). XRNA-methylation-dependent RNA processing controls the speed of the circadian clock. *Cell*, *155*(4), 793. https://doi.org/10.1016/j.cell.2013.10.026

Gatfield, D., & Schibler, U. (2007). Proteasomes Keep the Circadian Clock Ticking. *Science*, *316*(5828), 1135 LP – 1136. https://doi.org/10.1126/science.1144165

Gekakis, N., Staknis, D., Nguyen, H. B., Davis, F. C., Wilsbacher, L. D., King, D. P., Takahashi, J. S., & Weitz, C. J. (1998). Role of the CLOCK Protein in the Mammalian Circadian Mechanism. *Science*, *280*(5369), 1564 LP – 1569. https://doi.org/10.1126/science.280.5369.1564

Gibson, D. G., Young, L., Chuang, R. Y., Venter, J. C., Hutchison, C. A., & Smith, H. O. (2009). Enzymatic assembly of DNA molecules up to several hundred kilobases. *Nature Methods*, *6*(5), 343–345. https://doi.org/10.1038/nmeth.1318

Giovani, B., Byrdin, M., Ahmad, M., & Brettel, K. (2003). Light-induced electron transfer in a cryptochrome blue-light photoreceptor. *Nature Structural Biology*, *10*(6), 489–490. https://doi.org/10.1038/nsb933

Gomes, C. C., & Preto, S. (2015). Blue Light: A Blessing or a Curse? *Procedia Manufacturing*, *3*(Ahfe), 4472–4479. https://doi.org/10.1016/j.promfg.2015.07.459

Grandin, L. D., Alloy, L. B., & Abramson, L. Y. (2006). The social zeitgeber theory, circadian rhythms, and mood disorders: Review and evaluation. *Clinical Psychology Review*, *26*(6), 679–694. https://doi.org/10.1016/j.cpr.2006.07.001

Greenfield, N. J. (2007). Using circular dichroism spectra to estimate protein secondary structure. *Nature Protocols*, *1*(6), 2876–2890. https://doi.org/10.1038/nprot.2006.202

Gressel, J. (1979). Yearly review: Blue light photoreception. *Photochemistry and Photobiology*, *30*, 749–754.

Guillaumond, F., Dardente, H., Giguère, V., & Cermakian, N. (2005). Differential control of Bmal1 circadian transcription by REV-ERB and ROR nuclear receptors. *Journal of Biological Rhythms*, *20*(5), 391–403. https://doi.org/10.1177/0748730405277232

Guo, H., Yang, H., Mockler, T. C., & Lin, C. (1998). Regulation of Flowering Time by Arabidopsis Photoreceptors. *Science*, *279*(5355), 1360 LP – 1363. https://doi.org/10.1126/science.279.5355.1360

Gupta, N., Badeaux, M., Liu, Y., Naxerova, K., Sgroi, D., Munn, L. L., Jain, R. K., & Garkavtsev, I. (2017). Stress granule-associated protein G3BP2 regulates breast tumor initiation. *Proceedings of the National Academy of Sciences of the United States of America*, *114*(5), 1033–1038. https://doi.org/10.1073/pnas.1525387114

Gyurkó, M. D., Csermely, P., Soti, C., & Steták, A. (2015). Distinct roles of the RasGAP family proteins in C. elegans associative learning and memory. *Scientific Reports*, *5*, 1–10. https://doi.org/10.1038/srep15084

Hallett, R. A., Zimmerman, S. P., Yumerefendi, H., Bear, J. E., & Kuhlman, B. (2016). Correlating in Vitro and in Vivo Activities of Light-Inducible Dimers: A Cellular Optogenetics Guide. *ACS Synthetic Biology*, *5*(1), 53–64. https://doi.org/10.1021/acssynbio.5b00119

Harbach, P. H. P., Borowka, J., Bohnwagner, M.-V., & Dreuw, A. (2010). DNA (6−4) Photolesion Repair Occurs in the Electronic Ground State of the TT Dinucleotide Dimer Radical Anion. *The Journal of Physical Chemistry Letters*, *1*(17), 2556–2560. https://doi.org/10.1021/jz100898x

Hardin, P. E. (2005). The circadian timekeeping system of Drosophila. *Current Biology*, *15*(17), 714–722. https://doi.org/10.1016/j.cub.2005.08.019

Hatori, M., Gill, S., Mure, L. S., Goulding, M., O'leary, D. D. M., & Panda, S. (2014). Lhx1 maintains synchrony among circadian oscillator neurons of the SCN. *ELife*, *3*(July2014), 1–16. https://doi.org/10.7554/eLife.03357

Hauenschild, C. (1960). Lunar Periodicity. *Cold Spring Harbor Symposia on Quantitative Biology*, *25*, 491–497.

Heijde, M., Zabulon, G., Corellou, F., Ishikawa, T., Brazard, J., Usman, A., Sanchez, F., Plaza, P., Martin, M., Falciatore, A., Todo, T., Bouget, F.-Y., & Bowler, C. (2010). Characterization of two members of the cryptochrome/photolyase family from Ostreococcus tauri provides insights into the origin and evolution of cryptochromes. *Plant, Cell & Environment*, *33*(10), 1614–1626. https://doi.org/10.1111/j.1365-3040.2010.02168.x

Hemsley, M. J., Mazzotta, G. M., Mason, M., Dissel, S., Toppo, S., Pagano, M. A., Sandrelli, F., Meggio, F., Rosato, E., Costa, R., & Tosatto, S. C. E. (2007). Linear motifs in the C-terminus of D. melanogaster cryptochrome.

Biochemical and Biophysical Research Communications, *355*(2), 531—537. https://doi.org/10.1016/j.bbrc.2007.01.189

Hirano, A., Braas, D., Fu, Y.-H., & Ptáček, L. J. (2017). FAD Regulates CRYPTOCHROME Protein Stability and Circadian Clock in Mice. *Cell Reports*, *19*(2), 255–266. https://doi.org/10.1016/j.celrep.2017.03.041

Hitomi, K, Okamoto, K., Daiyasu, H., Miyashita, H., Iwai, S., Toh, H., Ishiura, M., & Todo, T. (2000). Bacterial cryptochrome and photolyase: characterization of two photolyase-like genes of Synechocystis sp. PCC6803. *Nucleic Acids Research*, *28*(12), 2353–2362. https://doi.org/10.1093/nar/28.12.2353

Hitomi, Kenichi, Arvai, A. S., Yamamoto, J., Hitomi, C., Teranishi, M., Hirouchi, T., Yamamoto, K., Iwai, S., Tainer, J. A., Hidema, J., & Getzoff, E. D. (2012). Eukaryotic class II cyclobutane pyrimidine dimer photolyase structure reveals basis for improved ultraviolet tolerance in plants. *The Journal of Biological Chemistry*, *287*(15), 12060–12069. https://doi.org/10.1074/jbc.M111.244020

Hitomi, Kenichi, DiTacchio, L., Arvai, A. S., Yamamoto, J., Kim, S. T., Todo, T., Tainer, J. A., Iwai, S., Panda, S., & Getzoff, E. D. (2009). Functional motifs in the (6-4) photolyase crystal structure make a comparative framework for DNA repair photolyases and clock cryptochromes. *Proceedings of the National Academy of Sciences of the United States of America*, *106*(17), 6962–6967. https://doi.org/10.1073/pnas.0809180106

Hitomi, Kenichi, Nakamura, H., Kim, S. T., Mizukoshi, T., Ishikawa, T., Iwai, S., & Todo, T. (2001). Role of Two Histidines in the (6-4) Photolyase Reaction. *Journal of Biological Chemistry*, *276*(13), 10103–10109. https://doi.org/10.1074/jbc.M008828200

Hoang, N., Schleicher, E., Kacprzak, S., Bouly, J.-P., Picot, M., Wu, W., Berndt, A., Wolf, E., Bittl, R., & Ahmad, M. (2008). Human and Drosophila cryptochromes are light activated by flavin photoreduction in living cells. *PLoS Biology*, *6*(7), e160–e160. https://doi.org/10.1371/journal.pbio.0060160

Hsu, D. S., Zhao, X., Zhao, S., Kazantsev, A., Wang, R. P., Todo, T., Wei, Y. F., & Sancar, A. (1996). Putative human blue-light photoreceptors hCRY1 and hCRY2 are flavoproteins. *Biochemistry*, *35*(44), 13871–13877. https://doi.org/10.1021/bi962209o

Hsu, J. L., Huang, S. Y., Chow, N. H., & Chen, S. H. (2003). Stable-Isotope Dimethyl Labeling for Quantitative Proteomics. *Analytical Chemistry*,

75(24), 6843–6852. https://doi.org/10.1021/ac0348625

Huang, Y., Baxter, R., Smith, B. S., Partch, C. L., Colbert, C. L., & Deisenhofer, J. (2006). Crystal structure of cryptochrome 3 from Arabidopsis thaliana and its implications for photolyase activity. *Proceedings of the National Academy of Sciences*, *103*(47), 17701 LP – 17706. https://doi.org/10.1073/pnas.0608554103

Imai, Y., Matsuo, N., Ogawa, S., Tohyama, M., & Takagi, T. (1998). Cloning of a gene, YT521, for a novel RNA splicing-related protein induced by hypoxia/reoxygenation. *Brain Research. Molecular Brain Research*, *53*(1–2), 33–40. https://doi.org/10.1016/s0169-328x(97)00262-3

Ishikawa, T., Matsumoto, A., Kato, T. J., Togashi, S., Ryo, H., Ikenaga, M., Todo, T., Ueda, R., & Tanimura, T. (1999). DCRY is a Drosophila photoreceptor protein implicated in light entrainment of circadian rhythm. *Genes to Cells : Devoted to Molecular & Cellular Mechanisms*, *4*(1), 57–65. https://doi.org/10.1046/j.1365-2443.1999.00237.x

Ivanova, I., Much, C., Di Giacomo, M., Azzi, C., Morgan, M., Moreira, P. N., Monahan, J., Carrieri, C., Enright, A. J., & O'Carroll, D. (2017). The RNA m6A Reader YTHDF2 Is Essential for the Post-transcriptional Regulation of the Maternal Transcriptome and Oocyte Competence. *Molecular Cell*, *67*(6), 1059-1067.e4. https://doi.org/10.1016/j.molcel.2017.08.003

Jakobi, A. J., Passon, D. M., Knoops, K., Stellato, F., Liang, M., White, T. A., Seine, T., Messerschmidt, M., Chapman, H. N., & Wilmanns, M. (2016). In cellulo serial crystallography of alcohol oxidase crystals inside yeast cells. *IUCrJ*, *3*, 88–95. https://doi.org/10.1107/S2052252515022927

Jia, G., Fu, Y., & He, C. (2013). Reversible RNA adenosine methylation in biological regulation. *Trends in Genetics : TIG*, *29*(2), 108–115. https://doi.org/10.1016/j.tig.2012.11.003

Jiang, C.-Z., Yee, J., Mitchell, D. L., & Britt, A. B. (1997). Photorepair mutants of Arabidopsis *Proceedings of the National Academy of Sciences*, *94*(14), 7441 LP – 7445. https://doi.org/10.1073/pnas.94.14.7441

Jonic, S., & Vénien-Bryan, C. (2009). Protein structure determination by electron cryo-microscopy. *Current Opinion in Pharmacology*, *9*(5), 636–642. https://doi.org/10.1016/j.coph.2009.04.006

Juhas, M., Von Zadow, A., Spexard, M., Schmidt, M., Kottke, T., & Büchel, C. (2014). A novel cryptochrome in the diatom Phaeodactylum tricornutum

influences the regulation of light-harvesting protein levels. *FEBS Journal*, *281*(9), 2299–2311. https://doi.org/10.1111/febs.12782

Julius, A. A., Yin, J., & Wen, J. T. (2019). Time optimal entrainment control for circadian rhythm. *PLoS ONE*, *14*(12), 1–30. https://doi.org/10.1371/journal.pone.0225988

Kanai, S., Kikuno, R., Toh, H., Ryo, H., & Todo, T. (1997). Molecular evolution of the photolyase-blue-light photoreceptor family. *Journal of Molecular Evolution*, *45*(5), 535–548. https://doi.org/10.1007/pl00006258

Kaniewska, P., Alon, S., Karako-Lampert, S., Hoegh-Guldberg, O., & Levy, O. (2015). Signaling cascades and the importance of moonlight in coral broadcast mass spawning. *ELife*, *4*(DECEMBER2015), 1–14. https://doi.org/10.7554/eLife.09991.001

Kao, Y.-T., Saxena, C., He, T.-F., Guo, L., Wang, L., Sancar, A., & Zhong, D. (2008). Ultrafast Dynamics of Flavins in Five Redox States. *Journal of the American Chemical Society*, *130*(39), 13132–13139. https://doi.org/10.1021/ja8045469

Kao, Y.-T., Saxena, C., Wang, L., Sancar, A., & Zhong, D. (2005). Direct observation of thymine dimer repair in DNA by photolyase. *Proceedings of the National Academy of Sciences of the United States of America*, *102*(45), 16128 LP – 16132. https://doi.org/10.1073/pnas.0506586102

Kao, Y.-T., Tan, C., Song, S.-H., Öztürk, N., Li, J., Wang, L., Sancar, A., & Zhong, D. (2008). Ultrafast Dynamics and Anionic Active States of the Flavin Cofactor in Cryptochrome and Photolyase. *Journal of the American Chemical Society*, *130*(24), 7695–7701. https://doi.org/10.1021/ja801152h

Kasahara, M., Torii, M., Fujita, A., & Tainaka, K. (2010). FMN binding and photochemical properties of plant putative photoreceptors containing two LOV domains, LOV/LOV proteins. *Journal of Biological Chemistry*, *285*(45), 34765–34772. https://doi.org/10.1074/jbc.M110.145367

Kavakli, I. H., Baris, I., Tardu, M., Gül, Ş., Öner, H., Çal, S., Bulut, S., Yarparvar, D., Berkel, Ç., Ustaoğlu, P., & Aydın, C. (2017). The Photolyase/Cryptochrome Family of Proteins as DNA Repair Enzymes and Transcriptional Repressors. *Photochemistry and Photobiology*, *93*(1), 93–103. https://doi.org/10.1111/php.12669

Kay, B. K., Williamson, M. P., & Sudol, M. (2000). The importance of being proline: the interaction of proline-rich motifs in signaling proteins with their cognate domains. *The FASEB Journal*, *14*(2), 231–241.

https://doi.org/10.1096/fasebj.14.2.231

Keith, S. A., Maynard, J. A., Edwards, A. J., Guest, J. R., Bauman, A. G., van Hooidonk, R., Heron, S. F., Berumen, M. L., Bouwmeester, J., Piromvaragorn, S., Rahbek, C., & Baird, A. H. (2016). Coral mass spawning predicted by rapid seasonal rise in ocean temperature. *Proceedings. Biological Sciences*, *283*(1830), 20160011. https://doi.org/10.1098/rspb.2016.0011

Kelner, A. (1949). Effect of Visible Light on the Recovery of Streptomyces Griseus Conidia from Ultra-violet Irradiation Injury. *Proceedings of the National Academy of Sciences of the United States of America*, *35*(2), 73–79. https://doi.org/10.1073/pnas.35.2.73

Khosravi-Far, R., & Der, C. J. (1994). The Ras signal transduction pathway. *Cancer Metastasis Reviews*, *13*(1), 67–89. https://doi.org/10.1007/BF00690419

Kikhney, A. G., & Svergun, D. I. (2015). A practical guide to small angle X-ray scattering (SAXS) of flexible and intrinsically disordered proteins. *FEBS Letters*, *589*(19), 2570–2577. https://doi.org/10.1016/j.febslet.2015.08.027

Kim, S. T., Malhotra, K., Smith, C. A., Taylor, J. S., & Sancar, A. (1994). Characterization of (6-4) photoproduct DNA photolyase. *The Journal of Biological Chemistry*, *269*(11), 8535–8540.

Kim, S. T., Malhotra, K., Taylor, J. S., & Sancar, A. (1996). Purification and partial characterization of (6-4) photoproduct DNA photolyase from Xenopus laevis. *Photochemistry and Photobiology*, *63*(3), 292–295. https://doi.org/10.1111/j.1751-1097.1996.tb03028.x

Kiontke, S., Geisselbrecht, Y., Pokorny, R., Carell, T., Batschauer, A., & Essen, L.-O. (2011). Crystal structures of an archaeal class II DNA photolyase and its complex with UV-damaged duplex DNA. *The EMBO Journal*, *30*(21), 4437–4449. https://doi.org/10.1038/emboj.2011.313

Klar, T., Kaiser, G., Hennecke, U., Carell, T., Batschauer, A., & Essen, L. O. (2006). Natural and non-natural antenna chromophores in the DNA photolyase from Thermus Thermophilus. *ChemBioChem*, *7*(11), 1798–1806. https://doi.org/10.1002/cbic.200600206

Klar, T., Pokorny, R., Moldt, J., Batschauer, A., & Essen, L. O. (2007). Cryptochrome 3 from Arabidopsis thaliana: Structural and Functional Analysis of its Complex with a Folate Light Antenna. *Journal of Molecular*

Biology, *366*(3), 954–964. https://doi.org/10.1016/j.jmb.2006.11.066

Kleine, T., Lockhart, P., & Batschauer, A. (2003). An Arabidopsis protein closely related to Synechocystis cryptochrome is targeted to organelles. *The Plant Journal : For Cell and Molecular Biology*, *35*(1), 93–103. https://doi.org/10.1046/j.1365-313x.2003.01787.x

Kloss, B., Price, J. L., Saez, L., Blau, J., Rothenfluh, A., Wesley, C. S., & Young, M. W. (1998). The Drosophila clock gene double-time encodes a protein closely related to human casein kinase Iepsilon. *Cell*, *94*(1), 97–107. https://doi.org/10.1016/s0092-8674(00)81225-8

Kloss, B., Rothenfluh, A., Young, M. W., & Saez, L. (2001). Phosphorylation of period is influenced by cycling physical associations of double-time, period, and timeless in the Drosophila clock. *Neuron*, *30*(3), 699–706. https://doi.org/10.1016/s0896-6273(01)00320-8

Ko, C. H., & Takahashi, J. S. (2006). Molecular components of the mammalian circadian clock. *Human Molecular Genetics*, *15*(SUPPL. 2), 271–277. https://doi.org/10.1093/hmg/ddl207

Kobayashi, K., Kanno, S., Takao, M., Yasui, A., Smit, B., & van der Horst, G. T. J. (1998). Characterization of photolyase/blue-light receptor homologs in mouse and human cells. *Nucleic Acids Research*, *26*(22), 5086–5092. https://doi.org/10.1093/nar/26.22.5086

Kobayashi, Y., Ishikawa, T., Hirayama, J., Daiyasu, H., Kanai, S., Toh, H., Fukuda, I., Tsujimura, T., Terada, N., Kamei, Y., Yuba, S., Iwai, S., & Todo, T. (2000). Molecular analysis of zebrafish photolyase/cryptochrome family: two types of cryptochromes present in zebrafish. *Genes to Cells : Devoted to Molecular & Cellular Mechanisms*, *5*(9), 725–738. https://doi.org/10.1046/j.1365-2443.2000.00364.x

Koh, K., Zheng, X., & Sehgal, A. (2006). JETLAG resets the Drosophila circadian clock by promoting light-induced degradation of TIMELESS. *Science (New York, N.Y.)*, *312*(5781), 1809–1812. https://doi.org/10.1126/science.1124951

Komori, H., Masui, R., Kuramitsu, S., Yokoyama, S., Shibata, T., Inoue, Y., & Miki, K. (2001). Crystal structure of thermostable DNA photolyase: Pyrimidine-dimer recognition mechanism. *Proceedings of the National Academy of Sciences*, *98*(24), 13560 LP – 13565. https://doi.org/10.1073/pnas.241371398

Kondoh, M., Shiraishi, C., Müller, P., Ahmad, M., Hitomi, K., Getzoff, E. D., &

Terazima, M. (2011). Light-induced conformational changes in full-length arabidopsis thaliana cryptochrome. *Journal of Molecular Biology*, *413*(1), 128–137. https://doi.org/10.1016/j.jmb.2011.08.031

Koopmann, R., Cupelli, K., Redecke, L., Nass, K., Daniel, P., White, T. A., Stellato, F., Rehders, D., Liang, M., Aquila, A., Bajt, S., Barthelmess, M., Barty, A., Michael, J., Bostedt, C., Boutet, S., Bozek, J. D., Caleman, C., Davidsson, J., … Duszenko, M. (2012). NIH Public Access biology. *Nature Methods*, *9*(3), 259–262. https://doi.org/10.1038/nmeth.1859.In

Koornneef, M., Rolff, E., & Spruit, C. J. P. (1980). Genetic Control of Light-inhibited Hypocotyl Elongation in Arabidopsis thaliana (L.) Heynh. *Zeitschrift Für Pflanzenphysiologie*, *100*(2), 147–160. https://doi.org/https://doi.org/10.1016/S0044-328X(80)80208-X

Korringa, P. (1947). Relations between the Moon and Periodicity in the Breeding of Marine Animals. *Ecological Monographs*, *17*(3), 347–381. https://doi.org/10.2307/1948665

Krishnan, B., Levine, J. D., Lynch, M. K. S., Dowse, H. B., Funes, P., Hall, J. C., Hardin, P. E., & Dryer, S. E. (2001). A new role for cryptochrome in a Drosophila circadian oscillator. *Nature*, *411*(6835), 313–317. https://doi.org/10.1038/35077094

Kristensen, O. (2015). Crystal structure of the G3BP2 NTF2-like domain in complex with a canonical FGDF motif peptide. *Biochemical and Biophysical Research Communications*, *467*(1), 53–57. https://doi.org/10.1016/j.bbrc.2015.09.123

Kronfeld-Schor, N., Dominoni, D., de la Iglesia, H., Levy, O., Herzog, E. D., Dayan, T., & Helfrich-Forster, C. (2013). Chronobiology by moonlight. *Proceedings of the Royal Society B: Biological Sciences*, *280*(1765). https://doi.org/10.1098/rspb.2012.3088

Kume, K., Zylka, M. J., Sriram, S., Shearman, L. P., Weaver, D. R., Jin, X., Maywood, E. S., Hastings, M. H., & Reppert, S. M. (1999). mCRY1 and mCRY2 are essential components of the negative limb of the circadian clock feedback loop. *Cell*, *98*(2), 193–205. https://doi.org/10.1016/S0092-8674(00)81014-4

Kutta, R. J., Archipowa, N., Johannissen, L. O., Jones, A. R., & Scrutton, N. S. (2017). Vertebrate Cryptochromes are Vestigial Flavoproteins. *Scientific Reports*, *7*, 1–11. https://doi.org/10.1038/srep44906

Kwon, I., Choe, H. K., Son, G. H., & Kim, K. (2011). Mammalian molecular clocks.

Experimental Neurobiology, *20*(1), 18–28. https://doi.org/10.5607/en.2011.20.1.18

Kyba, C. C. M., Mohar, A., & Posch, T. (2017). How bright is moonlight? *Astronomy & Geophysics*, *58*(1), 1.31-1.32. https://doi.org/10.1093/astrogeo/atx025

Kyriacou, C. P. (2009). Clocks, cryptochromes and Monarch migrations. *Journal of Biology*, *8*(6), 55. https://doi.org/10.1186/jbiol153

Lamia, K. A., Sachdeva, U. M., DiTacchio, L., Williams, E. C., Alvarez, J. G., Egan, D. F., Vasquez, D. S., Juguilon, H., Panda, S., Shaw, R. J., Thompson, C. B., & Evans, R. M. (2009). AMPK Regulates the Circadian Clock by Cryptochrome Phosphorylation and Degradation. *Science*, *326*(5951), 437 LP – 440. https://doi.org/10.1126/science.1172156

Landry, L. G., Stapleton, A. E., Lim, J., Hoffman, P., Hays, J. B., Walbot, V., & Last, R. L. (1997). An Arabidopsis photolyase mutant is hypersensitive to ultraviolet-B radiation. *Proceedings of the National Academy of Sciences*, *94*(1), 328 LP – 332. https://doi.org/10.1073/pnas.94.1.328

Levy, O., Appelbaum, L., Leggat, W., Gothlif, Y., Hayward, D. C., & Miller, D. J. (2007). Light-Responsive Cryptochromes from a Simple Multicellular Animal, the Coral Acropora millepora. *Science*, *318*, 467–470.

Lewis, P., Korf, H. W., Kuffer, L., Groß, J. V., & Erren, T. C. (2018). Exercise time cues (zeitgebers) for human circadian systems can foster health and improve performance: A systematic review. *BMJ Open Sport and Exercise Medicine*, *4*(1), 1–8. https://doi.org/10.1136/bmjsem-2018-000443

Li, Q.-H., & Yang, H.-Q. (2007). Cryptochrome signaling in plants. *Photochemistry and Photobiology*, *83*(1), 94–101. https://doi.org/10.1562/2006-02-28-IR-826

Li, X., Yang, J., Zhu, Y., Liu, Y., Shi, X., & Yang, G. (2016). Mouse Maternal High-Fat Intake Dynamically Programmed mRNA m^6A Modifications in Adipose and Skeletal Muscle Tissues in Offspring. *International Journal of Molecular Sciences*, *17*(8). https://doi.org/10.3390/ijms17081336

Li, Y. F., Kim, S. T., & Sancar, A. (1993). Evidence for lack of DNA photoreactivating enzyme in humans. *Proceedings of the National Academy of Sciences of the United States of America*, *90*(10), 4389–4393. https://doi.org/10.1073/pnas.90.10.4389

Lillywhite, H. B., & Brischoux, F. (2012). Is it better in the moonlight? Nocturnal

activity of insular cottonmouth snakes increases with lunar light levels. *Journal of Zoology*, *286*(3), 194–199. https://doi.org/10.1111/j.1469-7998.2011.00866.x

Lin, C, Robertson, D. E., Ahmad, M., Raibekas, A. A., Jorns, M. S., Dutton, P. L., & Cashmore, A. R. (1995). Association of flavin adenine dinucleotide with the Arabidopsis blue light receptor CRY1. *Science*, *269*(5226), 968 LP – 970. https://doi.org/10.1126/science.7638620

Lin, C, Yang, H., Guo, H., Mockler, T., Chen, J., & Cashmore, A. R. (1998). Enhancement of blue-light sensitivity of Arabidopsis seedlings by a blue light receptor cryptochrome 2. *Proceedings of the National Academy of Sciences of the United States of America*, *95*(5), 2686–2690. https://doi.org/10.1073/pnas.95.5.2686

Lin, Chentao. (2000). Plant blue-light receptors. *Trends in Plant Science*, *5*(8), 337–342. https://doi.org/https://doi.org/10.1016/S1360-1385(00)01687-3

Lin, Chentao, & Todo, T. (2005). The cryptochromes. *Genome Biology*, *6*(5). https://doi.org/10.1186/gb-2005-6-5-220

Liu, C., Hu, J., Qu, C., Wang, L., Huang, G., Niu, P., Zhong, Z., Hong, F., Wang, G., Postlethwait, J. H., & Wang, H. (2015). Molecular evolution and functional divergence of zebrafish (Danio rerio) cryptochrome genes. *Scientific Reports*, *5*, 8113. https://doi.org/10.1038/srep08113

Liu, N., & Zhang, E. E. (2016). Phosphorylation regulating the ratio of intracellular CRY1 protein determines the circadian period. *Frontiers in Neurology*, *7*(SEP), 1–9. https://doi.org/10.3389/fneur.2016.00159

Liu, Q., Su, T., He, W., Ren, H., Liu, S., Chen, Y., Gao, L., Hu, X., Lu, H., Cao, S., Huang, Y., Wang, X., Wang, Q., & Lin, C. (2020). Photooligomerization Determines Photosensitivity and Photoreactivity of Plant Cryptochromes. *Molecular Plant*, *13*(3), 398–413. https://doi.org/10.1016/j.molp.2020.01.002

Liu, W., Xie, Y., Ma, J., Luo, X., Nie, P., Zuo, Z., Lahrmann, U., Zhao, Q., Zheng, Y., Zhao, Y., Xue, Y., & Ren, J. (2015). IBS: An illustrator for the presentation and visualization of biological sequences. *Bioinformatics*, *31*(20), 3359–3361. https://doi.org/10.1093/bioinformatics/btv362

Lu, B., Sun, X., Chen, Y., Jin, Q., Liang, Q., Liu, S., Li, Y., Zhou, Y., Li, W., & Huang, Z. (2015). Novel function of PITH domain-containing 1 as an activator of internal ribosomal entry site to enhance RUNX1 expression and promote megakaryocyte differentiation. *Cellular and Molecular Life Sciences*, *72*(4),

821–832. https://doi.org/10.1007/s00018-014-1704-2

Lu, S., Wang, J., Chitsaz, F., Derbyshire, M. K., Geer, R. C., Gonzales, N. R., Gwadz, M., Hurwitz, D. I., Marchler, G. H., Song, J. S., Thanki, N., Yamashita, R. A., Yang, M., Zhang, D., Zheng, C., Lanczycki, C. J., & Marchler-Bauer, A. (2020). CDD/SPARCLE: the conserved domain database in 2020. *Nucleic Acids Research*, *48*(D1), D265–D268. https://doi.org/10.1093/nar/gkz991

Malhotra, K., Kim, S.-T., Batschauer, A., Dawut, L., & Sancar, A. (1995). Putative Blue-Light Photoreceptors from Arabidopsis thaliana and Sinapis alba with a High Degree of Sequence Homology to DNA Photolyase Contain the Two Photolyase Cofactors but Lack DNA Repair Activity. *Biochemistry*, *34*(20), 6892–6899. https://doi.org/10.1021/bi00020a037

Marguet, S., & Markovitsi, D. (2005). Time-Resolved Study of Thymine Dimer Formation. *Journal of the American Chemical Society*, *127*(16), 5780–5781. https://doi.org/10.1021/ja050648h

Martin, V. J. (2002). *Photoreceptors of cnidarians 1*.

Mastronarde, D. N. (2005). *Automated electron microscope tomography using robust prediction of specimen movements*. *152*, 36–51. https://doi.org/10.1016/j.jsb.2005.07.007

Maul, M. J., Barends, T. R. M., Glas, A. F., Cryle, M. J., Domratcheva, T., Schneider, S., Schlichting, I., & Carell, T. (2008). Crystal structure and mechanism of a DNA (6-4) photolyase. *Angewandte Chemie (International Ed. in English)*, *47*(52), 10076–10080. https://doi.org/10.1002/anie.200804268

Maurer, C., Hung, H. C., & Weber, F. (2009). Cytoplasmic interaction with CYCLE promotes the post-translational processing of the circadian CLOCK protein. *FEBS Letters*, *583*(10), 1561–1566. https://doi.org/10.1016/j.febslet.2009.04.013

McGuffin, L. J., Bryson, K., & Jones, D. T. (2000). The PSIPRED protein structure prediction server. *Bioinformatics*, *16*(4), 404–405. https://doi.org/10.1093/bioinformatics/16.4.404

Mees, A., Klar, T., Gnau, P., Hennecke, U., Eker, A. P. M., Carell, T., & Essen, L.-O. (2004). Crystal structure of a photolyase bound to a CPD-like DNA lesion after in situ repair. *Science (New York, N.Y.)*, *306*(5702), 1789–1793. https://doi.org/10.1126/science.1101598

Mehra, A., Baker, C. L., Loros, J. J., & Dunlap, J. C. (2009). Post-translational

modifications in circadian rhythms. *Trends in Biochemical Sciences*, *34*(10), 483–490. https://doi.org/10.1016/j.tibs.2009.06.006

Mei, Q., & Dvornyk, V. (2015). Evolutionary history of the photolyase/cryptochrome superfamily in eukaryotes. *PLoS ONE*, *10*(9), 1–20. https://doi.org/10.1371/journal.pone.0135940

Merbitz-Zahradnik, T., & Wolf, E. (2015). How is the inner circadian clock controlled by interactive clock proteins?: Structural analysis of clock proteins elucidates their physiological role. *FEBS Letters*, *589*(14), 1516–1529. https://doi.org/10.1016/j.febslet.2015.05.024

Mertens, H. D. T., & Svergun, D. I. (2010). Structural characterization of proteins and complexes using small-angle X-ray solution scattering. *Journal of Structural Biology*, *172*(1), 128–141. https://doi.org/10.1016/j.jsb.2010.06.012

Michel, S., & Meijer, J. H. (2020). From clock to functional pacemaker. *European Journal of Neuroscience*, *51*(1), 482–493. https://doi.org/10.1111/ejn.14388

Miranda-Vizuete, A., & Spyrou, G. (2000). Genomic structure and chromosomal localization of human thioredoxin-like protein gene (txl). *DNA Sequence : The Journal of DNA Sequencing and Mapping*, *10*(6), 419–424. https://doi.org/10.3109/10425170009015613

Miyamoto, Y., & Sancar, A. (1998). Vitamin B₂-based blue-light photoreceptors in the retinohypothalamic tract as the photoactive pigments for setting the circadian clock in mammals. *Proceedings of the National Academy of Sciences*, *95*(11), 6097 LP – 6102. https://doi.org/10.1073/pnas.95.11.6097

Mohawk, J. A., Green, C. B., & Takahashi, J. S. (2012). Central and peripheral circadian clocks in mammals. *Annual Review of Neuroscience*, *35*, 445–462. https://doi.org/10.1146/annurev-neuro-060909-153128

Moldt, J., Pokomy, R., Orth, C., Linne, U., Geisselbrecht, Y., Marahiel, M. A., Essen, L. O., & Batschauer, A. (2009). Photoreduction of the folate cofactor in members of the photolyase family. *Journal of Biological Chemistry*, *284*(32), 21670–21683. https://doi.org/10.1074/jbc.M109.018697

Moore MD, R. Y. (1997). CIRCADIAN RHYTHMS: Basic Neurobiology and Clinical Applications. *Annual Review of Medicine*, *48*(1), 253–266. https://doi.org/10.1146/annurev.med.48.1.253

Müller, M., & Carell, T. (2009). Structural biology of DNA photolyases and

cryptochromes. *Current Opinion in Structural Biology*, *19*(3), 277–285. https://doi.org/10.1016/j.sbi.2009.05.003

Murata, K., & Wolf, M. (2018). Cryo-electron microscopy for structural analysis of dynamic biological macromolecules. *Biochimica et Biophysica Acta - General Subjects*, *1862*(2), 324–334. https://doi.org/10.1016/j.bbagen.2017.07.020

Musacchio, A., Gibson, T., Lehto, V. P., & Saraste, M. (1992). SH3--an abundant protein domain in search of a function. *FEBS Letters*, *307*(1), 55–61. https://doi.org/10.1016/0014-5793(92)80901-r

Nagai, K., Oubridge, C., Ito, N., Avis, J., & Evans, P. (1995). The RNP domain: a sequence-specific RNA-binding domain involved in processing and transport of RNA. *Trends in Biochemical Sciences*, *20*(6), 235–240. https://doi.org/10.1016/S0968-0004(00)89024-6

Nawathean, P., & Rosbash, M. (2004). The doubletime and CKII kinases collaborate to potentiate Drosophila PER transcriptional repressor activity. *Molecular Cell*, *13*(2), 213–223. https://doi.org/10.1016/s1097-2765(03)00503-3

Nichols, R. C., Wang, X. W., Tang, J., Hamilton, B. J., High, F. A., Herschman, H. R., & Rigby, W. F. C. (2000). The RGG Domain in hnRNP A2 Affects Subcellular Localization. *Experimental Cell Research*, *256*(2), 522–532. https://doi.org/https://doi.org/10.1006/excr.2000.4827

Notredame, C., Higgins, D. G., & Heringa, J. (2000). T-coffee: A novel method for fast and accurate multiple sequence alignment. *Journal of Molecular Biology*, *302*(1), 205–217. https://doi.org/10.1006/jmbi.2000.4042

Okafuji, A., Biskup, T., Hitomi, K., Getzoff, E. D., Kaiser, G., Batschauer, A., Bacher, A., Hidema, J., Teranishi, M., Yamamoto, K., Schleicher, E., & Weber, S. (2010). Light-induced activation of class II cyclobutane pyrimidine dimer photolyases. *DNA Repair*, *9*(5), 495–505. https://doi.org/10.1016/j.dnarep.2010.01.014

Okamura, H., Miyake, S., Sumi, Y., Yamaguchi, S., Yasui, A., Muijtjens, M., Hoeijmakers, J. H. J., & van der Horst, G. T. J. (1999). Photic Induction of mPer1 and mPer2 in Cry-Deficient Mice Lacking a Biological Clock. *Science*, *286*(5449), 2531 LP – 2534. https://doi.org/10.1126/science.286.5449.2531

Oliveri, P., Fortunato, A. E., Petrone, L., Ishikawa-Fujiwara, T., Kobayashi, Y.,

Todo, T., Antonova, O., Arboleda, E., Zantke, J., Tessmar-Raible, K., & Falciatore, A. (2014a). The Cryptochrome/Photolyase Family in aquatic organisms. *Marine Genomics*, *14*(April), 23–37. https://doi.org/10.1016/j.margen.2014.02.001

Oliveri, P., Fortunato, A. E., Petrone, L., Ishikawa-Fujiwara, T., Kobayashi, Y., Todo, T., Antonova, O., Arboleda, E., Zantke, J., Tessmar-Raible, K., & Falciatore, A. (2014b). The Cryptochrome/Photolyase Family in aquatic organisms. *Marine Genomics*, *14*(April), 23–37. https://doi.org/10.1016/j.margen.2014.02.001

Ozturk, N. (2017). Phylogenetic and Functional Classification of the Photolyase/Cryptochrome Family. *Photochemistry and Photobiology*, *93*(1), 104–111. https://doi.org/10.1111/php.12676

Öztürk, N., Kao, Y.-T., Selby, C. P., Kavaklı, I. H., Partch, C. L., Zhong, D., & Sancar, A. (2008). Purification and Characterization of a Type III Photolyase from Caulobacter crescentus. *Biochemistry*, *47*(39), 10255–10261. https://doi.org/10.1021/bi801085a

Ozturk, N., Selby, C. P., Annayev, Y., Zhong, D., & Sancar, A. (2011). Reaction mechanism of Drosophila cryptochrome. *Proceedings of the National Academy of Sciences*, *108*(2), 516 LP – 521. https://doi.org/10.1073/pnas.1017093108

Palayam, M., Ganapathy, J., Guercio, A. M., Tal, L., Deck, S. L., & Shabek, N. (2020). Structural Insights into Photoactivation of Plant Cryptochrome-2 Equal contribution. *BioRxiv*, 2020.07.30.227371. https://doi.org/10.1101/2020.07.30.227371

Palmer, J. D. (2000). The clocks controlling the tide-associated rhythms of intertidal animals. *BioEssays : News and Reviews in Molecular, Cellular and Developmental Biology*, *22*(1), 32–37. https://doi.org/10.1002/(SICI)1521-1878(200001)22:1<32::AID-BIES7>3.0.CO;2-U

Park, H. W., Kim, S. T., Sancar, A., & Deisenhofer, J. (1995). Crystal structure of DNA photolyase from Escherichia coli. *Science*, *268*(5219), 1866 LP – 1872. https://doi.org/10.1126/science.7604260

Parker, F., Maurier, F., Delumeau, I., Duchesne, M., Faucher, D., Debussche, L., Dugue, A., Schweighoffer, F., & Tocque, B. (1996). A Ras-GTPase-activating protein SH3-domain-binding protein. *Molecular and Cellular Biology*, *16*(6), 2561 LP – 2569. https://doi.org/10.1128/MCB.16.6.2561

Partch, C. L., Clarkson, M. W., Özgür, S., Lee, A. L., & Sancar, A. (2005). Role of

Structural Plasticity in Signal Transduction by the Cryptochrome Blue-Light Photoreceptor. *Biochemistry*, *44*(10), 3795–3805. https://doi.org/10.1021/bi047545g

Payton, L., & Tran, D. (2019). Moonlight cycles synchronize oyster behaviour. *Biology Letters*, *15*(1). https://doi.org/10.1098/rsbl.2018.0299

Perrigault, M., & Tran, D. (2017). Identification of the molecular clockwork of the oyster Crassostrea gigas. *PLoS ONE*, *12*(1), 1–21. https://doi.org/10.1371/journal.pone.0169790

Perry, R. P., Kelley, D. E., Friderici, K., & Rottman, F. (1975). The methylated constituents of L cell messenger RNA: evidence for an unusual cluster at the 5' terminus. *Cell*, *4*(4), 387–394. https://doi.org/10.1016/0092-8674(75)90159-2

Peschel, N., Chen, K. F., Szabo, G., & Stanewsky, R. (2009). Light-Dependent Interactions between the Drosophila Circadian Clock Factors Cryptochrome, Jetlag, and Timeless. *Current Biology*, *19*(3), 241–247. https://doi.org/10.1016/j.cub.2008.12.042

Petoukhov, M. V., Franke, D., Shkumatov, A. V., Tria, G., Kikhney, A. G., Gajda, M., Gorba, C., Mertens, H. D. T., Konarev, P. V., & Svergun, D. I. (2012). New developments in the ATSAS program package for small-angle scattering data analysis. *Journal of Applied Crystallography*, *45*(2), 342–350. https://doi.org/10.1107/S0021889812007662

Petoukhov, M. V, Konarev, P. V, Kikhney, G., & Dmitri, I. (2007). ATSAS 2.1 - Supported Small-Angle Scattering Data Analysis. *Applied Crystallography*, *40*, s223–s228.

Polaino, S., Villalobos-Escobedo, J. M., Shakya, V. P. S., Miralles-Durán, A., Chaudhary, S., Sanz, C., Shahriari, M., Luque, E. M., Eslava, A. P., Corrochano, L. M., Herrera-Estrella, A., & Idnurm, A. (2017). A Ras GTPase associated protein is involved in the phototropic and circadian photobiology responses in fungi. *Scientific Reports*, *7*(February), 1–12. https://doi.org/10.1038/srep44790

Preitner, N., Damiola, F., Lopez-Molina, L., Zakany, J., Duboule, D., Albrecht, U., & Schibler, U. (2002). The orphan nuclear receptor REV-ERBalpha controls circadian transcription within the positive limb of the mammalian circadian oscillator. *Cell*, *110*(2), 251–260. https://doi.org/10.1016/s0092-8674(02)00825-5

Prigent, M., Barlat, I., Langen, H., & Dargemont, C. (2000). IκBα and IκBα/NF-κB

complexes are retained in the cytoplasm through interaction with a novel partner, RasGAP SH3-binding protein 2. *Journal of Biological Chemistry*, *275*(46), 36441–36449. https://doi.org/10.1074/jbc.M004751200

Raible, F., Takekata, H., & Tessmar-Raible, K. (2017). An overview of monthly rhythms and clocks. *Frontiers in Neurology*, *8*(MAY), 1–14. https://doi.org/10.3389/fneur.2017.00189

Ralph, M. R., Foster, R. G., Davis, F. C., & Menaker, M. (1990). Transplanted suprachiasmatic nucleus determines circadian period. *Science*, *247*(4945), 975–978. https://doi.org/10.1126/science.2305266

Rea, M. S., Bierman, A., Figueiro, M. G., & Bullough, J. D. (2008). A new approach to understanding the impact of circadian disruption on human health. *Journal of Circadian Rhythms*, *6*, 1–14. https://doi.org/10.1186/1740-3391-6-7

Reddy, A. B., Maywood, E. S., Karp, N. A., King, V. M., Inoue, Y., Gonzalez, F. J., Lilley, K. S., Kyriacou, C. P., & Hastings, M. H. (2007). Glucocorticoid signaling synchronizes the liver circadian transcriptome. *Hepatology*, *45*(6), 1478–1488. https://doi.org/10.1002/hep.21571

Reppert, S. M., & Weaver, D. R. (2002). Coordination of circadian timing in mammals. *Nature*, *418*(6901), 935–941. https://doi.org/10.1038/nature00965

Ritz, T., Yoshii, T., Helfrich-Foerster, C., & Ahmad, M. (2010). Cryptochrome: A photoreceptor with the properties of a magnetoreceptor? *Communicative & Integrative Biology*, *3*(1), 24–27. https://doi.org/10.4161/cib.3.1.9865

Rosato, E., Codd, V., Mazzotta, G., Piccin, A., Zordan, M., Costa, R., & Kyriacou, C. P. (2001). Light-dependent interaction between Drosophila CRY and the clock protein PER mediated by the carboxy terminus of CRY. *Current Biology*, *11*(12), 909–917. https://doi.org/https://doi.org/10.1016/S0960-9822(01)00259-7

Rosenfeldt, G., Viana, R. M., Mootz, H. D., von Arnim, A. G., & Batschauer, A. (2008). Chemically Induced and Light-Independent Cryptochrome Photoreceptor Activation. *Molecular Plant*, *1*(1), 4–14. https://doi.org/10.1093/MP/SSM002

Roundtree, I. A., & He, C. (2016). Nuclear m(6)A Reader YTHDC1 Regulates mRNA Splicing. *Trends in Genetics : TIG*, *32*(6), 320–321. https://doi.org/10.1016/j.tig.2016.03.006

RUPERT, C. S. (1960). Photoreactivation of transforming DNA by an enzyme

from bakers' yeast. *The Journal of General Physiology*, *43*(3), 573–595. https://doi.org/10.1085/jgp.43.3.573

Rutila, J. E., Suri, V., Le, M., So, W. V., Rosbash, M., & Hall, J. C. (1998). Cycle is a second bHLH-PAS clock protein essential for circadian rhythmicity and transcription of Drosophila period and timeless. *Cell*, *93*(5), 805–814. https://doi.org/10.1016/S0092-8674(00)81441-5

Sadeghian, K., Bocola, M., Merz, T., & Schütz, M. (2010). Theoretical Study on the Repair Mechanism of the (6−4) Photolesion by the (6−4) Photolyase. *Journal of the American Chemical Society*, *132*(45), 16285–16295. https://doi.org/10.1021/ja108336t

Sancar, A. (2003). Structure and function of DNA photolyase and cryptochrome blue-light photoreceptors. *Chemical Reviews*, *103*(6), 2203–2237. https://doi.org/10.1021/cr0204348

Sancar, A., & Rupert, C. S. (1978). Cloning of the phr gene and amplification of photolyase in Escherichia coli. *Gene*, *4*(4), 295–308. https://doi.org/10.1016/0378-1119(78)90047-1

Sang, Y., Li, Q. H., Rubio, V., Zhang, Y. C., Mao, J., Deng, X. W., & Yang, H. Q. (2005). N-terminal domain-mediated homodimerization is required for photoreceptor activity of Arabidopsis Cryptochrome 1. *Plant Cell*, *17*(5), 1569–1584. https://doi.org/10.1105/tpc.104.029645

Sawaya, M. R., Cascio, D., Gingery, M., Rodriguez, J., Goldschmidt, L., Colletier, J. P., Messerschmidt, M. M., Boutet, S., Koglin, J. E., Williams, G. J., Brewster, A. S., Nass, K., Hattne, J., Botha, S., Doak, R. B., Shoeman, R. L., DePonte, D. P., Park, H. W., Federici, B. A., … Eisenberg, D. S. (2014). Protein crystal structure obtained at 2.9 Å resolution from injecting bacterial cells into an X-ray free-electron laser beam. *Proceedings of the National Academy of Sciences of the United States of America*, *111*(35), 12769–12774. https://doi.org/10.1073/pnas.1413456111

Scheerer, P., Zhang, F., Kalms, J., Von Stetten, D., Krauß, N., Oberpichler, I., & Lamparter, T. (2015). The class III cyclobutane pyrimidine dimer photolyase structure reveals a new antenna chromophore binding site and alternative photoreduction pathways. *Journal of Biological Chemistry*, *290*(18), 11504–11514. https://doi.org/10.1074/jbc.M115.637868

Schenk, S., Bannister, S. C., Sedlazeck, F. J., Anrather, D., Minh, B. Q., Bileck, A., Hartl, M., Haeseler, A. Von, Gerner, C., Raible, F., & Tessmar-raible, K. (2019). Combined transcriptome and proteome profiling reveals specific molecular brain signatures for sex , maturation and circalunar clock phase.

ELife, *8*. https://doi.org/https://doi.org/10.7554/eLife.41556

Scholz, J., Besir, H., Strasser, C., & Suppmann, S. (2013). A new method to customize protein expression vectors for fast, efficient and background free parallel cloning. *BMC Biotechnology*, *13*, 1–11. https://doi.org/10.1186/1472-6750-13-12

Schönherr, R., Rudolph, J. M., & Redecke, L. (2018). Protein crystallization in living cells. *Biological Chemistry*, *399*(7), 751–772. https://doi.org/10.1515/hsz-2018-0158

Selby, C. P., & Sancar, A. (2006). A cryptochrome/photolyase class of enzymes with single-stranded DNA-specific photolyase activity. *Proceedings of the National Academy of Sciences of the United States of America*, *103*(47), 17696–17700. https://doi.org/10.1073/pnas.0607993103

Shao, K., Zhang, X., Li, X., Hao, Y., Xiaowei, H., Ma, M., Zhang, M., Fang, Y., Liu, H., & Zhang, P. (2020). The oligomeric structures of plant cryptochromes. *Nature Structural & Molecular Biology*, *27*, 480–488. https://doi.org/10.1038/s41594-020-0420-x

Shen, E. C., Henry, M. F., Weiss, V. H., Valentini, S. R., Silver, P. A., & Lee, M. S. (1998). Arginine methylation facilitates the nuclear export of hnRNP proteins. *Genes & Development*, *12*(5), 679–691. https://doi.org/10.1101/gad.12.5.679

Shi, H., Wang, X., Lu, Z., Zhao, B. S., Ma, H., Hsu, P. J., Liu, C., & He, C. (2017). YTHDF3 facilitates translation and decay of N(6)-methyladenosine-modified RNA. *Cell Research*, *27*(3), 315–328. https://doi.org/10.1038/cr.2017.15

Shlesinger, T., & Loya, Y. (2019). *Breakdown in spawning synchrony : A silent threat to coral persistence*. *1007*(September), 1002–1007. https://doi.org/10.1126/science.aax0110

Sitter, D. (1932). *2, 1932]*. *130*(3270), 9–10.

So, A. Y.-L., Bernal, T. U., Pillsbury, M. L., Yamamoto, K. R., & Feldman, B. J. (2009). Glucocorticoid regulation of the circadian clock modulates glucose homeostasis. *Proceedings of the National Academy of Sciences of the United States of America*, *106*(41), 17582–17587. https://doi.org/10.1073/pnas.0909733106

Somers, D. E., Devlin, P. F., & Kay, S. A. (1998). Phytochromes and Cryptochromes in the Entrainment of the Arabidopsis Circadian Clock. *Science*, *282*(5393),

1488 LP – 1490. https://doi.org/10.1126/science.282.5393.1488

Song, J. (2005). Solution structure of At3g04780.1-des15, an Arabidopsis thaliana ortholog of the C-terminal domain of human thioredoxin-like protein. *Protein Science*, *14*(4), 1059–1063. https://doi.org/10.1110/ps.041246805

Stanewsky, R., Kaneko, M., Emery, P., Beretta, B., Wager-Smith, K., Kay, S. A., Rosbash, M., & Hall, J. C. (1998). The cryb mutation identifies cryptochrome as a circadian photoreceptor in Drosophila. *Cell*, *95*(5), 681–692. https://doi.org/10.1016/s0092-8674(00)81638-4

Starr, C., Nekaris, K. A. I., & Leung, L. (2012). Hiding from the moonlight: Luminosity and temperature affect activity of Asian nocturnal primates in a highly seasonal forest. *PLoS ONE*, *7*(4), 1–8. https://doi.org/10.1371/journal.pone.0036396

Stephan, F. K., & Zucker, I. (1972). Circadian rhythms in drinking behavior and locomotor activity of rats are eliminated by hypothalamic lesions. *Proceedings of the National Academy of Sciences of the United States of America*, *69*(6), 1583–1586. https://doi.org/10.1073/pnas.69.6.1583

Sugama, N., Park, J.-G., Park, Y.-J., Takeuchi, Y., Kim, S.-J., & Takemura, A. (2008). Moonlight affects nocturnal Period2 transcript levels in the pineal gland of the reef fish Siganus guttatus. *Journal of Pineal Research*, *45*(2), 133–141. https://doi.org/10.1111/j.1600-079X.2008.00566.x

Suloway, C., Pulokas, J., Fellmann, D., Cheng, A., Guerra, F., Quispe, J., Stagg, S., Potter, C. S., & Carragher, B. (2005). Automated molecular microscopy: The new Leginon system. *Journal of Structural Biology*, *151*(1), 41–60. https://doi.org/10.1016/j.jsb.2005.03.010

Suyama, M., Doerks, T., Braun, I. C., Sattler, M., Izaurralde, E., & Bork, P. (2000). Prediction of structural domains of TAP reveals details of its interaction with p15 and nucleoporins. *EMBO Reports*, *1*(1), 53–58. https://doi.org/10.1093/embo-reports/kvd009

Svergun, D. (1999). Restoring low resolution structure of biological macromolecules from solution …. *Biophysical Journal*, *76*(June), 2879–2886. http://linkinghub.elsevier.com/retrieve/pii/S0006349599774436

Svergun, D. I. (1992). Determination of the regularization parameter in indirect-transform methods using perceptual criteria. *Journal of Applied Crystallography*, *25*(pt 4), 495–503. https://doi.org/10.1107/S0021889892001663

Tagaya, H., Murayama, N., & Fukase, Y. (2015). [Circadian rhythm sleep-wake disorder (circadian rhythm sleep disorder)]. *Nihon rinsho. Japanese journal of clinical medicine*, *73*(6), 942–948.

Tamada, T., Kitadokoro, K., Higuchi, Y., Inaka, K., Yasui, A., de Ruiter, P. E., Eker, A. P., & Miki, K. (1997). Crystal structure of DNA photolyase from Anacystis nidulans. In *Nature structural biology* (Vol. 4, Issue 11, pp. 887–891). https://doi.org/10.1038/nsb1197-887

Tamanini, F., Chaves, I., Bajek, M. I., & van der Horst, G. T. J. (2007). Structure function analysis of mammalian cryptochromes. *Cold Spring Harbor Symposia on Quantitative Biology*, *72*, 133–139. https://doi.org/10.1101/sqb.2007.72.066

Tanabe, A., Tanikawa, K., Tsunetomi, M., Takai, K., Ikeda, H., Konno, J., Torigoe, T., Maeda, H., Kutomi, G., Okita, K., Mori, M., & Sahara, H. (2016). RNA helicase YTHDC2 promotes cancer metastasis via the enhancement of the efficiency by which HIF-1α mRNA is translated. *Cancer Letters*, *376*(1), 34–42. https://doi.org/10.1016/j.canlet.2016.02.022

Team, R. C. (2016). *R: A language and environment for statistical computing*.

Teranishi, M., Nakamura, K., Morioka, H., Yamamoto, K., & Hidema, J. (2008). The native cyclobutane pyrimidine dimer photolyase of rice is phosphorylated. *Plant Physiology*, *146*(4), 1941–1951. https://doi.org/10.1104/pp.107.110189

Tessmar-Raible, K., Raible, F., & Arboleda, E. (2011). Another place, another timer: Marine species and the rhythms of life. *BioEssays*, *33*(3), 165–172. https://doi.org/10.1002/bies.201000096

Theler, D., Dominguez, C., Blatter, M., Boudet, J., & Allain, F. H. T. (2014). Solution structure of the YTH domain in complex with N6-methyladenosine RNA: A reader of methylated RNA. *Nucleic Acids Research*, *42*(22), 13911–13919. https://doi.org/10.1093/nar/gku1116

Thuy Nguyen, M., Indrawati, & Hendrickx, M. (2003). Model studies on the stability of folic acid and 5-methyltetrahydrofolic acid degradation during thermal treatment in combination with high hydrostatic pressure. *Journal of Agricultural and Food Chemistry*, *51*(11), 3352–3357. https://doi.org/10.1021/jf026234e

Todo, T, Ryo, H., Yamamoto, K., Toh, H., Inui, T., Ayaki, H., Nomura, T., & Ikenaga, M. (1996). Similarity among the Drosophila (6-4)photolyase, a human photolyase homolog, and the DNA photolyase-blue-light

photoreceptor family. *Science (New York, N.Y.)*, *272*(5258), 109–112. https://doi.org/10.1126/science.272.5258.109

Todo, T, Takemori, H., Ryo, H., Ihara, M., Matsunaga, T., Nikaido, O., Sato, K., & Nomura, T. (1993). A new photoreactivating enzyme that specifically repairs ultraviolet light-induced (6-4)photoproducts. *Nature*, *361*(6410), 371–374. https://doi.org/10.1038/361371a0

Todo, T, Tsuji, H., Otoshi, E., Hitomi, K., Kim, S. T., & Ikenaga, M. (1997). Characterization of a human homolog of (6-4) photolyase. *Mutation Research*, *384*(3), 195–204. https://doi.org/10.1016/s0921-8777(97)00032-3

Todo, Takeshi. (1999). Functional diversity of the DNA photolyase/blue light receptor family. *Mutation Research - DNA Repair*, *434*(2), 89–97. https://doi.org/10.1016/S0921-8777(99)00013-0

Tosini, G., Ferguson, I., & Tsubota, K. (2016). Effects of blue light on the circadian system and eye physiology. *Molecular Vision*, *22*(August 2015), 61–72.

Tsai, W.-C., Gayatri, S., Reineke, L. C., Sbardella, G., Bedford, M. T., & Lloyd, R. E. (2016). Arginine Demethylation of G3BP1 Promotes Stress Granule Assembly. *The Journal of Biological Chemistry*, *291*(43), 22671–22685. https://doi.org/10.1074/jbc.M116.739573

Turányi, C. Z., Rónai, K. Z., Zoller, R., Véber, O., Czira, M. E., Újszászi, Á., László, G., Szentkirályi, A., Dunai, A., Lindner, A., Szocs, J. L., Becze, Á., Kelemen, A., Lendvai, Z., Molnar, M. Z., Mucsi, I., & Novák, M. (2014). Association between lunar phase and sleep characteristics. *Sleep Medicine*, *15*(11), 1411–1416. https://doi.org/10.1016/j.sleep.2014.06.020

Tuukkanen, A. T., Kleywegt, G. J., & Svergun, D. I. (2016). Resolution of ab initio shapes determined from small-angle scattering. *IUCrJ*, *3*, 440–447. https://doi.org/10.1107/S2052252516016018

Uchida, N., Mitani, H., Todo, T., Ikenaga, M., & Shima, A. (1997). Photoreactivating Enzyme for (6-4) Photoproducts in Cultured Goldfish Cells. *Photochemistry and Photobiology*, *65*(6), 964–968. https://doi.org/10.1111/j.1751-1097.1997.tb07955.x

Ueda, H. R., Chen, W., Adachi, A., Wakamatsu, H., Hayashi, S., Takasugi, T., Nagano, M., Nakahama, K., Suzuki, Y., Sugano, S., Iino, M., Shigeyoshi, Y., & Hashimoto, S. (2002). A transcription factor response element for gene expression during circadian night. *Nature*, *418*(6897), 534–539.

https://doi.org/10.1038/nature00906

Upham, N. S. (2008). *Rodent activity in relation to moonlight in sandy and open habitats of the Great Basin Desert Morphological evolution and biogeography of Neotropical rodents View project*. *August 2008*. https://doi.org/10.13140/RG.2.2.33807.89765

Vaidya, A. T., Top, D., Manahan, C. C., Tokuda, J. M., Zhang, S., Pollack, L., Young, M. W., & Crane, B. R. (2013). Flavin reduction activates Drosophila cryptochrome. *Proceedings of the National Academy of Sciences of the United States of America*, *110*(51), 20455–20460. https://doi.org/10.1073/pnas.1313336110

Valverde, F., Mouradov, A., Soppe, W., Ravenscroft, D., Samach, A., & Coupland, G. (2004). Photoreceptor regulation of CONSTANS protein in photoperiodic flowering. *Science (New York, N.Y.)*, *303*(5660), 1003–1006. https://doi.org/10.1126/science.1091761

van der Horst, G. T., Muijtjens, M., Kobayashi, K., Takano, R., Kanno, S., Takao, M., de Wit, J., Verkerk, A., Eker, A. P., van Leenen, D., Buijs, R., Bootsma, D., Hoeijmakers, J. H., & Yasui, A. (1999). Mammalian Cry1 and Cry2 are essential for maintenance of circadian rhythms. *Nature*, *398*(6728), 627–630. https://doi.org/10.1038/19323

van der Schalie, E. A., Conte, F. E., Marz, K. E., & Green, C. B. (2007). Structure/function analysis of Xenopus cryptochromes 1 and 2 reveals differential nuclear localization mechanisms and functional domains important for interaction with and repression of CLOCK-BMAL1. *Molecular and Cellular Biology*, *27*(6), 2120–2129. https://doi.org/10.1128/MCB.01638-06

van Woesik, R., Lacharmoise, F., & Köksal, S. (2006). Annual cycles of solar insolation predict spawning times of Caribbean corals. In *Ecology letters* (Vol. 9, Issue 4, pp. 390–398). https://doi.org/10.1111/j.1461-0248.2006.00886.x

Vanselow, K., & Kramer, A. (2007). Role of phosphorylation in the mammalian circadian clock. *Cold Spring Harbor Symposia on Quantitative Biology*, *72*, 167–176. https://doi.org/10.1101/sqb.2007.72.036

Varghese, A. J., & Wang, S. Y. (1968). Photoreversible photoproduct of thymine. *Biochemical and Biophysical Research Communications*, *33*(1), 102–107. https://doi.org/10.1016/0006-291x(68)90262-3

Vinayak, P., Coupar, J., Hughes, S. E., Fozdar, P., Kilby, J., Garren, E., Yoshii, T.,

& Hirsh, J. (2013). Exquisite Light Sensitivity of Drosophila melanogaster Cryptochrome. *PLoS Genetics*, *9*(7), 1–10. https://doi.org/10.1371/journal.pgen.1003615

Vitaterna, M. H., Selby, C. P., Todo, T., Niwa, H., Thompson, C., Fruechte, E. M., Hitomi, K., Thresher, R. J., Ishikawa, T., Miyazaki, J., Takahashi, J. S., & Sancar, A. (1999). Differential regulation of mammalian Period genes and circadian rhythmicity by cryptochromes 1 and 2. *Proceedings of the National Academy of Sciences*, *96*(21), 12114 LP – 12119. https://doi.org/10.1073/pnas.96.21.12114

Volkov, V. V., & Svergun, D. I. (2003). Uniqueness of ab initio shape determination in small-angle scattering. *Journal of Applied Crystallography*, *36*(3 I), 860–864. https://doi.org/10.1107/S0021889803000268

Wahl, S., Engelhardt, M., Schaupp, P., Lappe, C., & Ivanov, I. V. (2019). The inner clock—Blue light sets the human rhythm. *Journal of Biophotonics*, *12*(12), 1–14. https://doi.org/10.1002/jbio.201900102

Wang, C.-Y., Yeh, J.-K., Shie, S.-S., Hsieh, I.-C., & Wen, M.-S. (2015). Circadian rhythm of RNA N6-methyladenosine and the role of cryptochrome. *Biochemical and Biophysical Research Communications*, *465*(1), 88–94. https://doi.org/10.1016/j.bbrc.2015.07.135

Wang, H., Ma, L.-G., Li, J.-M., Zhao, H.-Y., & Deng, X. W. (2001). Direct Interaction of Arabidopsis Cryptochromes with COP1 in Light Control Development. *Science*, *294*(5540), 154 LP – 158. https://doi.org/10.1126/science.1063630

Wang, J., Du, X., Pan, W., Wang, X., & Wu, W. (2015). Photoactivation of the cryptochrome/photolyase superfamily. *Journal of Photochemistry and Photobiology C: Photochemistry Reviews*, *22*, 84–102. https://doi.org/10.1016/j.jphotochemrev.2014.12.001

Wang, P., & Wilson, S. R. (2013). Mass spectrometry-based protein identification by integrating de novo sequencing with database searching. *BMC Bioinformatics*, *14 Suppl 2*(Suppl 2), S24. https://doi.org/10.1186/1471-2105-14-S2-S24

Wang, Q., & Lin, C. (2020). Mechanisms of Cryptochrome-Mediated Photoresponses in Plants. *Annual Review of Plant Biology*, *71*, 103–129. https://doi.org/10.1146/annurev-arplant-050718-100300

Wang, X., Lu, Z., Gomez, A., Hon, G. C., Yue, Y., Han, D., Fu, Y., Parisien, M., Dai,

Q., Jia, G., Ren, B., Pan, T., & He, C. (2014). N6-methyladenosine-dependent regulation of messenger RNA stability. *Nature*, *505*(7481), 117–120. https://doi.org/10.1038/nature12730

Wang, Y., & Wang, Y. (2015). *Protein Structure Determination from Cryo-electron Microscopy Density Maps*.

Wei, C. M., Gershowitz, A., & Moss, B. (1975). Methylated nucleotides block 5' terminus of HeLa cell messenger RNA. *Cell*, *4*(4), 379–386. https://doi.org/10.1016/0092-8674(75)90158-0

Woodcock, C. B., Horton, J. R., Zhou, J., Bedford, M. T., Blumenthal, R. M., Zhang, X., & Cheng, X. (2020). Biochemical and structural basis for YTH domain of human YTHDC1 binding to methylated adenine in DNA. *Nucleic Acids Research*, *48*(18), 10329–10341. https://doi.org/10.1093/nar/gkaa604

Worthington, E. N., Kavakli, I. H., Berrocal-Tito, G., Bondo, B. E., & Sancar, A. (2003). Purification and characterization of three members of the photolyase/cryptochrome family blue-light photoreceptors from vibrio cholerae. *Journal of Biological Chemistry*, *278*(40), 39143–39154. https://doi.org/10.1074/jbc.M305792200

Wu, H., Reynolds, A. B., Kanner, S. B., Vines, R. R., & Parsons, J. T. (1991). Identification and characterization of a novel cytoskeleton-associated pp60src substrate. *Molecular and Cellular Biology*, *11*(10), 5113–5124. https://doi.org/10.1128/mcb.11.10.5113

Xu, K., Zheng, X., & Sehgal, A. (2008). Regulation of feeding and metabolism by neuronal and peripheral clocks in Drosophila. *Cell Metabolism*, *8*(4), 289–300. https://doi.org/10.1016/j.cmet.2008.09.006

Xue, L., Yi, H., Huang, Z., Shi, Y.-B., & Li, W.-X. (2011). Global gene expression during the human organogenesis: from transcription profiles to function predictions. *International Journal of Biological Sciences*, *7*(7), 1068–1076. https://doi.org/10.7150/ijbs.7.1068

Yamada, D., Iwata, T., Yamamoto, J., Hitomi, K., Todo, T., Iwai, S., Getzoff, E. D., & Kandori, H. (2015). Structural role of two histidines in the (6-4) photolyase reaction. *Biophysics and Physicobiology*, *12*, 139–144. https://doi.org/10.2142/biophysico.12.0_139

Yamamoto, J., Plaza, P., & Brettel, K. (2017). Repair of (6-4) Lesions in DNA by (6-4) Photolyase: 20 Years of Quest for the Photoreaction Mechanism. *Photochemistry and Photobiology*, *93*(1), 51–66.

https://doi.org/10.1111/php.12696

Yang, Z., Liu, B., Su, J., Liao, J., Lin, C., & Oka, Y. (2017). Cryptochromes Orchestrate Transcription Regulation of Diverse Blue Light Responses in Plants. *Photochemistry and Photobiology*, *93*(1), 112–127. https://doi.org/10.1111/php.12663

Yanovsky, M. J., Mazzella, M. A., & Casal, J. J. (2000). A quadruple photoreceptor mutant still keeps track of time. *Current Biology*, *10*(16), 1013–1015. https://doi.org/https://doi.org/10.1016/S0960-9822(00)00651-5

Yasui, A., Eker, A. P., Yasuhira, S., Yajima, H., Kobayashi, T., Takao, M., & Oikawa, A. (1994). A new class of DNA photolyases present in various organisms including aplacental mammals. *The EMBO Journal*, *13*(24), 6143–6151.

Yi, H., Xue, L., Guo, M.-X., Ma, J., Zeng, Y., Wang, W., Cai, J.-Y., Hu, H.-M., Shu, H.-B., Shi, Y.-B., & Li, W.-X. (2010). Gene expression atlas for human embryogenesis. *FASEB Journal : Official Publication of the Federation of American Societies for Experimental Biology*, *24*(9), 3341–3350. https://doi.org/10.1096/fj.10-158782

Yifan, C. (2018). Single particle cryo-EM – how did it get here and where will it go. *Science*, *361*(6405), 876–880. https://doi.org/10.1016/j.physbeh.2017.03.040

Yu, W., & Hardin, P. E. (2006). Circadian oscillators of Drosophila and mammals. *Journal of Cell Science*, *119*(23), 4793–4795. https://doi.org/10.1242/jcs.03174

Yu, X., Klejnot, J., Zhao, X., Shalitin, D., Maymon, M., Yang, H., Lee, J., Liu, X., Lopez, J., & Lin, C. (2007). Arabidopsis cryptochrome 2 completes its posttranslational life cycle in the nucleus. *The Plant Cell*, *19*(10), 3146–3156. https://doi.org/10.1105/tpc.107.053017

Zaccara, S., & Jaffrey, S. R. (2020). A Unified Model for the Function of YTHDF Proteins in Regulating m(6)A-Modified mRNA. *Cell*, *181*(7), 1582-1595.e18. https://doi.org/10.1016/j.cell.2020.05.012

Zantke, J., Ishikawa-Fujiwara, T., Arboleda, E., Lohs, C., Schipany, K., Hallay, N., Straw, A. D., Todo, T., & Tessmar-Raible, K. (2013). Circadian and Circalunar Clock Interactions in a Marine Annelid. *Cell Reports*, *5*(1), 99–113. https://doi.org/10.1016/j.celrep.2013.08.031

Zhai, Y., Zhang, D., Yu, L., Sun, F., & Sun, F. (2019). SmartBac, a new baculovirus

system for large protein complex production. *Journal of Structural Biology: X*, *1*(February), 100003. https://doi.org/10.1016/j.yjsbx.2019.100003

Zhang, H, Zhang, S., He, H., Zhang, C., Yu, D., & Shao, R. (2013). Downregulation of G3BPs inhibits the growth, migration and invasion of human lung carcinoma H1299 cells by suppressing the Src/FAK-associated signaling pathway. *Cancer Gene Therapy*, *20*(11), 622–629. https://doi.org/10.1038/cgt.2013.62

Zhang, Hao, Ma, Y., Zhang, S., Liu, H., He, H., Li, N., Gong, Y., Zhao, S., Jiang, J.-D., & Shao, R.-G. (2015). Involvement of Ras GTPase-activating protein SH3 domain-binding protein 1 in the epithelial-to-mesenchymal transition-induced metastasis of breast cancer cells via the Smad signaling pathway. *Oncotarget*, *6*(19), 17039–17053. https://doi.org/10.18632/oncotarget.3636

Zhang, Z., Theler, D., Kaminska, K. H., Hiller, M., de la Grange, P., Pudimat, R., Rafalska, I., Heinrich, B., Bujnicki, J. M., Allain, F. H.-T., & Stamm, S. (2010). The YTH domain is a novel RNA binding domain. *The Journal of Biological Chemistry*, *285*(19), 14701–14710. https://doi.org/10.1074/jbc.M110.104711

Zhao, B. S., Wang, X., Beadell, A. V, Lu, Z., Shi, H., Kuuspalu, A., Ho, R. K., & He, C. (2017). m(6)A-dependent maternal mRNA clearance facilitates zebrafish maternal-to-zygotic transition. *Nature*, *542*(7642), 475–478. https://doi.org/10.1038/nature21355

Zhong, X., Yu, J., Frazier, K., Weng, X., Li, Y., Cham, C. M., Dolan, K., Zhu, X., Hubert, N., Tao, Y., Lin, F., Martinez-Guryn, K., Huang, Y., Wang, T., Liu, J., He, C., Chang, E. B., & Leone, V. (2018). Circadian Clock Regulation of Hepatic Lipid Metabolism by Modulation of m6A mRNA Methylation. *Cell Reports*, *25*(7), 1816-1828.e4. https://doi.org/10.1016/j.celrep.2018.10.068

Zhou, J., Wan, J., Gao, X., Zhang, X., Jaffrey, S. R., & Qian, S.-B. (2015). Dynamic m(6)A mRNA methylation directs translational control of heat shock response. *Nature*, *526*(7574), 591–594. https://doi.org/10.1038/nature15377

Zhu, H., Yuan, Q., Briscoe, A. D., Froy, O., Casselman, A., & Reppert, S. M. (2005). The two CRYs of the butterfly. In *Current biology : CB* (Vol. 15, Issue 23, pp. R953-4). https://doi.org/10.1016/j.cub.2005.11.030

Zoltowski, B. D., Chelliah, Y., Wickramaratne, A., Jarocha, L., Karki, N., Xu, W., Mouritsen, H., Hore, P. J., Hibbs, R. E., Green, C. B., & Takahashi, J. S.

(2019). Chemical and structural analysis of a photoactive vertebrate cryptochrome from pigeon. *Proceedings of the National Academy of Sciences of the United States of America*, *116*(39), 19449–19457. https://doi.org/10.1073/pnas.1907875116

Zoltowski, B. D., Vaidya, A. T., Top, D., Widom, J., Young, M. W., & Crane, B. R. (2011). Structure of full-length Drosophila cryptochrome. *Nature*, *480*(7377), 396–399. https://doi.org/10.1038/nature10618

7 Appendix

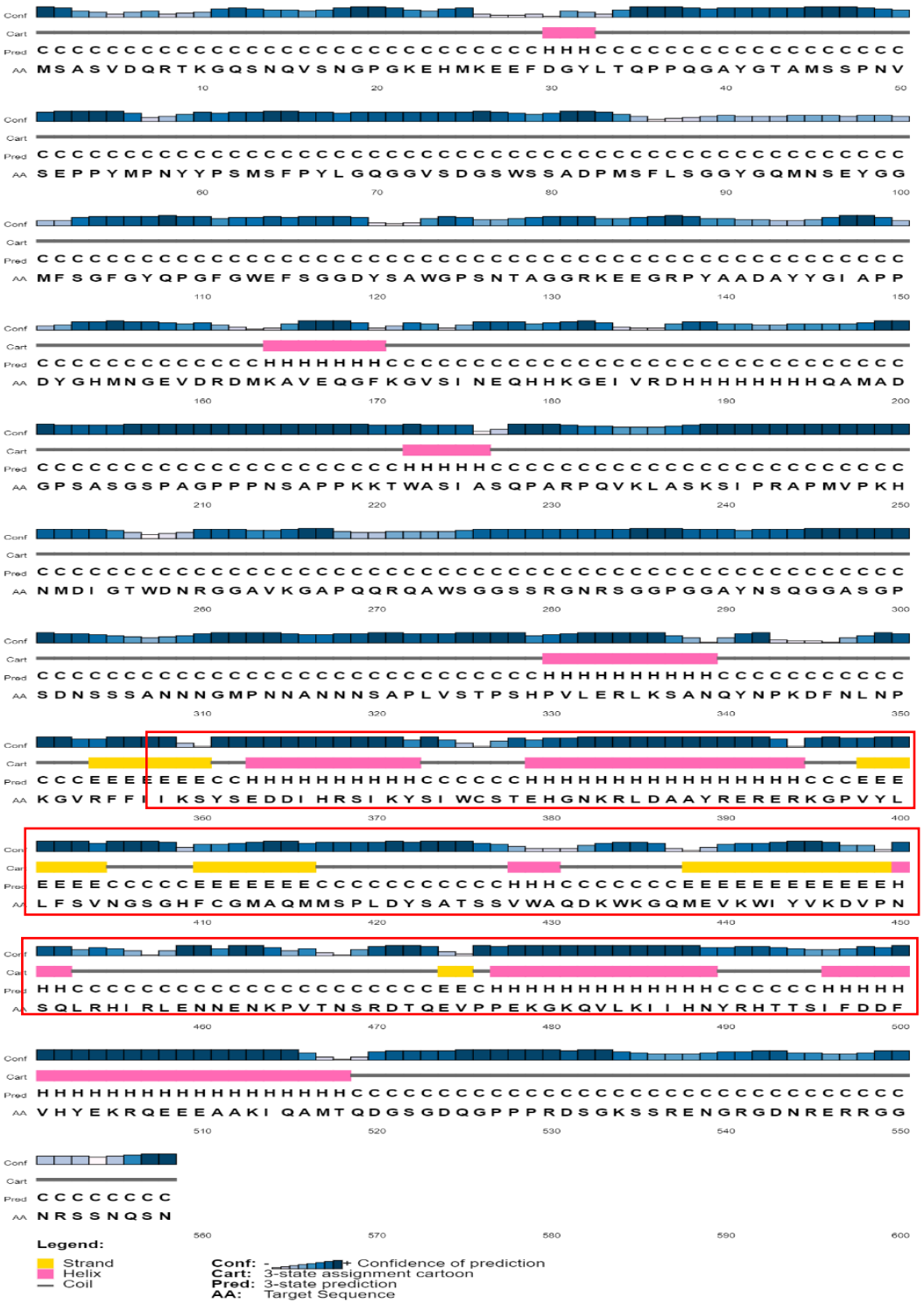

Figure A1: PSIPRED graphical output for the secondary structure prediction of YTHDF which indicated that the N-terminal region of the protein is predominantly composed of coils and the defined secondary structures lie mainly within the YTH domain of protein (red box).

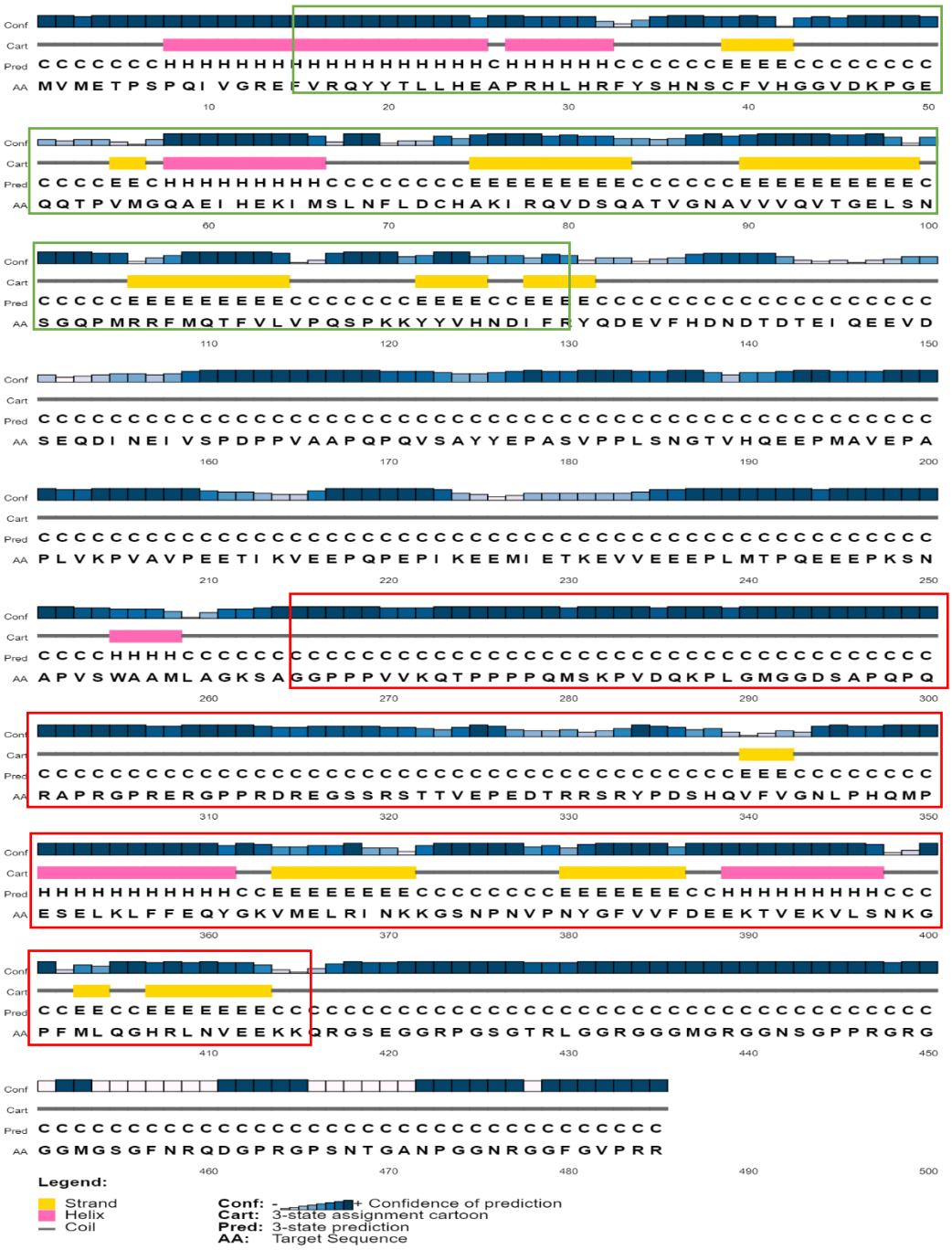

Figure A2: PSIPRED graphical output for the secondary structure prediction of G3BP which indicated mainly N-terminal and C-terminal strands and helices. The central sequence of the protein is composed of coils. The NFT2 domain (green box) and RRM-G3BP (red box) are marked.

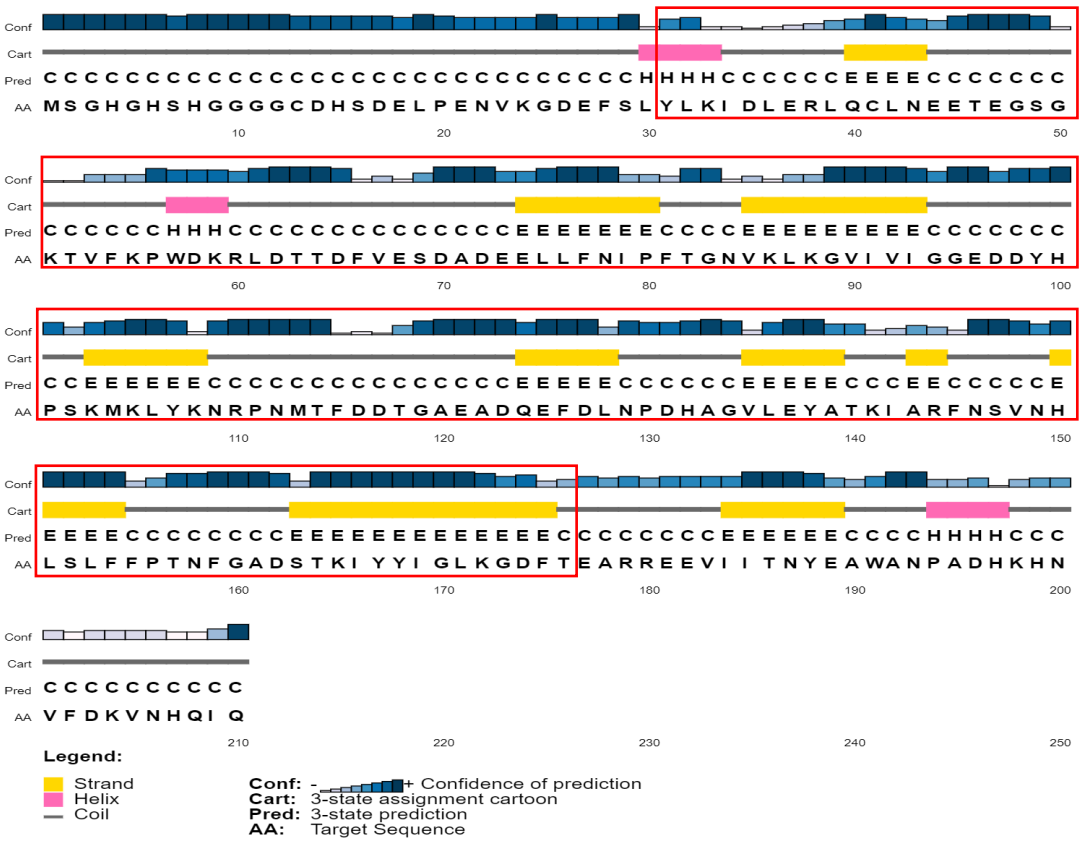

Figure A3: PSIPRED graphical output for the secondary structure prediction of PITHD1 which indicated that beta strand and coils as primary secondary structure feature of the protein. PITH domain (red box) is marked.

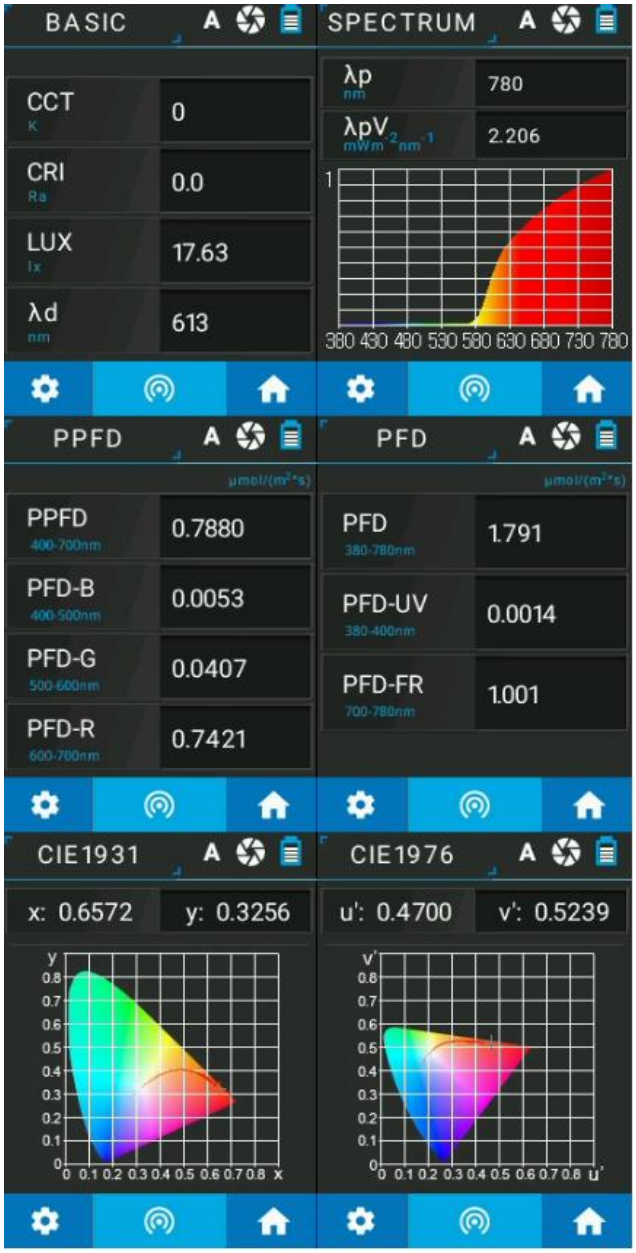

Figure A4: Spectrum and PFD measurement of red-light source used for L-CRY/P-CRY purification measured using LI 180 LICOR spectrometer (random distance in the room).

Figure A5: Spectrum and PFD measurement of red-light LED strips mounted in the cold room and centrifuge room used for L-CRY/P-CRY purification measured using LI 180 LICOR spectrometer (random distance in the room).

Figure A6: Spectrum and PFD measurement of red-light source used for P-CRY spectroscopy measured using LI 180 LICOR spectrometer at a distance of 1 cm.

Figure A7: Spectrum and PFD measurement of blue light source used for L-CRY spectroscopy measured using LI 180 LICOR spectrometer at a distance of 1 cm.

Figure A8: Spectrum and PFD measurement of moonlight source at full moon intensity used for L-CRY spectroscopy measured using LI 180 LICOR spectrometer at a distance of 7 cm.

Figure A9: Spectrum and PFD measurement of sunlight source used for L-CRY spectroscopy measured using LI 180 LICOR spectrometer at a distance of 7 cm.

8 Acknowledgment

The content is removed for privacy